INVESTIGATING THE MOLECULAR PARTICIPANTS OF PROGRAMMED CELL DEATH IN *PLASMODIUM FALCIPARUM*

Warren Antonio Vieira

The financial assistance of the National Research Foundation (NRF) towards this research is hereby acknowledged. Opinions expressed and conclusions arrived at, are those of the author and are not necessarily to be attributed to the NRF.

A thesis submitted to the Faculty of Health Sciences, University of the Witwatersrand, Johannesburg, in fulfilment of the requirements for the degree

of

Doctor of Philosophy

University of the Witwatersrand, Johannesburg, 2014

DECLARATION

I, Warren Antonio Vieira, declare that this thesis is my own work. It is being submitted for the degree of Doctor of Philosophy in the University of the Witwatersrand, Johannesburg. It has not been submitted before for any degree or examination at this or any other University.

…….

Warren Antonio Vieira

30th day of January, 2015

OUTPUTS ARISING FROM THE THESIS

Manuscript

Localization and interactions of Plasmodium falciparum SWIB/MDM2 homologues

Authors: W.A. Vieira and T.L. Coetzer

Manuscript under preparation

International conferences

Binding partners of putative SWIB domain proteins in Plasmodium falciparum

Authors: W.A. Vieira, P.M. Durand and T.L. Coetzer

Presentation: Poster

- At the 6th MIM Pan-African Malaria Conference in October 2013, Durban.

Recombinant p53 and MDM2 Homologues in Plasmodium falciparum

Authors: W.A. Vieira, P.M. Durand and T.L. Coetzer

Presentation: Poster

- At the South African Society for Biochemistry and Molecular Biology and the Federation of African Societies of Biochemistry and Molecular Biology (SASBMB-FASBMB) 2012 Congress in January 2012, Drakensburg

Local conferences

Localization and interactions of Plasmodium falciparum SWIB/MDM2 homologues

Authors: W.A. Vieira, P.M. Durand and T.L. Coetzer

Presentation: Poster

- At the Wits Faculty of Health Sciences Research Day 2014, September 2014, Johannesburg.

- At the South African Society for Biochemistry and Molecular Biology (SASBMB) 2014 Congress in July 2012, Western Cape.

Binding partners of putative SWIB domain proteins in <u>Plasmodium falciparum</u>

Authors: W.A. Vieira, P.M. Durand and T.L. Coetzer

Presentation: Oral

- At the Wits Molecular Bioscience Research Thrust (MBRT) Research Day in December 2013, Johannesburg. **The presentation won first prize in the oral category.**

Recombinant p53 and MDM2 Homologues in <u>Plasmodium falciparum</u>

Authors: W.A. Vieira, P.M. Durand and T.L. Coetzer

Presentation: Poster

- At the Wits Molecular Bioscience Research Thrust (MBRT) Research Day in December 2012, Johannesburg.
- At the Wits Faculty of Health Sciences Research Day 2012, September 2012, Johannesburg
- At the Wits Molecular Bioscience Research Thrust (MBRT) Research Day in December 2011, Johannesburg

ABSTRACT

Malaria, a disease resulting from infection by members of the *Plasmodium* genus, accounted for an estimated 627 000 deaths globally in 2012. The majority of these mortalities were due to *P. falciparum* infections and thus the species of focus in this study. Due to the rapid emergence of drug-resistant strains, novel avenues for research evaluating parasite survival and population regulation within the human host are now needed. Programmed cell death (PCD) is a well characterised means of self-regulation in metazoans, where a plethora of proteins and signals result in the destruction and/or removal of unnecessary, damaged or dangerous cells. A key protein participant is MDM2 which, via its SWIB/MDM2 domain, binds to the nuclear transcription factor p53 to promote p53 degradation and prevent apoptosis. SWIB/MDM2 domains additionally play key roles in transcription-dependent stress survival. No proven PCD molecular participants for *P. falciparum* exist but two SWIB/MDM2 homologues (PF3D7_0611400 (*Pf*SWIB) and PF3D7_0518200 (*Pf*MDM2)) and a putative p53 homologue (PF3D7_0522400 (*Pf*p53)) have been identified by bioinformatics. These were assessed experimentally in this study.

Structural features of the SWIB/MDM2 domains of *Pf*MDM2 and *Pf*SWIB, suggested that they are chromatin remodelling factors. The domains were amplified from 3D7 *P. falciparum* genomic DNA, directionally cloned into the pGEX-4T-2 vector, and used for recombinant GST-fusion protein expression in *E. coli*. The soluble, tagged, domains were isolated and purified by affinity chromatography (*Pf*MDM2, ~33kDa and *Pf*SWIB, ~42kDa) and used, in conjunction with *P. falciparum* phage display library technology, for the identification of several novel binding partners. Two of these interactions were verified with *in vitro* binding assays, proving concentration dependent interactions between *Pf*MDM2 and a conserved protein of unknown function; and *Pf*SWIB and a putative

serine-threonine protein kinase (*Pf*ARK3). Transgenic *P. falciparum* parasites were created by transfection with pARL2-GFP vector constructs containing the *Pf*SWIB and *Pf*MDM2 genes. *Pf*MDM2-GFP localized to the mitochondria under the control of an N-terminal signal sequence, under normal and heat stress conditions, the latter triggering PCD in the asexual intraerythrocytic parasite. *Pf*SWIB-GFP localized to the cytoplasm under normal and heat stress conditions, but in a subpopulation of trophozoites it moved to the nucleus after exposure to elevated temperatures. *Pf*MDM2 is hypothesized to play a role within the parasite mitochondrion, although its involvement in PCD is uncertain and may be unconventional, while *Pf*SWIB is suggested to be involved in a stage-specific heat stress response.

*Pf*p53 was found to have a putative DNA binding and tetramerization domain, based primarily on sequence alignments. A recombinant GST-tagged form (~87kDa) of these two domains was expressed in *E. coli* and purified by affinity chromatography. The ability of the recombinant protein to tetramerize was inconclusive, while in an electromobility shift assay it did not bind to a canonical p53 DNA binding consensus sequence identified in the parasite's genome. The precise cellular function(s) for this protein requires further evaluation.

This study represents the first characterisation of these three *P. falciparum* proteins. Several novel activities were identified for each and their role in PCD was evaluated by exposing parasites to febrile temperatures, which provided new information regarding heat stress regulation in *P. falciparum*.

ACKNOWLEDGMENTS

The last four years comprised an unexpected adventure. Although the road was rough, laced with a fair amount of heart ache and turmoil, there were times of joy, laughter and unforgettable memories. Every step, every word read and every idea exchanged enlightened me on all levels – intellectually, emotionally, personally, spiritually and physically. I am the man I am today because of the path I have walked and for that I could not be happier. Thankfully I did not walk this journey alone, and in accordance much thanks must be given to all who supported me.

First and foremost I must thank God – for giving me enough perseverance and dedication to carry on and face each new challenge and day; and enough unexplained and incorrect results to make sure I learnt and understood what I was doing.

Next I must bestow thanks upon my parents, Antonio and Stephanie, who toiled much to help and support me along this seemingly impossible journey. Without them I would not have been able to get this far. They have had an important hand in shaping the man I am today, intellectually and emotionally. I must also thank my brothers, Donovan and Justin, for being at my side through this journey.

An important and prominent woman, who must be thanked, is Professor Theresa L. Coetzer. She took the risk of accepting an eager student, not knowing much about molecular biology, into her laboratory and providing him with the knowledge needed to grow scientifically. Her faith and optimism, applied liberally, was an inspiration. Thank you for this life changing opportunity Prof.

My sanity was maintained in the laboratory due to the presence of warm and loving faces that toiled away with me, night and day. Alisje “Sunshine” Churchyard, Anthea Hean, Belinda Catherine Bezuidenhout, Dale Liebenberg, Dewaldt Engelbrecht, Kubendran “Kuben” Naidoo, Nadia Ebrahim, Nisha “Nishapoo” Dhar Kwatra, Melanie “Munchkin” Wepener, Rajdeep Choudhury and Sonja Brigitte Lautherbach – you are all family to me and will always hold special places in my heart. Thank you for your companionship. I give a special thanks to Kubendran and Sonja for showing me the ropes of molecular biology. Additionally, I would like to thank Sunshine, Muchkin and Nishapoo for becoming three of my best friends - I hope you will always know how precious you are!

Many people began this journey with me but not all remain in my life. This sorrow did teach me to cherish every moment and that even a brief presence can have a profound impact. For it is not how long someone is at your side, but how much life they lived with you while they were there. To those that are still at my side – all my family and friends (special thanks to Charles Henry Rall, Darren Lawrence, Drikus Saayman, Inga Theresa Baron, Johan van Niekerk, Melanie Kate Dickerson, Rachel Cooper, Sandra Pow Chong) – thank you for being lighthouses in the dark and pillars of strength. I hope that you will come with me as I begin my new chapter, making unforgettable memories. A special thank you to Michael James Laughland, although your impact has only been short so far, it has helped me greatly and I will forever be indebted to you for you patience, laughter, empathy and tolerance of my science induced insanity.

I would like to finally dedicate this thesis to

ଌ Aidan "**Binna**" **Joseph Powels** ଓ

(1933 - 1999)

The man who taught me the importance of the written word

"There are perhaps no days of our childhood we lived so fully as those we spent with a favourite book."

– *Marcel Proust*

ETHICS CLEARANCE

Ethics clearance was obtained for this project.

Ethics number M13-05-69; The University of the Witwatersrand; Committee for Research on Human Subjects (medical).

TABLE OF CONTENTS

LIST OF FIGURES

LIST OF TABLES

NOMENCLATURE, ABBREVIATIONS AND SYMBOLS

ABBREVIATIONS AND SYMBOLS	MEANING
A	Adenine
A260	Absorbance at 260nm
A280	Absorbance at 280nm
AIF	Apoptosis inducing factor
APAF-1	Apoptosis protease activating factor 1
ApiAP2	Apicomplexa Apetala2
ARK	Aurora related kinase
ATM	Ataxia telangiesctasia-mutated
BAK	Bcl-2 homologous antagonist killer
BAP60	Brahma-associated protein 60
BAX	Bcl-2-associated X protein
Bcl-2	B cell lymphoma 2
BID	BH3 interacting-domain death agonist protein
bp	Base pairs
BRG1	Brahma-related gene-1
BSA	Bovine serum albumin
C	Cytosine
CAD	Caspase activated DNase
CBCR	Computational Biology Research Centre
Cep-1	*C. elegans* transcription factor (p53 homologue)
cm	Centimetre
CoQ	Ubiquinone
CS	Circumsporozoite
DBD	DNA binding domain
DIG	Digoxigenin
DISC	Death inducing signalling complex
Dmp53	*D. melanogaster* p53 homologue
DNA	Deoxyribonucleic acid
DNaseI	Deoxyribonuclease I
EBA-175	Erythrocyte binding antigen 175
EDTA	Ethylenediaminetetraacetic acid
EMBL-EBI	European Molecular Biology Laboratory European Bioinformatics Institutes
EMSA	Electrophoretic mobility shift assay
ER	Endoplasmic reticulum
FIRE	Functional Inference using the Rates of Evolution
g	Gram
G	Guanine
GFP	Green fluorescent protein
Group C	SWIB/MDM2 domain homologues involved in chromatin remodelling, transcriptional regulation and unknown functions
Group M	SWIB/MDM2 domains homologues found in MDM2 proteins and facilitate p53 binding
GST	Glutathione S-transferase
GST-*Pf*MDM2	Recombinant GST-tagged *Pf*MDM2 SWIB/MDM2 domain
GST-*Pf*p53	Recombinant GST-tagged putative DBD and tetramerization domain of *Pf*p53

GST-*Pf*SWIB	Recombinant GST-tagged *Pf*SWIB SWIB/MDM2 domain
hDHFR	Human dihydrofolate reductase
His-*Pf*ALV5	Recombinant His-tagged *Pf*ALV5 domain
His-*Pf*ARK3	Recombinant His-tagged *Pf*ARK3 domain
His-*Pf*LisH	Recombinant His-tagged *Pf*LisH domain
His-*Pf*RS6	Recombinant His-tagged *Pf*RS6 domain
HRP	Horse radish peroxidise
HSBP	Heat shock binding protein
HSF	Heat shock factor
HSP	Heat shock protein
HSP70	Heat shock protein 70
HtrA2/Omi	High-temperature requirement factor A2/Omi stress regulated endoprotease
IAP	Inhibitor of apoptosis protein
iCAD	Inhibitor of CAD
IPTG	Isopropyl-β-D-1-thiogalactopyranoside
kDa	Kilodalton
l	Litre
LB	Luria Broth
LisH	Lis1 homology
M	Molar
MDa	Megadalton
MDMX	Mouse Double Minute X
MDM2	Mouse Double Minute 2
MDM4	Mouse Double Minute 4
mg	Milligram
ml	Millilitre
mM	Millimolar
n/a	Not applicable
NES	Nuclear export signal
ng	Nanogram
NLS	Nuclear localization signal
nm	Nanometer
nM	Nanomolar
OD	Optical density
OD_{600nm}	Optical density at 600nm
P. falciparum	*Plasmodium falciparum*
$p14^{ARF}$	Alternative reading frame tumour suppressor
p53	Protein 53
p63	Protein 63
p73	Protein 73
PBS	Phosphate buffered saline
PCD	Programmed cell death
PCR	Polymerase chain reaction
PFU	Plaque-forming unit
***Pf*ALV5**	Domain of PF3D7_1003600 (a membrane skeletal protein (Alveolin 5 (ALV5)) identified by biopanning
***Pf*ARK3**	Domain of PF3D7_1356800 (a putative serine/threonine protein kinase (Aurora related kinase 3 (ARK3)) identified by biopanning
***Pf*GFP**	Episomally expressed GFP protein

***Pf*LisH**	Domain of PF3D7_1303400 (a conserved *Plasmodium* protein of unknown function) identified by biopanning
***Pf*MDM2**	PF3D7_0518200, a putative SWIB/MDM2 domain-containing protein
***Pf*MDM2-GFP**	Episomally expressed GFP-tagged *Pf*MDM2
***Pf*p53**	PF3D7_0522400, a conserved *Plasmodium* protein and assessed as a potential p53 homologue in this study
***Pf*RS6**	Domain of PF3D7_1342000 (a putative 40S ribosomal protein S6) identified by biopanning
***Pf*SWIB**	PF3D7_0611400, the SWI/SNF-related matrix-associated actin-dependent regulator of chromatin
***Pf*SWIB-GFP**	Episomally expressed GFP-tagged *Pf*SWIB
pH	Potential of hydrogen
PS	Phosphatidylserine
PHYRE2	Protein Homology/analogy Recognition Engine V 2.0
PMRU	Plasmodium Molecular Research Unit
pI	Isoelectric point
pRBC	Parasitized red blood cells
PV	Parasitophorous vacuole
Pu	Purine
Py	Pyrimidine
R	Purine
RBC	Red blood cells
rcf	Relative centrifugal force
RIP	Receptor-interacting protein
RNA	Ribonucleic acid
RNase	Ribonuclease
RNase A	Ribonuclease A
rpm	Revolutions per minute
SDS	Sodium dodecyl sulphate
SDS-PAGE	Sodium dodecyl sulphate polyacrylamide gel electrophoresis
SMAC/DIABLO	Second mitochondria-derived activator of caspase/direct IAP binding protein with a low pI
SWI3	SWItch 3
SWI/SNF	SWItch/Sucrose NonFermentable
SWIB	SWI/SNF complex B
SWP73 (SNF12)	SWI/SNF associated protein 73
T	Thymine
T_a	Annealing temperature
TAE	Tris base, acetic acid and EDTA
TB	Terrific broth
TBE	Tris base, boric acid and EDTA
tBID	Truncated BID
TBS	Tris buffered saline
TCA	Tricarboxylic acid
TE	Tris EDTA
T_m	Melting temperature
™	Trade mark

TNFα	Tumour necrosis factor α
TRAP	Thrombospondin-related anonymous protein
Tris-HCl	Trisaminomethane hydrochloride
U	Uracil
UV	Ultra violet
V	Volts
W	Weakly binding nucleotide (A or T)
Y	Pyrimidine
Δm*Pf*MDM2	Truncated *Pf*MDM2 protein
Δm*Pf*MDM2-GFP	Episomally expressed GFP-tagged Δm*Pf*MDM2
µg	Microgram
µl	Microlitre
µM	Micromolar
®	Registered trademark

1 INTRODUCTION

1.1 The *Apicomplexa* phylum and malaria

The phylum *Apicomplexa* is constituted by a group of single celled eukaryotic organisms, referred to as protists, which are believed to have diverged from the eukaryotic lineage either at the time of or before the emergence of multicellularity (Escalante and Ayala, 1995, Adl *et al.*, 2005). All members of this phylum, classified according to molecular phylogeny, are obligatory intracellular parasites in nature and are commonly defined by the presence of apically located secretory organelles referred to as micronemes and rhoptries (Adl *et al.*, 2005, Morrison, 2009). One genus of great medical and social importance is *Plasmodium*, which lies in the order *Haemosporida* of the *Apicomplexa* phylum.

On the 6th of November 1880, a French army surgeon by the name of Charles Louis Alfonse Laveran noted the presence of unusual micro-organisms within the blood of malaria-infected soldiers while working in Algeria. He believed that the crescent and spherically shaped bodies he identified, and later watched transform into flagellated cells, were the causative agents of malaria (Bruce-Chwarr, 1988). This hypothesis, which received much criticism at the time, was later confirmed. Ronald Ross, in 1897, discovered that transmission was facilitated by a mosquito vector (Cox, 2010).

In 2013 97 countries were considered malaria endemic by the World Health Organization, with five *Plasmodium* species currently classified as the causative agents of human malaria. These species are *Plasmodium falciparum*, *P. vivax*, *P. ovale*, *P. malariae* and *P. knowlesi* (Singh *et al.*, 2004, World Health Organization, 2013). *P. vivax* infections are the most widely distributed globally, although infections by *P. falciparum* are the most

dangerous. It is estimated, in 2012, that malaria accounted for about 207 million clinical cases and about 627 000 deaths worldwide. About 80% of these cases and 90% of these deaths occurred in sub-Saharan Africa, with children under the age of five and pregnant women being the most severely affected (World Health Organization, 2013). Due to the high morbidity and mortality associated with *P. falciparum* infections, much scientific and medical focus has been placed on this species.

1.2 The origins and evolution of *Plasmodium falciparum*

rRNA studies suggest that the *Plasmodium* lineage may have evolved before the origin of vertebrates and radiated about 129 million years ago, paralleling the diversification of their vector's lineage and the divergence of birds from reptiles (Escalante and Ayala, 1995). The species constituting this genus fall into two distinct clades, one of which encompasses at least six distinct species, including *P. falciparum, P. reichenowi* and *P. gobani*, the latter two being the closest known relatives of *P. falciparum* (Escalante and Ayala, 1994, Ollomo *et al.*, 2009). The emergence of the *P. falciparum* species itself is a topic of much debate, with several hypotheses circulating in literature. These range from ancestral divergence of a common ancestral parasite at the time of the human-chimpanzee split to a cross-species transfer from a variety of possible primates to humans (Rich *et al.*, 1998, Rich *et al.*, 2009, Krief *et al.*, 2010, Liu *et al.*, 2010, Prugnolle *et al.*, 2011).

Originally, *P. falciparum* was assumed to be a strictly human pathogen but this notion has since proven to be false, with various primates being infected by many different *Plasmodium* species including *falciparum* (Krief *et al.*, 2010, Liu *et al.*, 2010, Prugnolle *et al.*, 2010). This observation that primates can naturally be infected with *P. falciparum*

implies the presence of a possible parasite reservoir, which needs to be considered for successful disease eradication (Prugnolle *et al.*, 2011).

1.3 The *P. falciparum* life cycle

All *Plasmodium* parasites require two hosts to complete their complex life cycle – an insect host, in the case of human malaria the female *Anopheles* mosquito, and a vertebrate host (Miller *et al.*, 2002, Cox, 2010, Hafalla *et al.*, 2011). Figure 1.1 presents an overview of the *P. falciparum* life cycle, which will be discussed in detail below.

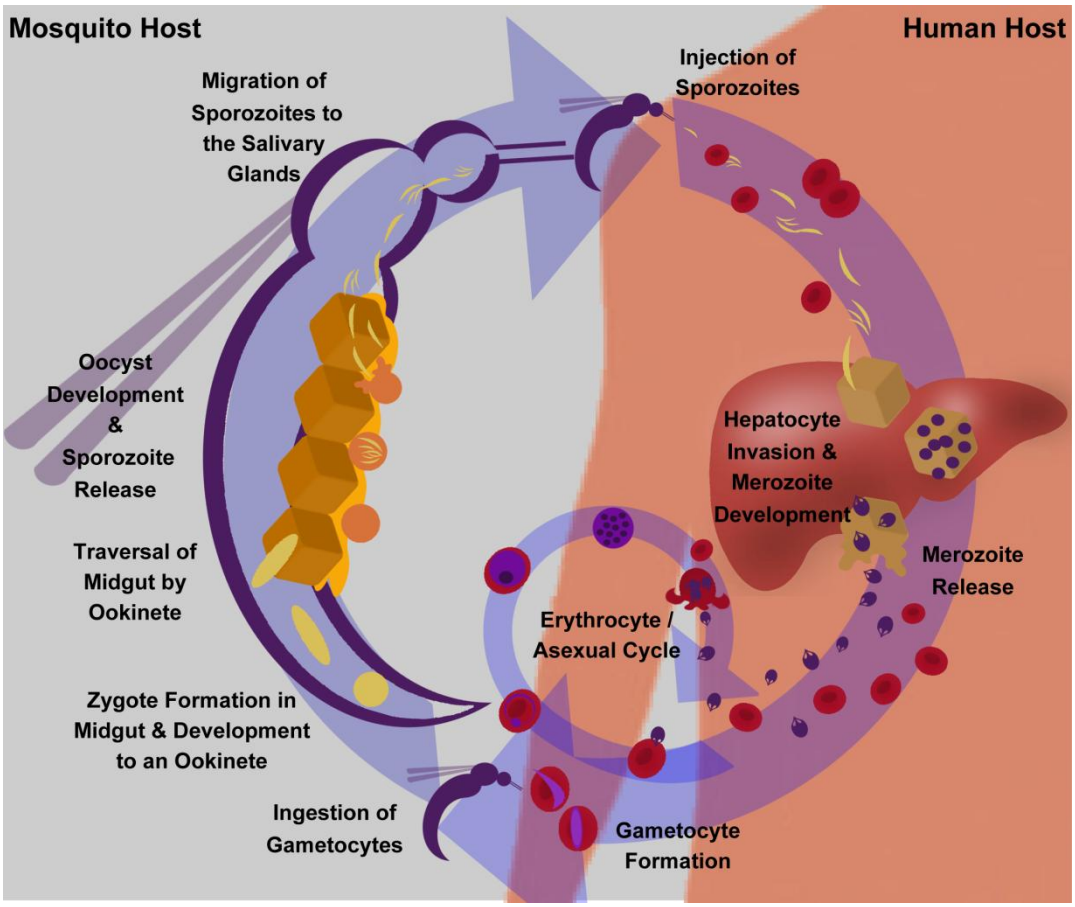

Figure 1.1: Diagram presenting the complete life cycle of *P. falciparum*.
Based on data from Miller *et al*., 2002.

1.3.1 The human host

1.3.1.1 The pre-erythrocytic stage

About fifteen parasites, resident in the mosquito's salivary ducts as sporozoites, are injected into the skin of the human host during the mosquito feeding process (Rosenberg *et al.*, 1990). The sporozoites traverse through the skin into the blood stream and proceed to the liver in the first 15 minutes to several hours after introduction into the skin (Hafalla *et al.*, 2011). The sporozoites specifically target and invade the liver hepatocytes through the use of sporozoite surface thrombospondin-related anonymous protein (TRAP) and circumsporozoite (CS) protein (Hafalla *et al*., 2011). Once inside the host hepatocyte each sporozoite takes about 140 hours to undergo complete schizogony and produce between 30 000 – 50 000 merozoites (Hafalla *et al.*, 2011). The fully developed merozoites are packed into a vesicle, a merosome, which buds from the infected hepatocytes and escapes into the blood where it disintegrates to allow the merozoites to invade host RBC (red blood cells) in as little as 30 seconds (Hafalla *et al.*, 2011). *P. falciparum*, unlike some of the other *Plasmodium* species, does not have a dormant liver stage (Fujioka and Aikawa, 1999). This obligatory pre-erythrocytic stage of the parasite's life cycle is clinically silent (Hafalla *et al.*, 2011).

1.3.1.2 The erythrocytic stage

The merozoite invades the host RBC in a four step process, utilizing an array of merozoite derived proteins and RBC membrane surface components. Ultimately this process results in a resealed erythrocyte membrane and the parasite located inside the RBC within a parasitophorous vacuole (PV) (Cowman *et al.*, 2012). *P. falciparum* does not solely depend on a single invasion pathway, instead using a wide variety of receptors for attachment and invasion (Cowman *et al*., 2012).

The majority of invaded merozoites enter into an asexual cycle and develop, through the ring stage, into a feeding amoeboid shape trophozoite (Tilley *et al.*, 2011). As the parasite develops it ingests RBC cytoplasm and haemoglobin to acquire nutrients. Glucose taken up by the parasite is almost entirely converted to lactate for energy production (MacRae *et al.*, 2013). The haemoglobin is degraded as an amino acid fuel source for the parasite in the acidic food vacuole, with the toxic haem group being processed and rendered harmless in the form of haemozoin, the dark pigment prominently seen in the trophozoite life stage (Tilley *et al.*, 2011, Pishchany and Skaar, 2012).

The *P. falciparum* trophozoite's cytoplasm contains a large number of ribonucleoprotein particles, pigment granules, a single digestive vacuole, a single membrane bound nucleus, and a primitive mitochondrial structure in contact with a generally round apicoplast (Tilley *et al.*, 2011). The parasite develops further, undergoing asexual amplification through the formation of a multinucleated schizont form, to ultimately produce 16 to 32 new merozoites (Hafalla *et al.*, 2011). Upon erythrocyte rupture, the newly formed merozoites are released into circulation and can infect new erythrocytes (Hafalla *et al.*, 2011). The *P. falciparum* asexual life cycle within human RBC is about 48-50 hours from invasion to egress (Tilley *et al.*, 2011). Escape from the infected RBC involves the initial PV membrane destruction and subsequent erythrocyte membrane rupture by a variety of parasite proteases (Wickham *et al.*, 2003).

This intraerythrocytic stage of the parasite's life cycle induces the clinical manifestations of the disease. The debris released during egress, both of human and parasite origin, is thought to have toxic effects on the human host and is the cause for some of the clinical symptoms, including fever (Hafalla *et al.*, 2011). *P. falciparum* infections are associated

with periodic fevers every 48 hours, although in early stages of infection the fever may be irregular (Miller *et al.*, 2002). Other clinical symptoms associated with a *falciparum* infection include anaemia, due to RBC loss; circulatory obstruction and its associated consequences, discussed below; and cerebral malaria which can lead to unconsciousness, coma and convulsions. These symptoms may present in isolation or in combination and may ultimately lead to death, particularly in malaria naïve individuals and children (Miller *et al.*, 2002). Malaria-infected pregnant women are at high risk of complications, not only to themselves but to the foetus. Mothers are at risk of anaemia; while the foetus risks abortion, stillbirth, premature delivery and a reduction in birth weight (Desai *et al.*, 2007).

Cytoadherence of parasitized RBC to vascular endothelium is responsible for impaired microcirculation, local hypoxia, vascular occlusions, inflammation and additionally, in the case of cerebral malaria, damage to the blood brain barrier (Hafalla *et al.*, 2011, White *et al.*, 2013). This cytoadherence, facilitated by parasite-induced RBC membrane alterations and knob-like protrusions, provides the trophozoite and schizont stage parasitized RBC the ability to avoid splenic clearance and thus effective elimination from the human host (Hafalla *et al*., 2011, Tilley *et al.*, 2011).

1.3.1.3 Gametocytogenesis

A small fraction of merozoites develop into sexually dimorphic gametocytes necessary for parasite transfer to the insect host, thus completing the life cycle. In *P. falciparum*, gametocytes reach maturity only eight to twelve days after the first asexual erythrocyte infection (Liu *et al.*, 2011). During the early stages of gametocytogenesis the infected RBC are sequestered to various tissues by cytoadherence but in the final stage of development

they are released into the peripheral circulation, allowing for uptake by the insect host during feeding (Hafalla *et al*., 2011, Liu *et al*., 2011).

1.3.1.4 Programmed cell death in P. falciparum in the human host

The parasite intraerythrocytic cycle is associated with a rapid amplification every 48 hours, which can quickly result in human host death, before the maturation and the transmission of gametocytes (Miller *et al.*, 2002, Hafalla *et al.*, 2011). This implies that the parasite maybe able to regulate its parasitaemia and one such mechanism has been hypothesized as parasite self-induced programmed cell death (PCD) (Deponte and Becker, 2004).

1.3.2 The mosquito host

1.3.2.1 Gamete formation

The female *Anopheles* mosquito, while feeding on infected human blood, consumes both the asexual and the sexual forms of the parasite. The asexual stages will simply perish but the gametocytes will survive. Rapid gamete development ensues due to a drop in temperature, an increase in pH and calcium concentration, and/or exposure to a relatively hydrophilic mosquito-derived molecule, xanthurenic acid (Guttery *et al*., 2012). The macrogametocytes (female gametocytes) become activated and leave their RBC but undergo no further nuclear changes. The microgametocytes (male gametocytes) on the other hand undergo three rapid rounds of DNA replication to release eight flagellated male gametes into the mosquito midgut (Guttery *et al.*, 2012).

1.3.2.2 Ookinete, oocyst and sporozoite formation and development

The mature haploid female and male gametes fuse to produce zygotes which undergo meiosis and ultimately give rise to ookinetes (Hurd *et al.*, 2006, Marois, 2011, Guttery *et al.*, 2012). This life stage, 26 – 36 hours post-infection, moves out of the blood bolus, traverses through the chitinous peritrophic matrix of the midgut, and localizes to the area

between the midgut epithelial cells and the midgut basal lamina (Guttery *et al.*, 2012). This invasion stimulates a wide range of immune responses by the mosquito, such as reactive oxygen and nitrogen species production and soluble immune proteins, which in part results in only a small fraction of the ookinetes emerging at the collagenous basal lamina of the midgut (Hurd *et al.*, 2006, Marois, 2011). Oocyst development ensues on the basal lamina surface, involving rapid cytoplasmic expansion and nuclear divisions to ultimately give rise to thousands of daughter cells called sporozoites (Guttery *et al.*, 2012). The oocyst ruptures in a protease dependant manner allowing sporozoites to escape into the haemocoel, of which about 25% successfully migrate to and invade the mosquito's salivary glands. Here they become competent for human host infection (Baton and Ranford-Cartwright, 2005).

1.3.2.3 PCD in P. falciparum in the mosquito host

Infection of the mosquito vector with *Plasmodium* is not an asymptomatic event, with the associated tissue damage and immune activation occurring in response to parasite invasion resulting in a loss of reproductive fitness and mosquito longevity (Hurd *et al.*, 2006). In order to keep the vector alive long enough for sporozoite development and transmission there needs to be a balance between parasite development and loss. Reduction in zygote, ookinete and sporozoite (Marois, 2011, Guttery *et al.*, 2012) levels have been well characterized during parasite development in the mosquito host, although the precise means of regulation is not. Partial limitation is maintained through the hostile environment created by the processing of the food bolus as well as the initiation of various mosquito immune responses, which are hypothesized to contribute towards the execution of a self controlled PCD-like phenotype within the parasite (Deponte and Becker, 2004, Hurd and Carter, 2004, Hurd *et al.*, 2006, Guttery *et al.*, 2012).

In both the human and insect hosts there is speculation regarding the means by which *P. falciparum* parasitemia is regulated to prevent host death before successful transmission. The association of this regulation with a PCD phenotype is a relatively recent concept in literature but has gathered support with time (Deponte and Becker, 2004). In order to understand this phenomenon within the parasite one needs first to address the concept of PCD itself.

1.4 Programmed cell death in multicellular organisms

The term PCD was first used in 1964 by Lockshin and Williams to describe controlled and autonomous death of cells within a silk moth, during metamorphosis, to bring about the breakdown of the abdominal intersegmental muscles. The phenomenon is currently best understood in the context of multicellular organisms as an active and genetically regulated process facilitating growth, development and homeostasis of an organism (Lockshin and Williams, 1964, Fuchs and Steller, 2011). Various forms of cell death, exhibiting numerous phenotypes, have been described and can be divided into three types – apoptosis, autophagy and necrosis – compared in table 1.1. It must be taken into account that many death regulatory genes are common to more than one death form and a single cell can present with a mixed phenotype, suggesting that the above mentioned cell death types form an interconnected network (Bialik *et al.*, 2010).

Table 1.1: A brief comparison of apoptosis, autophagy and necrosis (Kroemer *et al.*, 2009, Bialik *et al.*, 2010, Christofferson and Yuan, 2010, Fuchs and Steller, 2011, Fulda, 2012, Yonekawa and Thorburn, 2013, Mondal and Dutta, 2014).

Cell death term	**Apoptosis**		**Autophagy**	**Necrosis**	
Subtype	Intrinsic	Extrinsic	Macroautophagy	Accidental	Necroptosis
Initiator	Intracellular signals such as mitochondrial damage	Extracellular signals such as tumour necrosis factor α	Extra- and intracellular signals such as chemotoxic agents	Overt stress or injury	Extra- and intracellular signals such as tumour necrosis factor α
Basic biochemical process leading to death	Loss of mitochondrial membrane potential → Caspase activation	Death ligand-receptor complex formed → Caspase activation	**Poorly understood** Digestion of intracellular components or destabilization of lysosomes	No specific molecular pathways	**Poorly understood** Death ligand-receptor complex formed involving receptor interacting protein 1 and 3 → ?

The term apoptosis, originally coined in 1972 by Kerr *et al.*, describes an active form of PCD whereby cells, commonly single cells, eradicate themselves from a population by inherited biological mechanisms (Kerr *et al.*, 1972). The Nomenclature Committee on Cell Death guidelines stipulate that the term apoptosis should be used to describe the death phenotype expressing specific morphological features, while biochemical features should be used to support but not define the phenotype – morphological and biochemical features are described in table 1.2 (Kroemer *et al.*, 2009). This death form is regulated through intrinsic genetic programs, as well as extracellular and intracellular signals contributing to the activation of different biochemical pathways and the ultimate morphological phenotype (Bialik *et al.*, 2010, Fuchs and Steller, 2011).

Autophagy, more specifically macroautophagy, is an intracellular catabolic process commonly employed as a cell survival or recycling strategy in response to a variety of stimuli including starvation and growth factor withdrawal (Bialik *et al.*, 2010, Fuchs and

Steller, 2011, Yonekawa and Thorburn, 2013). Cytoplasmic long lived proteins or organelles as well as protein aggregates and damaged organelles are engulfed by autophagosomes, which fuse to lysosomes, and are degraded to resupply the cell with cellular building blocks. This cellular phenotype is claimed to additionally be associated with cell death under specific stimuli, although often the documentation is controversial as it may not reflect a natural death stimulus (Bialik *et al.*, 2010, Fuchs and Steller, 2011, Yonekawa and Thorburn, 2013). The exact cellular mechanism associated with this PCD-linked phenotype is uncertain but has been postulated to involve lysosomal destabilization in the autophagy process, resulting in death, or the excessive digestion of cellular components (Fulda, 2012). The morphological features of autophagic death are described in table 1.2.

Necrosis was originally thought to solely be an accidental or non-programmed form of death, occurring in response to overwhelming stress or injury and involving no specific molecular participants or pathways; although recent work suggests genetic control may be involved in some situations. The latter cases are termed necroptosis and appear, in part, to be activated by reactive oxygen species, mitochondrial defects, autophagy and some apoptotic induction factors, including tumour necrosis factor α (TNFα) (Kroemer *et al.*, 2009, Bialik *et al.*, 2010, Christofferson and Yuan, 2010, Fuchs and Steller, 2011). Although the molecular means by which death is executed is unknown, it is known that caspases are not involved and both subtypes present the same morphological features, as presented in table 1.2 (Christofferson and Yuan, 2010).

Table 1.2: Morphological and biochemical markers ascribed to the various PCD phenotypes. ☑ indicates presence and ☒ absence of a particular marker (Kroemer *et al.*, 2009, Bialik *et al.*, 2010, Christofferson and Yuan, 2010, Fuchs and Steller, 2011, Fulda, 2012, Yonekawa and Thorburn, 2013, Mondal and Dutta, 2014).

	Marker	PCD Phenotype		
		Apoptosis	**Autophagy**	**Necrosis**
Biochemical	Caspase-like activity	☑	☒	☒
	Cell disintegration	☑	☑	☑
	Early stage oligonucleosomal DNA fragmentation	☑	☒	☒
	Loss of mitochondrial membrane potential but mitochondria remains intact	☑	☒	☒
	Organelle dysfunction	☒	☒	☑
	Phosphatidylserine externalization	☑	☒	☒
Morphological	Apoptotic bodies	☑	☒	☒
	Chromatin condensation	☑	☒	☒
	Cytoplasmic condensation	☑	☒	☒
	Cytoplasmic swelling	☒	☒	☑
	Massive cytoplasmic autophagic vacuolization	☒	☑	☒
	Membrane blebbing	☑	☒	☒
	Organelle swelling	☒	☒	☑
	Phagocytosis of apoptotic bodies	☑	☒	☒

1.4.1 The need for apoptosis

Much of our understanding of apoptosis, in metazoan organisms, has been gained through a variety of studies using the nematode *Caenorhabditis elegans*, the fruit fly *Drosophila melanogaster*, and the mouse *Mus musculus*. These three models have highlighted the apparent reasons for the existence, the induction signals, as well as the cellular machinery involved in this phenotype.

Apoptosis, broadly speaking, is indispensable to a multicellular organism as it allows for correct growth, development and homeostasis. Firstly, it allows for utilitarian cell suicide, whereby healthy cells will perish for the good of the others, allowing for sufficient

resource availability, organogenesis and tissue remodelling (Fuchs and Steller, 2011, Mondal and Dutta, 2014). Secondly, it permits a means by which worn-out or aged cells or those no longer of functional importance, although still undamaged, can be removed from the body (Fuchs and Steller, 2011, Mondal and Dutta, 2014). Lastly, it facilitates a means of altruistic cell suicide, whereby abnormal or dangerous cells (such as those infected with a pathogen) can be removed from the body before inducing harm (Fuchs and Steller, 2011, Mondal and Dutta, 2014).

1.4.2 The pathways involved in apoptosis

Initiation of an apoptotic phenotype in metazoans has been shown to occur by both external (such as environmental stress or nutrient availability) and internal stimuli (such as DNA damage or infection with a pathogen) resulting in the activation of extrinsic and intrinsic pathways respectively. These two pathways can function independently or in an interrelated fashion, as depicted in figure 1.2, both ultimately resulting in the activation of the main executors of apoptosis - caspases (Fuchs and Steller, 2011, Mondal and Dutta, 2014). This family of cysteine-dependent aspartate-specific proteases participate in numerous cellular processes including cell death. The initiator caspase subgroup is responsible for the proteolytic activation of effector caspases while the effector caspase subgroup is responsible for the ordered destruction of the cell. In order to protect the cell from unregulated degradation, caspases are synthesized and stored in an inactive form – procaspases (Bialik *et al.*, 2010, Fuchs and Steller, 2011).

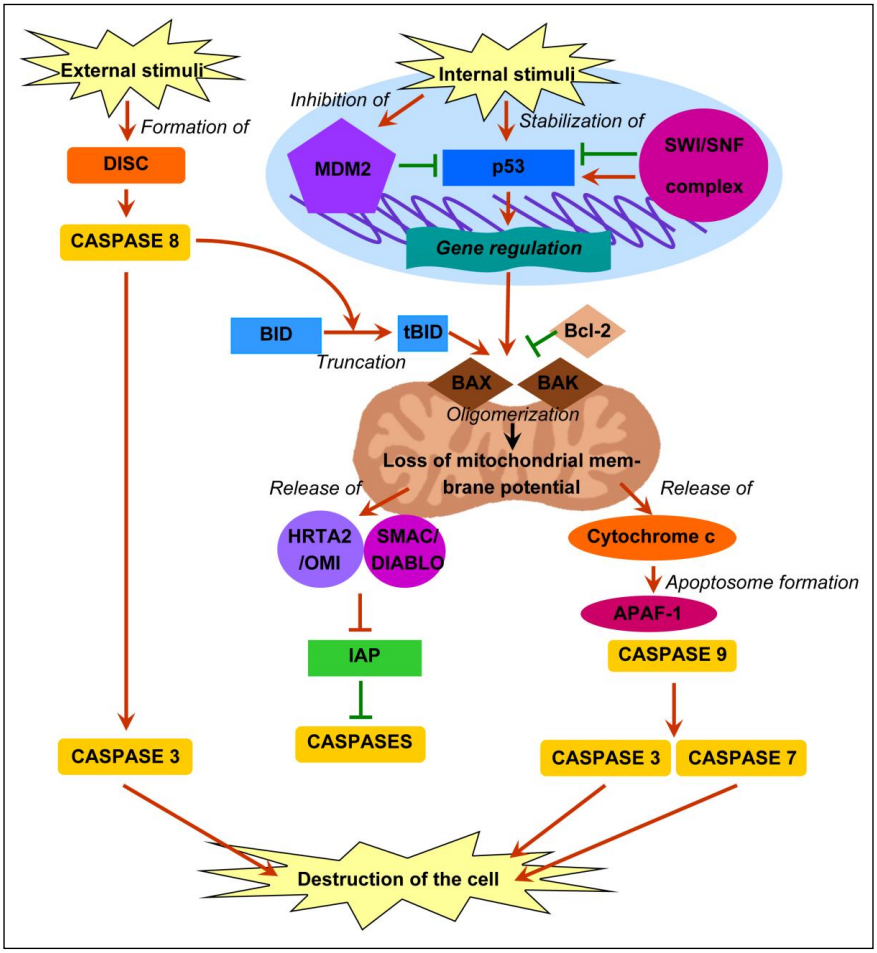

Figure 1.2: A simplified diagram depicting the extrinsic and intrinsic pathways which induce an apoptosis phenotype within metazoan cells.

Based on Lee *et al.*, 2002; Oh *et al.*, 2008; Park *et al.*, 2009; Amaral *et al.*, 2010; Bialik *et al.*, 2010; Wade *et al.*, 2010; Fuchs and Steller, 2011; Mondal and Dutta, 2014.

External stimulation induces the formation of a death-inducing signalling complex (DISC complex), where recruited pro-caspase 8 is activated by cleavage. Active caspase 8 directly activates caspase 3, or brings about caspase dependent cell destruction through a loss in mitochondrial membrane potential. This latter, in-direct process requires the truncation and activation of BID (BH3 interacting-domain death agonist), which affects the mitochondrial membrane potential. Internal stimuli frequently bring about apoptosis through changes in gene expression and an ultimate loss in mitochondrial membrane potential. The loss of this membrane potential is facilitated through mitochondrial pore opening, due to the B-cell lymphoma 2 (Bcl-2)-associated X protein (BAX) and Bcl-2 homologous antagonist killer (BAK) oligomerization. This releases mitochondrial resident inhibitor of apoptosis (IAP) inhibitors and cytochrome c into the cytoplasm. The latter factor is responsible for cytoplasmic apoptosome formation, bringing about caspase 3 and 7 activation.

Green lines represent inhibition under normal conditions; red arrows and lines represent activation or inhibition respectively under apoptotic conditions; and black arrows represent processes or activities leading to another. The presence of both red arrows and green lines implies the possibility of two different situations, each depending on the stimuli received by the cell. Abbreviations: MDM2 – murine double minute 2, p53 – protein 53, SWI/SNF – SWItch/Sucrose NonFermentable, HTRA2/OMI – high temperature requirement protein A2/Omi stress-regulated endoprotease, SMAC/DIABLO – second mitochondria-derived activator of caspase/direct IAP protein with a low pI.

Intrinsic pathways often involve the mitochondria, whereby various stimuli ultimately facilitate the loss in mitochondrial transmembrane potential through the opening of the mitochondrial permeability transition pores, which is controlled by the B cell lymphoma 2 (Bcl-2) protein family (Fuchs and Steller, 2011, Mondal and Dutta, 2014). Bcl-2-associated X protein (BAX) and Bcl-2 homologous antagonist killer (BAK), in response to apoptotic stimuli, overcome the inhibitory effects of the anti-apoptotic members of the Bcl-2 family and oligomerize to create pores within the outer mitochondrial membrane (figure 1.2). These facilitate a loss in mitochondrial transmembrane potential resulting in the release of death inducing factors, resident in the mitochondrial inter-membrane space, including cytochrome c, second mitochondria-derived activator of caspase/ direct IAP binding protein with a low pI (SMAC/DIABLO), high-temperature requirement factor A2/OMI stress-regulated endoprotease (HTRA2/OMI), apoptosis inducting factor (AIF) and endonuclease G (Bialik *et al.*, 2010, Fuchs and Steller, 2011). Cytochrome c binds to and activates apoptosis protease activating factor -1 (APAF-1) and the initiator caspase CASPASE-9, originally in its inactive form in the cytoplasm, to form the apoptosome. This complex activates the effector caspases CASPASE-3 and -7 which proceed to act upon a multitude of substrates to demolish the integrity of the cell skeleton, the nuclear lamin structure and DNA, as well as inhibiting the cell's natural repair mechanisms (Bialik *et al.*, 2010, Fuchs and Steller, 2011, Mondal and Dutta, 2014). DNA fragmentation is a prominent feature of apoptosis, brought about by the activities of AIF, endonuclease G and Caspase activated DNase (CAD). The latter requires caspase degradation of its inhibitor, iCAD, while the other two function in a caspase independent manner (Mondal and Dutta, 2014).

Caspase-dependent delamination of the intact plasma membrane from the cortical cytoskeleton as well as actomyosin-mediated contraction in conjunction with increased hydrostatic pressure results in the repeated formation and retraction of membrane blebs for sustained periods of time on the surface of the dying cell (Wickman *et al.*, 2012). These blebs may become packed with cellular organelles and condensed chromatin to form the basis of the apoptotic bodies which are ultimately released and dissociate from the dying mass (Wickman *et al.*, 2012). Phosphatidylserine (PS) under normal conditions is present on the inner leaflet of the cells plasma membrane. Caspase activation, in response to an apoptosis signal, brings about the accumulation of PS on the intact plasma membrane outer leaflet (Wickman *et al.*, 2012, Bendall and Green, 2014). This facilitates an ‘‘eat me’’ signal resulting in the removal of the dying cell by phagocytosis (Wickman *et al.*, 2012, Bendall and Green, 2014).

The extrinsic death pathway is initiated by the oligomerization of a death receptor, such as TNFα receptor type 1, in response to the binding of its death ligand, such as TNFα, and its subsequent recruitment of cytoplasmic adaptor proteins through its death domain, in order to form the death-inducing signalling complex (DISC) (Mondal and Dutta, 2014) (figure 1.2). The initiator caspase, CASPASE-8, is recruited to the DISC in its inactive procaspase form and subsequently activated (Mondal and Dutta, 2014). The activated CASPASE-8 can then participate in two pathways. Firstly, the cysteine protease can cleave and activate the effector caspase CASPASE-3, responsible for the breakdown of the cell and the activation of the effector caspase CASPASE-7 (Mondal and Dutta, 2014). Secondly, CASPASE-8 can cleave the BH3 interacting-domain death agonist (BID) protein into truncated BID (tBID) which induces oligomerization of BAX and BAK to induce a loss in

the mitochondrial outer membrane potential – linking the extrinsic pathways to the intrinsic pathway (Bialik *et al.*, 2010, Mondal and Dutta, 2014).

Regulation of caspases is vital for non-apoptotic cells and their inhibition is facilitated, in part, through the inhibitor of apoptosis proteins (IAP) , which are characterized by the presence of a variable number of N-terminal Baculoviral IAP repeat motifs that bind directly to and inhibit caspases. The released SMAC/DIABLO and HTRA2/OMI proteins, encoding IAP-binding motifs, are responsible for inhibiting the activity of IAP to allow for complete caspase activation (Bialik *et al.*, 2010, Fuchs and Steller, 2011).

1.4.3 Transcriptional control of apoptosis

Within a normal, healthy eukaryotic cell the default transcriptional state is considered repressed due to the natural packed state of its chromatin. According to the needs of the cell, often in response to specific stimuli, the chromatin structure is altered for the process of gene transcription. This change employs a variety of cellular factors and proteins (Li and Reinberg, 2011). Once transcription has been completed the DNA must then be returned to its repressed state (Li and Reinberg, 2011). During apoptosis the chromatin must be accessible to specific transcription factors necessary for the execution of specific death pathways. These factors include p53 and the SWI/SNF complex.

1.4.3.1 p53

The p53 protein, a 53kDa phosphoprotein with several functional domains as indicated in table 1.3, was originally discovered in a mutant form (DeLeo *et al.*, 1979). It has since been identified in its original form within mammalian cells, maintained in an inactive state at low concentrations in the cytoplasm under normal, healthy conditions, while under specific stress conditions its half life is dramatically increased, it is activated and it can be

relocalized to the nucleus to associate with the chromatin (Rotter *et al.*, 1983, Amaral *et al.*, 2010). Its activation and inactivation is dependent on a vast array of post-translational modifications, including phosphorylation and acetylation, directed against specific amino acid residues along its length (Amaral *et al.*, 2010).

Table 1.3: Important functional domains of human p53.

Name of region	Position (residues)	Function	Reference
Trans-activation domain	1-42	Interaction with various transcription factors	(Unger *et al.*, 1992)
Proline-rich region	61-94	Required for apoptosis induction	(Sakamuro *et al.*, 1997)
DNA-binding domain (DBD)	102-292	Required for the recognition of a specific DNA consensus sequence, in the presence of Zn^{2+}. This sequence is constituted by two copies of the 10-bp motif 5'-PuPuPuCWWGPyPyPy-3', separated by any 0-13 bps	(Kern *et al.*, 1991, El-Deiry *et al.*, 1992, Pavletich *et al.*, 1993)
Tetramerization domain	324-355	Facilitates tetramerization, which is enhanced in the presence of DNA	(Stenger *et al.*, 1992, Pavletich *et al.*, 1993, Wang *et al.*, 1995)
C-terminal regulatory domain	363-393	Aids in promoter binding and transactivation, apparently binding to DNA in a non-specific manner	(Pavletich *et al.*, 1993, McKinney *et al.*, 2004)
N-terminal nuclear export sequence (NES)	11-27	Allows for the export of p53 from the nucleus in an MDM2 independent manner, with phosphorylation of Ser residues in this region inhibiting nuclear export	(Zhang and Xiong, 2001)
C-terminal NES	340-351	Allows for the export of p53 from the nucleus in an MDM2 independent manner, with tetramerization of the protein masking this signal sequence in turn facilitating nuclear retention	(Stommel *et al.*, 1999)
C-terminal nuclear localization sequences (NLS)	NLSI: 316 - 325, NLSII: 369 – 375, NLSIII: 379 - 384	Allows for the import of the p53 protein into the nucleus	(Shaulsky *et al.*, 1990)

This transcription factor is thought to have evolved from an ancient stress response factor in metazoans that specialized, over evolutionary time, to play a key role in the regulation of apoptosis, autophagy, glycolysis, cell repair, cell survival and cell differentiation (Amaral *et al.*, 2010). The protein, as a tetramer, binds to DNA sequences in response to a variety of stimuli such as DNA damage. Although there exists a standard p53 DNA-binding consensus sequence, as presented in table 1.3, non-canonical binding sites have also been documented; both sequence types have been identified within the coding and non-coding regions of their target genes but are commonly situated in the promoter regions (Beckerman and Prives, 2010). Once bound, p53 recruits a variety of transcription factors including, amongst others, transcription machinery components and chromatin remodelling factors to regulate the expression of its target genes – RNA polymerase II transcribed genes being the most well studied (Beckerman and Prives, 2010).

The p53 protein is involved in the transcriptional activation of Bcl-2-family member genes, including pro-apoptotic BAX and p53 upregulated modulator of apoptosis (PUMA), and of factors that halt the cell-cycle, such as p21. Transcriptional repression by p53, although poorly understood, occurs for several anti-apoptotic factors including Bcl-2, Bcl-X, cyclin B1, survivin, and IAP (Amaral *et al.*, 2010, Beckerman and Prives, 2010). Although the primary involvement of p53 in apoptosis is dependent on its transcriptional role, the protein also plays transcription-independent apoptosis-related roles, as seen in cells undergoing apoptosis in the absence of nuclei (Speidel, 2010). The cytoplasmic pool of p53, conjugated to a single ubiquitin residue, is held in an inactive state through Bcl-XL binding. This association is disrupted by PUMA, in response to stress, and leads to p53 mitochondrial translocation, Bcl-2 anti-apoptotic factor inhibition, BAX oligomerization and BAK activation. The importance of the latter's activation in apoptosis *in vivo* is

currently controversial (Speidel, 2010). The proline rich domain and DNA binding domain DBD of p53 are involved in these binding events (Speidel, 2010).

1.4.3.2 SWIB/MDM2: the SWI/SNF complex and MDM2

Although the function of many SWIB/MDM2 domains is unknown, all have been shown to have a high degree of structural similarity and the conservation of several residues (Bennett-Lovsey *et al*., 2002). In light of this, it has been postulated that the domains of the MDM2 protein and the SWI/SNF complex may share a common evolutionary history and in turn a similar functional mechanism – specifically protein-protein interactions (Bennett-Lovsey *et al*., 2002).

The SWI/SNF complex

The SWI/SNF complex, a 2MDa multi-subunit nuclear assembly, was discovered in yeast and is an example of an ATP-dependent chromatin remodelling complex and transcriptional activator which binds to DNA and hydrolyses ATP in order to alter chromatin structure through nucleosome sliding and histone octamer insertion and/or ejection (Wilson and Roberts, 2011). It has been shown to directly activate a limited number of specific genes, including heat shock genes such as heat shock protein 70 (HSP70) (Sullivan *et al.*, 2001, Corey *et al.*, 2003, Wilson and Roberts, 2011). The ten polypeptide subunits of this complex are all interdependent in their function, with the SWI2/SNF2 protein being responsible for the observed DNA-dependent ATPase activity (Laurent *et al.*, 1991, Cairns *et al.*, 1994, Cote *et al.*, 1994, Wilson and Roberts, 2011). Within yeast, as well as other eukaryotic organisms, SWI/SNF and SWI/SNF-related complexes have been identified experimentally and by bioinformatics. The complexes are composed of constant units, believed to be core functional units, as well as other apparently variable units, proposed to aid in facilitating a degree of specificity and/or

functionality (Elfring *et al.*, 1994, Dingwall *et al.*, 1995, Wang *et al.*, 1996, Papoulas *et al.*, 1998, Wilson and Roberts, 2011). Although the SWI/SNF complex is often described as a transcriptional activator it has been shown in the yeast genome to transcriptionally repress a larger number of genes (Holstege *et al.*, 1998). This dual activation and repression ability has also been documented in the human genome for this ATP-dependent nucleosomal remodeller (Schnitzler *et al.*, 1998). In light of this the SWI/SNF complex should be seen as a transcriptional regulator facilitating a dynamic equilibrium between an activated and repressed state according to the cells needs (Schnitzler *et al.*, 1998, Wilson and Roberts, 2011).

The complex has documented involvement in various stress response pathways. It is required for the activation and repression of specific genes, such as *hsp*70 genes, in response to a plethora of stimuli including exposure to elevated temperatures, heavy metals and metabolic inhibitors (de la Serna *et al.*, 2000, Shivaswamy and Iyer, 2008). One core member of the yeast SWI/SNF complex is the SWI/SNF associated protein 73 (SWP73p)/SNF12, which encodes a SWIB/MDM2 domain, and whose absence can inhibit transcriptional activation in a promoter- and activator-dependent manner (Cairns *et al.*, 1996). Deletion of Swp73p/SNF12 has been documented to produce temperature sensitive mutants, highlighting a strong involvement of this protein in the transcriptional regulation of heat stress response genes (Cairns *et al.*, 1996). Homologues of this protein have been identified within the SWI/SNF related complexes of *Drosophila* and humans, *Brahma-associated protein 60* (BAP60) and Brahma-related gene-1 (BRG1) - associated factor 60 (BAF60) respectively (Treich *et al.*, 1998, Phelan *et al.*, 1999, Wu *et al.*, 2009, Wilson and Roberts, 2011).

Additionally, the human SWI/SNF complex has been shown to associate with and regulate the activities of p53. Direct p53 binding, facilitated at least in part, by the N-terminus of BAF60a, and not the originally predicted SWIB/MDM2 domain of the protein (Lee *et al.*, 2002, Oh *et al.*, 2008). This interaction appears to elicit cell cycle halting, DNA repair and apoptosis induction and/or repression responses (Lee *et al.*, 2002, Oh *et al.*, 2008, Park *et al.*, 2009).

MDM2

The mammalian MDM2 protein, originally identified in transformed mice fibroblasts, has several functional domains, as expressed in table 1.4, including a SWIB/MDM2 domain (Momand *et al.*, 1992, Kussie *et al.*, 1996). This protein shuttles between the nucleus and cytoplasm, moving into the nucleus under normal conditions in order to bind, commonly as an oligomer with itself or MDMX, directly to p53. This inhibits the transcriptional activity, enhances the nuclear export and accelerates the proteasomal degradation of p53 (figure 1.3) (Chen *et al.*, 1995, Roth *et al.*, 1998, Wade *et al.*, 2010). The MDM2 protein has intrinsic E3 ubiquitin-ligase activity which mediates ubiquitination and proteasome-dependent degradation of p53, this process is dependent on the RING and acidic domains of the protein. MDM2 oligomerization has been suggested to aid in the recruitment of E2 factors for poly-ubiquitination (Honda *et al.*, 1997, Kawai *et al.*, 2003, Chan *et al.*, 2006, Cheng *et al.*, 2009, Wade *et al.*, 2010). MDMX, also known as MDM4, is structurally related to MDM2, encoding a p53 binding domain and RING domain. It is believed that the two proteins arose due to duplication from a single ancestral gene (Wade *et al.*, 2010).

Table 1.4: Important functional domains of human MDM2.

Name of region	Position (residues)	Function	Reference
N-terminal p53 binding domain	18–101	SWIB/MDM2 domain, which binds to and inhibits p53	(Chen *et al.*, 1995, Kussie *et al.*, 1996)
Acidic domain	237–288	Interacts with a variety of regulatory factors. Required for effective p53 ubiquitination and degradation	(Argentini *et al.*, 2001, Kawai *et al.*, 2003, Wade *et al.*, 2010)
C-terminal RING finger domain	289-331	Provides E3 ubiquitin ligase activity and binds to specific RNA. Binds to MDMX to form a heterodimer, which stabilises MDM2.	(Honda *et al.*, 1997, Tanimura *et al.*, 1999)
Nuclear export sequence	197-205	Allows for export of MDM2, alone or bound to p53, from the nucleus.	(Roth *et al.*, 1998)
Nuclear localization sequence	181-185	Allows for import of MDM2 into the nucleus	(Chen *et al.*, 1995)
C-terminal nucleolar localization sequence	466-473	Allows for the import of the MDM2 protein into the nucleolus	(Lohrum *et al.*, 2000)

Under genotoxic conditions numerous processes occur to stabilize p53, one being the inhibition of its MDM2 association and subsequent degradation (figure 1.3) (Beckerman and Prives, 2010, Wade *et al.*, 2010). Ataxia telangiectasia mutated (ATM), a 370kDa protein, is a Mn^{2+} dependent kinase belonging to the phosphatidylinositide 3-kinase protein family that is held in an inactive dimeric or oligomeric state under normal conditions but in response to appropriate stimuli, such as DNA damage, it undergoes activation by autophosphorylation of Ser^{1981} leading to dimer dissociation (Canman *et al.*, 1998, Bakkenist and Kastan, 2003). ATM facilitates phosphorylation of various proteins involved in cell cycle regulation and apoptosis in response to ionizing radiation, such as p53 on Ser^{15} and MDM2 on Ser^{386} and Ser^{429} (Canman *et al.*, 1998, Bakkenist and Kastan, 2003, Cheng *et al.*, 2009, Waning *et al.*, 2010). Phosphorylation of p53 on Ser^{15} stabilizes it by reducing its contact with MDM2, while phosphorylation of MDM2 results in its inability to poly-ubiquitinate p53 and oligomerize (Cheng *et al.*, 2009, Waning *et al.*, 2010). An additional level of regulation also occurs in response to DNA damage where

MDM2 is phosphorylated on Tyr^{276}, by c-ABL, which activates its association with the alternative reading frame tumour suppressor (p14^{ARF}) and in turn p14^{ARF}-dependent nucleolar re-localization, further inhibiting a MDM2-p53 association (Lohrum *et al.*, 2000, Dias *et al.*, 2006).

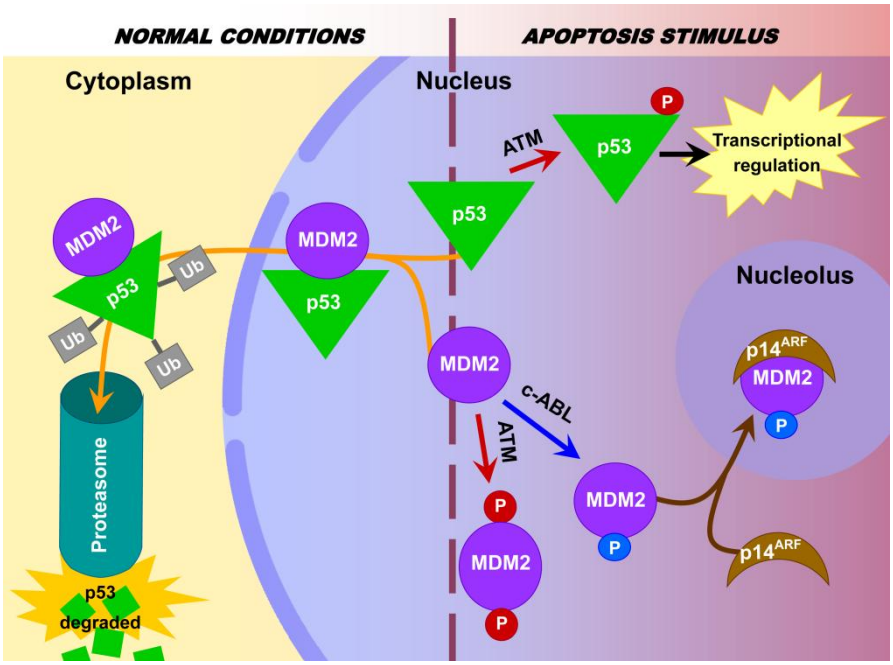

Figure 1.3: Diagrammatic representation of the interaction between MDM2 and p53 under normal conditions and during apoptosis.
Based on Chen *et al.*, 1995; Canman *et al.*, 1998; Roth *et al.*, 1998; Lohrun *et al.*, 2000; Bakkenist and Kastan, 2003; Chan *et al.*, 2006; Dias *et al.*, 2006; Cheng *et al.*, 2009; Beckerman and Prives, 2010; Wade *et al.*, 2010; Waning *et al.*, 2010.
Under normal conditions MDM2 binds and facilitates the nuclear export, ubiquitination and proteasome-dependent degradation of p53 (orange arrow). In response to an apoptosis stimulus, MDM2 is phosphorylated by ataxia telangiectasia mutated (ATM) (red arrow), on Ser^{386} and Ser^{429}, and c-ABL (blue arrows), on Tyr^{276}, resulting in its inactivation and nucleolus import respectively. Nucleolar import requires alternative reading frame tumour suppressor (p14^{ARF}) binding (brown arrow). ATM phosphorylates p53 (red arrow), on Ser^{15}, allowing for its stabilization and subsequent regulation of transcription.

Movement of MDM2 between the nucleus and cytoplasm has been suggested to regulate translation as well, where mRNA sequence export from the nucleus could be regulated through interactions with the MDM2 RING finger domain. This is believed to regulate

translation of cellular growth proteins and in turn the cell's growth and cycling (Roth *et al.*, 1998).

1.5 Programmed cell death in unicellular organisms

The concept of PCD amongst unicellular organism has been a controversial subject although both apoptotic- and autophagic-like features have been ascribed to numerous unicellular eukaryotes as well as prokaryotes (Ramsdale, 2012, Proto *et al.*, 2013, Bayles, 2014). Cornillon and colleagues have suggested that the PCD phenomenon may have arisen before the emergence of multicellularity (Cornillon *et al.*, 1994). This concept has received support by means of bioinformatic analysis and the identification of PCD markers in unicellular life forms, although it brings into question the original reason for the emergence of PCD (Cornillon *et al.*, 1994, Zangger *et al.*, 2002, Nedelcu, 2009).

A good example of the early origin of PCD tools is p53. The identification a p53-like protein family member within unicellular eukaryotes, such as *Entamoeba histolytica* and *Monosiga brevicollis*, indicates that this protein family may be present in all extant eukaryotic organisms, in some form, if not lost during the evolution of a particular lineage, phylum or species (Mendoza *et al.*, 2003, King *et al.*, 2008, Lu *et al.*, 2009, Belyi *et al.*, 2010). Duplication of the ancestral stress response factor is believed to have resulted in the three distinct family members – p53, p63 and p73 documented in higher vertebrates (Amaral *et al.*, 2010, Belyi *et al.*, 2010). The most well conserved domain amongst all the family members is the DBD, while significant diversification has been documented among the trans-activation and tetramerization domains, as well as the emergence of an additional domain, the sterile alpha-motif domain, within the p63 and p73 proteins (Lu *et al.*, 2009). Furthermore, amongst vertebrates and invertebrates the functional role of the DBD is

broadly conserved, highlighting a conserved role in death regulation (Lu *et al.*, 2009). Thus, current evidence suggests that the original role of the p53-ancestor was that of stress response and/or apoptotic death regulation. Meanwhile, its involvement in cell cycle regulation only appeared later in evolutionary history with the emergence of the vertebrate lineage. This highlights the fact that not all PCD machinery components are necessarily functionally conserved within all eukaryotes (Derry *et al.*, 2001, Lu *et al.*, 2009, Amaral *et al.*, 2010).

It has been suggested that the PCD machinery of multicellular organisms was originally recruited from proteins involved in other cellular functions, such as differentiation, which proceeded to specialize according to the organism's requirements. This theory has gained support due to the identification of many PCD homologues, in an array of species, involved in non-PCD activities (Dick and Megeney, 2013). Additionally, the apparent linkage between genes for cell cycle regulation and cell death in various unicellular and multicellular organisms supports the idea that the two systems are interlinked and, in part, worked together to facilitate appropriate cellular damage responses (Ameisen, 1996, Welburn *et al.*, 1997, Dick and Megeney, 2013). The precise driving forces behind the evolution and maintenance of PCD itself, as a cellular strategy, are poorly understood. It has been suggested that altruism, amongst clonal cells, may be a key factor or that PCD provided a mechanism for the development of multi-cellularity (Ramsdale, 2012, Dick and Megeney, 2013).

The study and comparison of PCD between unicellular and multicellular life forms should be conducted with the following in mind:

1) A degree of deviation from the metazoan machinery is anticipated amongst unicellular organisms, as genes would be lost, altered or gained during evolution to facilitate adaptation in biology, lifestyle and ecology (Nedelcu, 2009). For example, bioinformatic analysis has identified two families of caspase-like genes, paracapases and metacaspases, within the genomes of numerous eukaryotes, ranging from animals to protozoa (Uren *et al.*, 2000). Although both gene sets encode a conserved cysteine and histidine dyad required for cysteine protease functionality; they carry a diverse range of domains not typically associated with classical caspases. It was suggested that caspases, paracaspases and metacaspases all originated from a common ancestor, playing a role in stress response pathways, subsequently diverging and specializing during evolution (Uren *et al*., 2000). The metacaspase family has been proven to play a PCD-related execution role in yeast and plants, although this feature has not been proven in other unicellular eukaryotes that lack classical caspases, such as protozoan parasites (Dick and Megeney, 2013, Proto *et al.*, 2013).
2) Organisms may employ unique machinery to facilitate death. Bacteria, for example, utilize a unique toxin–antitoxin system which results in their demise in response to appropriate triggers which is not seen in metazoans (Sat *et al.*, 2001, Bayles, 2014).
3) Differences in cellular organisation and structure between various organisms may influence phenotypic expression. *Dinoflagellates,* for example, show a DNA fragmentation PCD response linked to limited carbon dioxide exposure and oxidative stress, although this pattern is distinct from the classical DNA laddering pattern. This difference is due to these organisms lacking the typical nucleosomal arrangement of their chromosomal material (Vardi *et al.*, 1999).

1.5.1 PCD and *Plasmodium*

Ameisen and colleagues were the first to hypothesise that the protozoan parasites may undergo PCD, after documenting apoptotic features in *Trypanosoma cruzi* (Ameisen *et al.*, 1995). In 1997 apoptosis-like phenotypes were linked to *P. falciparum* and *P. yoelli*, with Picot *et al.* (1997) postulating that the previously, well documented 'crisis form' may simply be a PCD phenotype (Picot *et al.*, 1997, Srivastava *et al.*, 1997). The term 'crisis form' has existed in literature for decades, commonly used to define a retardation in growth and development, loss of synchronicity and the ultimate death of asexual blood stage parasites, in response to a variety of conditions (Jensen *et al.*, 1982, Nkuo and Deas, 1988). Morphologically the phenomenon presents with vacuolization, abnormal stunted size, poorly stained cytoplasm and irregular nuclear divisions (Taliaferro and Taliaferro, 1944) – all of which are typical PCD-associated features. This phenotype has been documented under non-limiting nutrient and RBC conditions within cultured *P. falciparum* parasites, suggesting that it is a natural phenomena of the asexual life cycle (Mutai and Waitumbi, 2010).

Regulation of *P. falciparum* parasitaemia levels in both the human and mosquito host, to prevent premature host death and ensure effective transmission, has been hypothesised as parasite self-induced PCD (Deponte and Becker, 2004, Hurd and Carter, 2004). This idea would be supported evolutionarily as a form of altruism, whereby the death of some of the clonal individuals may facilitate resource availability and host survival to bring about propagation and transmission of its kin (Dick and Megeney, 2013, Proto *et al.*, 2013). There is some question as to whether this selection pressure would be valid in a high transmission area, as infections would commonly be mixed and thus benefit to all strains may not necessarily be ensured (Baton *et al.*, 2008). A non-altruistic mechanism was

suggested by Dick and Megeney (2013) in the *Trypanosoma* and *Leishmania*. They proposed that parasitaemia is regulated by individual cells utilizing paracrine signals to activate a PCD-like pathway in circulating neighbour cells, as a form of competition (Dick and Megeney, 2013). This form of population density regulation could be employed by *P. falciparum* as well, but would require an as of yet undefined means of quorum sensing (Al-Olayan *et al.*, 2002, Deponte and Becker, 2004, Mutai and Waitumbi, 2010).

Features of PCD have been documented in various *Plasmodium* species, at different stages of the parasite life cycle, in response to a plethora of stimuli, as described in tables 1.5 and 1.6 (Deponte and Becker, 2004, Engelbrecht *et al.*, 2012). As documented in table 1.5 the intraerythrocytic life stages of *P. falciparum* have shown facets of apoptotic, autophagic and necrotic death either individually or simultaneously suggesting that this stage of the parasite's life cycle may be associated with a mixed PCD-phenotype (Kwiatkowski, 1989, Porter *et al.*, 2008, Totino *et al.*, 2008, Engelbrecht *et al.*, 2012, Engelbrecht and Coetzer, 2013). Evaluation of *P. falciparum* and *P. berghei* ookinetes, as documented in table 1.6, has also demonstrated several apoptosis markers.

It is important to note that much controversy exists in relation to these markers, which may be due to the lack of uniformity in strain, life stage, species, stimuli type, stimuli duration and/or stimuli level used during analysis, and may explain the absence of one or all of these features during evaluation (Nyakeriga *et al.*, 2006, Le Chat *et al.*, 2007, Ali *et al.*, 2010, Engelbrecht *et al.*, 2012).

Table 1.5: Markers of PCD in various intraerythrocytic *P. falciparum* life stages.

PCD Marker	PCD-like phenotype	Reference
Caspase-like activity	Apoptosis	(Meslin *et al.*, 2007, Ch'ng *et al.*, 2010)
Chromatin condensation	Apoptosis	(Kwiatkowski, 1989, Porter *et al.*, 2008, Arambage *et al.*, 2009)
Cytoplasmic condensation	Apoptosis	(Porter *et al.*, 2008)
DNA fragmentation	Apoptosis	(Picot *et al.*, 1997, Meslin *et al.*, 2007, Oakley *et al.*, 2007, Totino *et al.*, 2008, Ch'ng *et al.*, 2010, Mutai and Waitumbi, 2010, Engelbrecht and Coetzer, 2013)
Erythrocyte membrane blebbing	Apoptosis	(Deponte and Becker, 2004)
Erythrocyte phosphatidylserine externalization	Apoptosis	(Engelbrecht and Coetzer, 2013)
Loss of mitochondrial membrane potential	Apoptosis	(Srivastava *et al.*, 1997, Meslin *et al.*, 2007, Porter *et al.*, 2008, Totino *et al.*, 2008, Ch'ng *et al.*, 2010, Mutai and Waitumbi, 2010, Engelbrecht and Coetzer, 2013)
Cytoplasmic vacuolization	Autophagy	(Porter *et al.*, 2008, Totino *et al.*, 2008, Engelbrecht and Coetzer, 2013)
Organelle lysis	Necrosis	(Porter *et al.*, 2008)
Organelle swelling	Necrosis	(Porter *et al.*, 2008)

Table 1.6: Markers of apoptosis in the *P. berghei* and *P. falciparum* ookinete life stage.

Apoptotic Marker	***Plasmodium* species**	Reference
DNA fragmentation	*P. berghei* and *P. falciparum*	(Al-Olayan *et al.*, 2002, Arambage *et al.*, 2009)
Chromatin condensation	*P. berghei*	(Al-Olayan *et al.*, 2002, Ali *et al.*, 2010)
Ookinete phosphatidylserine externalization	*P. berghei*	(Al-Olayan *et al.*, 2002, Arambage *et al.*, 2009, Ali *et al.*, 2010)
Caspase-like activity	*P. berghei*	(Arambage *et al.*, 2009, Ali *et al.*, 2010)
Loss of mitochondrial membrane potential	*P. berghei*	(Arambage *et al.*, 2009)
Apoptotic bodies	*P. berghei*	(Al-Olayan *et al.*, 2002)

1.5.1.1 Induction of a PCD-like phenotype

Although a degree of inconsistency exists in terms of the detection of a PCD-like phenotype, numerous stimuli have been documented as induction agents, as presented in table 1.7. Of these stimuli only three represent natural agents to which the parasite would normally be exposed to during its life cycle - febrile temperature mimics, reactive oxygen species and reactive nitrogen species. The use of these may provide more information about the naturally occurring phenotype(s) exhibited by the parasite at different life stages. Additionally, within the intraerythrocytic life stages of *P. falciparum*, PCD-markers have been documented in the absence of any discrete stimuli suggesting the possibility of death induction by means of quorum sensing (Al-Olayan *et al.*, 2002, Deponte and Becker, 2004, Mutai and Waitumbi, 2010).

Table 1.7: Factors documented to induce a PCD-like phenotype within various *Plasmodium* species.

Possible Inducers of PCD-like features	*Plasmodium* species	Life stage	Reference
Anti-malarial drugs such as chloroquine, staurosporine & atovaquone	*P. falciparum*	Intraerythrocytic	(Srivastava *et al.*, 1997, Meslin *et al.*, 2007, Totino *et al.*, 2008, Ch'ng *et al.*, 2010)
Apoptosis inducers such as etoposide	*P. falciparum*	Intraerythrocytic	(Meslin *et al.*, 2007)
Febrile temperature/heat shock	*P. falciparum*	Intraerythrocytic	(Oakley *et al.*, 2007, Engelbrecht and Coetzer, 2013)
Reactive nitrogen species such as nitric oxide	*P. falciparum*	Intraerythrocytic	(Totino *et al.*, 2008)
	P. berghei	Ookinete	(Ali *et al.*, 2010)
Reactive oxygen species such as hydrogen peroxide and superoxide anion	*P. falciparum*	Intraerythrocytic	(Deponte and Becker, 2004)
	P. berghei	Ookinete	(Ali *et al.*, 2010)

Several studies have considered the effects of elevated temperatures, 38.5°C and above, which mimic fever in malaria patients, on the growth and development of cultured parasites. Although some discrepancies exist in literature, for reasons discussed above,

elevated temperatures appeared to significantly inhibit the development and growth of all asexual intraerythrocytic parasite stages, as well as exhibiting several features of necrosis and/or PCD, with the effects apparently more severe in late trophozoites and schizonts (Kwiatkowski, 1989, Long *et al.*, 2001, Oakley *et al.*, 2007, Porter *et al.*, 2008, Engelbrecht and Coetzer, 2013). These late life stages have also been found to show a drastic reduction in metabolic activity under these conditions (Porter *et al.*, 2008). These phenomena are hypothesized to reduce the host's parasitic burden and synchronize the parasite population (Kwiatkowski, 1989, Long *et al.*, 2001, Porter *et al.*, 2008, Engelbrecht and Coetzer, 2013).

Reactive oxygen and nitrogen species are readily produced in the mosquito midgut lumen and epithelia by blood bolus digestion and nitric oxide synthetase induction, in response to the presence of blood and parasites (Hurd *et al.*, 2006). Research on these two reactive species has focused solely on *P. berghei* ookinetes, which have demonstrated apoptosis markers in response to exposure (Ali *et al.*, 2010). No work has determined the effects in the corresponding *P. falciparum* life stages but it is likely that a similar response would be noted.

1.5.1.2 PCD participants

Although numerous biochemical and morphological markers of PCD have been identified within the malaria parasite, as discussed earlier, no dedicated proteolytic and nuclease machinery or pathways have been proven experimentally. Thus far only a few homologues of metazoan PCD genes have been identified by bioinformatics within the *Plasmodium* genome (Nedelcu, 2009, Proto *et al.*, 2013).

Metacapsases and calpain

Work by various groups using caspase inhibitors, as highlighted in tables 1.5 and 1.6, supports the involvement of caspase-like proteins in the PCD phenotypes of *P. falciparum* and *P. berghei* (Al-Olayan *et al.*, 2002, Ch'ng *et al.*, 2010). The *P. falciparum* genome encodes three metacaspase and metacapase-like proteins, PF3D7_1354800 (metacaspase 1), PF3D7_1416200 (metacaspase-like protein 2) and PF3D7_1438400 (metacaspase-like protein 3); with *P. berghei* similarly encoding three metacaspase and metacapase-like proteins (Aurrecoechea *et al.*, 2009).

The *P. falciparum* metacaspase 1 candidate has been documented to have ubiquitous protein and mRNA expression in the sexual life stages but a parasite density-dependent variation in asexual stages (Mutai and Waitumbi, 2010). This fluctuation could be a contributing factor towards the absence or presence of caspase-like detection between studies and the efficiency of caspase inhibitors (Al-Olayan *et al.*, 2002, Nyakeriga *et al.*, 2006, Meslin *et al.*, 2007, Ch'ng *et al.*, 2010). This metacaspase homologue has further been shown to be a calcium-dependent, arginine-specific protease. It is able to induce death when expressed in yeast cells under oxidative stress conditions, but its role within *P. falciparum* was not assessed (Meslin *et al.*, 2011).

Knocking out the *P. berghei* metacaspase MCA1 gene failed to show any effect on ookinete PCD (Le Chat *et al.*, 2007). It is possible that other metacaspase-like genes (MCA2 and MCA3) may play a redundant role, masking the involvement of MCA1 (Le Chat *et al.*, 2007).

Although proteases have been implicated in parasite PCD, as explained above, the utilization of broad spectrum protease inhibitors does not target caspase-like homologues alone but rather any cysteine proteases (Al-Olayan *et al.*, 2002, Meslin *et al.*, 2007, Ch'ng *et al.*, 2010). The involvement of clan CA proteases, such as cathepsin and calpain-like

proteases has been suggested in *P. falciparum* intraerythrocytic PCD triggered by chloroquine (Ch'ng *et al.*, 2010), since the *Leishmannia* homologues have been documented to play a death role (Proto *et al.*, 2013). Calpains are calcium-dependent thiol proteases which participate in various cellular activities, including cell death in higher eukaryotes (Smith and Schnellmann, 2012). In the *P. falciparum* genome a single calpain homologue exists, PF3D7_1362400. This nucleolar protein has been shown to play a role in cell cycle regulation but its role in PCD remains elusive (Deponte and Becker, 2004, Aurrecoechea *et al*., 2009, Russo *et al*., 2009a, Russo *et al*., 2009b).

Endonuclease

The absence of an endonuclease G homologue within *Plasmodium*, but its presence in several other *Apicomplexa* species, suggests its deletion from the parasite during evolution. The Zinnia endonuclease 1 protein, for which *P. falciparum* has a single homologue, is suggested to perform the role of endonuclease G during PCD. This protein has not been studied within the parasite (Kaczanowski *et al.*, 2011).

The mitochondrion

The cytoplasm of the *P. falciparum* parasite contains only a single mitochondrion (Van Dooren *et al*., 2005, Torrentino-Madamet *et al.*, 2010). During the *P. falciparum* erythrocytic development from a trophozoite into a schizont, the small mitochondrion, lacking cristae, elongates and branches but only undergoes fission to produce several independent mitochondria very late in schizogony, during cytokinesis. This process allows each new merozoite to contain a single mitochondrion (Van Dooren *et al.*, 2005, Torrentino-Madamet *et al.*, 2010). During gametocytogenesis, the single mitochondrion branches and elongates, forming dense clusters around the small apicoplast (Okamoto et

al., 2009). This stage of the parasite's life cycle is also associated with the formation of cristate structures in the inner mitochondrial membrane; suggesting enhanced metabolic activity possibly as a preparation for entrance into the oxygen rich midgut of the mosquito (Torrentino-Madamet *et al.*, 2010).

All the proteins required for a functional respiratory chain have been identified. They are distributed across the various genomes of the parasite, but mainly located in the nuclear genome, and maybe responsible for the maintenance of an electropotential gradient across the mitochondrial inner membrane, and canonical oxidative TCA cycle, the latter's importance dependent on the life stage (Torrentino-Madamet *et al*., 2010, MacRae *et al*., 2013). Additionally the mitochondrion has been linked with various other metabolic pathways, such as *de novo* pyrimidine synthesis, iron-sulphur cluster biosynthesis, *de novo* ubiquinone (CoQ) synthesis, and PCD (Vaidya and Mather, 2009). Several studies, as presented in tables 1.5 and 1.6, have shown a loss in mitochondrial potential, a common PCD marker, in the *Plasmodium* genus. The downstream participants required for mitochondrial-related PCD have not been documented within the genus and thus the specific contribution of the mitochondrion to parasite death is uncertain.

1.5.1.3 Targeted identification of P.falciparum PCD homologues

In Professor Coetzer's unit, Dr Durand conducted a targeted PCD homologue search within the *P. falciparum* genome. Using novel bioinformatics procedures, homologues of the metazoan ATM, p53, SWIB/MDM2, CR6, IAP and caspase genes were identified (Coetzer *et al.*, 2010). Of importance to this study was the identification of a metazoan p53 (PFE1120w, currently known as PF3D7_0522400) and SWIB/MDM2 domain (PFE0910w, currently known as PF3D7_0518200) homologues, the latter being subsequently annotated

within PlasmoBD as a SWIB/MDM2 domain containing protein. Another SWIB/MDM2 homologue (PF3D7_0611400) has also been annotated on PlasmoDB (Aurrecoechea *et al.*, 2009). Laboratory evidence is now required to determine if these homologues act in a manner similar to their metazoan counterparts. Currently there are no true functional links established between any parasite PCD proteins and their metazoan homologues. Thus, laboratory evidence is now required to determine if these homologues act in a manner similar to their metazoan counterparts. They may participate in a PCD process that is unique to the parasite or *Apicomplexa* members or may play a role unrelated to cell death.

1.6 Aim and objectives

This study aims to investigate and characterize *P. falciparum* proteins that may be involved in PCD.

The objectives of this study are as follows:

1) SWIB/MDM2 domains
    - Clone the SWIB/MDM2 domains of PF3D7_0518200 (designated as *Pf*MDM2) and PF3D7_0611400 (designated as *Pf*SWIB).
    - Express recombinant *Pf*MDM2 and *Pf*SWIB proteins.
    - Identify protein binding partners via biopanning against *P. falciparum* phage display libraries.
    - Confirm the protein-protein interactions identified by biopanning.
    - Create transgenic parasites expressing GFP-tagged forms of *Pf*MDM2 and *Pf*SWIB.
    - Determine the cellular localization of these fluorescent proteins under normal and PCD conditions.

2) p53

- Clone the DNA binding domain (DBD) and tetramerisation domain of PF3D7_0522400 (designated as *Pf*p53)
- Express the domains as recombinant proteins
- Assess the function of the recombinant domains

2 MATERIALS AND METHODS

2.1 Bioinformatic analysis

2.1.1 Gene and protein sequence acquisition, multiple sequence alignments and p53-consensus sequence identification

The nucleotide sequences of the *P. falciparum* genes and the corresponding protein amino acid sequences were acquired from PlasmoDB: The *Plasmodium* genome resource database (www.plasmodb.org) (Aurrecoechea *et al.*, 2009). Amino acid sequences of proteins containing SWIB/MDM2 domains, as well as p53 or p53-like proteins were collected from a variety of prokaryotic and eukaryotic species, using the NCBI protein database (http://www.ncbi.nlm.nih.gov/). All data were saved in fasta format and various multiple sequence alignments were performed using on-line algorithms from the European Molecular Biology Laboratory European Bioinformatics Institute (EMBL-EBI) (http://www.ebi.ac.uk/Tools/sequence.html) (European Bioinformatics Institute, 2012) and the Computational Biology Research Centre (CBCR) (http://MAFFT.cbrc.jp/alignment/server/) (Computational Biology Research Centre, 2012):

- EMBL-EBI MAFFT v6.850b – using the strategy L-INS-i, a blosum62 matrix, gap-opening penalty of 1.53 and gap-extension penalty of 0.123
- EMBL-EBI MUSCLE 3.8
- EMBL-EBI CLUSTALw2 2.1 – a Gonnet matrix, gap-opening penalty of 10 and gap-extension penalty of 0.20
- EMBL-EBI CLUSTAL OMEGA
- CBCR MAFFT – using the strategy L-INS-i, a blosum62 matrix, gap-opening penalty of 1.53 and gap-extension penalty of 0

Multiple sequence alignments were expressed graphically using BioEdit Sequence Alignment Editor (Hall, 1999). Percentage identity and similarity was calculated using EMBOSS Needle (http://www.ebi.ac.uk/Tools/psa/emboss_needle/).

The metazoan p53 consensus sequence was defined as PuPuPuCWWGPyPyPyN PuPuPuCWWGPyPyPy where N represents a region of 0 to 13bp of random nucleotides (El-Deiry *et al.*, 1992). A p53-like sequence was identified in *Entamoeba histolytica* (AGAAATTCATGGGCTAGTGG), although it did deviate from the general form (Mendoza *et al.*, 2003). The *P. falciparum* genome was searched, using the DNA motif search function on PlasmoDB, for p53-consensus sequences, as well as variations thereof and for the putative p53-consensus sequence identified in the *E. histolytica* genome.

2.1.2 Protein structural analysis and modelling

2.1.2.1 Secondary structure predictions

The secondary structures of the *P. falciparum* proteins were assessed by means of the online Swiss Model Workspace Secondary Structure Prediction and Domain Assignment program (Guex and Peitsch, 1997, Jones, 1999, Arnold *et al.*, 2006); the Protein Homology/analogy Recognition Engine V 2.0 (Phyre2) online server (Kelley and Sternberg, 2009); the PSIPRED v3.0 online server (Jones, 1999, Buchan *et al.*, 2010) and the SSpro v 4.5 online server (Cheng et al., 2005). The likelihood of the presence of a particular secondary structure (alpha helix, beta-sheet or coil) within the proteins was determined by comparing the various secondary structure predictions within the BioEdit Sequence Alignment Editor. Areas were deemed to probably fold into a specific secondary structure if three or more of the servers predicted the same structure for the region. Regions presenting discordance between the different algorithms were classified as a coiled structure, often used by modelling programmes to depict uncertain topologies.

2.1.2.2 Tertiary structure predictions

Structural modelling of the proteins was conducted with the aid of the following online servers – Swiss Model Workspace Automatic Modelling Mode (Schwede *et al.*, 2003,

Arnold et al., 2006), Phyre2 (Kelley and Sternberg, 2009) and ESyPred3D Web Server 1.0 (Lambert *et al.*, 2002). For structural modelling against a crystal structure template, the putative p53 DNA binding was modelled upon the *Homo sapiens* p53 and *Caenorhabditis elegans* Cep-1 DNA binding domain crystal structures (PDB id: 2FEJ and 1T4W respectively) (Huyen *et al.*, 2004, Pérez-Cañadillas *et al.*, 2006); the putative p53 tetramerisation motif was modelled upon the *H. sapiens* p53 tetramerisation motif crystal structure (PDB id: 1AIE chain A) (Mittl *et al.*, 1998); and the putative SWIB/MDM2 proteins were modelled upon the *Xenopus laevis* MDM2 SWIB/MDM2 domain (PDB id: 1YCQ chain A) (Kussie *et al.*, 1996) and the *Mus musculus* SWI/SNF-related matrix-associated actin-dependent regulator of chromatin subfamily D member 1 SWIB/MDM2 domain (PDB id:1UHR). Graphical display, orientation and colouring of various PDB files were conducted using the Eduction-Use-Only PyMOL Molecular Graphics System (Schrodinger, 2010). The generated three dimensional models were assessed by means of the QMEAN Server (http://swissmodel.expasy.org/qmean/cgi/index.cgi) for estimation of the quality of the models (Benkert *et al.*, 2008, Benkert *et al.*, 2009).

2.1.2.3 pI, molecular mass determination and solubility predictions

The pI and molecular mass of the various *P. falciparum* proteins and domains were calculated with aid of ExPASy compute pI/MW program (Bjellqvist *et al.*, 1993, Bjellqvist *et al.*, 1994, Gasteiger *et al.*, 2005) (http://web.expasy.org/compute_pi/). The solubility of the malaria proteins, expressed as recombinant proteins in *E. coli*, was calculated with the Recombinant Protein Solubility Prediction program provided online by the University of Oklahoma (http://www.biotech.ou.edu/) (Wilkinson and Harrison, 1991).

2.1.3 Assessment of cellular localization

Various online prediction algorithms were employed to determine the likely cellular structure to which the proteins would localize. These included cNLS Mapper (http://nls-mapper.iab.keio.ac.jp/cgi-bin/NLS_Mapper_form.cgi) (Kosugi *et al.*, 2009a, Kosugi *et al.*, 2009b); MitoProt II - v1.101 (http://ihg.gsf.de/ihg/mitoprot.html) (Claros and Vincens, 1996); NucPred (http://www.sbc.su.se/~maccallr/nucpred/) (Brameier et al., 2007); PredSL (http://hannibal.biol.uoa.gr/PredSL/); PSORT Prediction (http://psort.hgc.jp/form.html); PREDOTAR V1.03 (http://urgi.versailles.inra.fr/predotar/predotar.html); PlasmoDB - PlasmoAP Results (http://v4-4.plasmodb.org/restricted/PlasmoAPcgi.shtml) (Foth *et al.*, 2003); PATS Version 1.2.1 (http://gecco.org.chemie.uni-frankfurt.de/pats/pats-index.php) (Waller *et al.*, 1998, Waller *et al.*, 2000, Zuegge *et al.*, 2001); PlasMit (http://gecco.org.chemie.uni-frankfurt.de/plasmit/) (Bender *et al.*, 2003) and iPSORT Prediction (http://ipsort.hgc.jp/).

2.2 Culturing of 3D7 *Plasmodium falciparum* parasites

2.2.1 Red blood cell preparation

The blood employed for culturing was freshly collected from human volunteers in 6ml acid citrate dextrose tubes. After centrifugation in a 5702R Eppendorf centrifuge at 2500rpm for 15 minutes at 4°C, the plasma and buffy coat were removed by aspiration using a vacuum pump, in a sterile hood. The remaining packed red blood cell (RBC) layer was washed in sterile PBS (10mM Na_2HPO_4, 1.5mM KH_2PO_4, 137mM NaCl, 2.7mM KCl, pH 7.4), centrifuged as described before and any residual plasma and buffy coat was subsequently removed by aspiration. This washing procedure was repeated twice and the washed erythrocytes were stored at 4°C, under sterile conditions for up to 14 days, in a 1:1 ratio in incomplete medium (79.45g RPMI in 5l with 250mg Gentamycin and 250mg Hypoxanthine, sterilized by filtration through a VacuCap® 90PF 0.8/0.2µm Filter Unit).

Laboratory chemicals and equipment and their suppliers can be found in Appendix E.

2.2.2 The culturing technique

Live cultures of the 3D7 *P. falciparum* parasite strain were donated towards the project by various members of the *Plasmodium* Molecular Research Unit (PMRU). Culturing of the 3D7 strain was conducted according to a modified version of the continuous culturing method (Trager and Jensen, 1976). In a sterile flow hood, parasitized red blood cells (pRBC) were dispensed into sterile culture flasks and maintained in fresh RBC, at a 5% haematocrit, and complete medium (0.5% Albumax and 0.2% $NaHCO_3$ in incomplete medium) at 37°C. The cultures, under sterile conditions, were gassed with a mixture of 5% carbon dioxide, 2% oxygen and 93% nitrogen and then sealed. On a daily basis, for each flask, the medium was removed by aspiration and replaced, along with the gaseous atmosphere. The specific volumes and gassing period for $25cm^3$ (small), $80cm^3$ (medium) and $175cm^3$ (large) flasks are presented in table 2.1 below. The parasitaemia of the cultures was maintained at a level of 10% or less and when necessary cultures were divided or moved to a larger culture flask.

Table 2.1: Culture flask volumes.

	Small	Medium	Large
Flask size (cm^3)	25	80	175
Total culture volume (ml)	5	20	35
Volume of complete medium (ml)	4.50	18	32.5
1:1 RBC (to give a haematocrit of 5%) (ml)	0.50	2.0	3.5
Gassing period (minutes)	1	2	3-5

The parasites were assessed by means of a pRBC smear, stained using the Giemsa-based staining system – Rapi-Diff Staining Kit, according to the manufacturer's specifications. Slides were viewed under an oil immersion Zeiss: Axiostar plus - Transmitted Light Microscope at 1000x magnification. On the blood smear slides five fields, each with more

than 100 erythrocytes, were examined and quantified in terms of their infected and uninfected erythrocytes and used to calculate the overall average percentage parasitaemia within the culture.

$$\textbf{\% parasitaemia} = \left(\frac{\text{Number of infected erythrocytes}}{\text{Number of infected and uninfected erythrocytes}}\right) \text{x } 100$$

2.2.3 Sorbitol treatment for culture synchronisation

Synchronisation of *P. falciparum* was facilitated by sorbitol treatment (Lambros and Vanderberg, 1979). The increased permeability of late stage infected RBC makes them more susceptible to sorbitol induced lysis, compared to early stage infections (Lambros and Vanderberg, 1979).

A 5ml culture of at least 3% ring stage parasites was transferred into a 15ml Nunc tube and centrifuged in a 5702R Eppendorf centrifuge at 2500rpm for 5 minutes at room temperature. The supernatant was aspirated and ten volumes of 5% D-sorbitol were added to the pelleted RBC. After incubation at room temperature for 20 minutes the tube was inverted slowly and then centrifuged as before. The supernatant was removed and replaced with complete medium and washed RBC to create a fresh 5ml culture. The culture was then transferred into a 25cm^3 culture flask, gassed, sealed and incubated at 37°C as described in section 2.2.2.

2.2.4 Freezing of the cultures

Parasite cultures were frozen according to a slightly modified form of a previously described protocol (Normark, 2008). Two 5ml cultures, having a ring stage parasitaemia of more than 3% were combined and frozen as a glycerol stock. The cultures were centrifuged in a 5702R Eppendorf centrifuge at 2500rpm for 5 minutes at room

temperature and the supernatant was removed. The packed RBC and pRBC were resuspended in a 2ml cryotube in a 1:1 ratio of 60% sterile freezing solution (60% glycerol in freezing PBS (123mM NaCl, 83mM Na_2HPO_4, 32mM KH_2PO_4, pH 7.4)), allowed to stand for 5 minutes and then stored in liquid nitrogen.

2.2.5 Thawing of frozen cultures

Frozen parasite cultures were thawed according to a slightly modified form of a previously described protocol (Blomqvist, 2008). A frozen culture was warmed at 37°C in its cryotube. Once thawed, 100µl of 12% NaCl was added and the suspension was transferred to a 15ml Nunc tube containing 9ml of 1.6% NaCl. After gentle mixing, the solution was centrifuged in a 5702R Eppendorf centrifuge at 1500rpm for 5 minutes at room temperature and the supernatant was removed. The pellet was resuspended in 9ml of a 0.9% NaCl and 0.2% glucose solution and centrifuged as before. After removal of the supernatant the pellet was transferred into a sterile 25cm^3 flask with complete medium, with an extra 500µl of 5% Albumax added, and 500µl prepared RBC, gassed, sealed and incubated at 37°C as described in section 2.2.2. The addition of extra Albumax was maintained until the culture exceeded a 1% parasitaemia.

2.3 Genomic DNA isolation

2.3.1 Extraction of genomic DNA from *P. falciparum*

Genomic DNA isolation was performed on 3D7 *P. falciparum* cultures with roughly 4% late trophozoite and/or schizont parasitaemia based on the hypotonic lysis method (Cowman *et al.*, 2008). These stages were used to maximize DNA yield due to the large amount of genomic material associated with these stages (Tilley *et al.*, 2011).

A 5ml culture was transferred into sterile 15ml Nunc tubes and centrifuged in a 5702R Eppendorf centrifuge at 2500rpm for 5 minutes at 4°C to pellet the pRBC and RBC. The supernatant was aspirated and the pellet was washed with 14ml PBS and centrifuged as before. The supernatant was aspirated and inversion was used to loosen the pellet.

Four pellet volumes of hypotonic solution (5mM KH_2PO_4, pH 7.4 with K_2HPO_4) were added to facilitate RBC lysis. The pellet was resuspended and one volume of 18% sodium dodecyl sulphate (SDS) was added to denature the released proteins (Birnboim and Doly, 1979). The solution was allowed to stand for 3 minutes at room temperature after which 8 volumes of 1:1 phenol:chloroform mixture was added, which facilitated the removal of any soluble proteins still present (Moore and Dowhan, 1987). The tube was inverted several times, centrifuged in the 5702R Eppendorf centrifuge at 4400rpm for 10 minutes at 4°C and the top aqueous layer, containing the chromosomal DNA, was carefully collected and transferred equally as 400µl aliquots into 1.5ml Eppendorf tubes, on ice. To each tube one tenth of a volume of 3M sodium acetate (CH_3COONa) (pH 5) and 2.5 volumes of ice cold 100% ethanol were added to induce chromosomal DNA aggregation (Moore and Dowhan, 1987).

The tubes were incubated for at least 15 minutes at -70°C, centrifuged in a 5415R Eppendorf centrifuge at 13200rpm for 30 minutes at 4°C and the supernatant decanted. One millilitre of 70% ethanol was added to the tube which was centrifuged in a 5415R Eppendorf centrifuge at 13200rpm for 5 minutes at 4°C to remove salt from the sample, which may hinder downstream applications (Moore and Dowhan, 1987). The supernatant was decanted and the pellets were allowed to air dry for about 15 minutes and then resuspended and pooled into a final volume of 600µl Tris EDTA (TE) buffer (10mM Tris-HCl, 1mM EDTA, pH 8).

A volume of 6µl of RNase A was added to remove contaminating single stranded RNA, mixed by swirling, and incubated for 30 minutes at 37°C in a water bath. One volume of 1:1 phenol:chloroform mixture was added and the tube was inverted several times and subsequently centrifuged as before for 5 minutes at 4°C. The top aqueous layer was carefully collected and transferred into a 1.5ml Eppendorf tube to which one volume (600µl) of chloroform was added; the tube was inverted and centrifuged as before. The top aqueous layer was collected and transferred into a 2ml Eppendorf tube, in which the DNA was precipitated as previously described after which the DNA pellet was allowed to air dry and subsequently resuspended in 20 - 50µl TE buffer. The DNA was stored at 4°C; long term storage was at -20°C.

2.3.2 Concentration and purity determination of isolated genomic DNA

2.3.2.1 NanoDrop

The NanoDrop® 1000 is able to determine the concentration of DNA within a solution. This is facilitated by DNA being able to absorb electromagnetic radiation strongly at a wavelength of about 260nm due, almost solely, to its constituent purine and pyrimidine bases (Blackburn *et al.*, 2006, NanoDrop Technologies, 2007).

2.3.2.2 Agarose gel electrophoresis

The integrity of the DNA was assessed by agarose gel electrophoresis. One percent agarose was dissolved in 50ml 1x TAE buffer (40mM Tris, 2mM acetic acid, 1mM EDTA, pH 8) by heating. The solution was cooled, to which 2.5µl of 10µg/µl ethidium bromide was added, and poured and set in a 10 x 8cm gel casting chamber. The samples and a mixed range base pair standard (80 – 10000bp) were added to the gel and electrophoresed, in 400ml 1x TAE buffer supplemented with 2.5µl of 10µg/µl ethidium bromide at the anode of the chamber, for one hour and forty minutes at 100V. The gel was then visualized under

ultra violet (UV) light using the GeneSnap GeneGenius Geldoc scanning system and version 6.05 image acquisition software (Syngene, UK).

2.4 Plasmid DNA isolation and preparation

2.4.1 Alkaline extraction procedure for plasmid DNA

The alkaline extraction procedure was conducted for the isolation of each of the following plasmid types – pARL2-GFP (donated by Dr Jude Przyborski, Marburg, Germany), pGEX-4T-2 (Amersham Biosciences, UK) and pET-15b (Millipore, USA) (vector maps presented in Appendix D) – from *E. coli* cells (Engebrecht *et al*., 1987).

A scraping of a 60% glycerol stock of *E. coli* cells, carrying the appropriate plasmid, was added to 5ml of Luria Broth (LB) (1% (w/v) Tryptone, 1% (w/v) NaCl, 0.5% (w/v) yeast extract, 10mM Tris-HCl, pH 8) containing 0.1mg/ml ampicillin antibiotic in a 50ml Erlenmeyer flask. After incubation for ~15 hours on a Labotec orbital shaker at 37°C at 250rpm, the optical density (OD) of the culture was determined at 600nm (OD_{600nm}), with the aid of a Thermo Biomate 5 Spectrophotometer (Thermo Fisher Scientific Inc, USA). If the OD was greater than 3 for this culture, 500µl of this culture was transferred to 10ml LB, containing 0.1mg/ml of ampicillin, in a 100ml flask and allowed to incubate for ~15 hours with shaking. Only after the 10ml bacterial culture had a minimum OD_{600nm} of above 3, was it transferred into a 15ml Nunc tube and centrifuged in a 5702R Eppendorf centrifuge at 4400rpm for 10 minutes at 4°C. The supernatant was discarded and 500µl ice cold re-suspension solution (50mM glucose, 10mM EDTA, 25mM Tris, pH 8) was added and the pellet was completely resuspended and incubated at room temperature for 5 minutes. One millilitre of freshly prepared lysis solution (0.2M NaOH, 1% SDS) was added, mixed by inversion and allowed to stand at room temperature for 5 minutes. The SDS aids in denaturing the bacterial proteins while the high pH of the sodium hydroxide

denatures the linear chromosomal bacterial DNA but not the covalent, circular plasmid DNA (Birnboim and Doly, 1979, Engebrecht *et al.*, 1987). A freshly prepared 750µl aliquot of ice cold neutralization solution (1.6M potassium acetate and 3.2M acetic acid, pH 4.8) was added, mixed gently by inversion and allowed to incubate for 5 minutes on ice. During the neutralization step the chromosomal DNA will aggregate to form an insoluble network and precipitate, along with the SDS-protein complexes and high molecular weight RNA molecules due to the high concentration of sodium acetate present (Birnboim and Doly, 1979). Any covalently closed plasmid DNA which had denatured during lysis will renature correctly into a soluble form during the neutralization step (Engebrecht *et al.*, 1987).

The sample was centrifuged in a 5702R Eppendorf centrifuge at 4400rpm for 20 minutes at 4°C and the supernatant, containing the plasmid DNA, collected and transferred as roughly 1ml aliquots into 2ml Eppendorf tubes. One volume of 1:1 phenol:chloroform was added to each tube, mixed and centrifuged in a 5415R Eppendorf centrifuge at 13200rpm for 5 minutes at 4°C, to remove any soluble proteins still present (Moore and Dowhan, 1987). The aqueous phase was transferred as roughly 450µl aliquots into 2ml Eppendorf tubes. A volume of 1.2ml of ice cold 100% ethanol was added to each tube and incubated for 5 minutes at room temperature to precipitate the plasmid DNA and then centrifuged in a 5415R Eppendorf centrifuge at 13200rpm for 10 minutes at 4°C. The supernatant was decanted and the pellets were allowed to air dry and resuspended in 100µl of TE buffer.

Samples were pooled to produce a single Eppendorf tube holding 400µl solution, to which 4µl of RNase A was added and allowed to incubate at 37°C for 30 minutes, as the alkaline extraction procedure does not remove residual low molecular weight RNA (Birnboim and Doly, 1979). Subsequently 40µl of freshly prepared ice cold neutralization solution was added to each tube, after which 500µl of 1:1 phenol:chloroform was added. The solution

was mixed and then centrifuged in a 5415R Eppendorf centrifuge at 13200rpm for 5 minutes at 4°C, the aqueous phase collected and transferred into new 2ml tubes, each holding about 400µl supernatant. To each tube 500µl chloroform was added, mixed and centrifuged in a 5415R Eppendorf centrifuge at 13200rpm for 5 minutes at 4°C. The aqueous phase was transferred into a new tube, to which one tenth of a volume of 3M sodium acetate and two and a half volumes of 100% ice cold ethanol were added.

The tubes were kept at -70°C for 15 minutes, centrifuged in a 5415R Eppendorf centrifuge at 13200rpm for 30 minutes at 4°C and the pellet washed with 1ml of ice cold 70% ethanol to remove any salt from the sample which may hinder downstream applications (Moore and Dowhan, 1987). After re-centrifugation the pellet was allowed to air dry and resuspended in 20-50µl TE buffer.

2.4.2 Restriction enzyme digestion and alkaline phosphatase treatment of plasmids

The extracted plasmids were cut with specific FastDigest® restriction endonucleases and dephosphorylated using FastAP™ Thermosensitive Alkaline Phosphatase according to the manufacturer's specifications.

pGEX-4T-2 was digested with FastDigest® *Bam*HI and FastDigest® *Xho*I

pARL2-GFP was digested with FastDigest® *Avr*II and FastDigest® *Xho*I

pET-15b was digested with FastDigest® *Nde*I and FastDigest® *Bam*HI

The digested and dephosphorylated plasmids were purified using the QIAgen QIAquick PCR Purification kit® or the Macherey-Nagel NucleoSpin® Gel and PCR Clean-up Kit, according to the manufacturers' instructions, and eluted into 50µl nuclease free water.

2.5 Polymerase chain reaction (PCR)

2.5.1 Primer design

Based on the gene sequences derived from the *Plasmodium* genome database, PlasmoDB version 7.2 (www.plasmodb.org (Aurrecoechea *et al.*, 2009, The EuPathDB Project Team, 2012)), primers were designed with the aid of Integrated DNA Technologies SciTools Oligo Analyzer 3.1 (www.idtdna.com (Integrated DNA Technologies, 2012)) for the amplification of various *P. falciparum* genes or domains. The primers were assessed to ensure that the formation of any hairpins or primer dimers during the PCR process would be non-consequential. Specific restriction endonuclease cleavage sites were included at the 5' end to facilitate directional cloning of the PCR products into plasmid vectors – pARL2-GFP, pGEX-4T-2 and pET-15b. The reverse primers for the pGEX-4T-2 and pET-15-b vectors were created to include a stop codon while the forward primers for the pARL2-GFP vector were created with a start codon. Primer sequences are given in appendix B.

The primers were synthesised by Inqaba Biotec^{TM}, South Africa, and supplied in lyophilised form. Reconstitution of the primers was conducted in nuclease free water as a concentrated 100µM stock, used to make working stocks of 10µM for the PCR reactions.

2.5.2 Insert amplification for cloning

High fidelity PCR was carried out for the amplification of the various inserts required for cloning using either the High Fidelity PCR Enzyme kit® or the Phusion® Flash High-Fidelity PCR Master Mix. Both mixes contained a thermostable *Taq* DNA Polymerase with proofreading ability, thus enhancing accuracy during replication (Thermo Fisher Scientific, 2011). High fidelity PCRs were conducted in an Eppendorf Mastercycler Gradient Thermocycler according to the manufacturer's specifications, using the forward and reverse primers at a concentration of 0.5µM. Table 2.2 presents the annealing

temperatures (T_a) and elongation times used during the various hot start PCRs – four cycles of the PCR were carried out using the *P. falciparum* specific T_a followed by twenty nine cycles using the T_a of the full length primers.

Table 2.2: PCR parameters for the amplification of *P. falciparum* genes/domains.

Enzyme	Gene being amplified	Vector to be used with the insert	*P. falciparum* specific T_a (°C)	Full length primer T_a (°C)	Elongation time (seconds)
High Fidelity	Putative DNA binding domain and tetramerization domain of *Pf*p53	pGEX-4T-2	45	55	120
High Fidelity	MDM2/SWIB domain of *Pf*MDM2	pARL2-GFP	40	53	30
High Fidelity	MDM2/SWIB domain of *Pf*MDM2	pGEX-4T-2	40	51	30
Phusion® Flash	Entire PfMDM2	pARL2-GFP	43	55	15
Phusion® Flash	Putative MDM2/SWIB domain of *Pf*SWIB	pGEX-4T-2	43	55	15
Phusion® Flash	Entire *Pf*SWIB	pARL2-GFP	44	51	45
Phusion® Flash	Biopanning identified domain of *Pf*LisH	pET15-b	43	55	15
Phusion® Flash	Biopanning identified domain of *Pf*ALV5	pET15-b	45	55	15
Phusion® Flash	Biopanning identified domain of *Pf*RS6	pET15-b	37	55	15
Phusion® Flash	Biopanning identified domain of *Pf*ARK3	pET15-b	47	55	15

2.5.3 Restriction endonuclease digestion of the PCR products

The PCR products were purified using the QIAgen QIAquick PCR Purification kit® or the Macherey-Nagel NucleoSpin® Gel and PCR Clean-up Kit, according to the manufacturers' instructions, and eluted in 50µl nuclease free water . The purified product was digested with the appropriate restriction endonucleases, according to the Fermentas guidelines (Thermo Fisher Scientific Inc, 2011).

The digested PCR products were again purified using the QIAgen QIAquick PCR Purification kit® or Macherey-Nagel NucleoSpin® gel and PCR Clean-up and eluted in 50µl nuclease free water to remove salts and other contaminants which may influence the subsequent cloning steps.

2.6 Ligation reaction

The In-Fusion® Molar Ratio Calculator (http://bioinfo.clontech.com/infusion/molarRatio.do (ClonTech, 2012)) was used to calculate the amounts of vector and PCR product required for ligation. The molar ratio employed was one vector unit to three PCR insert units and the total amount of DNA present in the reaction was not allowed to exceed 200ng, as specified in the ligation kit (Roche Applied Science, 2011).

The digested and purified PCR inserts and plasmids were quantified on a 1% agarose gel against a mixed range of base pair standards, using the GeneSnap GeneGenius Geldoc scanning system. The necessary volumes were used accordingly to set up ligation reactions using the Roche Rapid DNA Ligation Kit, according to the manufacturer's specifications, with a 16°C incubation for 30 minutes (Roche Applied Science, 2011). Control ligation reactions were set up using nuclease free water instead of PCR product.

2.7 Transformation of XL10 and DH5α cells

Once ligation had been completed, *E. coli* cells were transformed with 10µl of the ligation reaction. Two different cell strains were used. The XL10 cells are more suitable for effective transformation with larger vector constructs and as a result were used for the pARL2-GFP plasmid (Stratagene, 2004). Commercial XL10 cells were obtained from Stratagene and used according to the manufacturer's specifications (Stratagene, 2004). A

100µl aliquot of the chemically competent cells were thawed on ice and then incubated with 4µl β-mercaptoethanol for 10 minutes. While gently swirling, 10µl of ligation reaction was added and the cells were incubated on ice for 30 minutes. Heat shock was conducted at 42°C for 90 seconds, after which the cells were incubated on ice for 2 minutes and then seeded into 450µl LB and incubated for 1 hour at 37°C. These cells were plated at 50µl and 500µl, on 1.5% agar plates in LB containing 100µg/ml ampicillin and incubated for at least 18 hours at 37°C.

The smaller vector constructs, those involving the pGEX-4T-2 and pET-15b plasmids, were used to transform DH5α cells. In-house chemically competent DH5α cells were donated by Dr Sonja Lauterbach, from the PMRU, and used according to an in-house transformation protocol, which differed slightly from that of the Stratagene method - the chemically competent cells were not exposed to β-mercaptoethanol after thawing and they were not incubated in LB for 1 hour before plating.

Single colonies were picked off the experimental plates using a pipette and suspended in 10µl nuclease free water. A 5µl aliquot of the suspension was added to 14ml BD Falcon™ round bottom tubes with 2ml LB containing 100µg/ml ampicillin and incubated at 37°C on a Labotec orbital shaker overnight at 250rpm. Glycerol stock solutions were made from these overnight cultures by adding 500µl of the transformed cells to 500µl 60% sterile glycerol and stored at -70°C. The remaining overnight bacterial culture was utilized for plasmid extraction with the GenElute Plasmid Miniprep Kit or the Macherey-Nagel NucleoSpin® plasmid extraction kit, according to the manufacturers' specifications, and eluted into 50µl nuclease free water.

2.7.1 Verification of transformation

2.7.1.1 Colony PCR verification

A volume of 2µl of the colony suspension, described above, was used for a colony PCR to detect the presence of inserts in the constructs. The aliquots were heated to 94°C for 5 minutes in the Eppendorf Mastercycler Gradient Thermocycler, in order to lyse the bacterial cells, and then used to set up 20µl GoTaq® Green Master Mix PCR reactions, as specified by the manufacturer's instructions. Vector or insert specific primers were used for the PCR (primers presented in appendix B).

2.7.1.2 Restriction digestion verification of extracted plasmid constructs

The extracted vector constructs were digested with FastDigest® restriction endonucleases, according to the manufacturer's specifications, in order to detect the presence of the correctly sized insert and vector backbone (Thermo Fisher Scientific Inc, 2011). Digestion of the pET15-b and pGEX-4T-2 constructs was conducted as described in section 2.4.2. For the pARL2-GFP vector the FastDigest® *Eco*RV and FastDigest® *Xho*I enzymes were used. Control digests were conducted simultaneously on the original vector constructs. The digested vectors were assessed by agarose gel electrophoresis, against a mixed range base pair standard for 1 hour, as described in section 2.3.2.2.

Constructs with the correctly sized insert were sent to Inqaba Biotec^{TM}, South Africa, for sequencing.

2.8 Transformation of Rosetta™ 2 (DE3) cells

Rosetta™ 2 (DE3) cells were designed for enhanced expression of eukaryotic proteins requiring codons which are rarely utilized by *E. coli* – specifically the AUA, AGG, AGA, CUA, CCC, GGA and CGG codons, and thus prevents the need for codon optimization (Novagen, 2004). These cells were transformed with the pGEX-4T-2 and pET-15b

constructs containing the verified sequences according to the manufacturer's protocol (Novagen, 2004). After 18 hours or more of incubation at 37°C, transformed colonies found on each of the experimental 100µg/ml ampicillin and 50µg/ml chloramphenicol plates were picked off and each resuspended in ten microliters of nuclease free water. Five microliters of the suspension was added to BD Falcon™ round bottom tubes holding two millilitres of LB with 100µg/ml ampicillin and 50µg/ml chloramphenicol and incubated at 37°C on a Labotec orbital shaker overnight at 250rpm. Glycerol stock solutions were made as described in section 2.7 and the remaining overnight culture was used for plasmid extraction and digestion, as described in sections 2.7 and 2.7.1.2 to confirm transformation with the correct construct.

2.9 Protein expression, extraction, purification and visualization

2.9.1 Protein expression

The following procedure was optimized for recombinant protein expression:

A scraping of a glycerol stock of transformed Subcloning Efficiency™ Rosetta™ 2 (DE3) cells, containing the appropriate vector construct, was added to 5ml LB containing 100µg/ml ampicillin and 50µg/ml chloramphenicol. The culture was incubated overnight on a Labotec orbital shaker at 37°C at 250 rpm. A volume of 500µl of this overnight culture was used to seed 20ml of Overnight Express™ Instant TB Medium (60g Overnight Express™ instant TB Medium Powder, 10ml glycerol, made up to 1l and autoclaved) containing 100µg/ml ampicillin and 50µg/ml chloramphenicol and incubated for 22 hours while vigorously shaking at 250rpm on a Hoefer PR250 orbital bench top shaker, at room temperature (~ 20°C). Overnight Express™ Instant TB Mediums promotes high density cell growth, several fold higher than that of conventional protocols such as isopropyl-β-D-1-thiogalactopyranoside inducible bacterial systems, due to its specific carbon source blend

and magnesium; while its unique blend of nitrogen sources sustains high protein expression, induced through lactose using the Lac promoter (Grabski *et al*., 2005).

For a comparative un-induced control of the *E. coli* protein expression system, 500µl of the 5ml LB grow was seeded into a 2% glucose LB mixture. In this growth medium a glucose effect will be induced, which will reduce Lac transcription and so prevent the expression of the recombinant proteins (Novy and Morris, 2001).

The cultures were analysed with a Thermo Biomate 5 Spectrophotometer. They were used for protein purification if the OD_{600nm} was 3 or above.

2.9.2 Protein extraction and purification of GST-tagged recombinant proteins

The following procedure was optimized for GST-tagged recombinant protein extraction (Promega, 2009a):

The Overnight Express™ Instant TB Medium cultures were pelleted and frozen at -70°C for at least 15 minutes. The pellet was thawed at 37°C for 5 minutes, resuspended in 1.5ml GST Binding/Wash buffer (4.2mM Na_2HPO_4, 2mM K_2HPO_4, 500mM NaCl, 10mM KCl, pH 7.2) (Promega, 2009a) with 1.5µl Calibiochem® Protease Inhibitor cocktail Set III (100mM 4-(2-Aminoethyl) benzenesulphonyl fluoride hydrochloride, 80µM Aprotinin, 5mM Bestatin; 1.5mM E-64; 2mM Leupeptin, 1mM Pepstatin A) and 1.5µl DNaseI, frozen at -70°C for 15 minutes and then thawed at 37°C for five minutes again.

The thawed suspension was transferred into 15ml Nunc tube and sonicated for 4 cycles, while immersed in ice water, at an 80% amplitude; each cycle lasting for 30 seconds, having an on pulse of one second and an off pulse for half a second and a 30 second break between each cycle. A 75µl aliquot was collected after the final round of sonication, representing the total protein aliquot. The remaining solution was centrifuged in a 5415R

Eppendorf centrifuge at 16000rpm for 20 minutes at 4°C and the supernatant collected - 75µl was taken as the soluble protein aliquot. The pellet was resuspended in 1.5ml of GST Binding/Wash buffer, 75µl taken as the insoluble protein aliquot. The total, soluble and insoluble aliquots were diluted in 75µl GST Binding/Wash buffer and processed further, as described in section 2.9.4.

Purification of the GST-tagged proteins was performed using a magnetic particle separator and the MagneGST^{TM} Kit according to the manufacturer's specifications, with slight modifications:

A 10µl aliquot of the MagneGST™ particle slurry was washed 3 times with the GST Binding/Wash buffer and then resuspended in 100µl of GST Binding/Wash buffer and added to the extracted soluble protein solution, containing the GST-tagged protein of interest. The mixture was incubated at 4°C while rotating at 25rpm on an Intelli-mixer for one hour after which the supernatant was removed and the beads were washed five times in 1ml GST Binding/Wash buffer for five minutes while rocking vigorously at a 90° angle at 90rpm on the Intelli-mixer. The unbound supernatant was re-applied to the washed beads and incubated and washed again, as described above. From each wash step a 50µl aliquot was kept (wash aliquots) and a 75µl aliquot of the unbound supernatant was suspended in 75µl of GST Binding/Wash buffer (unbound aliquot).

Depending on the downstream application of the purified protein the GST fusion proteins could either be eluted from the beads or retained on the beads. For elution of the protein, 150µl of GST-Elution buffer (500mM L-Glutathione, 500mM NaCl, 50mM Tris-HCl, pH 8.1) was added to the beads and incubated while rocking at 90° at 99rpm on an Intelli-

mixer for 15 minutes. The elution was collected and the beads were then suspended in 50µl GST Binding/Wash buffer (bead aliquot).

2.9.3 Protein extraction and purification of His-tagged recombinant proteins

The procedure optimized for His-tagged recombinant protein extraction and purification was similar to that of the GST-tagged recombinant proteins, as described in section 2.9.2, with the following differences (Promega, 2009b):

- The thawed pellet was resuspended in 1.5ml His-Binding buffer (50mM Na_2HPO_4/NaH_2PO_4 buffer, 150mM NaCl, pH 8) with 1.5µl Protease Inhibitor cocktail Set III and 1.5µl DNaseI.
- Purification of the His-tagged proteins was performed using the magnetic particle separator and MagneHis™ Kit, where 30µl of MagneHis™ particle slurry was washed three times with His-Binding buffer, resuspended in 100µl of His-Binding buffer and added to the extracted soluble protein solution, along with imidazole at a final concentration of 10mM.
- The beads were washed in 1ml His-Wash buffer (20mM imidazole in His-Binding buffer). For elution 1 100µl of His-Elution buffer 1 (50mM Na_2HPO_4/NaH_2PO_4 buffer, 150mM NaCl, pH 7.5, 0.5M imidazole) was added to the beads, while for elution 2 100µl His-Elution buffer 2 (50mM Na_2HPO_4/NaH_2PO_4 buffer, 150mM NaCl, pH 7.5, 1M imidazole) was added to the beads.

2.9.4 SDS-PAGE and Coomassie blue staining

Three volumes of various protein aliquots, described in sections 2.9.2 and 2.9.3, were mixed with 1 volume of boiling solution (composed of 40µl 5x suspension solution (50mM Tris-HCl, 5mM EDTA, 5% SDS, 25% sucrose, pH 8.0), 5µl dye mix (2.5% sucrose, 0.5% bromophenol blue) and 5µl β-mercaptoethanol), vortexed thoroughly, boiled for 7 minutes

and resolved on the Laemmli sodium dodecyl sulfate polyacrylamide gel electrophoresis (SDS-PAGE) system (Laemmli, 1970). A 6cm 12% polyacrylamide SDS resolving gel was poured, allowed to polymerize for 20 minutes at room temperature, and then overlaid with a 2cm 4% stacking gel within a Mighty Small II SE250 gel cassette, as described in table 2.3. A 10- or 15-well comb was inserted into the stacking gel and then it was allowed to polymerize for 20 minutes at room temperature.

Table 2.3: Laemmli SDS-Polyacrylamide resolving and stacking gels.

Reagent	12% Resolving gel	4% Stacking gel
MilliQ water	2.3ml	1.63ml
10% (w/v) SDS	53µl (Final concentration 0.05%)	6.7µl (Final concentration 0.02%)
4X resolving buffer (1.5M Tris, pH 8.8)	2.5ml (Final concentration 375mM)	n/a
4X stacking buffer (0.5M Tris, pH 6.8)	n/a	833µl (Final concentration 125mM)
1% (w/v) Bis-acrylamide	1.1ml (Final concentration 0.11%)	333µl (Final concentration 0.11%)
30% (w/v) Acrylamide	4ml (Final concentration 12%)	433µl (Final concentration 4%)
10% (w/v) fresh ammonium persulfate	67µl (Final concentration 0.07%)	67µl (Final concentration 0.2%)
TEMED	5µl	2.5µl
Final volume	10.0ml	3.3ml

A protein molecular mass marker was loaded concurrently with the samples, which was either prepared from human red blood cells by Dr K. Naidoo, of the PMRU, or acquired commercially – Spectra^{TM} Protein Ladder or the QIAgen 6xHis Protein Ladder. The gel was electrophoresed at a constant 20mA and a maximum voltage of 250V in Laemmli running buffer (25mM Tris, 192mM Glycine, 0.1% SDS), maintained at 4°C with the aid of a Labcon CPE 50 circulator.

The resultant SDS-PAGE gel was stained with Coomassie blue (0.05% Coomassie Brilliant Blue R-250 (w/v), 25% Isopropanol (v/v), 10% acetic acid (v/v)) overnight and

destained in 10% acetic acid and 10% methanol for two hours and then 10% acetic acid overnight. The gel was photographed using the GeneSnap GeneGenius Geldoc scanning system.

The amount of recombinant protein eluted was determined relative to a bovine serum albumin (BSA) standard. The processed sample was loaded onto a gel with a series of solubilized BSA standards of 100ng, 200ng, 300ng, 400ng and 500ng. The Coomassie Brilliant Blue stained gel was scanned and the area of the BSA standard bands quantified using the GeneSnap GeneGenius Geldoc scanning system. From these data a linear BSA standard curve was constructed of peak area versus amount. The peak area of the recombinant protein band was then used to determine its relative amount.

2.9.5 Western blotting

The resolved proteins were transferred from the polyacrylamide gel onto a Hybond^{TM}-C extra nitrocellulose membrane using the liquid transfer method at 35V overnight at 4°C in transblot buffer (25mM Tris, 192mM Glycine, 0.1% (w/v) SDS, 20% (v/v) methanol) (Towbin et al., 1979). The gel, from which the proteins had been transferred, was stained as in section 2.9.4 to detect if any proteins were retained during transfer. The membrane was washed in Tris-buffered saline (TBS) (50mM Tris-HCl, 150mM NaCl, pH 7.5) for five minutes and then stained with Ponceau S (1% Ponceau S, 7% glacial acetic acid), a non-permanent protein stain, to ensure transfer had occurred. The membrane was rinsed in water twice for 5 minutes to remove the Ponceau S stain and then washed in TBS for 10 minutes.

The membrane was placed in either a 3% BSA in TBS blocking solution or QIAgen Anti-His HRP conjugate blocking solution, for the detection of GST-tagged and His-tagged

proteins respectively, for one hour on a shaking platform to cover the membrane to prevent the antibody binding to the nitrocellulose. The membrane was then placed in either a 1:100 000 dilution of anti-GST horse radish peroxidise (HRP)-conjugated primary antibody in 1% BSA in TBS or a 1: 2 000 dilution of anti-His HRP conjugate primary antibody, for GST-tagged and His-tagged proteins respectively, while gently shaking for one hour at room temperature.

The membrane was washed three times in 0.25% Tween-TBS and once in TBS, each for ten minutes on a shaking platform. A volume of 2ml of SuperSignal® West Pico Chemiluminescent Substrate was applied to cover the membrane for 5 minutes before visualization of the chemiluminescent signal using the GeneSnap GeneGenius Geldoc scanning system. After visualization the membrane was stained in amido black (10% acetic acid, 25% isopropanol, 0.1% amido black) for five minutes and then destained for 30 minutes in 10% acetic acid 10% methanol, 30 minutes in 10% acetic acid and then photographed using the GeneSnap GeneGenius Geldoc scanning system.

2.10 Biopanning against *P. falciparum* Phage Display Libraries

Biopanning and the related procedures were conducted according to the Novagen's T7Select® System Manual (Novagen, 2011), with slight modificationsin order to identify binding partners of the putative MDM2/SWIB domains.

2.10.1 BLT5403 cell growth

A 5ml overnight culture of BLT5403 *E. coli* cells in M9LB medium (18.7mM NH_4Cl, 22mM KH_2PO_4, 22mM Na_2HPO_4, 0.4% (w/v) glucose, 1mM $MgSO_4$, in LB) with 50µg/ml ampicillin was set up and used either directly for titering, described in section 2.10.2, or alternatively for phage amplification. In the case of phage amplification, 200µl of the

overnight culture was transferred into 50ml M9LB medium with 50µg/ml ampicillin and incubated at 37°C on a Labotec orbital shaker at 250rpm until log phase (OD_{600} of 0.5 – 0.6) was reached.

2.10.2 Titering

Titering was conducted by the plating assay. A volume of 250µl of BLT5403 *E. coli* cells, grown in M9TB medium and at an OD_{600} of 1, was combined with 100µl of a series of phage lysate dilutions in TBS ranging from 10^{-5} – 10^{-10}. This mixture was combined with 3ml of melted top agarose (1% (w/v) tryptone, 0.5% (w/v) yeast extract, 85.6mM NaCl, 0.6% (w/v) agarose) and plated onto pre-warmed 50µg/ml ampicillin agar plates. Plates were allowed to stand for 10 minutes, for the top agarose to set, and then inverted and incubated for 3-4 hours at 37°C or overnight at room temperature. Resultant plaques were quantified and the titre, multiplicity of infection (MOI) and library size calculated.

$$\textbf{phage titre } \left(\frac{\textbf{pfu}}{\textbf{ml}}\right) = (\text{number of plaques on plate}) \text{ x dilution x } 10$$

Where 10 takes into account the 0.1ml of the dilution plated

$$\textbf{library size (pfu)} = \text{phage titer x total sample volume}$$

2.10.3 Biopanning

Several *P. falciparum* cDNA phage display libraries were used, created by Dr Sonja Lauterbach, Dr Roberto Lanzillotti and Mr Dale Liebenberg in the PMRU. The following screening protocol was employed:

The original phage display library was titered, as described in section 2.10.2, and used at ~$1x10^7$ pfu/ml, in a total volume of 500µl TBS. This solution was mixed with MagneGST

beads bound with at least 8µg of GST for one hour at room temperature on the Intelli-mixer using the F3 function at 25rpm. This pre-screening step facilitated the removal of any phage which bound to the GST protein, the MagneGST beads or any *E. coli* proteins attached to the beads. These background binding beads were removed magnetically and the phage were then mixed with MagneGST beads bound to at least 8µg of recombinant *Pf*MDM2- or *Pf*SWIB-GST proteins and incubated as described above.

The beads were removed magnetically and washed 5 times with 2ml of 0.05% Tween-TBS for 10 minutes with continuous inversion on the Intelli-mixer to remove any non-specifically bound phage. The washed beads were added to 50ml of log phase BLT5403 cells, as described in section 2.10.1, and incubated at 37°C overnight until lysis was noted. Sodium chloride was added to the phage-infected culture, to a final concentration of 0.5M, to further aid in *E. coli* lysis, which was then centrifuged in a Beckman Coulter Avanti ® J-E centrifuge at 10000rpm for 10 minutes. The supernatant was used as the starting library for the next round of biopanning, with 2ml being used for the creation of glycerol stocks, section 2.10.3, and for bateriophage titering, section 2.10.2.

In total, four sequential rounds of biopanning were conducted to enrich for phage binding specifically to the *Pf*MDM2 and *Pf*SWIB proteins. After the final round of titering the resultant plaques were used for PCR analysis.

2.10.4 Bacteriophage glycerol stock and plug extraction

Long term storage of the bacteriophage was facilitated by adding 0.1 volume 80% sterile glycerol to the phage lysate and storing at -70°C. For bacteriophage derived from a plate, plugs were sterilely removed and placed in 1ml extraction buffer (20mM Tris-HCl,

100mM NaCl, 12mM $MgSO_4$, pH 8), incubated at 4°C overnight and then combined with 0.1 volume of 80% sterile glycerol and stored at -70°C.

2.10.5 PCR and sequencing of phage

2.10.5.1 PCR amplification of T7 phage

From a top agarose plate containing individual, well isolated plaques, plugs were sterilely removed and placed in 100µl of 10 mM EDTA, pH 8.0; vortexed briefly and then boiled for 10 minutes. The solution was centrifuged in a 5415R Eppendorf centrifuge at 14000rpm for 3 minutes at 4°C and used for a GoTaq screening PCR.

Phage T7Select10-3b amplification, using T7 promoter and terminator primers (see appendix B for primers)*:*

1. Initial denaturation: 94°C for 2 minutes
2. Denaturation: 94°C for 50 seconds
3. Primer annealing: 50°C for 60 seconds
4. Elongation: 72°C for 60 seconds
5. Repeat steps 2 to 4 thirty five times
6. Final extension: 72°C for 6 minutes

The resultant products were separated by agarose gel electrophoresis for 1 hour against a mixed range base pair ladder, as described in section 2.3.2.2. The empty cassette PCR product was 216bp and plaque PCR products ≥ 300bp were sent for sequencing at Inqaba Biotec™, South Africa.

2.11 *In vitro* binding assays

In vitro binding assays were conducted in order to confirm the interactions identified using biopanning, described in section 2.10. The eluted His- and GST-tagged proteins were

dialysed against three changes of their respective binding buffers or TBS, depending on whether they were to be reattached to the magnetic beads or remain in solution, using a Slide-A-Lyzer MINI dialysis unit (molecular weight cut off of 10kDa), at 4°C for 30 minutes. An amount of 1µg of dialysed recombinant His-fusion *Pf*LisH and *Pf*ARK proteins, reattached to 5µl MagneHis beads, were exposed to increasing concentrations of their respective GST-tagged binding partners for 1 hour at room temperature on a rotating Intelli-mixer platform at 45rpm in a total volume of 150µl TBS. The beads were collected with a magnetic particle separator and rinsed twice in 1ml TBS for 5 minutes with vigorous rocking on an Intelli-mixer platform (90°, 90rpm). The protein complexes on the beads were solubilised, electrophoresed and stained as described in section 2.9.4. Control reactions were conducted as described above using equivalent amounts of recombinant GST protein as well heat denatured (70°C for 15 minutes) SWIB/MDM2 proteins, to account for non-specific binding.

The reactions were also conducted in a reciprocal fashion, whereby dialysed recombinant GST-fusion *Pf*SWIB and *Pf*MDM2 proteins were reattached to MagneGST beads and exposed to increasing concentrations of their respective His-tagged binding partners. This interaction was assessed by western blotting as described in section 2.9.5.

2.12 Creation of transgenic *Plasmodium falciparum* lines

2.12.1 Preparation of constructs

A scraping of a glycerol stock of transformed XL10 cells, containing the appropriate vector construct as described in section 2.7, was added to 5ml of LB containing 100µg/ml ampicillin. The culture was incubated for 8 hours on a Labotec orbital shaker at 37°C at 250rpm. A 1ml volume of this starter culture was transferred to two flasks of 250ml LB containing 100µg/ml ampicillin and incubated overnight as described before. The cultures

were used for the plasmid DNA preparation protocol if the OD_{600nm} was ≥3. The NucleoBond® Xtra Maxi Plus plasmid DNA preparation kit was used according to the manufacturer's specifications and the plasmid construct was eluted into 1ml of the provided Tris buffer. A 1 in 10 dilution of the eluted construct was digested with FastDigest® *Eco*RV, as specified by the manufacturer's instructions, and quantified by agarose gel electrophoresis for 1 hour against a mixed range base pair standard, as described in section 2.3.2.2.

A minimum of 100µg plasmid DNA was used for each transfection. To 1ml elution 1ml 1:1 phenol:chloroform was added, mixed and then centrifuged in a 5415R Eppendorf centrifuge at 16 000rpm for 5 minutes at 4°C. The aqueous phase was collected and transferred into a new tube to which 1ml of chloroform was added, mixed and then centrifuged in a 5415R Eppendorf centrifuge at 16 000rpm for 5 minutes at 4°C. The aqueous phase was collected and divided into ~450µl aliquots, in two new 2ml Eppendorf tubes. To each tube 45µl 3M sodium acetate, and 1125µl 100 % ethanol was added. The plasmid DNA was precipitated at -70 °C overnight and was then centrifuged in a 5415R Eppendorf centrifuge at 16 000rpm at 4°C for 30 minutes. The supernatant was decanted and the pellet was washed in 70% ethanol and centrifuged in a 5415R Eppendorf centrifuge at 16 000rpm at 4 °C for 5 minutes. The pellet was allowed to air-dry in a sterile flow hood and resuspended in 30µl sterile TE buffer, to be used for the transfection.

2.12.2 Transfection of *P. falciparum*

The following method was conducted under sterile conditions. The 30µl plasmid DNA was added to 370µl pre-warmed cytomix (120mM KCl, 0.15mM $CaCl_2$, 8.7mM K_2HPO_4, 1.3mM KH_2PO_4, 25mM Hepes, 2mM EGTA, 5mM $MgCl_2$, pH 7.6) and 200µl packed, unwashed RBC in a 1ml Eppendorf tube. The solution was transferred to a 2 mm BioRad

Gene Pulser® Cuvette and electroporated using the Bio-Rad GenePulse Xcell™ electrophorator, at 310 V, with a resistance of 950 μF and a time of less than 15 milliseconds. The RBC were then added to a 25cm^3 culturing flask with 5ml of complete medium and a 1% parasitaemia of synchronized ring stage parasites. The flask was gassed, sealed and incubated as described in section 2.2.2.

From the next day (day one) the medium was changed daily, as described in section 2.2.2, with stock 10μM WR99210 drug, suspended in DMSO, being added to the culture, at a final concentration of 2nM, from day two. The parasites which had taken up the pARL2-GFP construct would carry the human dihydrofolate reductase (hDHFR) gene, providing resistance to WR99210, and thus survive the drug treatment (Fidock and Wellems, 1997). The parasites were cultured daily, in the presence of the drug, until no parasites were detected; after which the culturing protocol was implemented only every second day. Once parasites, containing the vector construct, were visible, daily culturing resumed, still in the presence of the drug. Glycerol stocks were subsequently prepared for the transgenic parasites, as described in section 2.2.4. A control transgenic line was donated by Dr Belinda Bezuidenhout towards this study, which expressed GFP alone.

2.12.3 Verification of transgenic lines

2.12.3.1 Verification by detection of GFP fluorescence in living transgenic parasites

A volume of 300μl of a mixed culture, with a parasitaemia of about 3%, was suspended in 700μl incomplete medium to which 5mg/ml stock DAPI suspended in water, at a final concentration of 0.2μg/ml, or 1mg/ml stock Hoechst 33258 pentahydrate suspended in water, at a final concentration of 6μg/ml, was added and incubated for 5 minutes at room temperature or 2 hours at 37°C respectively, to identify the parasite nucleus. The sample was centrifuged in a 5415R Eppendorf centrifuge at 3300rpm for 3 minutes at 4°C and the

supernatant was removed. The pRBC were washed by gentle resuspension in incomplete medium and then centrifugation in a 5415R Eppendorf centrifuge at 2500rpm for 3 minutes at 4°C. This step was repeated, after which the pRBC were resuspended in 200µl incomplete medium.

A volume of 5µl of the stained cell suspension was placed on a clean microscope slide, mounted with a cover slip and viewed at 1000x magnification, using the BX41 Olympus Microscope system. The system included the following features – an U-MWU2 filter (excitation between 330-385nm and emission above 410nm, for DAPI visualization), an U-MWB2 filter (excitation between 460-490nm and an emission above 510nm, for GFP visualization), a U-25ND25 Olympus neutral density filter, an Olympus DP72 camera; and CellSense Dimensions 1.7 Software.

2.12.3.2 PCR verification of plasmid

Once parasites were observed and the parasitaemia had increased to ≥4% trophozoites parasite DNA was extracted (Tirasophon *et al.*, 1991, Vu *et al.*, 1995). A volume of 1ml of resuspended culture was centrifuged in a 5702R Eppendorf centrifuge at 1400rpm for 5 minutes at room temperature. The supernatant was removed and the pellet resuspended in 100µl quick lysis buffer (34mM NaCl, 1% Triton-X-100, 1.2mM EDTA), vortexed vigorously and centrifuged in a 5702R Eppendorf centrifuge at 16000rpm for 10 minutes at room temperature. The following step was repeated twice, whereby the supernatant was removed and the pellet resuspended in 100µl quick boiling buffer (10mM Tris-HCl, 50mM KCl, pH 8.3), vortexed vigorously and centrifuged in a 5702R Eppendorf centrifuge at 16000rpm for 10 minutes at room temperature. The supernatant was removed and the pellet was resuspended in 100µl quick PCR buffer (10mM Tris-HCl, 50mM KCl, 3mM $MgCl_2$, pH 8.8) and boiled for 10 minutes. A volume of 200µl of 1:1 phenol:chloroform

was added, mixed and then centrifuged at 13200rpm for 5 minutes at 4°C. The aqueous phase was collected and transferred into a new tube to which 100µl of chloroform was added, mixed and then centrifuged at 16000rpm for 5 minutes at 4°C. The aqueous phase was collected and stored at 4°C in a new 1.5ml Eppendorf tube.

PCR was conducted using the pARL2-GFP vector specific primers (see appendix B), as the endogenous genes would be amplified by the gene specific primers.

2.13 Localization of fluorescently tagged *P. falciparum* proteins

2.13.1 Localization studies using fixed transgenic parasite and anti-EBA175 antibodies

A volume of 2.5ml of a mixed culture, with a parasitaemia of at least 3% late stage parasites, was prepared for analysis (Tonkin *et al.*, 2004). The aliquot of culture was centrifuged in a 5415R Eppendorf centrifuge at 2500rpm for 3 minutes at 4°C, the supernatant removed and the pRBC pellet was washed by gentle resuspension in PBS followed by centrifugation as before. The supernatant was removed and the pRBC pellet fixed in 2ml of fixing solution (4% electron microscopy grade formaldehyde and 0.0075% electron microscopy grade glutaraldehyde in PBS) for 30 min. The pRBC were washed as described above and the pRBC pellet was resuspended in permeabilization solution (0.1% TritonX-100 in PBS) for 10 minutes. The cells were washed again although from this point on wash steps involved centrifugation in a 5415R Eppendorf centrifuge at 16000rpm for 3 minutes at 4°C. The pRBC pellet was treated with 2ml of 0.1 mg/ml sodium borohydride ($NaBH_4$) in PBS for 10 minutes to remove any free aldehyde groups. The cells were washed, as described above, resuspended in 3% BSA in PBS blocking solution for one hour. The cells were washed and then exposed to 1ml of 3% BSA in PBS with 1:500 anti-GFP rabbit antibody Alexa Fluor® 488 Conjugate and 1:1000 erythrocyte binding antigen – 175 (EBA-175) mouse primary antibody for one hour, and then washed three times,

whereby the cells were resuspended and incubated in 1ml PBS for 10 minute on a rotating Intelli-Mixer platform at 12rpm and then centrifuged for 10 minutes in a 5415R Eppendorf centrifuge at 16000rpm at 4°C and the supernatant removed. The pRBC pellet was resuspended in 250µl of 3% BSA in PBS with 5µg/ml Alexa Fluor® 594 Goat Anti-Mouse antibody and a final concentration of 0.2µg/ml DAPI, and then washed three times, as described before with 10 minute incubation and centrifugation steps. The resultant cell pellet was resuspended in 20µl PBS, of which 5µl was viewed with a BX41 Olympus Microscope and an Olympus DP72 camera as described in section 2.13.1, with the additional use of the 49306 filter (excitation between 567 – 596nm and emission between 609 – 640nm) to visualize the Alexa Fluor® 594 antibody.

2.13.2 Mitochondrial localization studies using live transgenic parasites

MitoTracker, a fluorescent mitochondrial stain that accumulates in the active mitochondria of a cell (Molecular Probes, 2008), has previously been used in *P. falciparum* (Tonkin *et al.*, 2004). However, MitoTracker Green FM has an identical excitation and emission spectrum as GFP and therefore MitoSOX™ Red mitochondrial superoxide indicator had to be used. This stain is selectively targeted to the mitochondria of living cells and then oxidized by mitochondrial superoxides into a fluorescent form (Molecular Probes, 2005). No previous work regarding the use of MitoSOX™ in *P. falciparum* has been published to date although the mitochondrion of *P. falciparum* has been shown to have superoxides (Torrentino-Madamet *et al.*, 2010). Therefore the localization of MitoSOX™ was compared to that of MitoTracker Green FM in control parasites to confirm the specificity of MitoSOX™.

Lyophilized MitoTracker Green FM and MitoSOX™ were dissolved in dimethylsulfoxide to prepare 1mM and 5mM stock solutions respectively. Aliquots of the MitoTracker Green FM and MitoSOX™, at a final concentration of 20nM and 0.5µM respectively, were added

to 300µl of wild type 3D7 *P. falciparum* parasites, with a parasitaemia of about 3%, suspended in 700µl incomplete medium and incubated for 15 minutes at 37°C. Cells were washed twice by resuspension in 1ml incomplete medium and centrifugation in a 5415R Eppendorf centrifuge at 2500rpm for 3 minutes at room temperature, with the supernatant removed by aspiration. Nuclear staining was then conducted and the parasites visualized as described in section 2.13.1, with the additional use of the U-MWG2 filter (excitation between 510 – 550nm and emission maximum at 590nm, for MitoSOX^{TM} visualization) and the MWB2 filter (excitation between 460-490nm and an emission above 510nm, for MitoTracker Green FM visualization). The MitoSOX^{TM} stain can only be used for live cell imaging and could not be used in conjunction with the fixation protocol (Molecular Probes, 2005).

2.14 PCD induction by elevated temperatures

Previous work has indicated that exposing *P. falciparum* parasites to 41°C, a temperature equivalent to malaria-induced febrile illness, induces a time-dependent apoptosis-like death mechanism (Oakley *et al.*, 2007, Engelbrecht and Coetzer, 2013). One percent synchronized ring and trophozoite stage transgenic parasites were exposed to 41°C for 2 hours and then returned to 37°C. The parasites were viewed immediately and then at set time points (2, 4 and 24 hours later) by fluorescence microscopy as described in sections 2.13.1 and 2.13.2.

2.15 Tetramerization assay

The ability of the *Pf*p53 protein to form oligomers was assessed using previously documented protocols (Payne, 1973, Stenger *et al.*, 1992, Wang *et al.*, 1994), whereby low concentrations of glutaraldehyde were employed as a protein cross-linking agent (Payne,

1973). Initial verification was conducted with BSA in 0.1M sodium phosphate buffer (0.1M Na_2HPO_4/NaH_2PO_4 pH 7.5) and GST-elution buffer. Subsequently the assay was employed on the GST-*Pf*p53 protein, both in the GST-elution buffer and the electrophoretic mobility shift assay (EMSA) binding buffer (20mM HEPES, 1mM EDTA, 10mM $(NH_4)_2SO_4$, 1mM DTT, 30mM KCl, 0.2% Tween 20). Glutaraldehyde, at a final concentration of 0.02%, was added to the samples while vortexing for 1 minute. The samples were incubated at room temperature for 2 hours and then solubilized and assessed by SDS-PAGE and western blotting as described in section 2.9.4 and 2.9.5 respectively, as well as on an exponential gradient Fairbanks gel with silver staining as described in section 2.15.1 and 2.15.2 respectively. Control assays were conducted on purified GST protein to determine the influence of GST on oligomerization.

2.15.1 3.5-17.5% exponential gradient Fairbanks gel

A 10 well, 16cm x 18cm 3.5-17.5% exponential gradient Fairbanks SDS polyacrylamide gel was poured, as described in table 2.4, and allowed to polymerize at room temperature (Fairbanks *et al.*, 1971). The tetramerization samples were loaded and gel was electrophoresed in the Hoefer SE 400 Sturdier™ Air-Cooled Vertical Electrophoresis System at a constant voltage of 45V in Fairbanks running buffer (40mM Tris, 20mM $C_2H_3NaO_2$, 2mM EDTA, 0.1% (w/v) SDS, pH7.5) for 17 hours.

Table 2.4: Fairbanks SDS polyacrylamide gel.

Reagent	3.5%	17.5%
40% Acrylamide and 1.5% Bis-acrylamid solution	3ml (Final acrylamide concentration 3.5%; bis-acrylamide 0.13%)	3.4ml (Final acrylamide concentration 17.5%; bis-acrylamide 0.6%)
10X TAE buffer (400mM Tris, 200mM $C_2H_3NaO_2$, 20mM EDTA, pH 7.4)	3.4ml (Final concentrations 40mM Tris, 20mM $C_2H_3NaO_2$, 2mM EDTA)	0.8ml (Final concentrations 40mM Tris, 20mM $C_2H_3NaO_2$, 2mM EDTA)
10% (w/v) SDS	0.68ml (Final concentration 0.2%)	0.16ml (Final concentration 0.2%)
MilliQ water	26.9ml	1.62ml
25% Glycerol	-	2ml (Final concentration 6%)
10% (w/v) fresh ammonium persulphate	0.4ml (Final concentration 0.1%)	0.02ml (Final concentration 0.02%)
TEMED	11µl	-
0.5% TEMED	-	0.5ml
Final volume	34.4ml	8.5ml

2.15.2 Silver staining

Silver staining of polyacrylamide gels was conducted according to a previously described protocol (Porro *et al.*, 1982). The gel was fixed in 50% ethanol, 12% acetic acid, 0.02% formaldehyde, washed 3x for 20 minutes with 50% ethanol and then treated for 1 minute with 0.01% (w/v) sodium thiosulfate ($Na_2S_2O_3$). Three sets of 20 second washes in water were conducted, after which the gel was stained for 30 minutes in 0.1% (w/v) silver nitrate ($AgNO_3$) and washed again with water as before. The bands of interest were developed in 3% (w/v) Na_2CO_3, 0.0002% $Na_2S_2O_3$ and the reaction was stopped with 25mM EDTA, pH 8.

2.16 Electrophoretic mobility shift assay

The EMSA is based on the principle that during electrophoresis an oligonucleotide would migrate at a faster rate when alone relative to it being bound by a protein, which would retard its movement (Hellman and Fried, 2007). Commonly radioisotope-labelled

oligonucleotides are used in this assay due to the high sensitivity they confer during detection (Hellman and Fried, 2007). In this study the DNA binding ability of *Pf*p53 was determined using an EMSA and the Digoxigenin (DIG) Gel Shift Kit, 2nd generation, as specified by the manufacturer.

2.16.1 Oligonucleotide annealing and labelling

Complementary p53 consensus sequence oligonucleotides (*P. falciparum* specific sequence: 5'-AAACATGCTTTTAAAAACAAGCTT-3') (El-Deiry *et al.*, 1992) were mixed in equal concentrations and annealed by heating for 10 minutes at 95°C and subsequent slow cooling to room temperature. One hundred ng of the double stranded oligonucleotides were labelled with DIG in a 25µl kit labelling reaction at 37°C for 1 hour. Labelling efficiency was conducted using the DIG visualization protocol, as described in section 2.16.2, against a DIG-labelled control.

2.16.2 Electrophoretic mobility shift assay

The electrophoretic mobility shift assay (EMSA) was conducted according to the kit specifications in the EMSA binding buffer, described in section 2.15, in the presence of 0.1µg poly-L-lysine, a basic protein which enhances the DNA binding of some proteins. The kit control reaction and a GST control reaction were included in each experiment, to ensure the assay was working correctly and to ensure the absence of non-specific GST DNA binding, respectively.

The 20µl assay was incubated for 20 minutes at room temperature in the presence of various amounts of labelled p53 oligonucleotides – 4, 2 and 0.8ng per reaction, and dialysed GST-*Pf*p53 protein – ~50ng, ~100ng, ~150ng, ~200ng and ~300ng per reaction. The specificity of DNA binding was evaluated in the presence of 10- and 100-fold excess

of unlabelled competitor p53 oligonucleotide as well as 100-fold excess of a random, unlabelled oligonucleotide sequence (5'-ATATTTGAGAACTGGATGAACAGA-3').

The reactions were then separated on 9cm 6% native polyacrylamide gels as well as 9cm 3.5 – 5% native polyacrylamide linear gradient gels in a Mighty Small II SE250 gel system, constituted as described in table 2.5.

Table 2.5: Constituents of a 6% polyacrylamide native gel.

Reagent	Volume
MilliQ water	2.655ml
1X TBE buffer (89mM Tris, 89mM Boric acid, 2mM EDTA pH 8)	2.75ml (Final concentration 0.25xTBE)
1% (w/v) Bis-acrylamide	3.3ml (Final concentration 0.3%)
30% (w/v) Acrylamide	2.2ml (Final concentration 6%)
10% (w/v) fresh ammonium persulphate	75µl (Final concentration 0.07%)
TEMED	20µl
Final volume	11.0ml

The wells were washed thoroughly and the 6% and 3.5-5% linear gradient gels were pre-electrophoresed at 160V and 50V respectively to remove any residual ammonium persulphate. Samples were then electrophoresed at 100V and 70V respectively in 0.25x TBE buffer, maintained at 4°C with the aid of a Labcon CPE 50 circulator, until the dye front reached the bottom of the gel. Electro-blotting was performed in 0.5x TBE buffer at 400mA for 45mins using Hybond^{TM}-N nylon membrane. The membrane was placed in SSC buffer (0.3M NaCl, 30mM sodium citrate, pH 7) and exposed to UV radiation for 5 minutes to crosslink the oligonucleotides to the membrane.

The membrane was rinsed for 5 minutes in DIG washing buffer (0.1M Maleic acid, 0.15M NaCl, 0.3% Tween 20, pH 7.5), incubated for 30 minutes in 100ml of 1x DIG blocking

buffer (1g DIG blocking buffer into 100ml Maleic acid buffer (0.1M Maleic acid, 0.15M NaCl, pH 7.5)) and then exposed to 20ml of 1:10 000 Anti-DIG-alkaline phosphatase antibody in 1x DIG blocking buffer for 30 minutes. The membrane was then rinsed twice for 15 minutes in DIG washing buffer, equilibrated in DIG detection buffer (0.1M Tris-HCl, 0.1M NaCl, pH9.5) for 5 minutes before being overlayed with 2ml of the 25mM chemiluminescent substrate CDP-star for 5 minutes. Excess substrate was removed and the signal visualized using the GeneSnap GeneGenius Geldoc scanning system.

3 RESULTS

3.1 Analysis of *P. falciparum* SWIB/MDM2 homologues

3.1.1 Identification of SWIB/MDM2 genes

The *Pf*MDM2 gene (PF3D7_0518200) is annotated as coding for a protein of unknown function, containing a putative SWIB/MDM2 domain (Arambage *et al.*, 2009), previously identified by Dr Pierre Durand (Coetzer *et al.*, 2010). The gene is located on the negative strand (Crick orientation) of chromosome 5 from base 758,503 to 758,898 and lacks introns (Aurrecoechea *et al.*, 2009). The C-terminal SWIB/MDM2 domain comprises almost all of the 131 amino acid protein, with no other functional domains ascribed to the protein, as depicted in figure 3.1 (Aurrecoechea *et al.*, 2009).

The genome also encodes the *Pf*SWIB gene (PF3D7_0611400), annotated as a SWI/SNF-related matrix-associated actin-dependent regulator of chromatin, with a SWIB/MDM2 domain towards the N terminus of the corresponding protein (Figure 3.1). The single exon gene is located on the negative strand (Crick orientation) of chromosome 6 from base 471,658 to 474,150 (Aurrecoechea *et al.*, 2009).

3.1.1.1 Primary sequence alignments for PfMDM2 and PfSWIB

Two broad groups of SWIB/MDM2 domains have been identified. The first group is involved in p53 binding and identified in MDM2 proteins, thus this group will be designated as group M within this study. The second group is identified in a variety of eukaryotic proteins and participates in chromatin remodelling, transcriptional regulation and unknown functions. This group will be designated as group C. Primary sequence analysis was conducted to determine the group to which each parasite SWIB/MDM2 homologue would belong. Clustal Omega alignments, presented in figure 3.2, revealed a highly conserved sequence for a wide range of vertebrate (fish to mammal) group M

homologues. This feature was only partially extended to the SWIB/MDM2 domains of the two *P. falciparum* proteins.

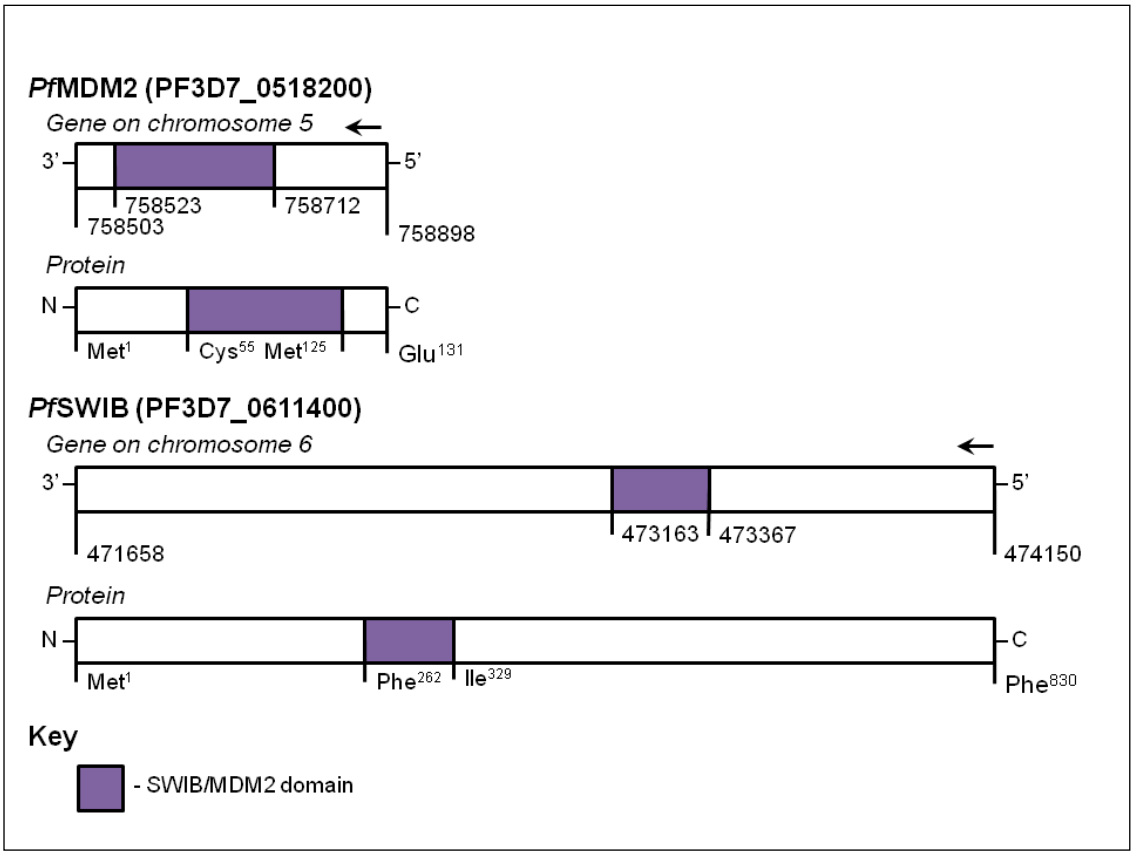

Figure 3.1: Diagrammatic representation of the two *P. falciparum* SWIB/MDM2 homologues (derived from Aurrecoechea *et al.*, 2009).
The numbers represent nucleotide positions situated along the respective chromosomes while the arrows indicate transcriptional direction for the genes.

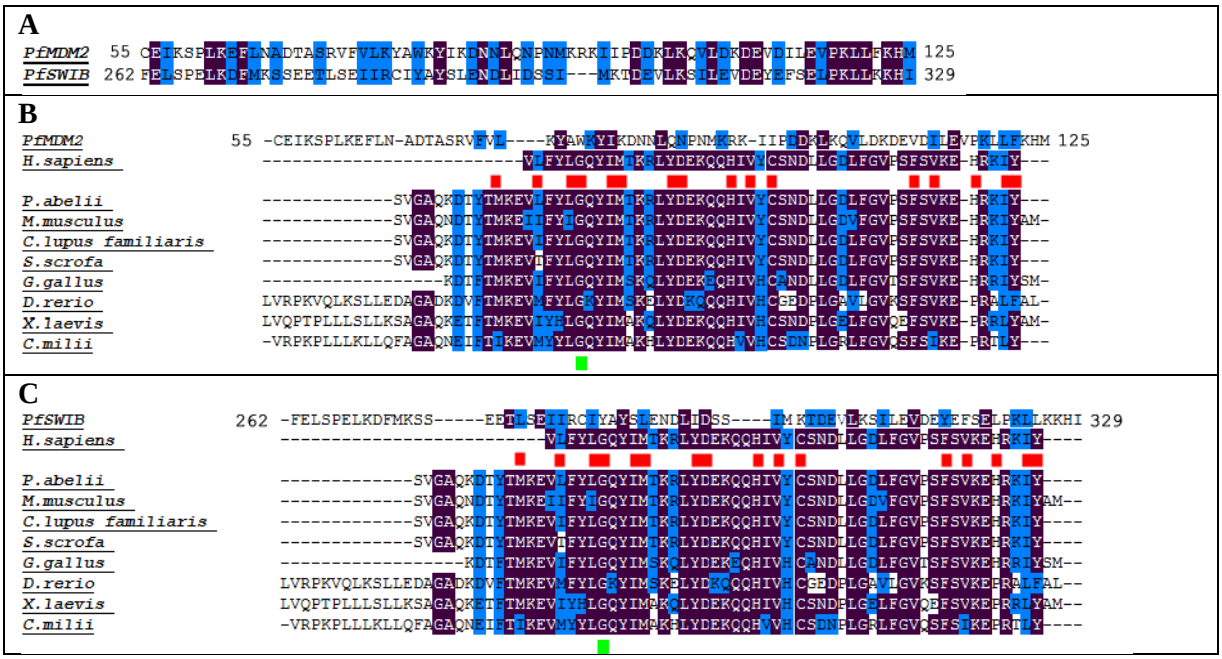

Figure 3.2: Clustal Omega primary amino acid sequence alignments for *Pf*MDM2 and *Pf*SWIB against each other and group M SWIB/MDM2 domains.
A) Alignment of *Pf*MDM2 to *Pf*SWIB. In relation to each other the two domains have 28.2% identity and 57.7% similarity.
B) Alignment of *Pf*MDM2 to group M SWIB/MDM2 domains.
C) Alignment of *Pf*SWIB to group M SWIB/MDM2 domains.
The high degree of conservation between Group M SWIB/MDM2 domains was only partly extended to the two parasite domains. The red blocks indicate critical amino acid residues for p53 binding (Kussie *et al.*, 1996; Freedman *et al.*, 1997), which show limited conservation in the two parasite domains. The green block indicates a conserved Gly residue identified in all group M domains. Purple blocks indicate identical amino acids; blue blocks indicate similar amino acids; threshold set at 80%.

Binding of MDM2 to p53 is mainly the result of van der Waals forces, facilitated by a high proportion of aromatic and hydrophobic residues within the SWIB/MDM2 domain (Kussie *et al.*, 1996, Freedman *et al.*, 1997) – 46.8% in humans for example. The *P. falciparum* SWIB/MDM2 domains have a slightly lower hydrophobic and aromatic amino acid residue composition (39.4% for *Pf*MDM2 and 40.6% for *Pf*SWIB). Of the 16 residues marked as critical for p53 binding in figure 3.2, only one is identical in each *P. falciparum* protein – Ile^{83} in *Pf*MDM2 and Asp^{297} in *Pf*SWIB. There are five residues (Leu^{76}, Asn^{90}, Ile^{114}, Leu^{121} and Phe^{122}) and seven residues (Leu^{279}, Ile^{283}, Ile^{286}, Leu^{291}, Ile^{300}, Tyr^{316} and Leu^{324}) for *Pf*MDM2 and *Pf*SWIB respectively that show semi-conservation to the critical p53 binding residues of the human MDM2 protein. The *P. falciparum* homologues could

deviate in essential amino acids due to potential sequence and structural differences in their binding partner(s), relative to the human p53 protein. Several residues within group M domains, not involved in direct p53 binding, are also identical in both parasite SWIB/MDM2 domains (Tyr^{78}, Leu^{88}, Asp^{101}, Leu^{103} and Glu^{116} for *Pf*MDM2, and Thr^{278}, Glu^{281}, Tyr^{289}, Leu^{295}, Leu^{307}, Val^{313} and Glu^{320} for *Pf*SWIB). Roughly half of these identical residues are hydrophobic and/or aromatic and possibly participate in creating a suitable environment for protein-protein interactions.

The SWIB/MDM2 domains of *Pf*MDM2 and *Pf*SWIB were also compared to group C SWIB/MDM2 domains, identified within a wide range of unicellular and multicellular eukaryotic proteins ranging from *Toxoplasma* to humans (figure 3.3). The residues which are critical for function are unknown, although there is a high proportion of hydrophobic and aromatic amino acid residues. Eight residues were identical in *Pf*MDM2 (Leu^{61}, Arg^{72}, Trp^{80}, Tyr^{82}, Ile^{83}, Lys^{84}, Leu^{88}, Gln^{89} and Asp^{100}) and one was semi-conserved (Ile^{57}). In the case of *Pf*SWIB, six of residues were identical (Leu^{265}, Leu^{269}, Tyr^{290}, Leu^{296}, Asp^{298}, and Asp^{305}) and one was semi-conserved (Tyr^{288}) relative to other group C SWIB/MDM2 domains.

Although the function is unknown, all group C SWIB/MDM2 domains contain a conserved Trp residue. This was identical for *Pf*MDM2 (Trp^{80} marked in green in figure 3.3) relative other group C SWIB/MDM2 domains. In group M SWIB/MDM2 domains, this residue has been converted to a Gly (marked in green in figure 3.2) and plays a critical role in p53 binding (Bennett-Lovsey *et al.*, 2002). The *Pf*SWIB domain did not have the Trp or Gly residue but instead a different aromatic residue – Tyr^{288}.

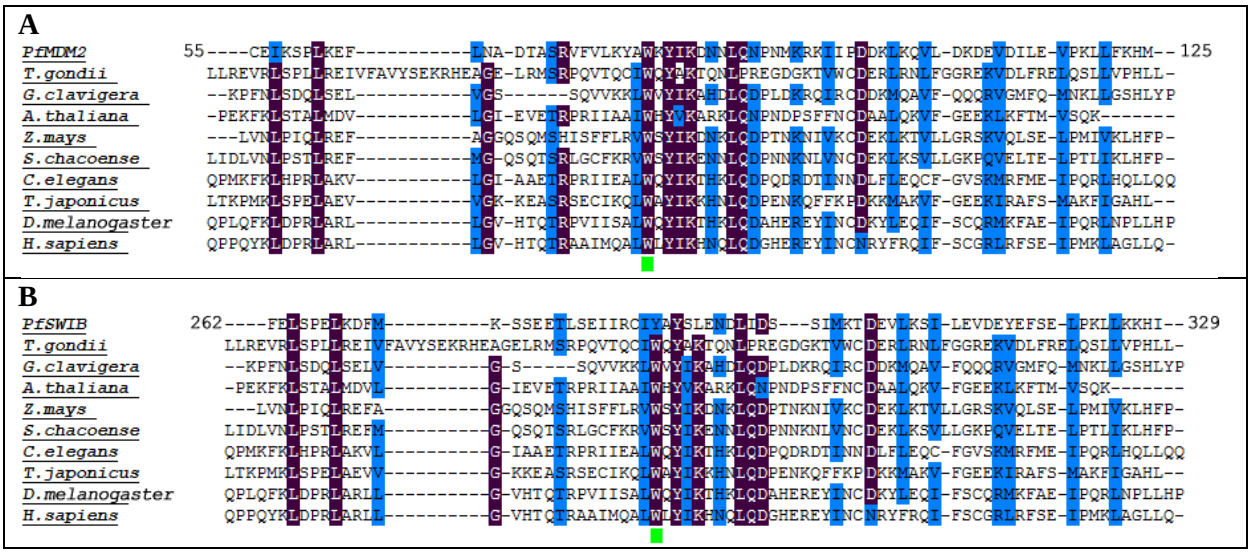

Figure 3.3: Clustal Omega primary amino acid sequence alignments for *Pf*MDM2 and *Pf*SWIB against group C SWIB/MDM2 domains.
A) Alignment of *Pf*MDM2 to group C SWIB/MDM2 domains.
B) Alignment of *Pf*SWIB to group C SWIB/MDM2 domains.
A similar degree of conservation was documented between group C SWIB/MDM2 domains and the two *P. falciparum* domains. The green block highlights a previously described group C conserved Trp residue (Bennett-Lovsey *et al*., 2002). Purple blocks indicate identical amino acids; blue blocks indicate similar amino acids; threshold set at 80%.

Primary sequence identity and similarity were calculated using EMBOSS Needle analysis, relative to *Pf*MDM2 and *Pf*SWIB, for representative members of group M (the SWIB/MDM2 domain of the *H. sapiens* MDM2 protein and the *X. laevis* E3 ubiquitin-protein ligase MDM2 protein) and group C (the *A. thaliana* SWI/SNF complex component SNF12 homolog, the *D. melanogaster* Brahma associated protein 60kD and the *H. sapiens* SWI/SNF-related matrix-associated actin-dependent regulator of chromatin subfamily D) homologues. As documented in tables 3.1 and 3.2, both *P. falciparum* SWIB/MDM2 domains demonstrated a greater sequence identity and similarity to group C SWIB/MDM2 homologues, in particular to the *H. sapiens* group C member.

Table 3.1: EMBOSS needle analysis for *Pf*MDM2 relative to representative SWIB/MDM2 domains.

Organism of comparison	SWIB/MDM2 homologue Group	Percentage identity (%)	Percentage similarity (%)
H. sapiens	M	16.7	25.6
X. laevis	M	17.5	35.0
A. thaliana	C	18.1	36.1
D. melanogaster	C	22.1	42.9
H. sapiens	C	23.4	48.1

Table 3.2: EMBOSS needle analysis for *Pf*SWIB relative to representative SWIB/MDM2 domains.

Organism of comparison	SWIB/MDM2 homologue Group	Percentage identity (%)	Percentage similarity (%)
H. sapiens	M	9.7	26.4
X. laevis	M	19.2	38.5
A. thaliana	C	24.0	40.0
D. melanogaster	C	22.1	41.6
H. sapiens	C	24.7	42.9

Sequence similarity was greater than identity in all these alignments. Logically, greater sequence similarity, relative to identity, correlates to a greater likelihood of homology as certain residue exchanges may have little or no effect on tertiary structure and/or protein function (Rost, 1999). Protein structure, as opposed to sequence, often shows greater conservation during evolution and was therefore characterized for both *P. falciparum* SWIB/MDM2 homologues (Rost, 1999, Geourjon *et al.*, 2001).

3.1.1.2 Secondary structure predictions for PfMDM2 and PfSWIB are rich in helices

Secondary structure predictions and tertiary structure analyses (section 3.1.1.3), were conducted with the aid of group C and M domains for which crystallized structures were available (figure 3.3). These included the following group M homologues:

- The SWIB/MDM2 domain of the *H. sapiens* MDM2 protein (PBD id: 2VG2) (Sakurai *et al.*, 2006)

- The SWIB/MDM2 domain of the *X. laevis* E3 ubiquitin-protein ligase MDM2 protein (PDB id: 1YCQ) (Kussie *et al.,* 1996)

The following C homologues were used:

- The SWIB/MDM2 domain of the *A. thaliana* SWI/SNF complex component SNF12-like protein At5g14170 (PBD id: 1V31) (Yoneyama *et al.,* 2004b)
- The SWIB/MDM2 domain of the *M. musculus* SWI/SNF-related matrix-associated actin-dependent regulator of chromatin subfamily D member 1 protein (PBD id: 1UHR) (Yamada *et al.,* 2004)

Predicted secondary structure analyses and comparisons were of importance as they, in contrast to crystal structures, may show greater similarities between distantly related domains (Geourjon *et al.,* 2001). Overall, a specific secondary structure was deemed probable in areas where three or more algorithms predicted the same topology. It was assumed that one or two residues predicted as alpha helices would not contribute towards the overall tertiary structure of the domain but beta-strands conmposed of two residues would participate in the formation of beta-sheets, based on crystallized structures (example 1V31 – see section 3.1.1.3). For additional information the group C SWIB/MDM2 domain of the *S. cerevisiae* SNF12 protein was used, which is a unicellular homologue implicated in chromatin remodelling but has no crystal structure.

The secondary structures of the crystallized group M SWIB/MDM2 domains were predicted to fold into two long alpha helical stretches and two to three short beta-sheets with several interspersing random coil regions (figure 3.3A-B). Crystallized group C SWIB/MDM2 domains were very similar, although they had more helical stretches and only a single, short beta-sheet preceding the third helical run (figure 3.3C-D). The regions of random coils are believed to act as hinges or folding areas facilitating the interactions

between the alpha helices and beta-strands and in turn aiding in overall tertiary structure formation (Bennett-Lovsey *et al.*, 2002).

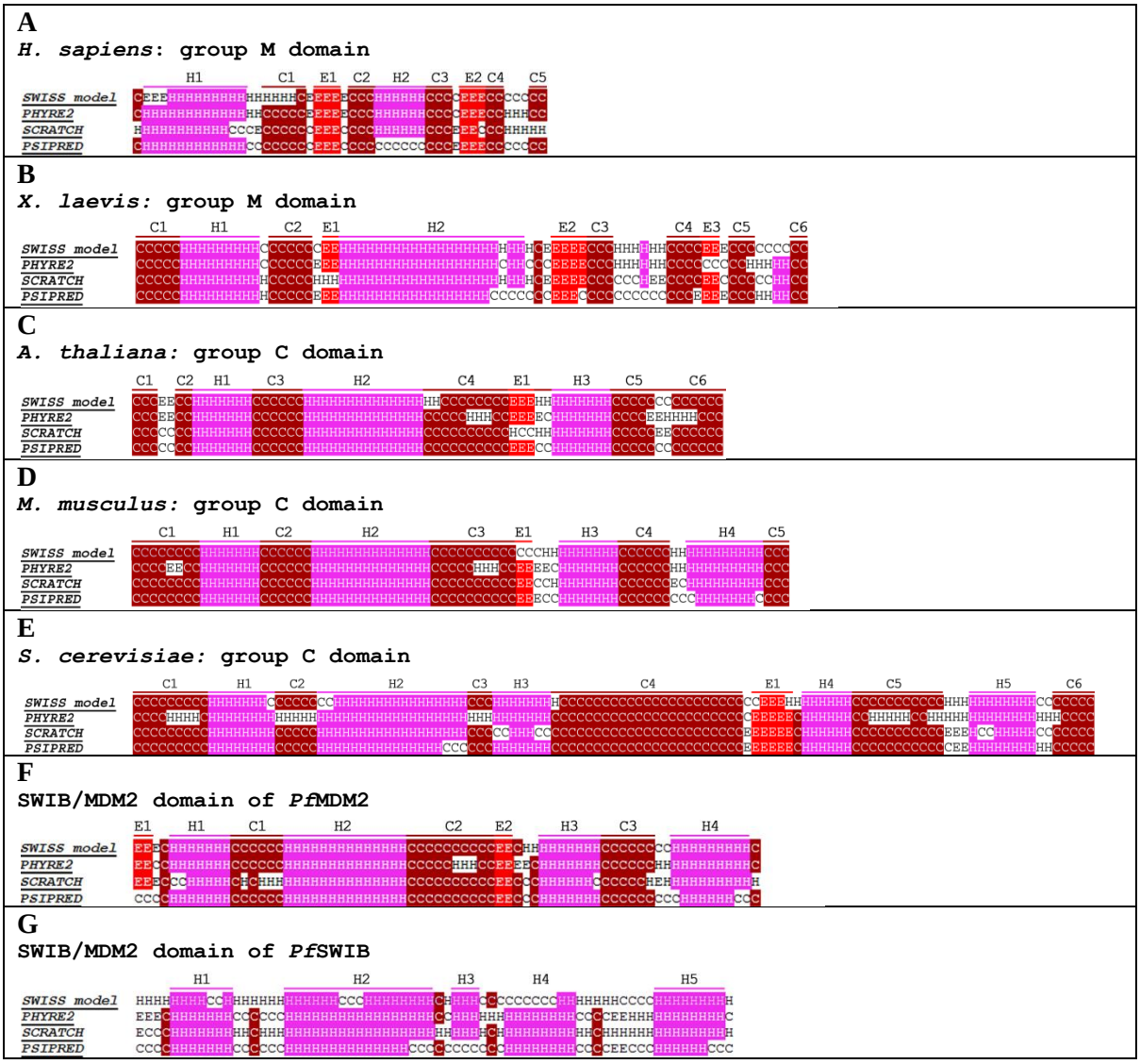

Figure 3.3: Secondary structure predictions for various SWIB/MDM2 domains.
A and B: The two group M SWIB/MDM2 domains analysed were predicted to fold into two long alpha helical stretches and at least two short beta-strands.
C and D: The two group C domains were predicted to fold into at least three long stretches of alpha helices, with the third helical run preceded by a short beta-strand.
The *Pf*MDM2 (F) and *S. cerevisiae* (E) domains conformed to a group C predicted secondary structure, while *Pf*SWIB (G) was rich in alpha helices.
Blocked areas indicate identical predictions by three or more algorithms. C represents random coils; E represents beta-strands; H represents alpha helices. Any unblocked areas represent areas where no secondary structure could be determined.

The overall predicated secondary structure of the *Pf*MDM2 domain was similar to that of the group C domains – rich in helices, with a short beta-strand preceding the third helical

run – but deviated with the presence of an additional, short beta-strand at the N-terminus of the domain (figure 3.3F). The yeast domain was also similar to other group C domains and to the *Pf*MDM2 domain, rich in helices and having only a single beta-strand. This latter structure had an altered spatial location, preceding the fourth helical stretch (figure 3.3 E). As the random coiled region (C3 in figure 3.3E) which separates helical stretch two and three (H2 and H3 in figure 3.3E) is so small, these two helical stretches may actually represent a single unit, explaining the discrepancy in the position of the beta-strand relative to other group C domains.

The *Pf*SWIB domain was mainly helical in nature suggestive of a group C domain, although there was some difficulty in deciding the probable secondary structures in many regions of this protein.

3.1.1.3 Tertiary structure predictions for PfMDM2 and PfSWIB conform to a partial twisted cleft topology

All crystallized SWIB/MDM2 domains, irrespective of their functional roles, show a similar topology, referred to as a twisted cleft, constituted by four alpha helices creating a twisted barrel- or basket-like structure, capped on one or both sides by beta-sheets (figure 3.4 A-E) (Kussie *et al.*, 1996, Bennett-Lovsey *et al.*, 2002, Yamada *et al.*, 2004, Yoneyama *et al.*, 2004b, Yoneyama *et al.*, 2004a, Sakurai *et al.*, 2006). The only exception to this is the SWIB/MDM2 domain of the *H. sapiens* MDM2 protein. Here the complete topology requires an adjacent, neighbouring helix (figure 3.4A) (Sakurai *et al.*, 2006).

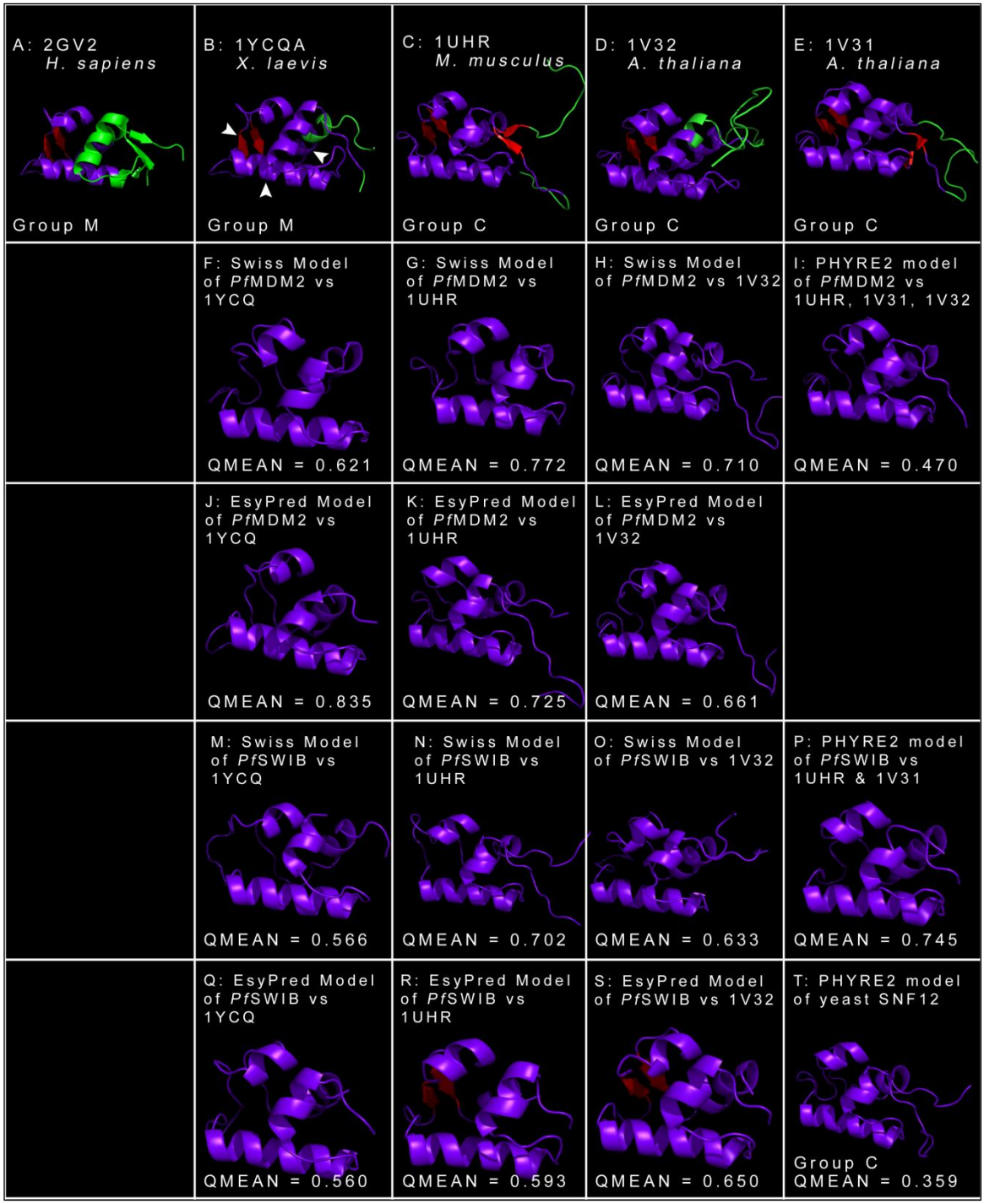

Figure 3.4: Crystallised SWIB/MDM2 domains and various predicted tertiary structures of the SWIB/MDM2 domains of *Pf*MDM2, *Pf*SWIB and the *S. cerevisiae* SNF12 protein.
For descriptions of the crystallized domains refer to section 3.1.1.2 and 3.1.1.3. The purple regions represent the amino acid residues constituting the SWIB/MDM2 domains, as classified by the NCBI database; the red regions denote the beta-sheets in the SWIB/MDM2 domains; and the green regions represent flanking domains in the structures. The white arrows in (B) indicate the three critical folds within the *X. laevis* SWIB/MDM2 domain required for p53 binding – the left beta-sheet, the bottom alpha helix and a rear, almost hidden, alpha helix (Kussie *et al.*, 1996). The modelled structure of the yeast SWIB/MDM2 domain corresponds to that seen for most of the parasite domains, a helical barrel with no beta-sheets (S).

Discrepancy existed between crystallized and predicted secondary structures when comparing figures 3.3 and 3.4 in terms of group M domains – an inappropriate number of helices and beta-sheets were predicted. A correlation was documented for helices in group C domains, but a greater number of beta-strands were evident in the crystal structures. This finding highlights the suggestion of Geourjon *et al*., (2001) that the predicted secondary structure of a protein or domain does not always correlate to that which is crystallized.

The two parasite proteins have not previously been crystallized and so they were assessed in terms of their putative tertiary structures, with the aid of three template-based modelling algorithms. All three predicted an incomplete twisted cleft topology for both parasite domains, using a variety of SWIB/MDM2 crystal templates (figure 3.4 F-S). The four most prominent crystal templates used were 1UHR, 1YCQA, 1V31 and 1V32 (The SWIB/MDM2 domain of the *A. thaliana* SWI/SNF complex component SNF12-like protein At5g08430 (Yoneyama *et al.*, 2004a)), although the percentage identity was always less than 30% regardless of the template employed. The SWIB/MDM2 domain of the 2GV2 template was part of a complex (other participating proteins removed in figure 3.4A for simplicity), and therefore not used during the modelling process.

All the predicted tertiary structures of *Pf*MDM2 had an appropriate helical composition but no beta-strands when compared to the classical twisted cleft topology. This absence of beta-strands deviated from the domains secondary structure predictions. All but one of the models showed fair to high quality and reliability when assessed using QMEAN analysis (figure 3.4F-L, QMEAN >0.5) (Benkert *et al.*, 2009). The most reliable prediction was that created by the EsyPred algorithm using the 1YCQ template (QMEAN score of 0.835; figure 3.4J).

Unlike the unclear secondary structure predictions for *Pf*SWIB, all the tertiary models showed four distinct helical regions, with fair to high quality and reliability based on QMEAN analysis (figure 3.4M-S). All but two of these lacked beta-strands, in line with secondary structure predictions. Two of the lower scoring models had correctly positioned beta-sheets and thus conformed to the full classical topology (figure 3.4R-S) but the lower quality, relative to the some of the other incomplete models, suggests that the domain may indeed lack beta-strands. The most reliable prediction was created by the PHYRE2 server (QMEAN score of 0.745, figure 3.4P). The apparent absence of beta-sheets in the modelled *Pf*MDM2 and *Pf*SWIB domains respectively suggests their inability to bind to a p53-homologue in a conventional manner.

Further analysis was conducted using the yeast SNF12 protein, which has not been crystallized. When modelled, using the PHYRE2 algorithm (figure 3.4T), the same incomplete twisted cleft topology was predicted as for the two parasite domains, although the quality and reliability of this model was poor (QMEAN = 0.359). This helical rich structure, like *Pf*MDM2, failed to correlate to its predicated secondary structure in terms of beta-strands. Whether this modelled absence of beta-sheets is of functional importance is unknown but appears to be a conserved feature of unicellular eukaryotic SWIB/MDM2 domains. Based on secondary structure predictions and tertiary modelling both parasite SWIB/MDM2 domains are likely group C homologues. Both, but more so for *Pf*MDM2, show strong relation to the yeast SNF12 SWIB/MDM2 domain.

3.1.2 Binding partner identification for *P. falciparum* SWIB/MDM2 homologues

Although the precise molecular mechanism by which the SWIB/MDM2 family induces transcriptional regulation is often unknown, protein-protein interactions appear to be

essential (Bennett-Lovsey *et al.*, 2002). Thus, this study aimed to identify novel or known homologous binding partners for the two recombinant *P. falciparum* SWIB/MDM2 domains with the aid of phage display library technology.

3.1.2.1 Isolation of pure genomic DNA

Genomic DNA was isolated from wild type 3D7 *P. falciparum* parasites and the purity and concentration thereof was determined spectrophotometrically. The DNA was free of protein and organic contaminants based on the A260/A280 and A260/A230 values (table 3.3) (Sambrooke and Russell, 2001, Rapley, 2005, NanoDrop Technologies, 2007). The high A260/A280 ratio indicated the possibility of RNA contamination (Rapley, 2005, Hoffmann-Rohrer and Kruchen, 2011) but agarose gel electrophoresis failed to reveal any RNA (figure 3.5). The sample migrated as a single, intact band of high molecular mass and was used successfully for PCR.

Table 3.3: Spectrophotometric assessment of isolated *P. falciparum* genomic DNA

DNA concentration (ng/µl)	A260/A280 value	A260/A230 value
28.4	3.19	2.01

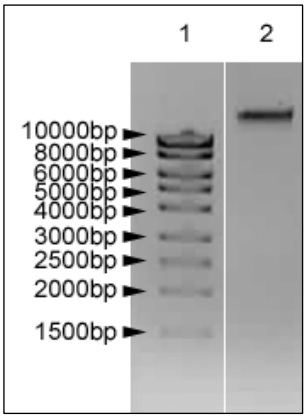

Figure 3.5: Isolated *P. falciparum* genomic DNA.
Assessment of genomic DNA was performed by 1% agarose gel electrophoresis, with size validation relative to a base pair standard.
Lane 1 – MassRuler™ high range DNA ladder; Lane 2 – isolated *P. falciparum* genomic DNA.

3.1.2.2 Preparation of the P. falciparum SWIB/MDM2 domain constructs

The SWIB/MDM2 domains of *Pf*MDM2 and *Pf*SWIB were amplified and prepared for directional insertion into the pGEX-4T-2 vector, as presented in figures 3.6A and 3.6B. The prepared amplicons migrated as single bands, at their theoretically expected sizes (273bp for *Pf*MDM2 and 480bp for *Pf*SWIB) during electrophoresis. The pGEX-4T-2 plasmid was employed for this section of the study, to produce GST-tagged recombinant proteins (Appendix D). The quantified pGEX-4T-2 plasmid DNA and PCR amplicons were ligated and the resultant constructs were used for the transformation of DH5α *E. coli* cells.

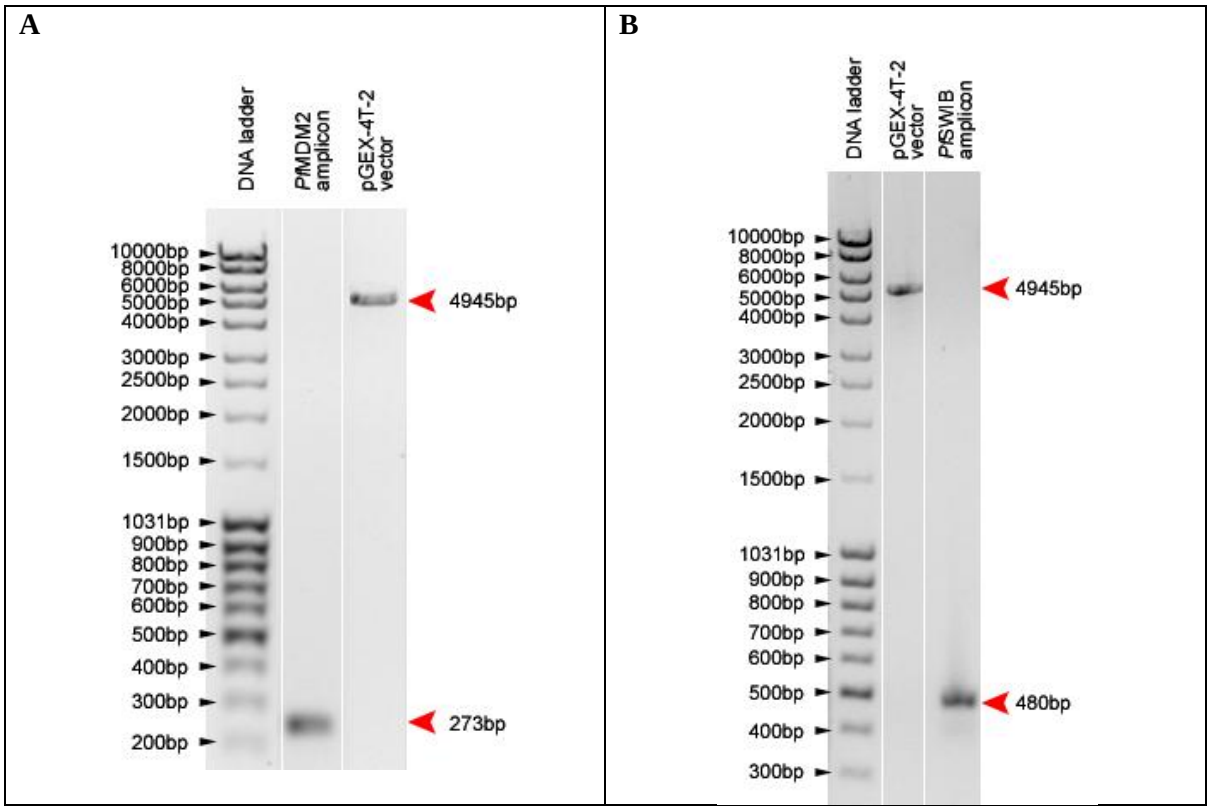

Figure 3.6: The pGEX-4T-2 plasmid and the *P. falciparum* SWIB/MDM2 domain amplicons. Assessment conducted by 1% agarose gel electrophoresis, with size validation relative to a base pair standard.
A) Lane 1 – MassRuler™ mixed range DNA ladder; Lane 2 – *Pf*MDM2 SWIB/MDM2 domain amplicon; Lane 3 – linearized pGEX-4T-2 plasmid.
B) Lane 1 – MassRuler™ mixed range DNA ladder; Lane 2 – linearized pGEX-4T-2 plasmid; Lane 3 – *Pf*SWIB SWIB/MDM2 domain amplicon.

3.1.2.3 Verification of the pGEX-4T-2 constructs

A minimum of five transformed colonies, of each construct, were assessed to determine the success of cloning. Extracted plasmids underwent restriction endonuclease digestion, as shown in figures 3.7 – 3.8, to determine if the appropriately sized insert was ligated into the plasmid backbone. Correctly sized constructs were validated by sequencing, to ensure the absence of mutations and that in-frame ligation had occurred, and used for the transformation of Rosetta™ 2 (DE3) cells and used for recombinant protein expression.

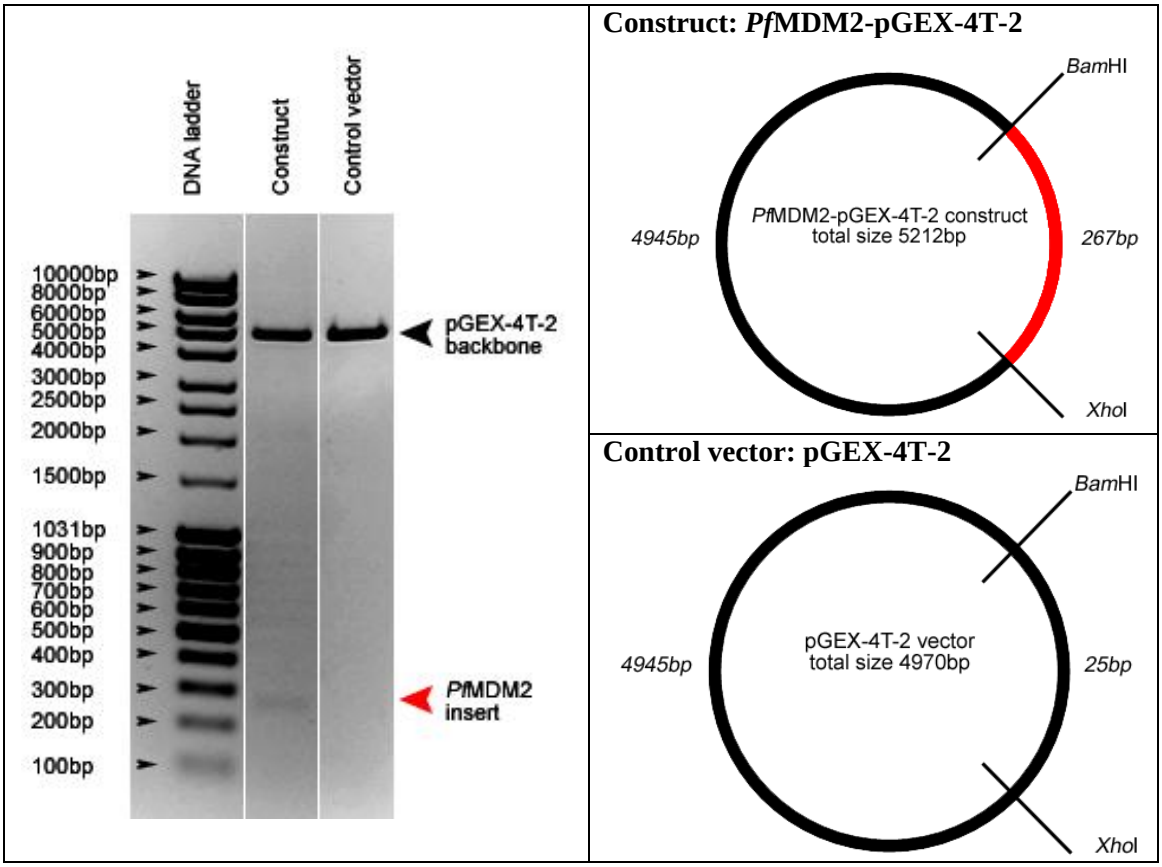

Figure 3.7: Validation of the *Pf*MDM2-pGEX-4T-2 construct by restriction endonuclease digestion.

*Bam*HI and *Xho*I were used to excise the *Pf*MDM2 amplicon (marked by the red arrow) from the *Pf*MDM2-pGEX-4T-2 construct. A control digestion reaction was conducted on the pGEX-4T-2 vector. The vector maps on the right indicate the band sizes expected after construct and control plasmid digestion.

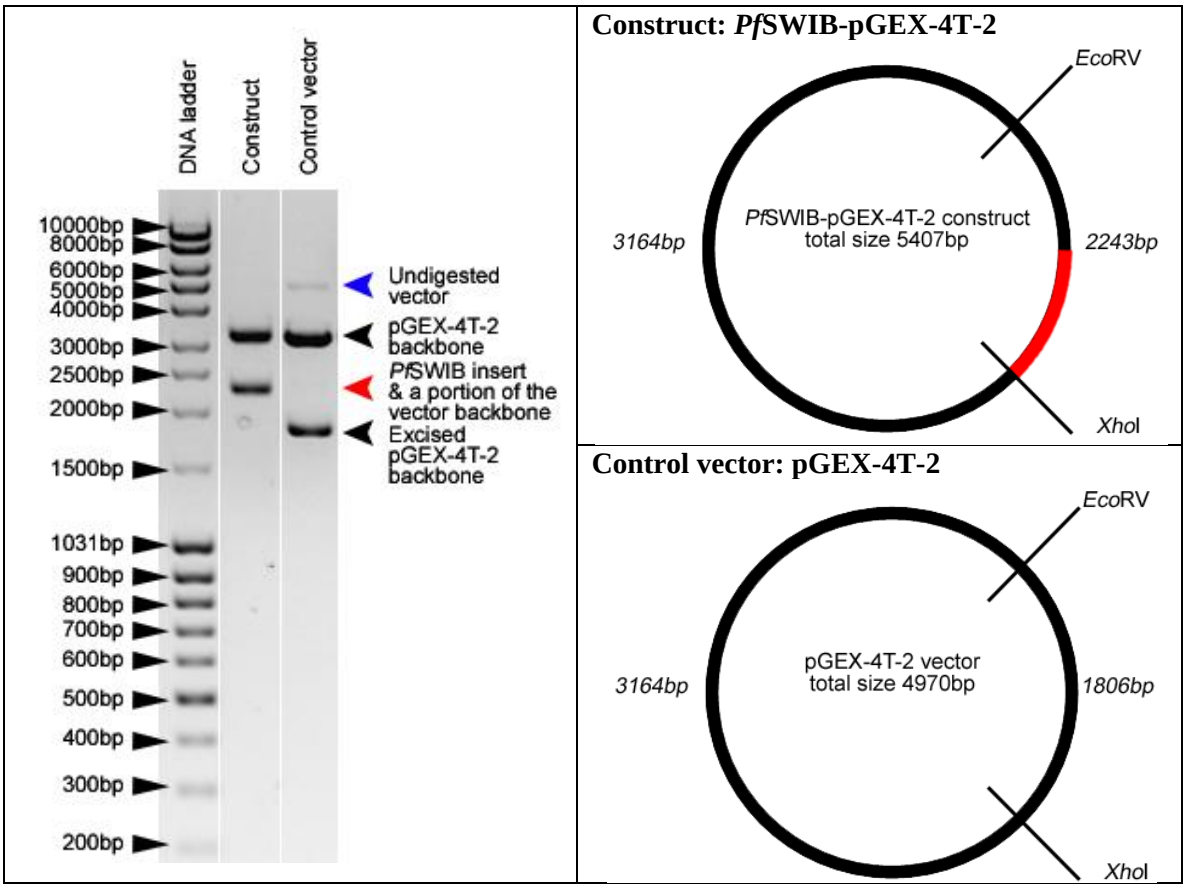

Figure 3.8: Validation of the *Pf*SWIB-pGEX-4T-2 construct by restriction endonuclease digestion.
*Eco*RV and *Xho*I were used to excise the *Pf*SWIB amplicon and a portion of the vector backbone (marked by the red arrow) from the *Pf*SWIB-pGEX-4T-2 construct. A control digestion reaction was conducted on the pGEX-4T-2 vector. The vector maps on the right indicate the band sizes expected after construct and control plasmid digestion.

3.1.2.4 Recombinant expression of GST-tagged proteins

From this point on the term GST-*Pf*MDM2 will represent the GST-tagged recombinant *Pf*MDM2 SWIB/MDM2 domain while GST-*Pf*SWIB will represent the GST-tagged recombinant *Pf*SWIB SWIB/MDM2 domain. Through the optimization of the expression, extraction and purification protocol, successful isolation was achieved for both parasite SWIB/MDM2 domains (figures 3.9 – 3.10). For both proteins, a large proportion remained in the unbound fraction after one round of affinity purification. The use of more magnetic beads did not proportionally increase the yield but did decrease the elution purity, due to elevated non-specific protein binding. Yield was increased by washing the beads after the first round of protein binding to remove non-specifically bound proteins, and then

reapplying the beads to the unbound fraction. This allowed for additional recombinant fusion protein to bind to the beads. As seen in figures 3.9A and 3.10A recombinant protein was lost during the wash steps, although the amount lost was reduced with each successive round of washing, which was conducted to enhance elution purity.

GST-*Pf*SWIB was expressed with a lower than theoretically expected solubility (<50% based on immunoblot densitometry vs. 74.9% calculated – figure 3.9B and table 3.4). This was unexpected as the acidic pI (pI of 5) of GST-*Pf*SWIB should have promoted protein solubility (Mehlin *et al.*, 2006). An average yield of 24μg was attained per 20ml bacterial culture and, as seen in figure 3.9A, was essentially pure. Purity was based on densitometry of gels stained with Coomassie blue, implying that contaminating proteins of less than 100ng would not be detected.

Immunoblotting of eluted GST-*Pf*SWIB revealed a single band, whereas two additional bands were detected in the unpurified fractions. The lowest band, with a relative molecular mass of about 21kDa, was probably endogenous *E. coli* GST protein (theoretical mass of 22.9kDa). Its absence from the GST-*Pf*SWIB elution may have been due to the relatively small proportion of total elution assessed. The identity of the higher band, with a relative molecular mass of about 39kDa, is unknown, but it was not present in the soluble fraction. The curving of some of the protein bands at the edge of the gels in figure 3.9 and 3.10, attributed to uneven heat distribution across the gel during electrophoresis (Takahashi *et al.*, 1991).

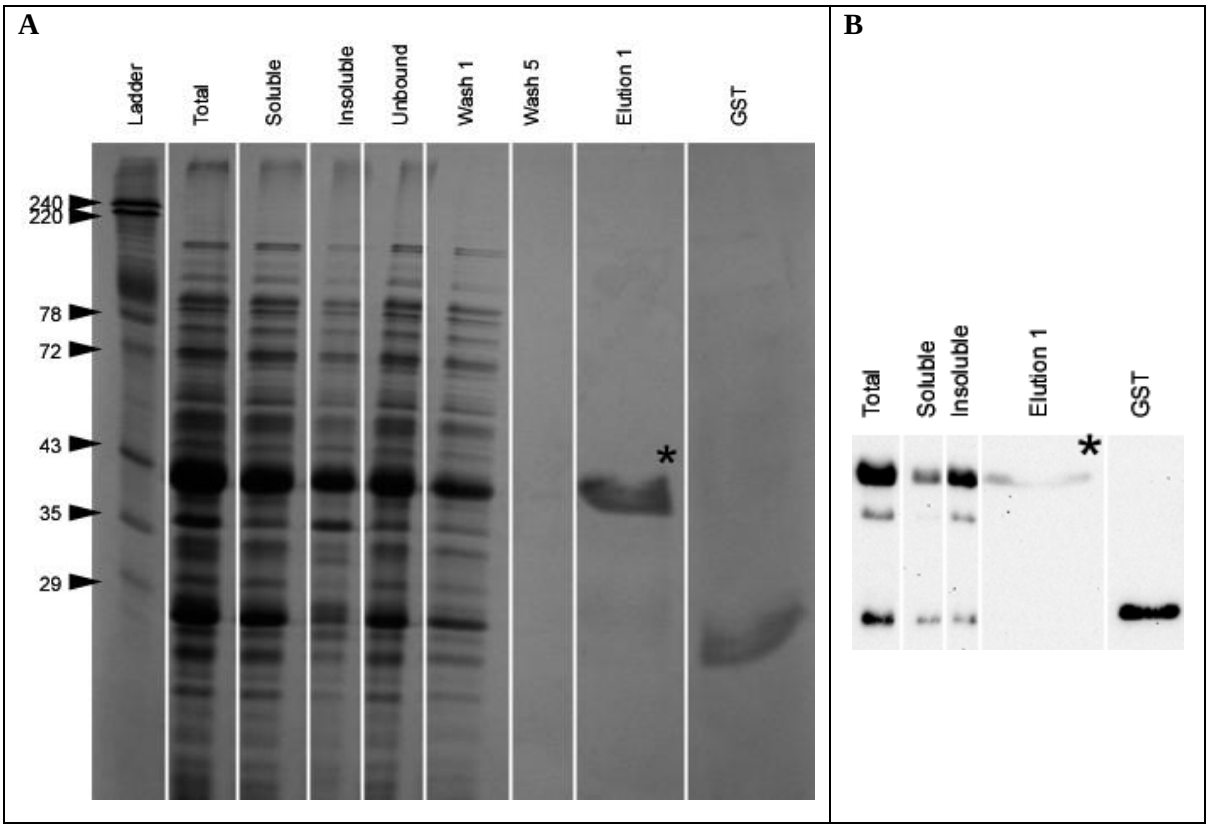

Figure 3.9: Expression and immunoblot analysis of GST-*Pf*SWIB.
A) A Coomassie blue stained SDS-polyacrylamide gel. Aliquots assessed: 5µl of the red cell membrane ladder; 1.5µl of 1.5ml total, soluble, insoluble and unbound fractions; 20µl of 1ml washes; 20µl of 150µl elution 1; and 10µl of 150µl GST elution (control). The *Pf*SWIB fusion protein migrated at 42kDa, roughly its correct theoretically expected molecular mass of 44.1kDa.
B) An immunoblot using an anti-GST antibody verified the 42kDa protein band as GST-*Pf*SWIB. The same volumes of aliquots were assessed as stated above expect for the use of 10µl of 150µl elution 1 and 5µl of 150µl GST elution (control).
* indicates GST-*Pf*SWIB

Table 3.4: The properties of GST-*Pf*MDM2 and GST-*Pf*SWIB.

Protein name	N-terminal tag	Molecular mass (kDa)		Predicted solubility‡ (%)	pI†	Purity (%)	Average concentration of elution (ng/µl) ± standard deviation (n=3)	Yield per 20ml *E. coli* culture (µg)**
		Calculated †	*Based on SDS-PAGE**					
***Pf*SWIB**	GST	44.1	42	74.9	5.0	99	162 ± 21.4	~24
***Pf*MDM2**	GST	36.4	33	35.4	8.4	72	59 ± 18.1	~9

†Entire fusion protein, tag included, assessed using ExPASy (Gasteiger *et al.*, 2005);* A standard red cell membrane marker was used for relative molecular mass determination; ‡ Calculated using the Recombinant Protein Solubility Prediction program (Wilkinson and Harrison, 1991) for the entire fusion protein, tag included; ** Average from three elutions.

GST-*Pf*MDM2 was expressed with a low, but theoretically expected, solubility (~40% vs. 35.4% respectively – figure 3.10B and table 3.4). The protein's relatively high pI of 8.4 was a possible contributing factor, as previous studies have correlated high pI values to reduced recombinant *P. falciparum* protein expression within bacterial systems (Mehlin *et al.*, 2006). The average yield for GST-*Pf*MDM2 was 9µg per 20ml bacterial culture, significantly lower than that of GST-*Pf*SWIB. A basic pI not only contributes to poor solubility but affects protein expression, with a pI below 6 or above 8 commonly being associated with low expression (Mehlin *et al.*, 2006). The low level of GST-*Pf*MDM2 expression was expected in light of its high pI.

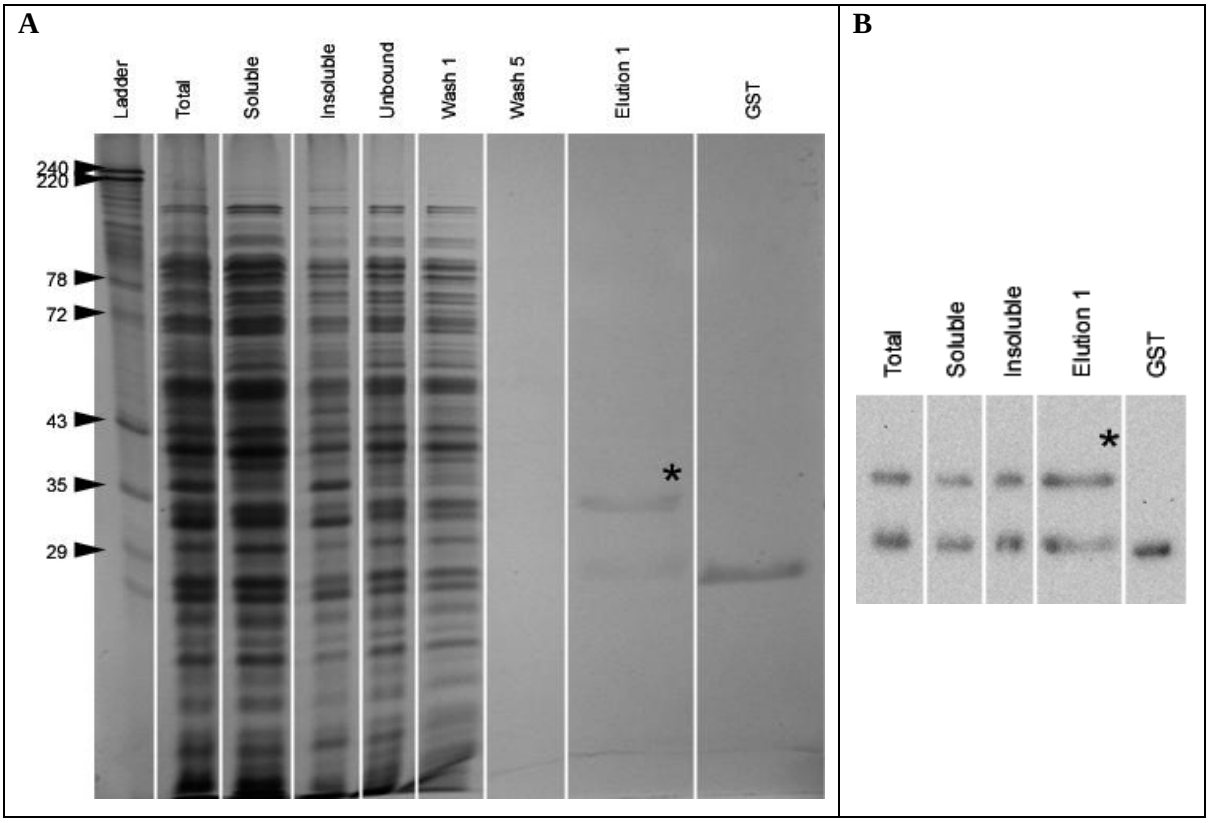

Figure 3.10: Expression and immunoblot analysis of GST-*Pf*MDM2.
A) A Coomassie blue stained SDS-polyacrylamide gel. Aliquots assessed: 5µl of the red cell membrane ladder; 1.5µl of 1.5ml total, soluble, insoluble and unbound fractions; 20µl of 1ml washes; 10µl of 150µl elution 1; and 10µl of 150µl GST elution (control). The *Pf*MDM2 fusion protein migrated at 33kDa, roughly its correct theoretically expected molecular mass of 36.4kDa. A truncated form of GST-*Pf*MDM2 was documented at a molecular mass of roughly 27kDa.
B) An immunoblot using an anti-GST antibody verified the 33kDa protein band as GST-*Pf*MDM2. The same volumes of aliquots were assessed as stated above expect for the use of 20µl of 150µl elution 1 and 5µl of 150µl GST elution (control).
* indicates GST-*Pf*MDM2

As seen in figure 3.10 the GST-*Pf*MDM2 protein expressed in two forms; the full length form with a relative molecular mass of 33kDa and a truncated form with a relative molecular mass of 27kDa. The latter form was only slightly larger than the GST tag alone (figure 3.10) suggesting early truncation, just after the N-terminus tag. Recombinant expression of *P. falciparum* proteins as truncated forms is not an uncommon event (Flick *et al.*, 2004, Mehlin *et al.*, 2006). One general contributing factor is the use of rare codons, not recognized by *E. coli*. Nucleotide analysis of *Pf*MDM2-pGEX-4T-2 construct revealed a rare Arg codon (AGA) present near the 5'end of the parasite specific domain and truncation at this point would correlate to a 27kDa protein. The Rosetta™ 2 (DE3) cell line was employed in this study, which encodes six tRNAs for rare codons, one being AGA (Novagen, 2004). This modified *E. coli* cell ensured that not all the protein products were truncated but could not prevent it entirely.

The truncated GST-*Pf*MDM2 could not be separated from its corresponding full length form due to their small size difference and identical N-terminal tags. It is unlikely that this truncation was due to protein degradation as a protease inhibitor cocktail was employed during the extraction process and the band was consistent, constant in size and proportion for every protein preparation. The truncated GST-*Pf*MDM2 was not considered problematic as it would simply represent the GST-tag, with very little of the SWIB/MDM2 domain actually expressed.

3.1.2.5 Four putative binding partners identified for the P. falciparum SWIB/MDM2 homologues

The GST-*Pf*MDM2 and GST-*Pf*SWIB proteins were biopanned against *P. falciparum* phage display libraries (Lauterbach *et al.*, 2003) and after the fourth round of biopanning the resultant plaques, presenting as clearly defined, non-overlapping clear areas on the lawn of *E. coli* on the titering plates (as depicted in figure 3.11) were utilized for PCR assessment to determine the size of the *P. falciparum* cDNA inserts in the phage. Plaques were screened for each recombinant GST-SWIB/MDM2 protein and a diverse range of insert sizes were found, although the majority were no more than 100bp larger than the control empty cassette PCR product, indicating resultant peptides of approximately 30 amino acids (figure 3.12). Multiple, similarly sized bands suggested specific phage enrichment and amplification. The large quantity of small sized inserts was expected as previous studies involving the same libraries presented similar results (Lauterbach *et al.*, 2003). PCR products ≥300bp were sequenced and analysed as well as selected small *P. falciparum* cDNA inserts, ≥40bp relative to the empty cassette.

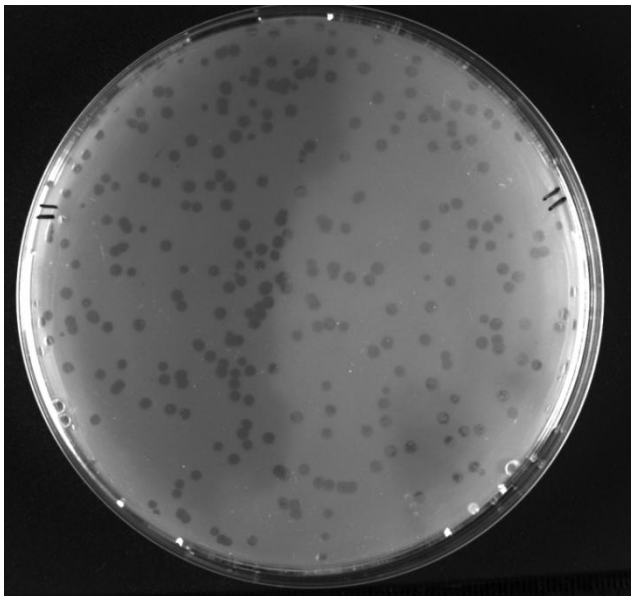

Figure 3.11: A titering plate after four rounds of biopanning.
A 10^6 dilution of a phage library plated after the fourth round of biopanning against GST-*Pf*SWIB. The high number of plaques indicated successful phage amplification.

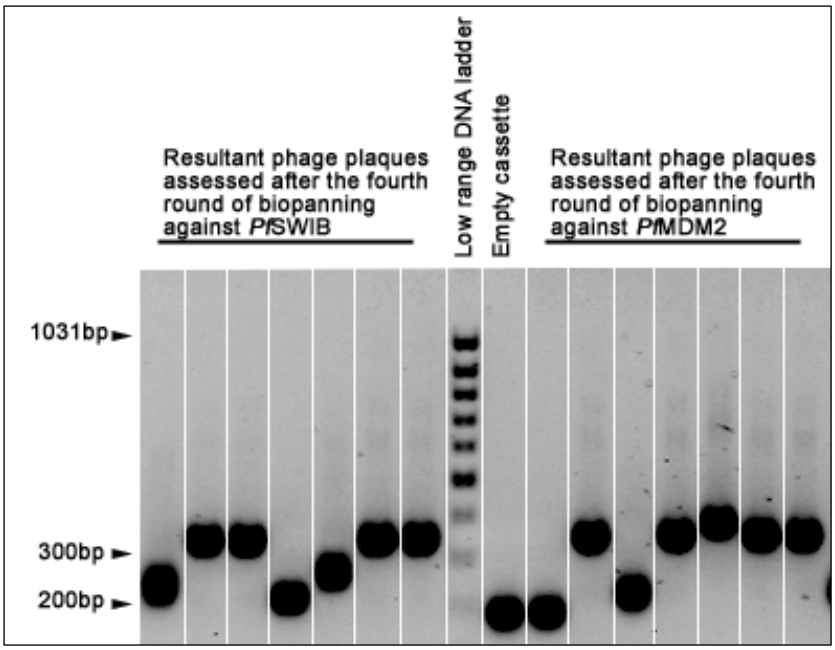

Figure 3.12: A representation of the cDNA inserts present in the phage isolated after four rounds of biopanning.
A range of PCR products (up to ~150bp), relative to the empty cassette (214bp), were identified.

The sequenced inserts were converted to amino acids, four of which correlated to in-frame *P. falciparum* peptides, representing three *Pf*SWIB and one *Pf*MDM2 binding partners (tables 3.5 and 3.6 and the sequencing results in appendix C). The first *Pf*SWIB partner was a C-terminal region of the protein encoded by the PF3D7_1342000 gene, 41 amino acids after the annotated ribosomal protein S6e domain. The protein has been annotated as a putative 40S ribosomal protein S6 and the domain identified by biopanning will be referred to as *Pf*RS6 (Aurrecoechea *et al.*, 2009). The second was an N-terminal region of the PF3D7_1356800 protein annotated as a putative serine/threonine protein kinase (Aurora related kinase 3 (ARK3)), which localises to the nucleus (table 3.6) (Aurrecoechea *et al.*, 2009). The domain is situated 434 amino acids upstream of the kinase domain and will be designated as *Pf*ARK3. Thirdly, an N-terminal region of the protein translated from the PF3D7_1003600 gene was identified and correlated to part of the inner membrane

complex domain of this membrane skeletal protein (Alveolin 5 (ALV5)) (Aurrecoechea *et al.*, 2009, Hu *et al.*, 2010, Kono *et al.*, 2012). This domain will be designated as *Pf*ALV5.

Table 3.5: GST-*Pf*MDM2 and GST-*Pf*SWIB binding partners

Reference Protein		*GST-PfMDM2*	*GST-PfSWIB*	*GST-PfSWIB*	*GST-PfSWIB*
Binding partner characteristics	***Identity***	PF3D7_1303400 (conserved Plasmodium protein, unknown function)	PF3D7_1003600 (membrane skeletal protein IMC1-related (ALV5))	PF3D7_1356800 (serine/threonine protein kinase, putative (ARK3))	PF3D7_1342000 (40S ribosomal protein S6, putative)
	Total number of amino acids	1022	281	4044	306
	Previously annotated domains (location)†	LisH domain (8-34)	Inner membrane complex protein domain (58-153)	Ser/Thr protein kinase domain, putative (1282-1528)	Ribosomal protein S6e domain (1-219)
	Location of putative SWIB/ MDM2 binding domain (amino acids)	505-538	58-107	788-847	260-298
	Animo acid sequence of putative binding domain	KKKKKKEQTNEGKKSVKGINKKDKKRNSKVESKKK	PKTIIQEKIIHVPKNVTHIVEKIVEVPEVKYIEKIVEVPHIHYKNKYVPKKK	IYEKVNIDNDKVKKKNLHSINDKKIKINKTFMNEKDMKGNNRKKYNTEKRDNIKRNENDNEKK	EKKQNKTNNIKNDKSEKKEQAKKKTKTNENPQQTKQNKPNKKK
	E-value*	2E-13	1.9E-24	6.2E-30	1.3E-18

† According to PlasmoDB (Aurrecoechea *et al.*, 2009); * Probability score for the correlation of the identified sequence to the *P. falciparum* protein sequence.

Only a single high affinity binding partner for *Pf*MDM2 was identified, corresponding to a centrally located region of the PF3D7_1303400 protein of unknown function. It contains an N-terminal Lis1 homology (LisH) domain, 466 amino acids upstream from the *Pf*MDM2 binding site, which will be designated as *Pf*LisH in this study. The cellular location of this protein was predicted to be nuclear (table 3.6). A rRNA sequence (malmito_rna_10) was also identified, but due to the high A/T bias of the *P. falciparum*

genome, non-coding RNA molecules can frequently be purified with the mRNA and subsequently inserted into the phage arms, resulting in the expression of unnatural proteins (Lanzillotti and Coetzer, 2008).

PCR products with equal size and restriction endonuclease digestion patterns relative to *Pf*ALV5 and *Pf*LisH were identified several times. This indicates strong enrichment of these phage from the original starting library.

Table 3.6: Predicted and/or proven cellular locations of the putative binding partners of GST-*Pf*MDM2 and GST-*Pf*SWIB

Cellular location		***Bioinformatic analysis†***	***Experimentally Proven***
Identified binding partner	***PfALV5***	Cytoplasm	Inner membrane complex (Hu *et al.*, 2010)
	PfARK3	Nucleus	Nucleus (Doerig, 2014 Personal communication)
	PfLisH	Nucleus	Not determined
	PfRS6	Nucleus	Not determined

† No annotated signal sequences exist for any of these proteins (Aurrecoechea *et al.*, 2009); a variety of bioinformatic tools were employed to determine their possible cellular locations – the highest scoring location was deemed as most likely (see appendix A for more details).

The biopanning system is not error free and can be associated with the detection of non-specific interactions (Lanzillotti and Coetzer, 2008). Thus, the identified interactions were verified through binding partner recombinant protein expression and subsequent *in vitro* binding assays.

3.1.2.6 Preparation of the binding partner constructs

The four protein domains identified by biopanning were amplified by PCR and prepared for directional insertion into the pET-15b plasmid (Appendix D). This plasmid was used to express the binding partner domains as recombinant His-tagged fusion proteins – a different tag to the SWIB/MDM2 domains. As presented in figure 3.13 the prepared amplicons migrated at their expected sizes (735bp *Pf*ALV5, 1008bp *Pf*ARK3, 558bp *Pf*Lish and 627bp *Pf*RS6), relative to a standard of base pair markers.

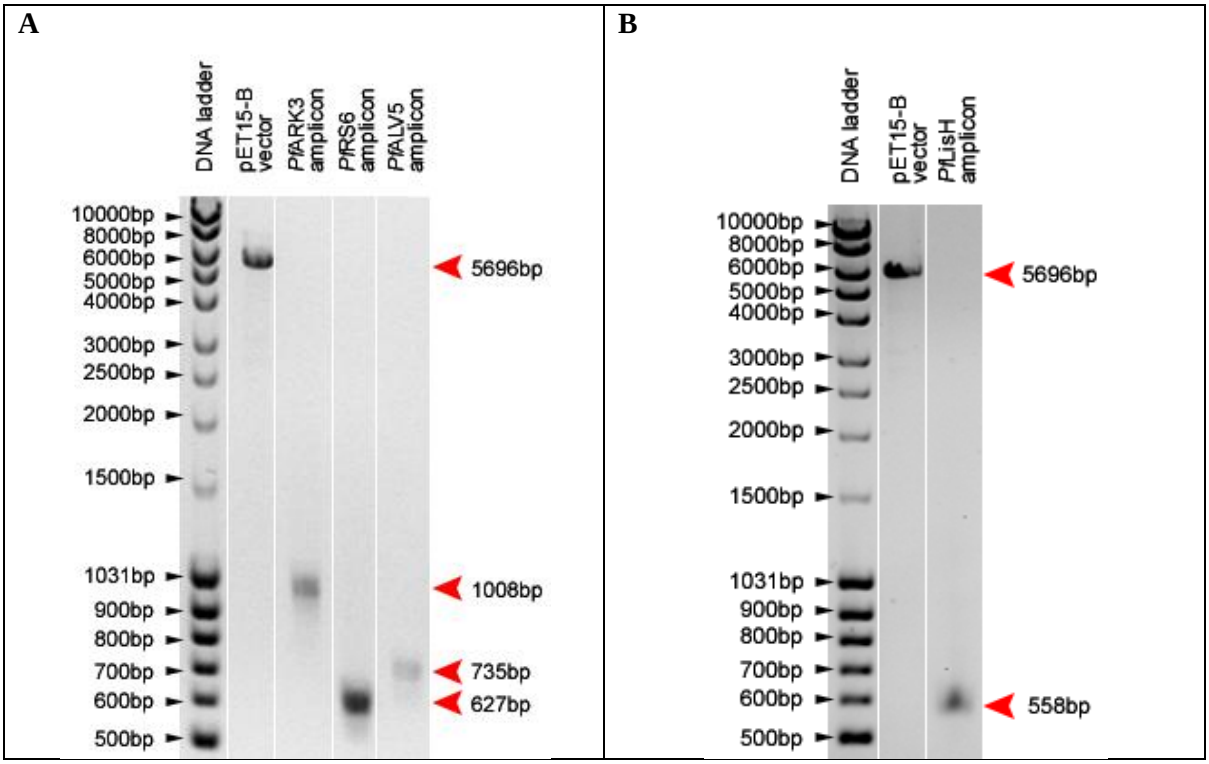

Figure 3.13: The pET15-B plasmid and the binding domain amplicons.
Assessment conducted by 1% agarose gel electrophoresis, with size validation relative to a base pair standard.
A) Lane 1 – MassRuler™ mixed range DNA ladder; Lane 2 – linearized pET15-B plasmid; Lane 3 – *Pf*ARK3 amplicon; Lane 4 – *Pf*RS6 amplicon; Lane 5 –*Pf*ALV5 amplicon.
B) Lane 1 – MassRuler™ mixed range DNA ladder; Lane 2 – linearized pET-15b plasmid; Lane 3 – *Pf*LisH amplicon.

3.1.2.7 Verification of the pET15-B constructs

As described in section 3.1.2.3, positive colonies were assessed (figures 3.14 – 3.15) and sequenced and error-free constructs were used for recombinant protein expression in Rosetta™ 2 (DE3) cells.

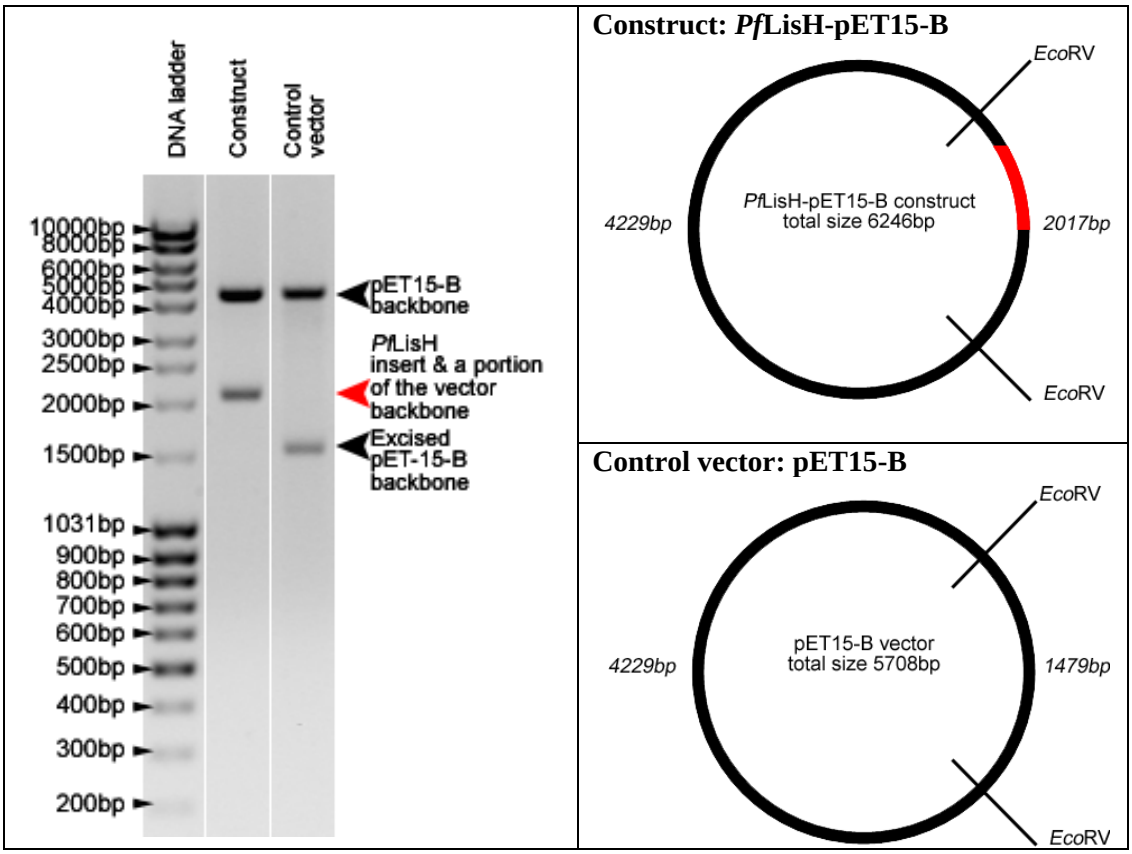

Figure 3.14: Validation of the *Pf*LisH-pET15-B construct by restriction endonuclease digestion.

*Eco*RV was used to excise the *Pf*LisH amplicon and a portion of the vector backbone (marked by the red arrow) from the *Pf*LisH-pET15-B construct. A control digestion reaction was conducted on the pET15-B vector. The vector maps on the right indicate the band sizes expected after construct and control plasmid digestion.

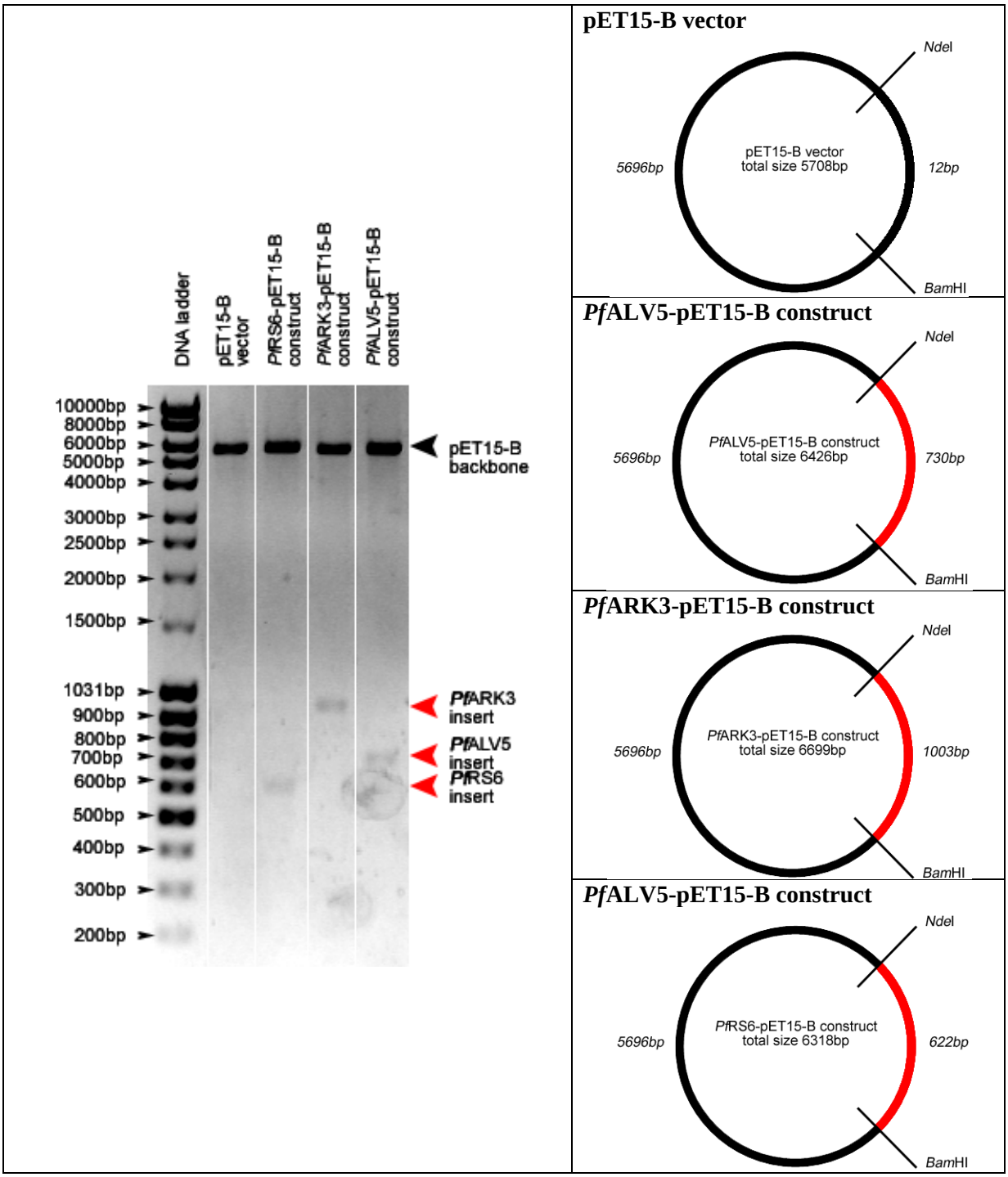

Figure 3.15: Validation of the GST-*Pf*SWIB binding partner pET15-B constructs by restriction endonuclease digestion.

*Nde*I and *Bam*HI were used to excise the binding partner amplicons (marked by the red arrows) from the pET15-B constructs. A control digestion reaction was conducted on the pET15-B vector. The vector maps on the right indicate the band sizes expected after construct and control plasmid digestion.

3.1.2.8 Recombinant protein expression of His-tagged proteins

From this point an example of the nomenclature which will be used is His-*Pf*LisH, denoting the recombinant His-tagged *Pf*LisH domain. Protein extraction and purification were previously described (section 3.1.2.4) but here nickel affinity magnetic beads were used.

His-*Pf*LisH was expressed as a soluble protein (≥90% based on immunoblot densitometry) and at a high level with an average yield of 13.4μg per 20ml bacterial culture, despite its basic pI of 8.9 (Mehlin *et al.*, 2006) and theoretically expected insolubility (figure 3.16 and table 3.7). The highly pure protein, based on densitometry of gels stained with Coomassie blue, migrated with a relative molecular mass of 41kDa, approximately 1.8 times greater than theoretically expected (22.9kDa), even though the sequence of the vector construct was correct. Unnatural migration patterns have been documented for proteins characterised by a high proportion of low complexity regions and enrichment in amino acids such as lysine (Tompa, 2002), features of numerous malaria proteins – His-*Pf*LisH has two low complexity regions (Aurrecoechea *et al.*, 2009). This unusual amino acid composition leads to a proportionally lower amount of SDS binding to the protein, in turn shifting migration and resulting in a perceived molecular mass greater than expected (Tompa, 2002).

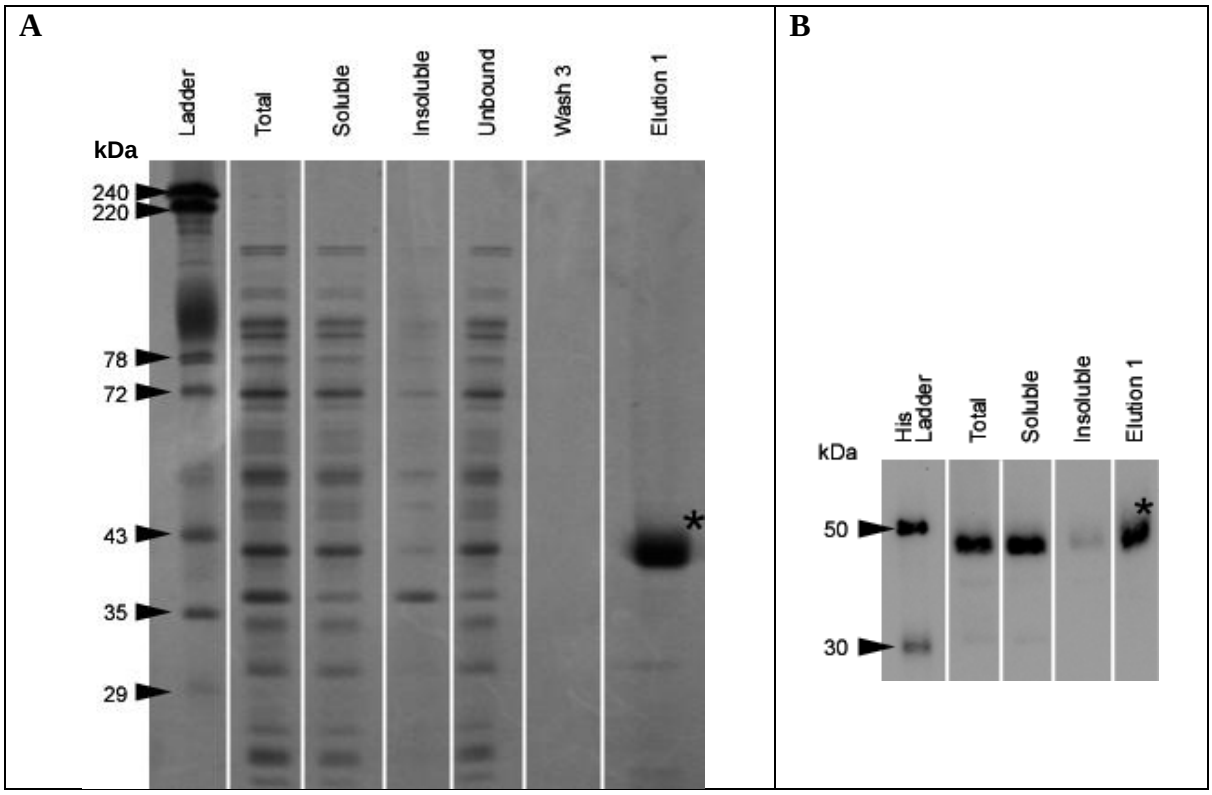

Figure 3.16: Expression and immunoblot analysis of His-*Pf*LisH.

A) A Coomassie blue stained SDS-polyacrylamide gel. Aliquots assessed: 3µl of the red cell membrane ladder; 1.5µl of 1.5ml total, soluble, insoluble and unbound fractions; 20µl of 1ml final wash; and 15µl of 100µl elution 1. His-*Pf*LisH migrated at 41kDa, roughly double its theoretically expected molecular mass (22.9kDa).

B) An immunoblot using an anti-His antibody verified the 41kDa protein band as His-*Pf*LisH. The same volumes of aliquots were assessed as stated above expect for the use of 1µl of 100µl elution 1 and 3µl of the commercial His-ladder (control).

* indicates His-*Pf*LisH

Table 3.7: The properties of the recombinant binding partners.

Protein Name	N-terminal tag	Molecular mass (kDa)		Predicted solubility‡ (%)	pI†	Purity (%)	Average concentration of elution (ng/µl) ± standard deviation (n=3)	Yield per 20ml *E. coli* culture (µg)**
		Calculated †	*Based on SDS-PAGE**					
***Pf*LisH**	His	22.9	41.0	0	8.9	99	134 ± 16.9	~ 13.4
***Pf*ARK3**	His	42.0	40.0	5.7	10.5	35	15.0 ± 2.4	~ 1.5
***Pf*ALV5**	His	30.3	29.0	32.1	8.4	-	-	-
***Pf*RS6**	His	26.0	26.0	97	9.2	-	-	-

†Entire fusion protein, tag included, assessed using ExPASy (Gasteiger *et al.*, 2005);* A standard red cell membrane marker was used for relative molecular mass determination; ‡ Calculated using the Recombinant Protein Solubility Prediction program (Wilkinson and Harrison, 1991) for the entire fusion protein, tag included; ** Average from three elutions; - data could not be determined due to poor expression or insolubility.

His-*Pf*ARK3 was expressed with a far greater solubility than theoretically expected (~50% based on immunoblot densitometry relative to 5.7% calculated – figure 3.17B and table 3.7) but had low expression and was isolated with a poor yield of 1.5μg per 20ml bacterial culture. A pI below 6 and above 8 is known to reduce protein expression while a basic pI results in insolubility (Mehlin *et al.*, 2006). His-*Pf*ARK3 had a pI of 10.5 and thus low soluble expression was expected. Literature does show that recombinant proteins with a molecular mass of between 30 to 40 kDa, although not that large in size, often express in an insoluble manner (Mehlin *et al.*, 2006). His-*Pf*ARK3 has a molecular mass of 40kDa and may well fall into category. His-*Pf*ARK3 purity based on densitometry was poor due to numerous truncated forms – the most prominent at a molecular mass of 31.4kDa, which implies that truncation occurred in a flanking region just after or at the end of the SWIB/MDM2 binding domain. Therefore the truncated protein may participate in *in vitro* binding assays. The *Pf*ARK3-pET-15B construct carries several rare tRNA codons. A rare AGA codon is positioned such that it could be responsible for the prominent truncation documented. A modified bacterial line which expressed all six rare tRNAs, for the codons AGA, AGG, AUA, CCC, CUA and GGA (Novagen, 2004) documented in the *Pf*ARK3-pET-15B construct, was used in this study. This, even in conjunction with lower expression rates due to reduced incubation temperatures (~20°C), was only able to reduce but not prevent truncation of the recombinant parasite protein. The use of a protease inhibitor cocktail ensured that the truncations were not due to protein degradation.

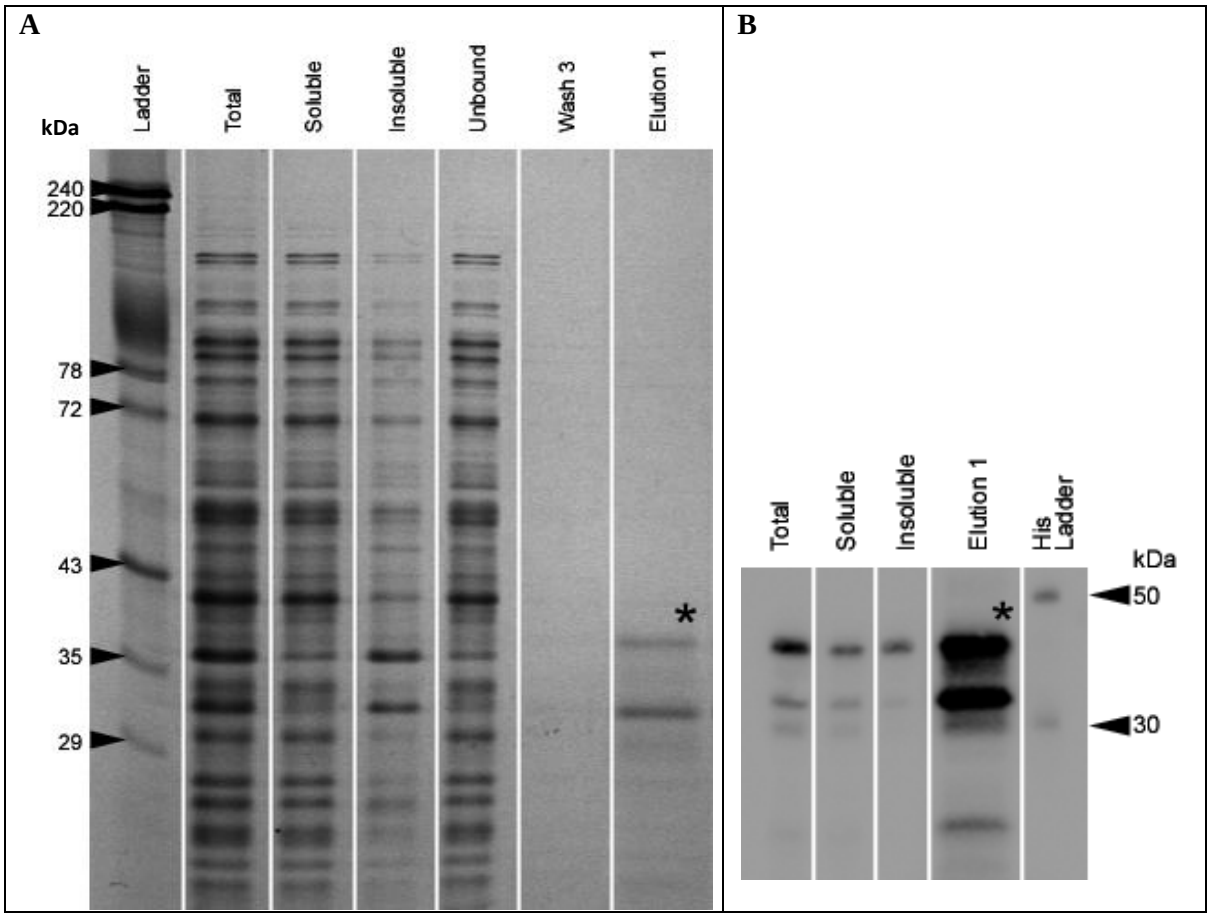

Figure 3.17: Expression and immunoblot analysis of His-*Pf*ARK3
A) A Coomassie blue stained SDS-polyacrylamide gel. Aliquots assessed: 5µl of the red cell membrane ladder; 1.5µl of 1.5ml total, soluble, insoluble and unbound fractions; 20µl of 1ml final wash; and 20µl of 150µl elution 1. His-*Pf*ARK3 migrated at 40kDa, roughly its correct theoretically expected molecular mass of 42kDa. A prominent truncated form was documented at a relative molecular mass of roughly 31.4kDa.
B) An immunoblot using an anti-His antibody verified the 40kDa protein band as His-*Pf*ARK3. The same volumes of aliquots were assessed as stated above expect for the use of 15µl of 100µl elution 1 and 3µl of a commercial His-ladder (control).
* indicates His-*Pf*ARK3.

Extremely low expression was documented for His-*Pf*RS6. This could be due to its very basic pI (9.2), although His-*Pf*ARK3 expressed at sufficient levels for use with pI of 10.5 (Mehlin *et al.*, 2006). The small amount of fusion protein which did express was apparently all soluble, as predicted bioinformatically (calculated as 97% – figure 3.18 and table 3.7). His-*Pf*ALV5 was associated with high levels of expression but was insoluble (<5% solubility based on immunoblot densitometry). This latter result was worse than theoretically predicted (32.1% solubility – table 3.7). Membrane components are known to

be difficult to express in a soluble manner (Dearnley *et al.*, 2012). Various unsuccessful attempts were conducted to improve the expression and purification of His-*Pf*ALV5, including increased culture volume and amount of Nickel beads (data not shown). Due to the very low yield of soluble recombinant His-*Pf*ALV5 and His-*Pf*RS6 proteins they were not used further experimentally.

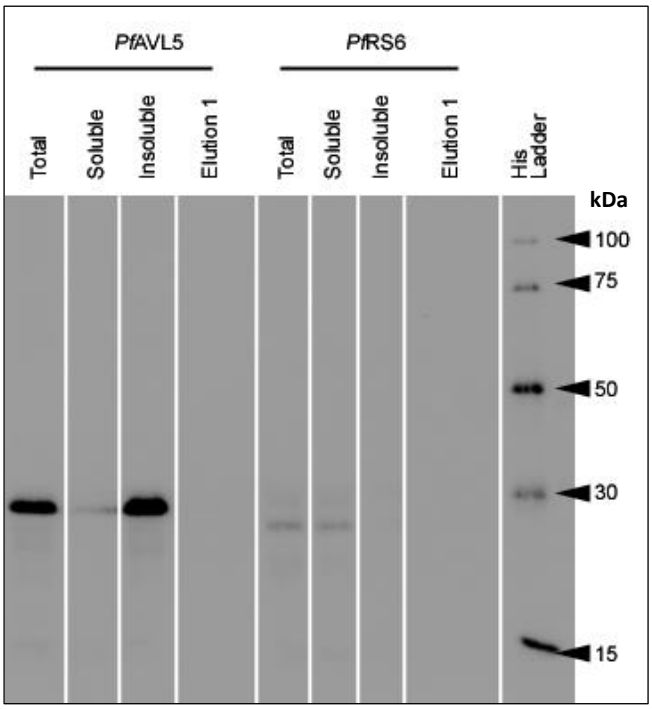

Figure 3.18: Immunoblot analysis of His-*Pf*ALV5 and His-*Pf*RS6.
An immunoblot using an anti-His antibody verified that the 29kDa protein band was His-*Pf*ALV5 and the 26kDa protein band was His-*Pf*RS6. Aliquots assessed: 1.5µl of 1.5ml total, soluble and insoluble fractions; 20µl of 100µl elution 1; and 3µl of a commercial His-ladder (control).

3.1.2.9 In vitro binding assays confirmed interaction between the two P. falciparum SWIB/MDM2 domains and their binding partners

In vitro binding assays were conducted as a means to verify the biopanning data. When a constant amount of His-*Pf*LisH or His-*Pf*ARK3 was immobilized on magneHis beads and exposed to increasing concentrations of their respective GST-tagged SWIB/MDM2 domain (also referred to as the ligands), a dose-dependent association was documented which began to achieve asymptotic saturation (figures 3.19A, 3.19D, 3.20A and 3.20C).

This pattern represents a classical protein-ligand binding association and validates the biopanning data (Nelson and Cox, 2005). Reverse binding experiments were performed whereby GST-*Pf*MDM2 and GST-*Pf*SWIB were immobilized on magneGST beads and exposed to increasing concentrations of their respective binding partners in solution, which also indicated a dose dependent association (figures 3.19B-C and 3.20B). As presented in figure 3.20B full length His-*Pf*ARK revealed stronger binding affinity than the prominent truncated form indicating that the early truncation removed some residues critical for effective binding.

Additional controls were included to ensure the specificity of binding. First, heat denatured ligand was allowed to interact with immobilized protein and revealed a substantially reduced binding association (figure 3.19A and 3.20A). Secondly, recombinant GST protein was allowed to interact with the immobilized His-tagged proteins and showed negligible association. The observed interactions between the recombinant parasite proteins therefore verified the biopanning data.

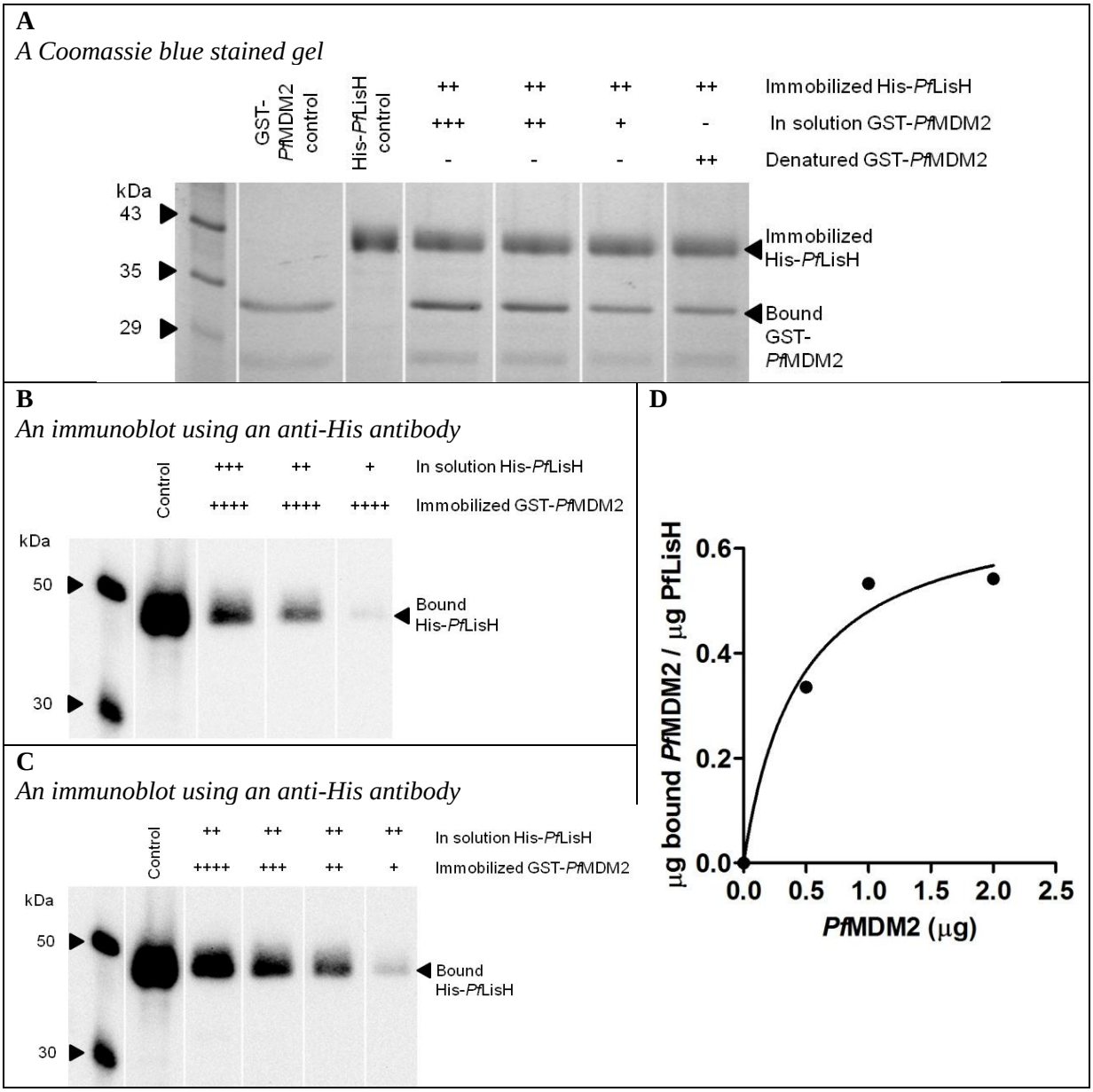

Figure 3.19: Dose-dependent interactions between GST-*Pf*MDM2 and His-*Pf*LisH.
In all gels lane 1 represents a molecular mass marker.
A) Lane 2 represents the GST-*Pf*MDM2 protein and lane 3 the His-*Pf*LisH protein, which were included as controls to verify the position of the proteins on the gel. Lanes 4-7 represent the binding assays conducted whereby 1µg immobilized His-*Pf*LisH interacted with increasing concentrations (0.5 - 2µg) of GST-*Pf*MDM2 in solution.
B) Lane 2 represents the control His-*Pf*LisH protein. Lanes 3-5 represent the binding assays where a total of 1.3µg immobilized GST-*Pf*MDM2 interacted with increasing concentrations (0.1, 0.5 and 1µg) of His-*Pf*LisH in solution.
C) Lane 2 represents the control His-*Pf*LisH protein. Lanes 3-6 represent the binding assays where increasing concentrations (0.4-2.6µg) of immobilized GST-*Pf*MDM2 interacted with 1µg in solution His-*Pf*LisH.
D) A graphical interpretation of the dose-dependent association between His-*Pf*LisH and GST-*Pf*MDM2, starting to reach asymptotic saturation.

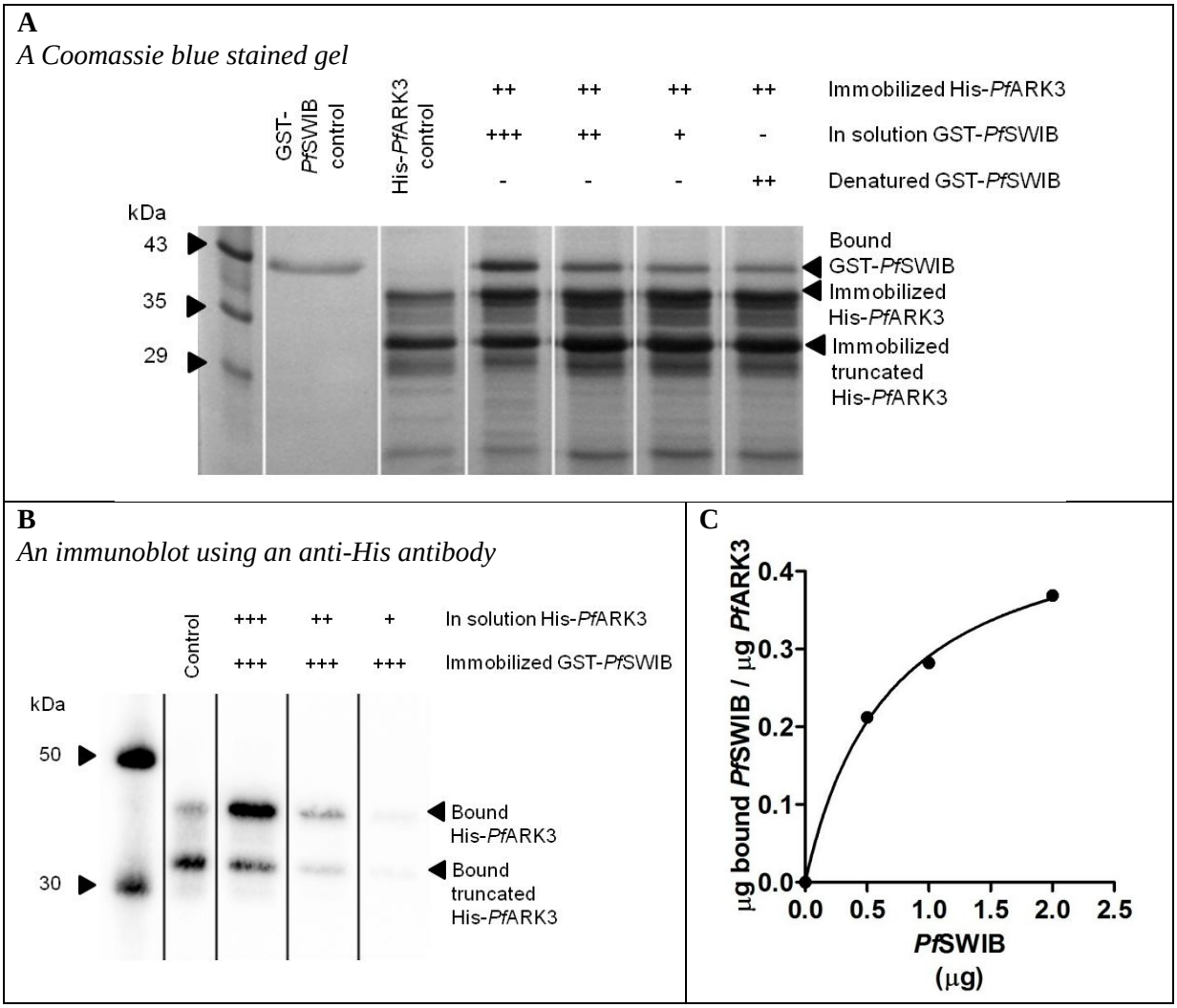

Figure 3.20: Dose-dependent interactions between GST-*Pf*SWIB and His-*Pf*ARK3.
In all gels lane 1 represents a molecular mass marker.
A) Lanes 2 and 3 represent the GST-*Pf*SWIB and His-*Pf*ARK3 proteins respectively which were included as controls to verify the position of the proteins on the gel. Lanes 4 – 7 represent the binding assays where 1µg immobilized His-*Pf*ARK3 interacted with increasing concentrations (0.5 - 2µg) of in solution GST-*Pf*SWIB.
B) Lane 2 represents the control His-*Pf*ARK3 protein. Lanes 3-5 represent the binding assays where a total of 1.5µg immobilized GST-*Pf*SWIB interacted with increasing concentrations (0.1, 0.5 and 1µg) of His-*Pf*ARK3 in solution.
C) A graphical interpretation of the dose-dependent association between His-*Pf*ARK3 and GST-*Pf*SWIB, approaching asymptotic saturation.

3.1.3 Cellular localization of two *P. falciparum* SWIB/MDM2 homologues under normal and PCD conditions

The next step in elucidating the role of the two SWIB/MDM2 domains in the parasite was to determine their localization under various growth conditions using an episomal protein expression system. A variety of stress stimuli have been proven to affect SWIB/MDM2 domain localization in other eukaryotic organisms (Mosser *et al.*, 1988, de la Serna *et al.*, 2000, Wade *et al.*, 2010, Catalano and O'Day, 2012). Previous work failed to elucidate the precise cellular location of *Pf*MDM2 and the protein was simply concluded to reside in either the cytoplasm, mitochondria or apicoplast (Hu *et al*., 2010). No previous localization work has been conducted on *Pf*SWIB.

3.1.3.1 Predicted localisation of PfMDM2 and PfSWIB

As the two *P. falciparum* homologues lacked any annotated localization signals a variety of bioinformatic tools were employed to determine their possible sites of cellular residence within the parasite (table 3.8 and appendix A). For *Pf*SWIB mitochondrial and apicoplast localization was unlikely, based on the algorithms used. Only two out of four algorithms predicted nuclear localization, although these latter two algorithms did highlight several putative nuclear localization signal sequences (black and blue lines, figure 3.21A). These findings suggested that *Pf*SWIB maybe in the cytoplasm.

On the other hand, *Pf*MDM2 revealed a strong probability of nuclear localization, with several putative nuclear localization signal sequences (black and blue lines, figure 3.21B). Four algorithms suggested mitochondrial localization for *Pf*MDM2, with the iPSORT prediction algorithm identifying a putative N-terminal mitochondrial localization sequence, highlighted in figure 3.21B, between amino acids Met^{1} and Lys^{30} (LLRTNIFSA denoted as being of specific importance). A *Plasmodium* specific algorithm (PlasMit) failed to detect this signal sequence, suggesting its atypical nature (Bender *et al.*, 2003). A truncated form

of *Pf*MDM2 lacking the N-terminus will be designated as Δm*Pf*MDM2, and was used to assess the functional role of the predicted mitochondrial localization sequence (green line of figure 3.21B)

Table 3.8: Predicted cellular locations of *Pf*MDM2 and *Pf*SWIB.

Protein	Predicted localization*		
	Nucleus	Mitochondria	Apicoplast
***Pf*SWIB**	2 out of 4	1 out of 7	0 out of 5
***Pf*MDM2**	4 out of 4	4 out of 7	1 out of 5

* In this study multiple prediction algorithms were employed as detailed in section 2.1.3.

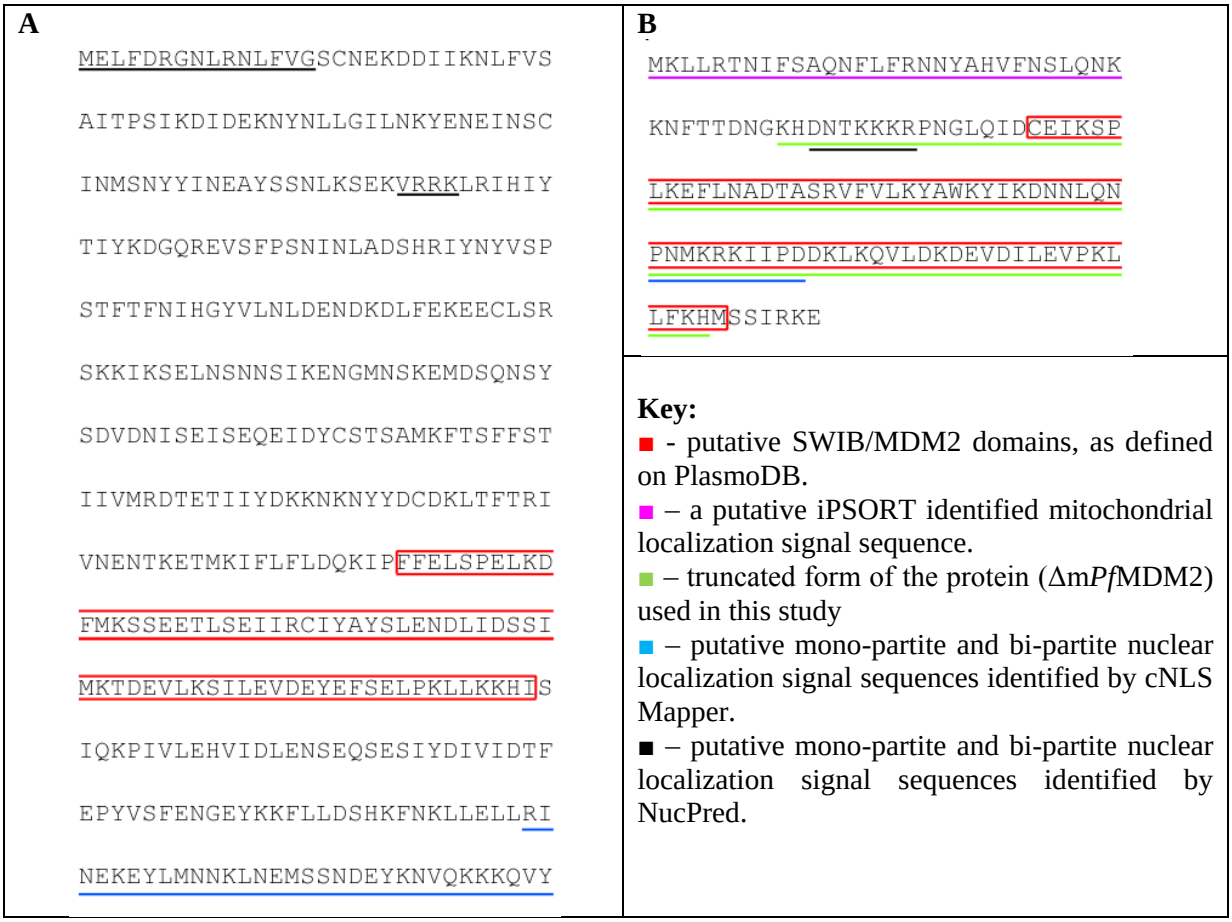

Figure 3.21: Predicted signal sequences and functional domains of *Pf*SWIB and *Pf*MDM2.
(A) The N-terminal region of the *Pf*SWIB protein. (B) The full length *Pf*MDM2 protein.

3.1.3.2 Preparation of the pARL2-GFP constructs

The full length *Pf*MDM2, Δm*Pf*MDM2 and the full length *Pf*SWIB sequences were amplified by PCR and prepared for insertion into the pARL2-GFP vector (Appendix D). This vector allows for C-terminal GFP-tagged episomal protein expression within the parasite. As presented in figures 3.22 the amplicons migrated as single bands at their theoretically expected sizes (288bp for Δm*Pf*MDM2, 411bp for *Pf*MDM2 and 2508bp for *Pf*SWIB) during electrophoresis. The constructs were used to transform the XL10 *E. coli* cell line.

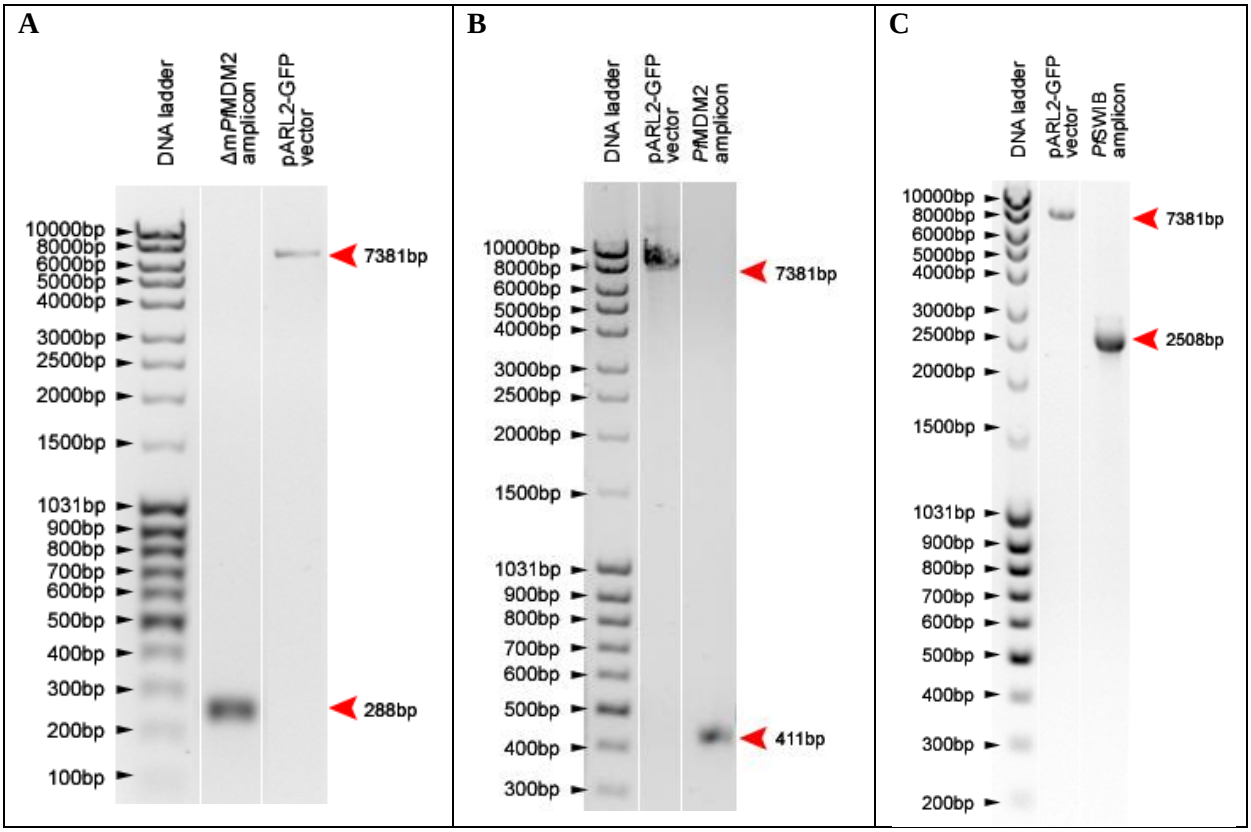

Figure 3.22: The pARL2-GFP vector and the Δm*Pf*MDM2, *Pf*MDM2 and *Pf*SWIB amplicons. Assessment preformed by 1% agarose gel electrophoresis, with size validation relative to a base pair standard.
A) Lane 1 – MassRuler™ mixed range DNA ladder; Lane 2 – Δm*Pf*MDM2 amplicon; Lane 3 – linearized pARL2-GFP plasmid.
B) Lane 1 – MassRuler™ high range DNA ladder; Lane 2 – linearized pARL2-GFP vector; Lane 3 – *Pf*MDM2 amplicon.
C) MassRuler™ mixed range DNA ladder; Lane 2 – linearized pARL2-GFP; Lane 3 – *Pf*SWIB amplicon.

3.1.3.3 Verification of the pARL2-GFP constructs

As described in section 3.1.2.3, the pARL2-GFP constructs were assessed with the aid of restriction endonuclease digestion (figures 3.23 – 3.24). Correctly sized constructs were then validated by sequence analysis and were amplified in XL-10 *E. coli*, extracted and used for transfection of 3D7 ring stage *P. falciparum* parasites.

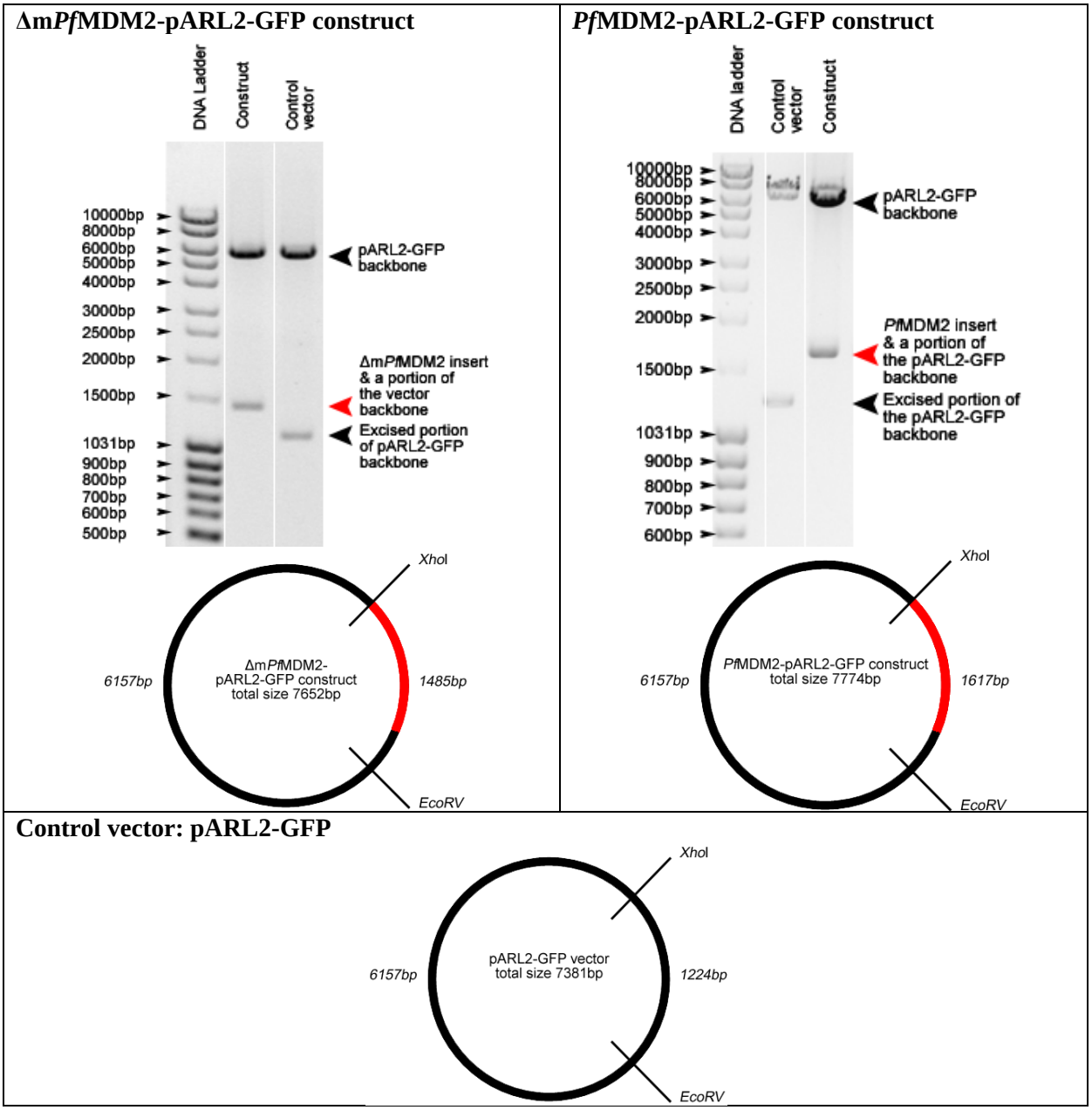

Figure 3.23: Validation of the *Pf*MDM2-pARL2-GFP and Δm*Pf*MDM2-pARL2-GFP constructs by restriction endonuclease digestion.
*Eco*RV and *Xho*I were used to excise the *Pf*MDM2 and Δm*Pf*MDM2 amplicons, along with portions of the vectors backbone, (marked by the red arrow) from the construct. A control digestion reaction was conducted on the pGEX-4T-2 vector. The vector maps indicate the band sizes expected after construct and control plasmid digestion.

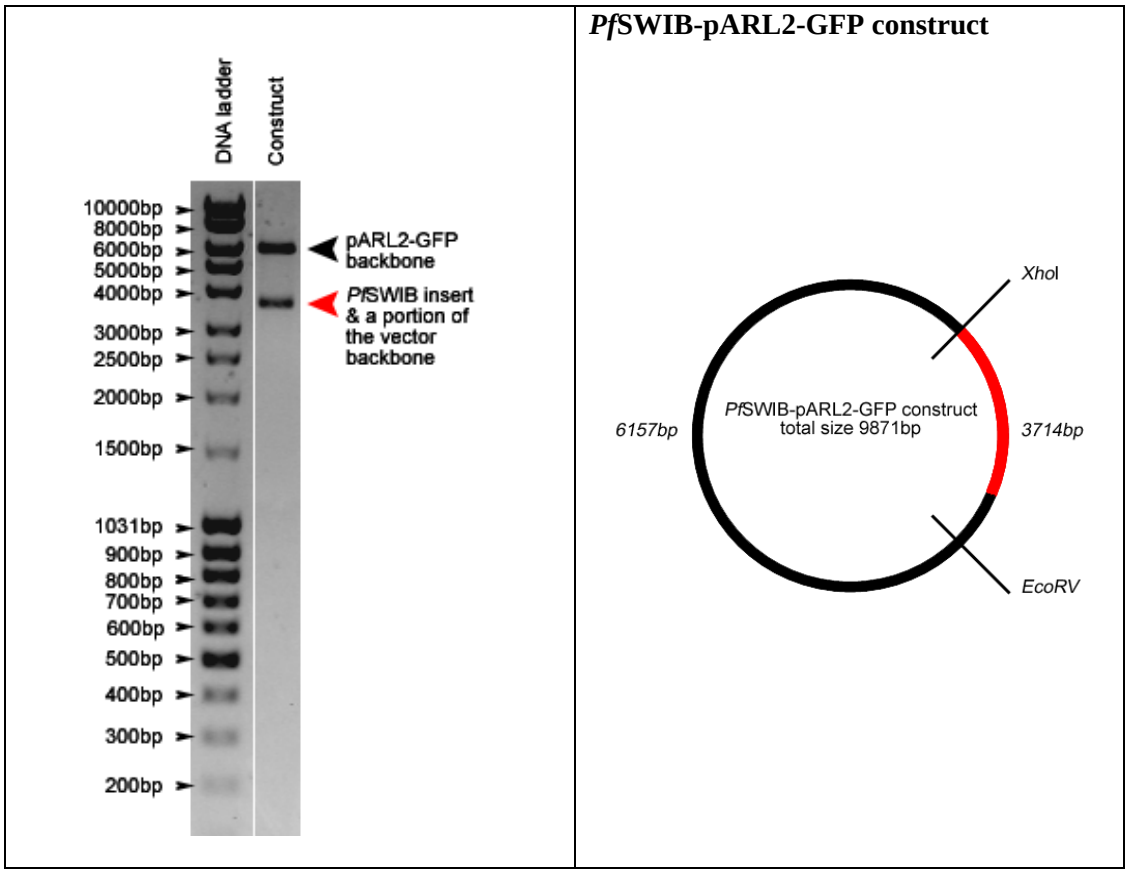

Figure 3.24: Validation of the *Pf*SWIB-pARL2-GFP construct by restriction endonuclease digestion.
*Eco*RV and *Xho*I were used to excise the *Pf*SWIB amplicon, along with a portion of the vector backbone, (marked by the red arrow) from the construct. A control digestion reaction was conducted on the pARL2-GFP vector. The vector map indicates the expected band sizes after construct digestion.

3.1.3.4 Creation and verification of three P. falciparum transgenic parasite lines

Each of the pARL2-GFP constructs were used for transfection of sorbitol-synchronized ring stage 3D7 strain *P. falciparum* parasites. The transgenic parasites were detected between 23 and 43 days after RBC electroporation and used for localization studies under normal and stress conditions. The GFP-tag allowed for subcellular location of the tagged proteins by fluorescence microscopy (Van Wye and Haldar, 1997).

From this point on the term *Pf*GFP will be used to denote episomally expressed GFP protein in a parasite transgenic line, *Pf*MDM2-GFP will represent the full length *Pf*MDM2 protein with a GFP tag, Δm*Pf*MDM2-GFP will represent the truncated *Pf*MDM2 protein with a GFP tag, and *Pf*SWIB-GFP will represent the full length *Pf*SWIB protein with a

GFP tag. All transgenic lines had a GFP signal while the wild type 3D7 parasites did not (data not shown), indicating transfection had occured. PCR analysis verified that each transfected *Plasmodium* line carried the appropriate constructs (Waters *et al.*, 1997), based on amplicon size relative to the pARL2-GFP plasmid (165bp, 558bp, 429bp, and 2655bp amplicon sizes for *Pf*GFP, *Pf*MDM2-GFP, Δm*Pf*MDM2-GFP, *Pf*SWIB-GFP respectively) (figure 3.25 and 3.26). The poor PCR signal strength could be attributed to the poor and unstable transfection efficiency, known to be associated with *P. falciparum*, or due to variations in plasmid copy number within the host, dictated by the construct itself (Waters *et al.*, 1997).

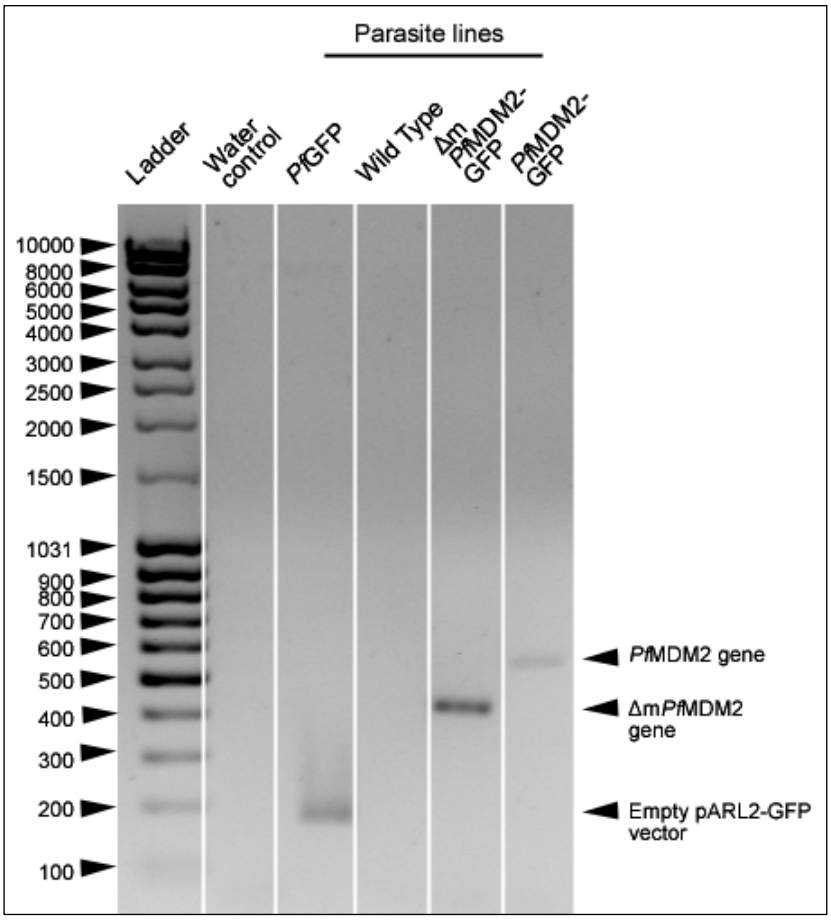

Figure 3.25: PCR verification of the two different *Pf*MDM2-GFP lines.
The ladder represents the MassRuler™ mixed range DNA ladder. The PCR amplicons were of the correct sizes for each of the constructs, relative to the pARL2-GFP vector.

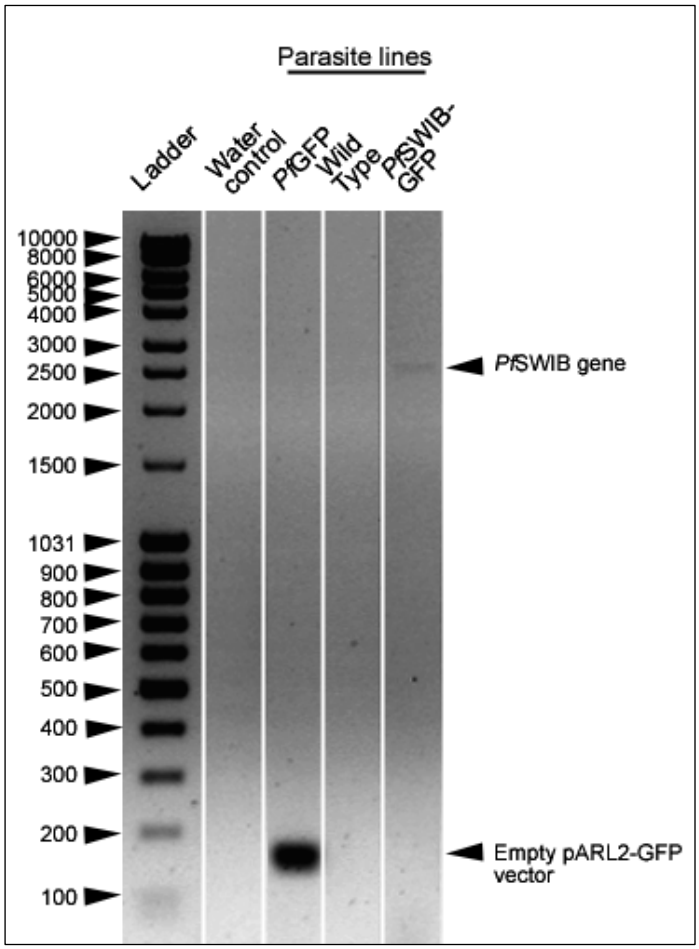

Figure 3.26: PCR verification of the *Pf*SWIB-GFP line.
The ladder represents the MassRuler^{TM} mixed range DNA ladder. The PCR amplicon was of the correct size, relative to the pARL2-GFP vector.

3.1.3.5 Imaging of the PfGFP transgenic line

Due to the episomal protein expression being driven by the *crt* promoter, the GFP protein was expressed throughout the asexual intraerythrocytic life cycle of the parasite. As expected, the GFP-tag alone accumulated within the cytoplasm of the parasite during all these stages (figure 3.27) (Van Wye and Haldar, 1997). The signal became punctuate in schizont stages reflecting individual merozoites. Although GFP is associated with a high quantum yield, implying a strong fluorescent signal, the molecule was still susceptible to rapid photo-bleaching (Lichtman and Conchello, 2005, Shaner *et al.*, 2005) which complicated live imaging. Various means were employed to improve this – the use of a neutral density filter, reduced light exposure of the sample; as well the use of a GFP-

directed labelled antibody on fixed parasitized RBC. As expected in fixed, late stage parasites the episomal GFP was located in the cytoplasm (Van Wye and Haldar, 1997) and failed to co-localize with a red microneme marker, EBA-175 (Sim *et al.*, 1992) (figure 3.28).

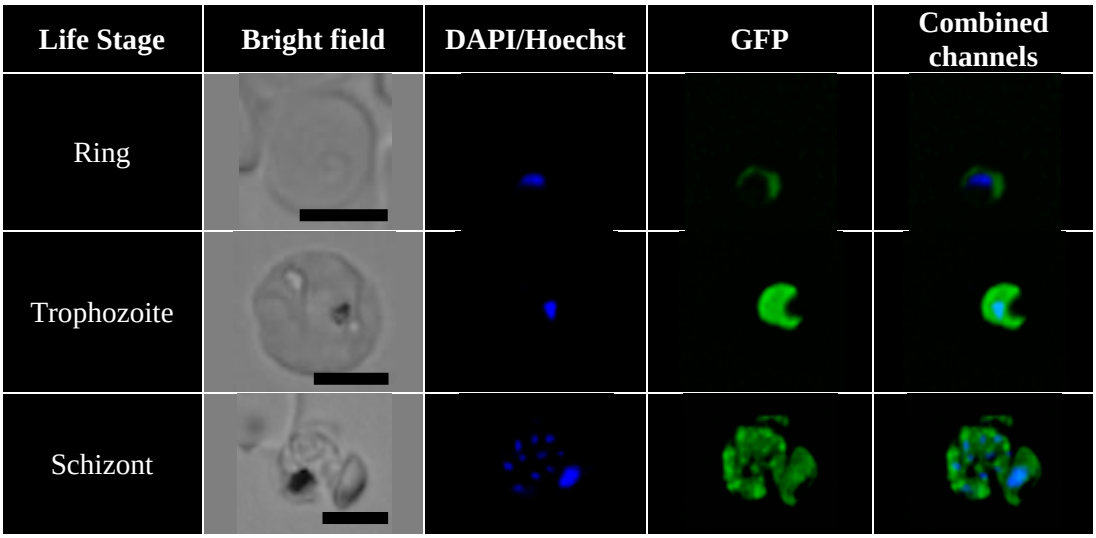

Figure 3.27: Live imaging of the *Pf*GFP transgenic parasite.
Hoechst dye was utilized for nuclear visualization within the ring parasites, while DAPI staining was employed for all the others. The GFP signal was located in the cytoplasm of all of the intraerythrocytic life stages. Scale bar in bright field represents 2.5µm

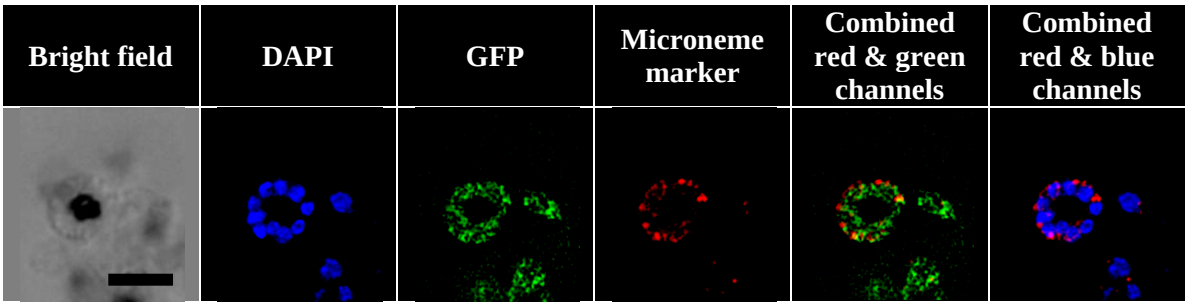

Figure 3.28: Fluorescent imaging of fixed schizont *Pf*GFP parasites.
Nuclear material was stained with DAPI, the GFP signal was amplified with the aid of an anti-GFP antibody-conjugate, and microneme detection was facilitated by an EBA-175 primary antibody and a secondary antibody, conjugated to a red fluorophore. *Pf*GFP was punctate throughout the cytoplasm and showed no distinct correlation to the red microneme pattern. Scale bar in bright field represents 5µm.

3.1.3.6 The effect heat on GFP localization

Numerous stress factors induce PCD-like phenotypes within *P. falciparum*, one of the most physiologically important being elevated temperatures of 38.5°C and above encountered in malaria patients during fever. *In vitro* incubation of cultured parasites at these temperatures severely effects their growth and development of, especially in the late asexual intraerythrocytic life stages (Kwiatkowski, 1989, Long *et al.*, 2001, Oakley *et al.*, 2007, Porter *et al.*, 2008, Engelbrecht and Coetzer, 2013). Furthermore, heat stress is a valuable tool as the yeast SWIB/MDM2 homologue protein, Swp73p/SNF12, is involved in the transcriptional regulation of heat stress response genes (Cairns *et al.*, 1996). In this study ring stage transgenic parasites were synchronized and 24 hours later, as trophozoites and schizonts, exposed to 41°C for 2 hours (Oakley *et al.*, 2007, Engelbrecht and Coetzer, 2013). As represented in figure 3.29, the cellular distribution of the GFP protein was unaffected by heat shock at all time points, relative to controls (figure 3.27). Cytoplasmic vacuolization was documented in some of the stressed parasite (white arrow in figure 3.29) and high mortality was seen in the cultures 24 hours later. A parasite lacking any intracellular movement was deemed dead. The development of the survivors lagged, still residing in the late life stage twenty-four hours after heat stress termination. This feature has previously been documented under the same conditions (Engelbrecht and Coetzer, 2013).

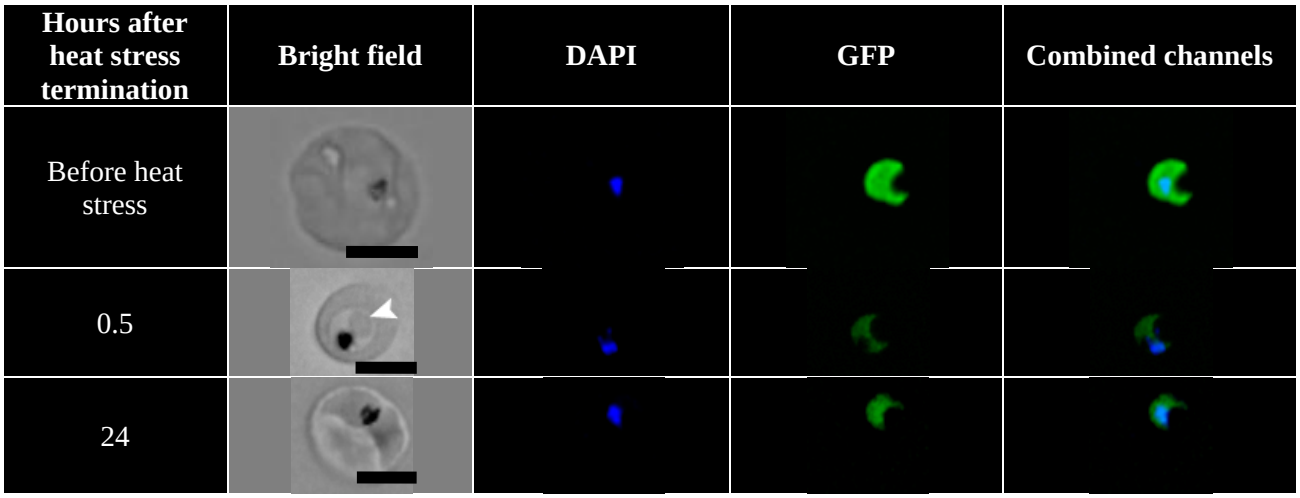

Figure 3.29: Heat stress had no effect on GFP distribution in late stage transgenic parasites.
DAPI staining was utilized for nuclear visualization. The GFP signal presented no alteration in response to heat stress within the late life stages. The white arrow denotes a vacuole, indicative of a PCD-like phenotype, in response to elevated temperatures. Scale bar in bright field represents 2.5µm.

3.1.3.7 Live imaging of the PfMDM2-GFP transgenic line

Based on mRNA profile analysis, there are very few *Pf*MDM2 gene transcripts in the ring and early trophozoite stages but a relatively high expression in late trophozoites and schizonts (Aurrecoechea *et al.*, 2009). Proteomic data, although incomplete, have only documented the protein within schizonts (Aurrecoechea *et al.*, 2009). Therefore, the cellular location of the *Pf*MDM2-GFP protein was considered to be of physiological relevance only in the late asexual intraerythrocytic life stages.

As the transgenic parasite developed into a trophozoite and then a schizont, there was an associated expansion and subsequent division of nuclear material. The punctate *Pf*MDM2-GFP signal increased with life cycle progression but did not go to the nucleus (figure 3.30). Δm*Pf*MDM2-GFP was found dispersed within the cytoplasm, like GFP (figure 3.30). This latter result suggests that the N-terminus of *Pf*MDM2-GFP controls localization. This region was predicted to have a mitochondrial localization signal sequence but the punctate *Pf*MDM2-GFP signal did not have a typical branched mitochondrial architecture (Tonkin

et al., 2004). In order to determine if the protein did move to the mitochondrion, two sets of experiments were conducted.

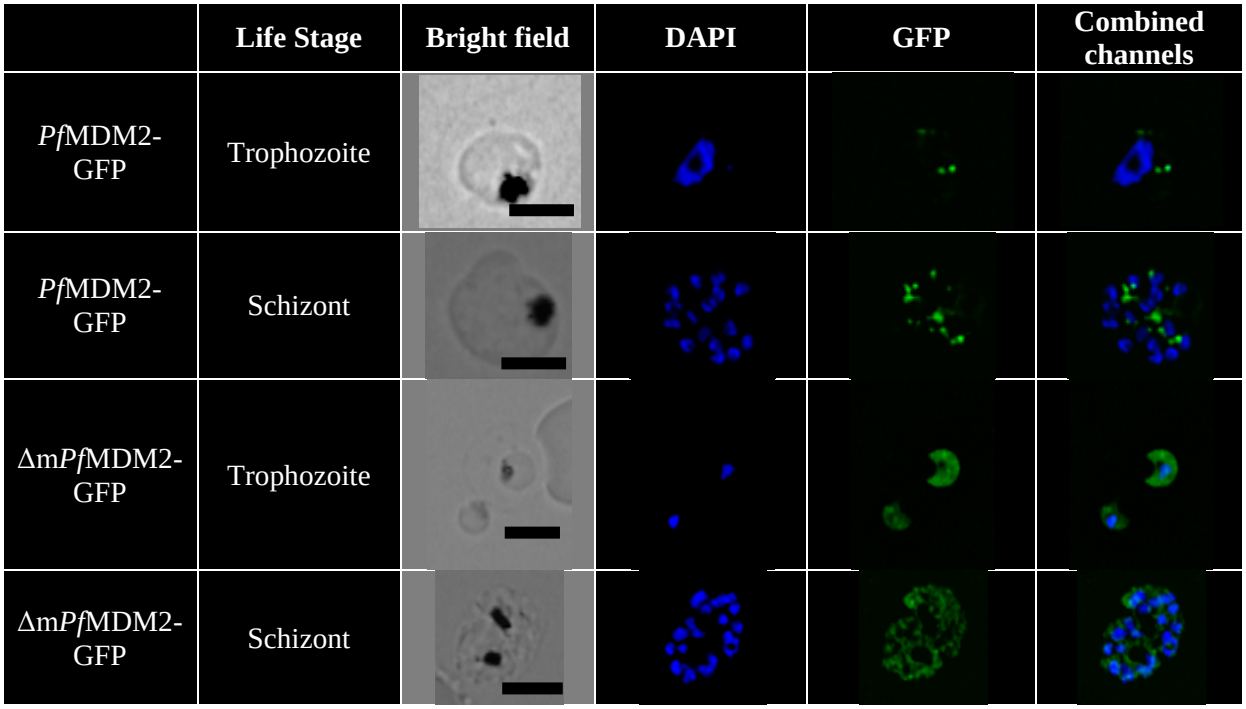

Figure 3.30: Live imaging of late stage *Pf*MDM2-GFP and Δ*Pf*MDM2-GFP transgenic parasite lines.
DAPI staining was utilized for nuclear visualization. *Pf*MDM2-GFP showed a distinct, non-nuclear localization pattern while Δm*Pf*MDM2-GFP was cytoplasmic in all assessed life stages. Scale bar in bright field represents 2.5μm.

First, trophozoite and schizont *Pf*MDM2-GFP parasites were fixed and assessed with a green fluorescently labelled anti-GFP antibody. As represented in figure 3.31, the enhanced *Pf*MDM2-GFP signal was cord-like in appearance, a pattern documented for a branching and dividing parasite mitochondrion (Tonkin *et al.*, 2004). This pattern was distinctly different to and failed to co-localize with the dot-like EBA-175 microneme signal, confirming previous findings (Hu *et al.*, 2010) that *Pf*MDM2 is not an apical invasion protein (figure 3.31). Under fixed conditions Δm*Pf*MDM2-GFP was still found within the cytoplasm and did not co-localize with the micronemes (figure 3.31).

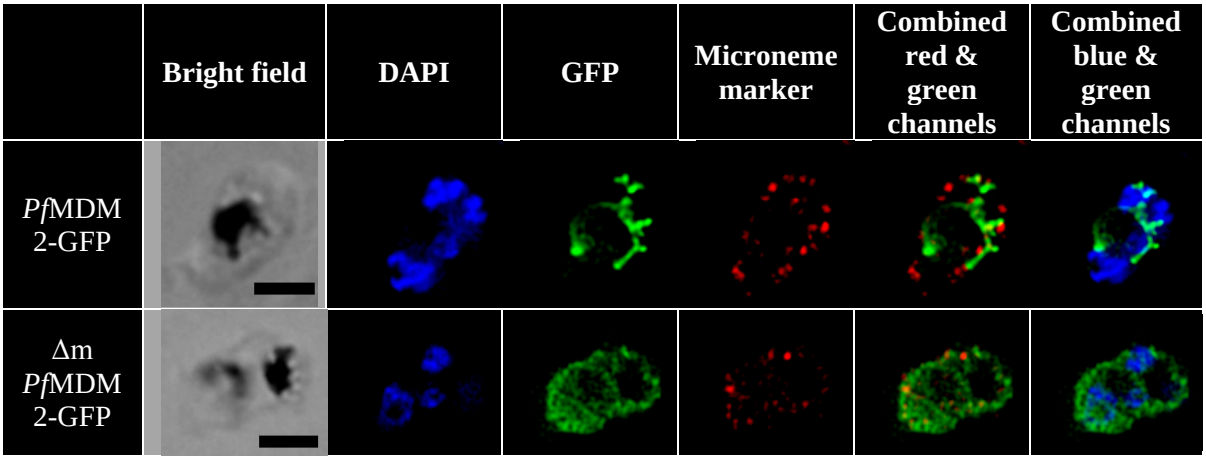

Figure 3.31: Fluorescent imaging of fixed *Pf*MDM2-GFP and Δm*Pf*MDM2-GFP transgenic parasites in the schizont life stage.
DAPI was utilized for nucleus visualization. The GFP signals were amplified with the aid of anti-GFP antibody conjugates. The use of a primary EBA-175 antibody allowed for the detection of the micronemes. *Pf*MDM2-GFP presented a distinct non-nuclear, branched, cord-like pattern, whereas Δm*Pf*MDM2-GFP was present in the cytoplasm. Neither showed co-localization with the micronemes. Scale bar in bright field represents 2.5µm.

Secondly, mitochondrial co-localization was assessed with a mitochondrial stain MitoSOX^{TM}. As no previous work had evaluated this fluorophore in *P. falciparum*, its localization was compared to a well characterized *P. falciparum* mitochondrial stain – MitoTracker^{TM} Green FM (Tonkin *et al.*, 2004). The latter stain has almost identical emission and excitation spectra properties to GFP and therefore could not be used directly in the study (Molecular Probes, 2008). Neither stain could be used on fixed samples and were thus only employed for live imaging (Molecular Probes, 2005, Molecular Probes, 2008). MitoTracker^{TM} and MitoSOX^{TM} showed co-localization in the wild type 3D7 parasites, as presented in figure 3.32. There existed a small degree of variation between the two stains. This may have been due to different localisation mechanisms (a thiol-reactive chloromethyl moiety directed MitoTracker^{TM} while a cationic triphenylphosphonium substitution directed MitoSOX^{TM}); the MitoSOX^{TM} stain required activation once in the mitochondrion which the MitoTracker^{TM} stain did not; and lastly MitoSOX^{TM} has a variable quantum yield (Molecular Probes, 2005, Molecular Probes, 2008, Zielonka and

Kalyanaraman, 2010). Nevertheless, MitoSOX™ distinctly localized to the *P. falciparum* mitochondrion and was used in the transgenic parasite line.

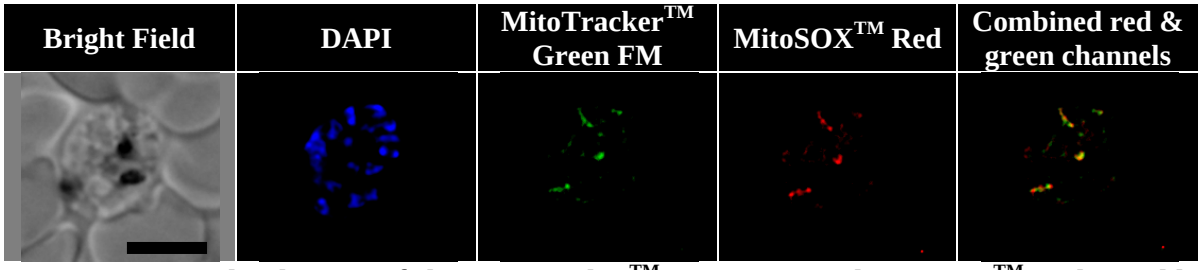

Figure 3.32: Co-localization of the MitoTracker™ Green FM and MitoSOX™ Red in wild type schizont parasites.
DAPI was utilized for nuclear visualization. The two fluorescent signals colocalised, proving that MitoSOX™ stains *P. falciparum* mitochondria. Neither showed co-localization with the micronemes. Scale bar in bright field represents 5µm.

As expected, GFP alone had no influence on the mitochondrion staining in late asexual intraerythrocytic life stages of *P. falciparum* (figure 3.33 top panel). In these physiologically relevant life stages *Pf*MDM2-GFP showed distinct co-localization with MitoSOX™ except for one large red dot in the bottom panel of figure 3.33.The red and green signal intensities were not always equivalent, as seen in the bottom panel for one of the parasites, which influenced the yellow colocalisation signal.

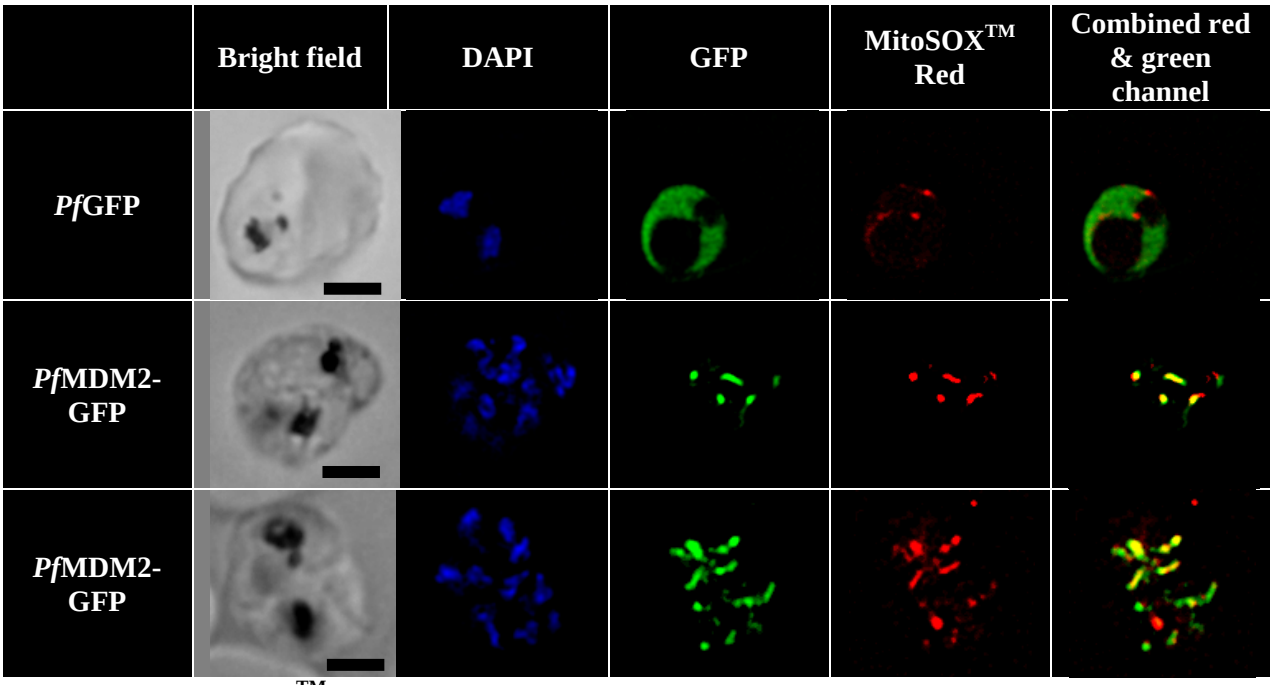

Figure 3.33: MitoSOX™ Red stained mitochondria in transgenic schizonts.
DAPI was utilized for nuclear visualization. The MitoSOX™ Red stain co-localized with *Pf*MDM2-GFP and not the GFP-tag alone. Scale bar in bright field represents 2.5µm.

3.1.3.8 The effect heat on PfMDM2-GFP localization

Late stage *Pf*MDM2-GFP parasites were exposed to 41ºC for 2 hours and as represented in figure 3.34, there was no alteration in the mitochondrial localization of *Pf*MDM-GFP 30 minutes after stress termination. Visualization of living parasites 24 hours later was complicated by the high mortality rate (Engelbrecht and Coetzer, 2013), poor MitoSOX staining and the rapid movements by the survivors. The latter process could not be circumvented with fixation since the MitoSOX™ stain required live parasites with active mitochondria. The heat stress conditions employed did not to significantly affect mitochondrial membrane polarization, (Engelbrecht and Coetzer, 2013) and is therefore an unlikely cause of poor staining. The altered reactive oxygen species content and compartmentalisation within the parasite may have affected the visualization pattern of MitoSOX™ (Zielonka and Kalyanaraman, 2010).

In the cases where MitoSOX™ staining was detected in surviving parasites after 24 hours, the pattern was similar to that of *Pf*MDM2-GFP but when overlaid the signals appeared to have shifted (figure 3.34). This shift may have been an artefact resulting from the rapid cellular movement of the parasite and a delay in image capturing through a non-automated system. Alternatively it could indicate that the protein has moved out of the mitochondrion. The survivors were, as expected, delayed in their development and were still in the late intraerythrocytic life.

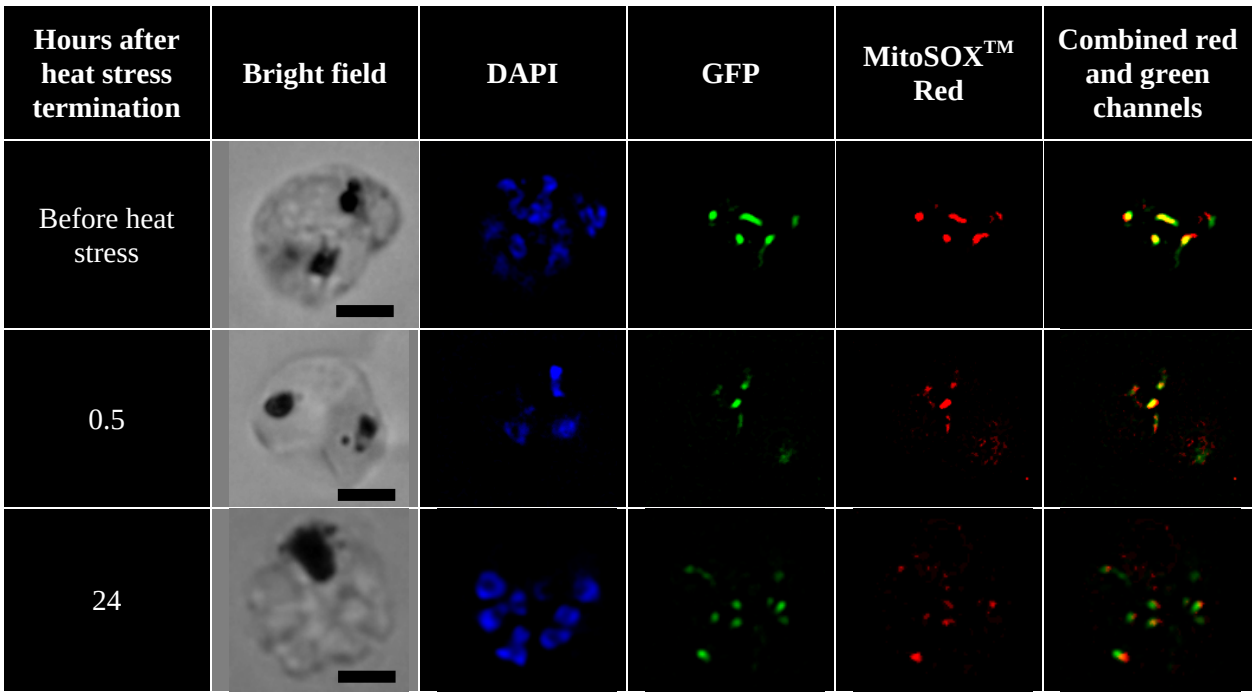

Figure 3.34: Live imaging of *Pf*MDM2-GFP in late stage parasites, after exposure to 41ºC for 2 hours.
DAPI was utilized for nuclear visualization. The MitoSOX™ red signal co-localized with *Pf*MDM2-GFP before heat stress and 30 minutes after heat stress termination. Twenty-four hours after heat stress the two signals appeared to be next to each other as opposed to overlapping. Scale bar in bright field represents 2.5µm.

3.1.3.9 Live imaging of the PfSWIB-GFP transgenic line

Transcriptome analysis of *Pf*SWIB indicated continual mRNA production throughout all the intraerythrocytic asexual life stages, highest in the ring life stage. Current proteomic data has only identified the protein in the trophozoite and schizont stages (Aurrecoechea *et al.*, 2009) and therefore focus was placed on the late asexual intraerythrocytic life stages, although the protein maybe of physiological importance in the early stages as well. Although *Pf*SWIB was predicted to have several mono-partite and bi-partite nuclear localization signals, evaluation of *Pf*SWIB-GFP localization demonstrated a cytoplasmic distribution, in both living and fixed parasites (figures 3.35 and 3.36). This pattern was akin to that documented for GFP, indicating that the protein's predicted nuclear localization signals were not used.

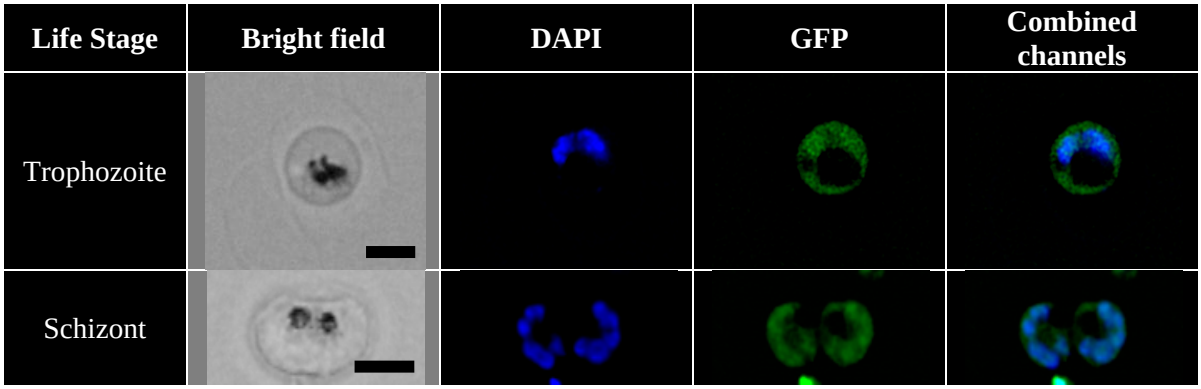

Figure 3.35: Live imaging of the *Pf*SWIB-GFP transgenic parasite line.
DAPI staining was utilized for nuclear visualization. *Pf*SWIB-GFP was present in the cytoplasm for both intraerythrocytic life stages. Scale bar in bright field represents 2.5µm.

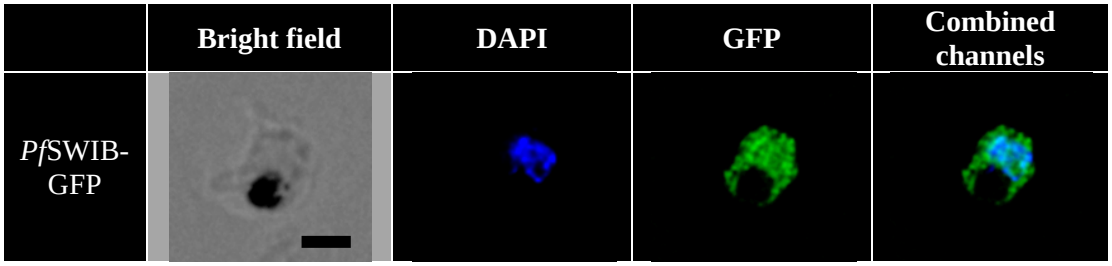

Figure 3.36: Fluorescent imaging of fixed *Pf*SWIB-GFP transgenic late stage parasites
Nuclear material was visualized with DAPI staining while the GFP signal was amplified with an anti-GFP antibody conjugate. *Pf*SWIB-GFP was located in the cytoplasm of late stage intraerythrocytic transgenic parasites. Scale bar in bright field represents 2.5µm.

3.1.3.10 The effect heat on PfSWIB-GFP localization

Late stage *Pf*SWIB-GFP parasites were stressed at 41°C for 2 hours and then analysed at several time points thereafter. After 30 minutes approximately 90% of the trophozoite population revealed a cytoplasmic *Pf*SWIB-GFP distribution pattern, identical to control parasites, while the remaining showed a clear nuclear signal, as represented in figure 3.37. Interestingly, all the early and some of the late trophozoites showed precise nuclear colocalisation, while some of the late trophozoites had some GFP signal either moving into or out of the nucleus. It is possible that activation of one or more of the predicted nuclear localization signals could drive this nuclear targeting. Schizonts retained a cytoplasmic *Pf*SWIB-GFP distribution. Therefore, the heat stress distribution pattern of *Pf*SWIB-GFP appeared to be stage specific.

The nuclear signal in the trophozoite subpopulation was not sustained, since two hours after the termination of heat stress all the trophozoites only had cytoplasmic *Pf*SWIB-GFP, which remained there up to 24 hours later (figure 3.37). Very few parasites survived 24 hours after heat stress, as expected and their development was delayed.

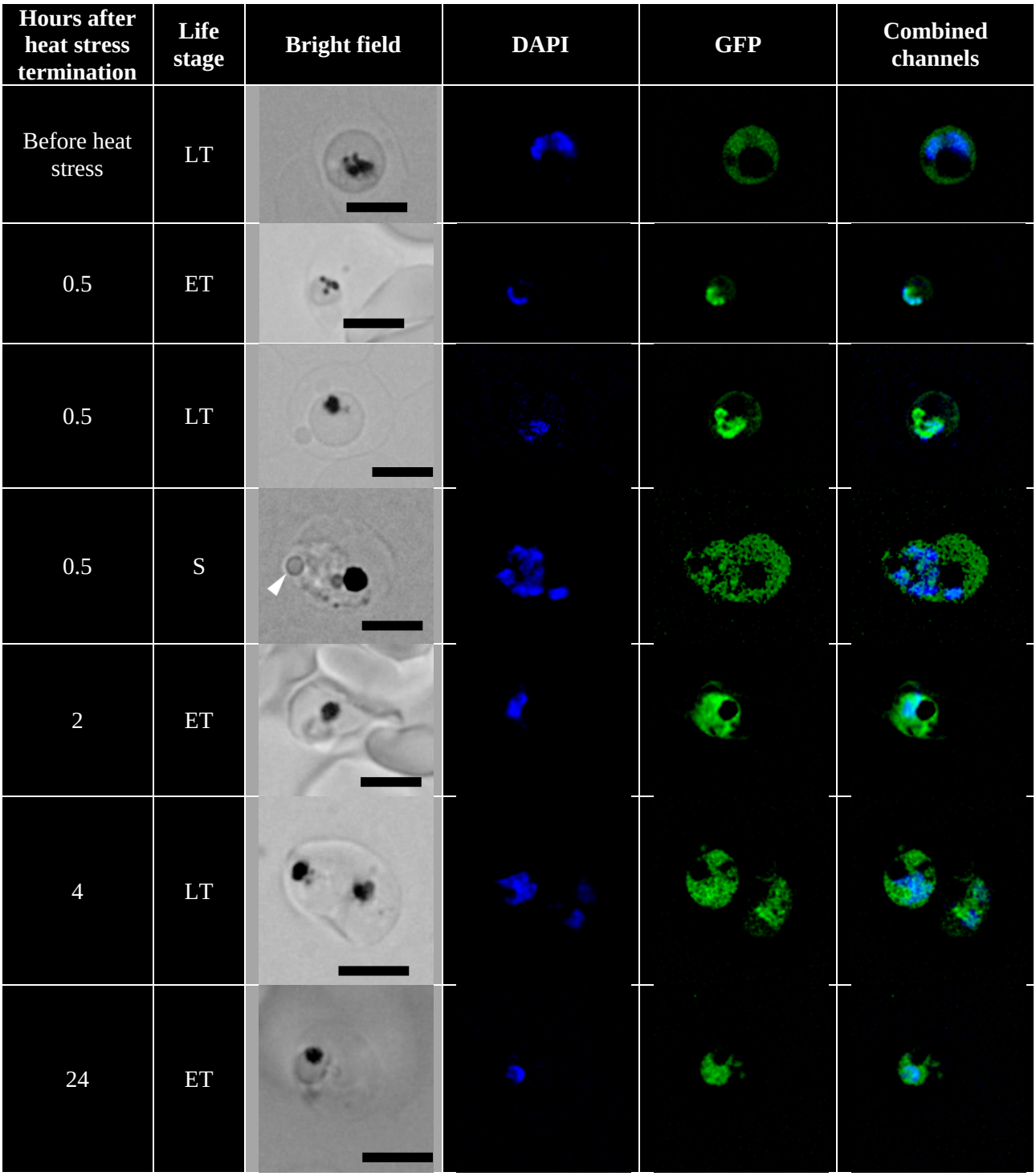

Figure 3.37: Effects of exposure to 41ºC for 2 hours on late stage *Pf*SWIB-GFP parasites.
DAPI was utilized for nuclear visualization. The cytoplasmic GFP signal was maintained in all schizonts and about 90% of the trophozoites, up to 24 hours after heat stress termination. In the remaining trophozoite population, a short lived nuclear GFP signal was documented, which was lost 2 hours post heat stress termination. The white arrow highlights a heat stress induced cytoplasmic vacuole. ET = early trophozoite, LT = late trophozoite and S = schizont. Scale bar in bright field represents 5µm.

3.2 Analysis of a putative p53 homologue within *P. falciparum*

3.2.1 Identification of a putative *P. falciparum* p53 gene

Within the *P. falciparum* genome no p53-like homologue has been annotated. Identification of p53 homologues within organisms outside the vertebrate lineage has often been complicated by low similarity and therefore requires the use of additional algorithms (Jin *et al.*, 2000, Derry *et al.*, 2001). Previous work conducted by Dr Pierre Durand, using a variety of novel computational methods such as the evolutionary rate-based alignment algorithm FIRE (Functional Inference using the Rates of Evolution (Durand *et al.*, 2010)), highlighted the PF3D7_0522400 gene (*Pf*p53) as a potential p53 DBD homologue within the *P. falciparum* genome (Coetzer *et al.*, 2010). This gene is currently described as coding for a conserved, hypothetical protein with no annotated function. The gene is located on the positive strand (Watson orientation) of chromosome 5 from base 907837 to 936315, comprising of four exons, as depicted in figure 3.38 (Aurrecoechea *et al.*, 2009). A portion of this 9307 amino acid protein was found, as will be described in sections 3.2.1.1-3.2.1.6, to carry a putative DNA binding and tetramerization domain.

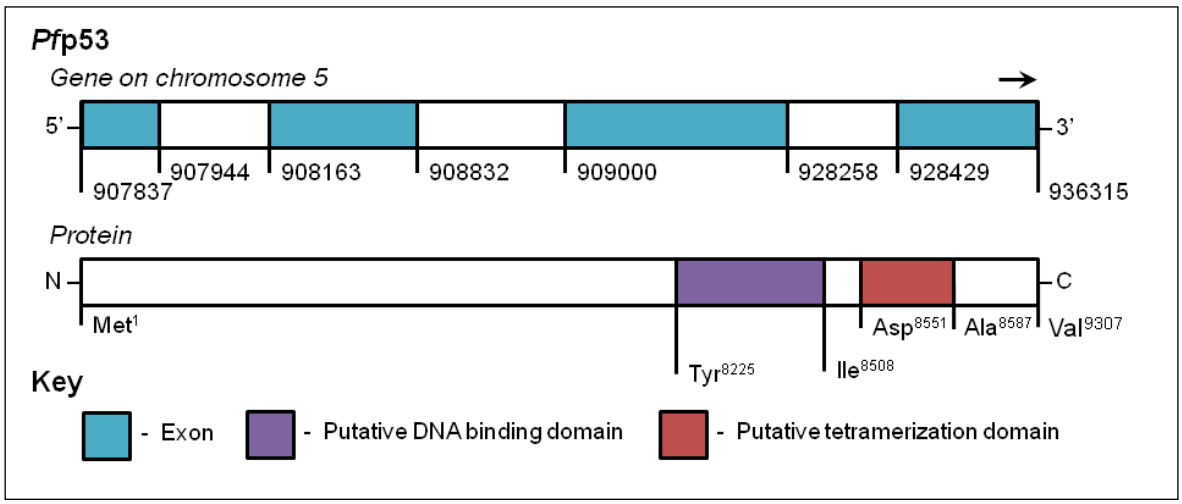

Figure 3.38: Diagrammatic representation of the putative *P. falciparum* p53 homologue (derived from Aurrecoechea *et al.*, 2009).
The numbers represent nucleotide positions situated along the chromosome while the arrow

indicates transcriptional direction for the gene. The putative DNA binding and tetramerisation domains were predicted using bioinformatics algorithms.

3.2.1.1 Primary sequence alignments for the putative DBD of Pfp53

Several standard multiple sequence alignment programs, different to those used by Dr Durand (Coetzer *et al.*, 2010, Durand *et al.*, 2010), were employed to define the location of the putative DBD within the parasite protein. As there exists a significant degree of diversification in the p53 gene during evolution (Belyi *et al.*, 2010), analysis was streamlined by assessing the *Pf*p53 protein relative to distinct multicellular lineages and low degrees of similarity and identity were anticipated. Greatest homology between p53 homologues is often confined solely to the DBD – with several amino acid residues critical for DNA interactions showing identical conservation regardless of the lineage (Ollmann *et al.*, 2000, Schumacher *et al.*, 2004, Pankow and Bamberger, 2007, King *et al.*, 2008, Holbrook *et al.*, 2009). Unlike the work done by Dr Durand, all of the standard algorithms revealed poor primary sequence conservation for the *P. falciparum* protein. Amongst the spatially different and often broken primary sequence alignments, two lineage specific Clustal omega comparisons highlighted overlapping regions of the parasite protein as a putative p53 DBD. The first employed a range of vertebrate (fish to mammal) p53 proteins and the second used the *C. elegans* transcription factor Cep-1 (a p53 homologue), as presented in figures 3.39 and 3.40 respectively.

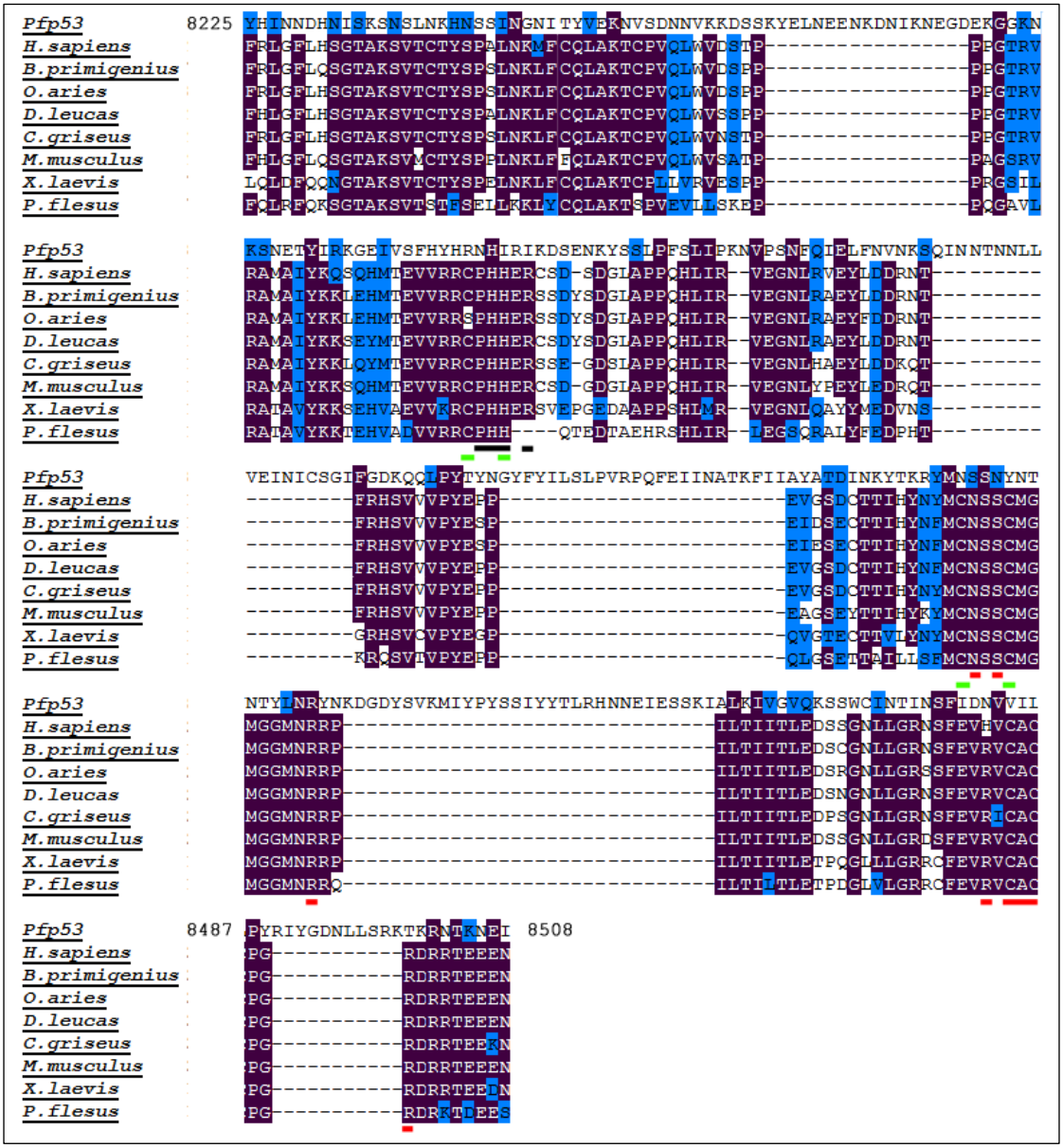

Figure 3.39: Clustal Omega primary amino acid sequence alignments for residues 8225 to 8508 of *Pf*p53 against vertebrate p53 DBDs.
The assessed portion of *Pf*p53 showed poor conservation to the DBDs of vertebrate p53 proteins. Green lines represent residues critical for Zinc binding (none conserved); black lines represent residues critical for protein dimerization (identical His^{8311}); red lines represent residues critical for nucleotide binding (Ser^{8417} and Asn^{8419} semi-conserved, Arg^{8426} identical); purple blocks indicate identical amino acids; and blue blocks indicate similar amino acids; threshold set at 80%.

Alignment of the putative *Pf*p53 DBD to the highly conserved vertebrate p53 proteins revealed a low degree of conservation. Two (Ser^{8417} and Asn^{8419}) of the eight amino acid residues stipulated as critical for vertebrate p53 nucleotide binding were semi-conserved while one (Arg^{8426}) was identical (red lines in figure 3.39). There was low conservation in

terms of the residues required for protein dimerization (only His^{8311} was identical, black lines in figure 3.39) and none involved in zinc binding (green lines in figure 3.39).

This alignment revealed a common feature documented in many *falciparum* proteins – size expansion relative to their metazoan counterparts (Pizzi and Frontali, 2000, Pizzi and Frontali, 2001). This contributed to residues 8225 to 8508 of the *Pf*p53 protein sharing only 6.6% identity and 10.3% similarity to the human p53 DBD (based on EMBOSS Needle analysis). Removal of the large intervening regions improved the sequence identity and similarity significantly (21.5% and 37.7% respectively) and was comparable to that documented for other non-vertebrate p53 homologues relative to the vertebrate p53 DBD.

The same region of *Pf*p53 could also be aligned to the DBD of Cep-1, with intervening gaps, although the alignment only started at residue 8233 and ended at residue 8506. The residues 8225 to 8508 of *Pf*p53 showed 13.1% identity and 25.4% similarity to the Cep-1 DBD (figure 3.40) but critical residues were poorly conserved. Removal of the large intervening regions from *Pf*p53 did not markedly improve the degree of identity and similarity noted (15.4% and 35.6% respectively). Only a single zinc binding residue was identical (Cys^{8362}, black lines in figure 3.40), while one identical (Tyr^{8488}) and two semi-conserved residues (Arg^{8468} and Val^{8486}) were noted for the DNA binding residues (red lines figure 3.40). Although Cep-1 is most closely related to the *D. melanogaster* p53 homologue (Dmp53), this latter protein's DBD showed very poor conservation with the putative DBD of *Pf*p53 – 8.2% identity and 17.1% similarity.

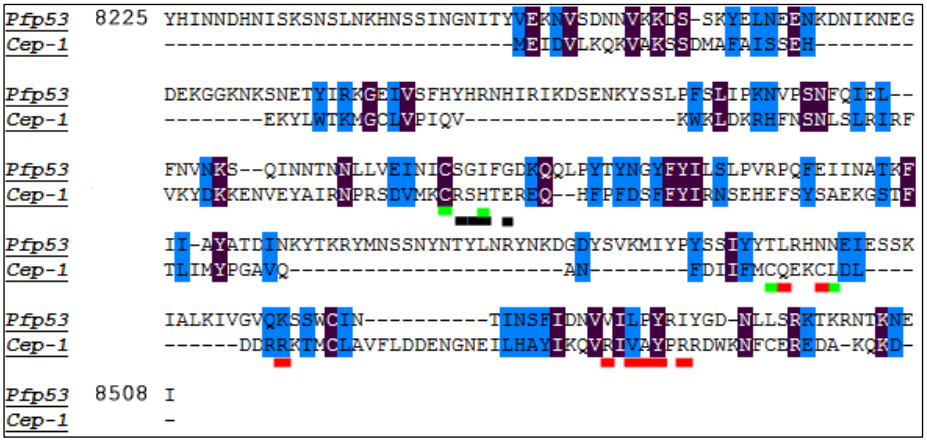

Figure 3.40: Clustal Omega primary amino acid sequence alignments for residues 8225 to 8508 of *Pf*p53 against the *C. elegans* p53 homologue (Cep-1) DBD.
A poorly conserved alignment was documented between a portion of *Pf*p53 and the DBD of Cep-1. Green lines represent residues critical for Zinc binding (Cys[8362] identical); black lines represent residues critical for protein dimerization (none conserved); red lines represent residues critical for nucleotide binding (Arg[8468] and Val[8486] semi-conserved, Tyr[8488] identical); purple blocks indicate identical amino acids; and blue blocks indicate similar amino acids; threshold set at 80%.

Sequence similarity, rather than identity, would correlate more strongly to homology as certain residue exchanges could bestow little, if any, alteration on tertiary structure and/or protein function (Rost, 1999). For this reason protein structure often shows greater conservation during evolution, as opposed to primary sequence, and was therefore investigated for the putative *Pf*p53 DBD (Rost, 1999, Geourjon *et al.*, 2001). The portion of the parasite protein selected for further analysis stretched from residue 8225 to 8508, based on the better than expected similarities with the vertebrate p53 and Cep-1 DBDs.

3.2.1.2 Secondary structure predictions for the putative DBD of Pfp53

Secondary structure predictions and tertiary structure analyses (section 3.2.1.3), were conducted with the aid of crystallized p53 homologue DBD structures. These included:

- The *C. elegans* p53 tumour suppressor-like transcription factor (Cep-1) (PBD id: 1T4W) (Huyen *et al.*, 2004)
- The in solution structure of human p53 DBD (PBD id: 2FEJ) (Pérez-Cañadillas *et al.*, 2006)

The *D. melanogaster* p53 homologue Dmp53 was also used, although it has not been crystallized.

A particular secondary structure was concluded in regions where three or more of the algorithms predicted the same topology. Overall helical predictions constituted by only one or two residues were not considered to contribute towards the overall tertiary structure of the domain. Two residues noted as beta-strands were considered as viable topological features as assessment of crystallized structures revealed that two residues can participate in beta-strand formation (example 1V31 – see section 3.1.1.3).

The secondary structures predicted for the DBD of the *H. sapiens* p53 and the *D. melanogaster* Dmp53 were similar in beta-sheet number and spatial positioning but both were poor in terms of alpha helices, having only a single helical fold of 4 residues each (figures 3.41A and 3.41B). Cep-1 had 10 beta-strands, although with a different spatial location relative to the human p53 and Dmp53 due the greater number of alpha helices predicted (figure 3.41C). The portion of the parasite protein evaluated (residue 8225 to 8508) was devoid of helices but had 14 beta-strands, as presented in figure 3.41D. The large size of the domain shifted the location of beta-strands relative to the other assessed DBDs.

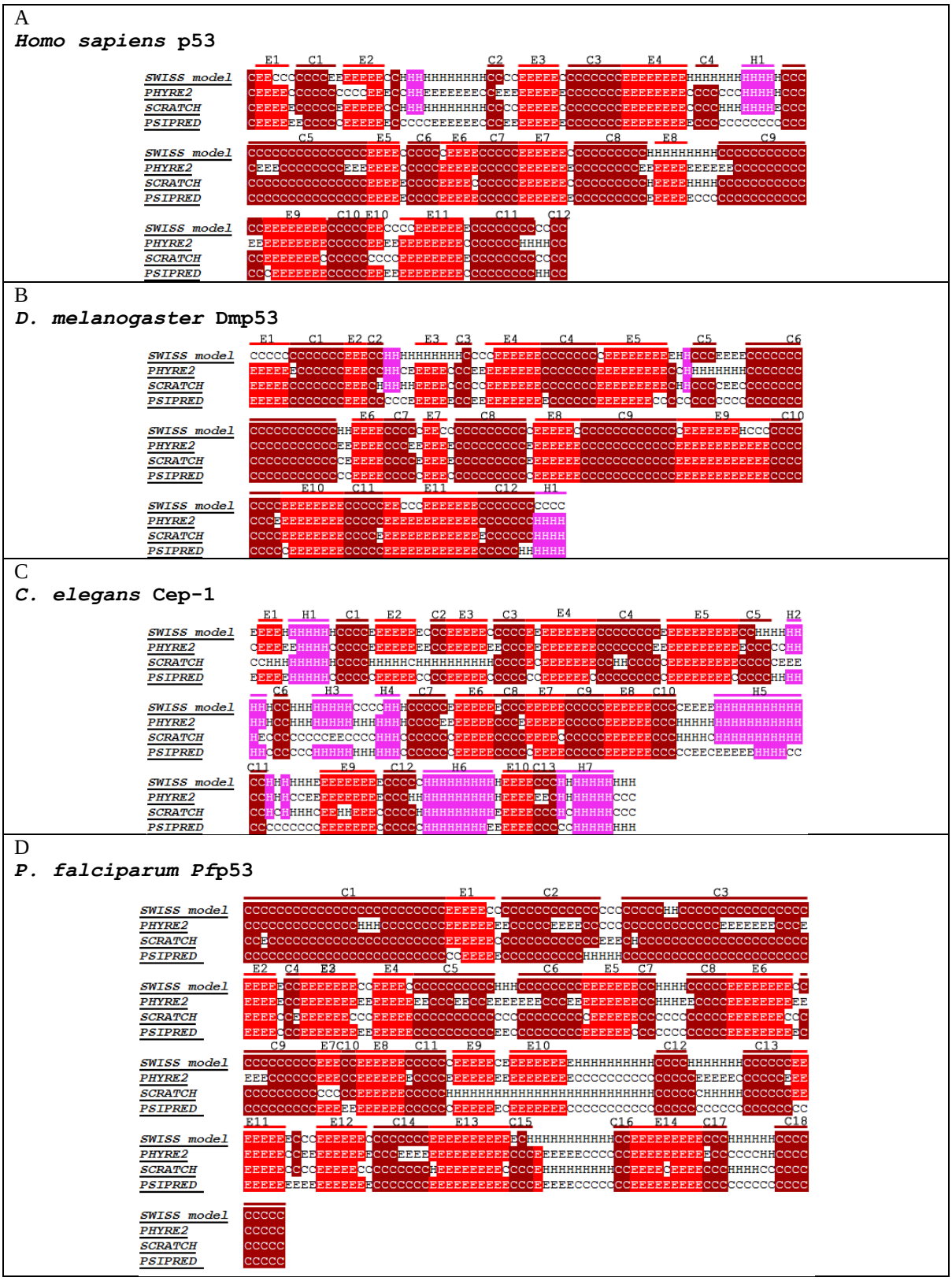

Figure 3.41: Secondary structure predictions for various p53 homologue DBDs.
The DBD domain of *H. sapiens* p53 was similar to that of *D. melanogaster* Dmp53 in terms of beta-strand content. The *C. elegans* Cep-1 DBD was richer in helices, while the parasite domain was predicted to be devoid of helices but folded into 14 beta-strands.
Blocked areas indicate identical predictions by three or more algorithms. C represents random coils; E represents beta-strands; H represents alpha helices.

3.2.1.3 Tertiary structure predictions for the DBD of Pfp53

Although the *C. elegans* Cep-1 and human p53 DBDs share low sequence similarity they share similar folds and key structural elements. The structure is constituted by a beta-sandwich of 2 antiparallel beta-sheets forming a 'Greek key' topology (green regions of figures 3.42A and 3.42B); a helix-loop-hairpin motif (red regions of figures 3.42A and 3.42B), packed tightly against the beta-sandwich; and three, so called, loop structures (white, purple and cyan regions of figures 3.42A and 3.42B) (Cho *et al.*, 1994, Huyen *et al.*, 2004, Pérez-Cañadillas *et al.*, 2006). DNA is bound by the helix-loop-hairpin motif and one of the large loops, while the beta-sandwich acts as a large scaffold to correctly position these structural elements (Cho *et al.*, 1994, Huyen *et al.*, 2004). The slight deviations in terms of DNA-binding consensus sequence affinities between the human p53 and Cep-1 are the result of slight structural variations between the two domains (Huyen *et al.*, 2004). The *C. elegans* crystallized DBD corresponds closely to its secondary structure, with the required number of beta-sheets and helical runs often in the correct spatial location, but some predicted topologies were incorrect – for example the sixth predicted alpha helix (figure 3.41C) crystallized as a beta-strand (figure 3.42A). The secondary structure prediction of the *H. sapiens* DBD corresponded closely to its crystallized form but there too discrepancies existed, such as it lacking a C-terminal helical run. Such discrepancies have been documented for proteins, where secondary structure predictions can deviate from the crystallized structure (Geourjon *et al.*, 2001).

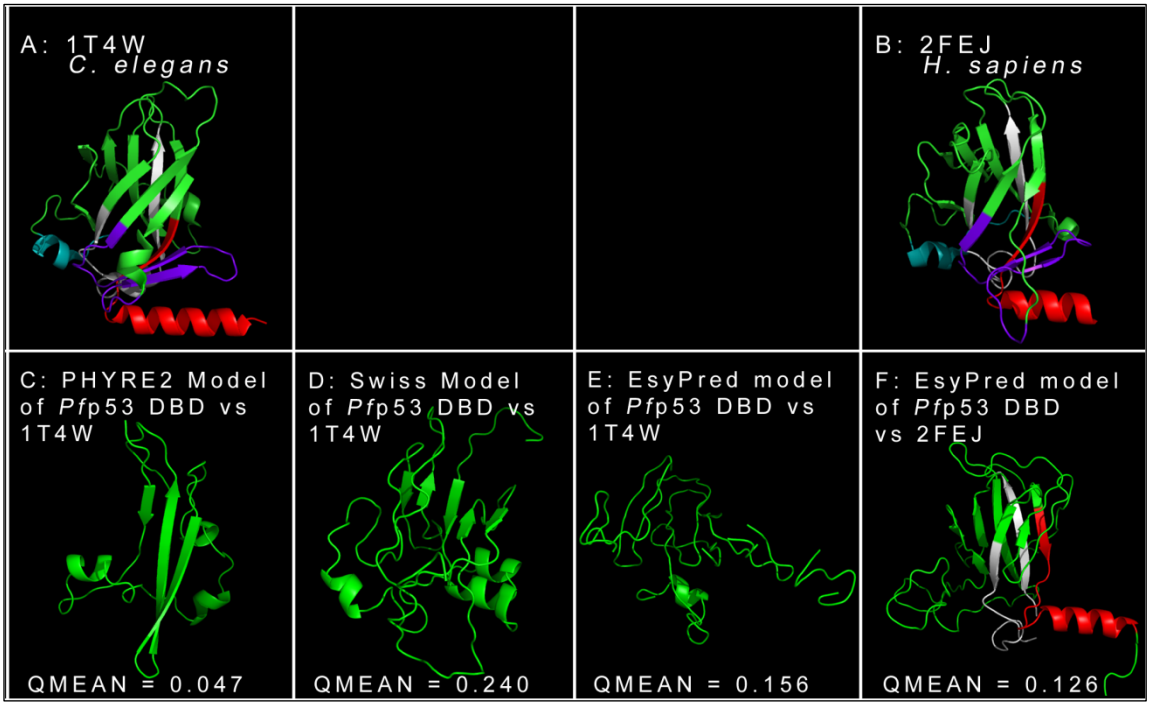

Figure 3.42: Crystallized DBDs of two p53 homologues and the various predicted tertiary structures of the putative DBD of *Pf*p53.
The green regions represent the beta-sandwich, 2 antiparallel beta-sheets forming a 'Greek key' topology, in the crystallized domains; the red region represents the helix-loop-hairpin motif and the white, purple and cyan regions denote the three large loops (Cho *et al.*, 1994; Huyen *et al.*, 2004). The putative parasite domain was modelled with poor reliability and quality, based on QMEAN analysis. All have at least one helical stretch and varying numbers of coiled regions. The model with greatest similarity to the classical p53 topology was constructed relative to 2FEJ (F).

*Pf*p53 has not been previously crystallized and was thus assessed with the aid of several standard template-based modelling algorithms. QMEAN analysis of the resultant models were extremely low (<0.25), implying that they were all highly unreliable and poor representations of the domain's native conformation (figure 3.42C – 3.42F). All the tertiary structures were rich in coiled regions, as in the predicted secondary structure, but varied in location and number of beta-sheets. All models show the presence of at least a single helical stretch, which was not predicted in the secondary structure.

All three template based algorithms could model the parasite domain against the 1T4W template (figure 3.42C – 3.42E). Only EsyPred could be forced to use the human p53 DBD crystal template, 2FEJ, to model the parasite domain. This, although unreliable when

considering the associated QMEAN score of 0.126, was constituted by a beta-sheet sandwich of anti-parallel beta-strands (green region in figure 3.42F), one of the classical loop structures (white region in figure 3.42F) and a helix-loop-hairpin motif (red region in figure 3.42F). The structural deviations compared to 2FEJ and 1T4W, in relation to topology, size and orientation, were anticipated, in part, due to the domain's proposed alterations during evolution and low relative similarity (Jin *et al.*, 2000).

Modelling based on bioinformatics, especially when using standard techniques for p53 homologues, is not always reliable. Therefore, based on primary sequence alignments the putative DBD of *Pf*p53 (residues 8225 to 8508) was expressed as a recombinant protein and used for biochemical assessments to determine if it could bind to DNA (section 3.1.3).

3.2.1.4 Primary sequence alignments for the putative tetramerization domain of Pfp53

The p53 tetramerization domain has been hypothesized to have undergone broad diversification during evolution and therefore a low degree of homology, if any, would be anticipated in *Pf*p53 (Lu *et al.*, 2009). Several multiple sequence alignment programs were employed to determine if a putative tetramerization domain could be identified within a portion of the parasite protein. A small degree of similarity was only identified relative to the vertebrate domain (figure 3.43), with amino acid residues 8551 to 8587 showing 14.3% identity and 18.4% similarity to the human p53 tetramerization domain. This was less than that seen amongst other p53 homologues. Hydrophobic interactions are critical for the function of the domain (Miller *et al.*, 1996). This region of the parasite protein (8551 to 8587) is constituted by 49% hydrophobic amino acids residues, while the human domain is composed of 33%. Additionally, the vertebrate p53 tetramerization domain is situated in

close proximity to the C-terminal end of the DBD, a feature extended to the putative parasite domain.

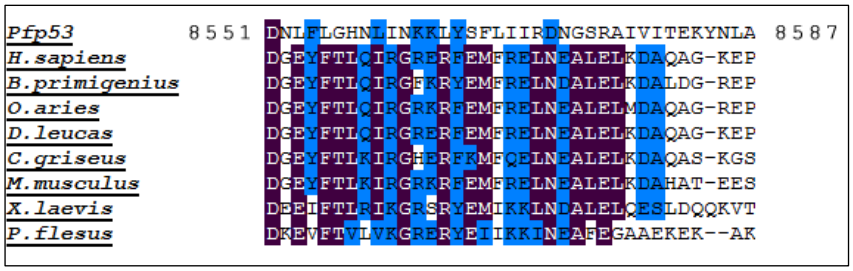

Figure 3.43: Clustal Omega primary amino acid sequence alignment of various vertebrate p53 tetramerization domains against *Pf*p53.
A small degree of conservation was documented between the vertebrate p53 tetramerization domain and a portion (residues 8551 to 8587) of *Pf*p53. Purple blocks indicate identical amino acids; blue blocks indicate similar amino acids; threshold set at 80%.

As for the putative DBD, or any other protein homologue for that matter, sequence similarity was not used as a sole indicator of homology as some sequence alterations can have little or no effect on tertiary structure and/or protein function (Rost, 1999). Hence the structure of the putative tetramerization domain was analysed with the aid of various bioinformatic algorithms.

3.2.1.5 Secondary structure predictions for the putative tetramerization of Pfp53

The secondary structures were predicted for the human p53 tetramerization domain and for the residues 8551 to 8587 of *Pf*p53. Three or more of the algorithms predicted that the human p53 tetramerization domain folded into a single beta-strand and an alpha helix (figure 3.44A). The parasite domain was predicted to fold into three beta-strands and a single, shorter helical run (figure 3.44B).

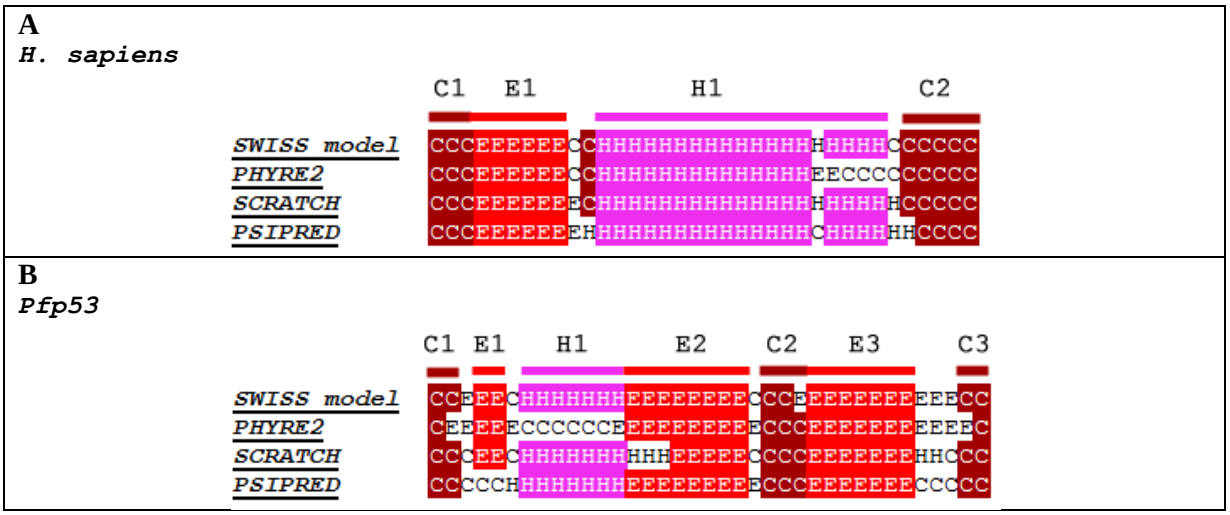

Figure 3.44: Secondary structure predictions for the *H. sapiens* p53 tetramerization domain and residues 8551 to 8587 of *Pf*p53.
The two predicted topologies are significantly different from one another, both in frequency and location of specific secondary structures.
Blocked areas indicate identical predictions by three or more algorithms. C represents random coils; E represents beta-strands; H represents alpha helices.

3.2.1.6 A tertiary structure prediction for the putative tetramerization domain of Pfp53

The p53 protein is able to form dimers without the tetramerization domain; facilitated by interactions between residues of the DBD itself. The tetrameric structure of the transcription factor relies on the tetramerization domain, whereby the dimeric structures are linked (Miller *et al.*, 1996)**.** The annotated domain is constituted by a single alpha-helix, according to NCBI database and work by Miller *et al.*,(1996), which is responsible for two orthogonally positioned p53 dimers forming a tetramer (Miller *et al.*, 1996). A neighbouring beta-sheet has been stated as constituting part of the functional structure, although it does not participate in direct binding (Miller *et al.*, 1996). The crystallized human p53 tetramerization domain, a single helical stretch preceded by random coils, was different to its corresponding secondary structure prediction (figure 3.45A) since no beta-sheets were seen (Mittl *et al.*, 1998).

The only template-based modelling algorithm which could predict the topology of region 8551 to 8587 of *Pf*p53 was EsyPred, using the 1AIE template. The model was constituted

by a much smaller, single alpha helix relative to the human domain (figure 3.46B), flanked by long stretches of random coils on both sides and no beta sheets. The location of the helix did not correlate to that predicted in the secondary structure, beginning at the end of the helix prediction and running through the beta-strand portion.

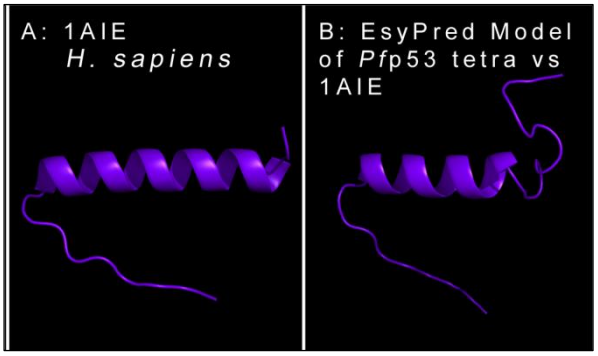

Figure 3.45: Crystallized human p53 tetramerization domain and a tertiary model of residues 8551 to 8587 of *Pf*p53.
The modelled parasite domain was predicted to fold into a single, short helix, with a similar topology to the alpha helix of the human p53 tetramerization domain. Tetra denotes tetramerization domain.

Although the evidence was poor, residues 8551 to 8587 of *Pf*p53 were expressed as a recombinant protein and their involvement in protein tetramerization was assessed (section 3.1.4).

3.2.2 Predicted nuclear localization for *Pf*p53

An important consideration for a functional p53 homologue within the parasite would be nuclear localization, critical for a transcriptional PCD-regulatory role. The *Pf*p53 protein has not been shown to carry any signal sequence on the *Plasmodium* database and thus was assessed by a variety of bioinformatic tools. Several cellular locations were predicted, the nucleus being the most strongly and commonly predicted location (a more detailed report is presented in Appendix A). Several regions of the protein were highlighted to contain putative nuclear localization sequences, a common feature of p53 homologues. Sequence

alignments and EMBOSS Needle assessments indicated that the *Pf*p53 sequences STNSLKEP, IKNKKGK and KKKKMM had 37.5%, 57.1% and 50% identity to the three human p53 nuclear localization sequences, respectively. The locations of these three signals in the parasite protein are presented in figure 3.46.

Nuclear export sequences were not as strongly conserved in *Pf*p53 based on sequence alignments and EMBOSS Needle assessments. The *Pf*p53 sequences DTFYRPWVSLV and IYLRNMHKF had 23.5% and 16.7% identity to the two human p53 nuclear export sequences respectively.

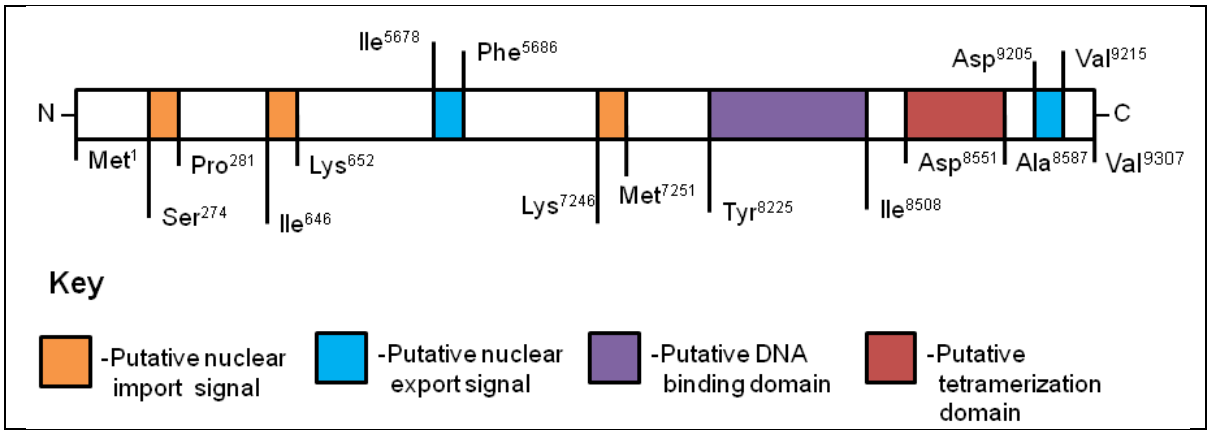

Figure 3.46: Diagrammatic representation of the nuclear localization signal sequences situated in the putative *P. falciparum* p53 homologue.

3.2.3 Assessment of the DNA binding ability of *Pf*p53

The predicted DBD and nuclear localization signals (sections 3.2.1 and 3.2.2) prompted EMSA studies to assess the DNA binding ability of *Pf*p53.

3.2.3.1 Preparation of a Pfp53 construct

The putative DNA binding and tetramerization domains of *Pf*p53 were amplified, as a single unit, by PCR and prepared for directional insertion into the pGEX-4T-2 vector. As presented in figure 3.47, below the correctly sized amplicon (molecular mass of 1602bp)

there were two faint bands. These non-specific products, which can occur during PCR, did not hinder the cloning process due to their greatly reduced quantity relative to the correct amplicon.

Previous studies have shown that the human p63 DBD, sharing 55.4% identity to the human p53 DBD, was unable to bind to the p53 consensus sequence in the absence of a GST-tag. The tag allowed for artificial domain dimerization facilitating consensus sequencing binding, detected via an EMSA (Klein *et al.*, 2001). Thus, in this study to ensure that any possible lack of intrinsic domain-domain dimerization did not prevent DNA binding, the GST-tag was fused to the *Pf*p53 recombinant protein.

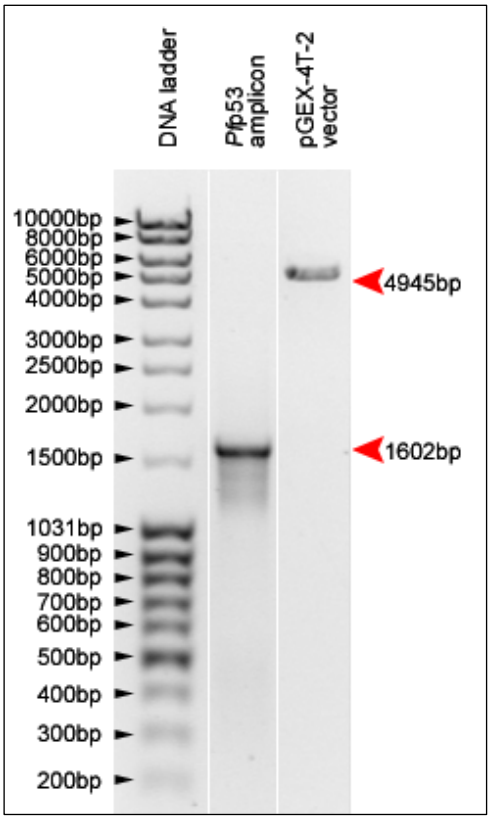

Figure 3.47: The pGEX-4T-2 plasmid and the *Pf*p53 domain amplicon.
Assessment conducted by 1% agarose gel electrophoresis, with size validation relative to a base pair standard.
Lane 1 – MassRuler^{TM} mixed range DNA ladder; Lane 2 – *Pf*p53 domain amplicon; Lane 3 – linearized pGEX-4T-2 plasmid.

3.2.3.2 Verification of the Pfp53 construct

A minimum of five bacterial colonies where assessed to verify transformation with the *Pf*p53 construct, with the aid of restriction endonuclease digestion (figure 3.48), as previously described in section 3.1.2.3. The construct was subsequently validated by sequence analysis and used for the transformation of Rosetta™ 2 (DE3) cells and recombinant protein expression.

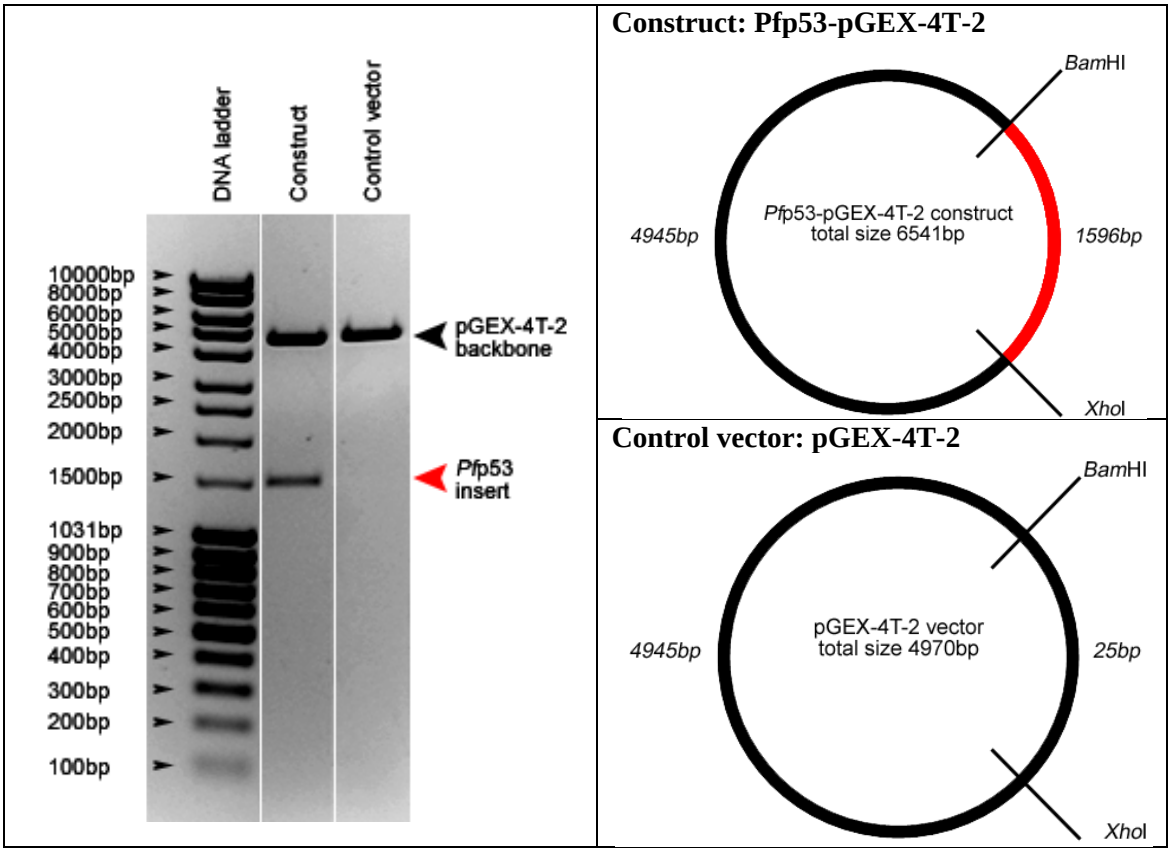

Figure 3.48: Validation of the *Pf*p53-pGEX-4T-2 construct by restriction endonuclease digestion.
*Bam*HI and *Xho*I were used to excise the *Pf*p53 amplicon (marked by the red arrow) from the *Pf*p53-pGEX-4T-2 construct. A control digestion reaction was conducted on the pGEX-4T-2 vector. The vector maps on the right indicate the band sizes expected after construct and control plasmid digestion.

3.2.3.3 Recombinant expression of the GST-tagged protein

From this point on the term GST-*Pf*p53 will represent the recombinant GST-tagged DBD and tetramerization domain of *Pf*p53. Optimization of recombinant GST-tagged protein

expression was discussed in section 3.1.2.4 and applied to GST-*Pf*p53. The protein was purified and isolated, as presented in figure 3.49, at a better than theoretically expected solubility (~40% as determined by immunoblot densitometry vs. 7% calculated, figure 3.49 and table 3.9). The nevertheless low solubility was probably induced, in part, by the protein's basic pI of 9 (Mehlin *et al.*, 2006).

The GST-tagged protein was isolated with ~73% purity, based on densitometry of Coomassie blue-stained gels, although the associated yield was relatively low when compared to other GST-fusion proteins expressed during this study – ~1.9µg per 20ml bacterial culture. GST-*Pf*p53 migrated at a molecular mass of 87kDa, close to its theoretically expected mass of 88.4kDa (table 3.9 and figure 3.49). The relatively large size of the protein was likely to have played a significant role in reducing its expression and thus its yield (Mehlin *et al.*, 2006).

Table 3.9: The properties of GST-*Pf*p53

Protein name	**N-terminal tag**	**Molecular mass (kDa)**		**Predicted solubility‡ (%)**	**pI†**	**Purity (%)**	**Average concentration of elution (ng/µl) ± standard deviation (n=3)**	**Yield per 20ml *E. coli* culture (µg)****
		Calculated †	*Based on SDS-PAGE**					
***Pf*p53**	GST	88.4	87.0	7,0	9.0	~73	37 ± 17.7	~1.9

†Entire fusion protein, tag included, assessed using ExPASy (Gasteiger *et al.*, 2005);* A standard red cell membrane marker was used for relative molecular mass determination; ‡ Calculated using the Recombinant Protein Solubility Prediction program (Wilkinson and Harrison, 1991) for the entire fusion protein, tag included; ** Average from three elutions.

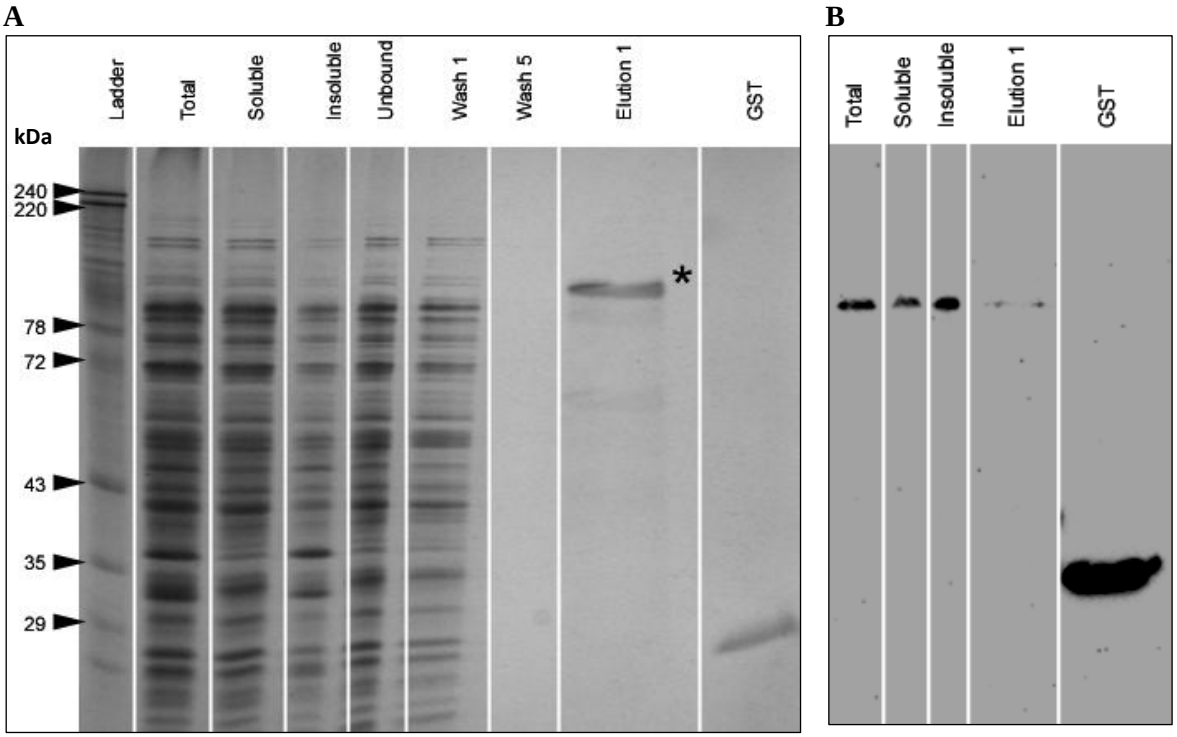

Figure 3.49: Expression and immunoblot analysis of GST-*Pf*p53.
A) A Coomassie blue-stained SDS polyacrylamide gel. Aliquots assessed: 5µl of the red cell membrane ladder; 1.5µl of 1.5ml total, soluble, insoluble and unbound fractions; 20µl of 1ml of washes; 10µl of 150µl of elution 1; and 10µl of 150µl of GST elution (control). The *Pf*p53 fusion protein migrated at 87kDa, roughly its correct theoretically expected molecular mass of 88.4kDa.
B) An immunoblot using an anti-GST antibody verified the 87kDa protein band as GST-*Pf*p53. The volumes of aliquots were assessed as stated above expect for the use of 10µl of 150µl of elution 1 and 5µl of 150µl of GST elution (control).
* indicates GST-*Pf*p53

3.2.3.4 p53 DNA binding consensus sequence identification

Binding assays have proven that a wide range of p53 homologues, regardless of the eukaryotic lineage, are able to bind to the standard p53 DNA-binding consensus sequence (PuPuPuCWWGPyPyPy duplicated and separated by no more than 13 random bp), suggesting that the protein and sequence evolved as a conserved unit (Pankow and Bamberger, 2007).

Using the DNA motif search function on the *Plasmodium* database 3662 genomic sequences were identified to encode half of the generic canonical p53 DNA-binding

consensus sequence (PuPuPuCWWGPyPyPy). Of these only two matched the full length consensus sequence, where the base pair gap between the two halves was no more than 13. There were four additional sequences where the two halves of the canonical consensus sequence were separated by a gap of 13 – 25bp. Results are presented in table 3.10. All six sequences are present in coding regions which is a described characteristic of p53 DNA-binding consensus sequences (Beckerman and Prives, 2010). No pattern of association was noted between the genes in which these sequences were identified and a cellular function and/or role.

Table 3.10: p53 DNA-binding consensus sequences identified within the *P. falciparum* genome.

Consensus sequence*	Sequence identified†	Gene identity (gene annotation)	Start and end site in chromosome
PuPuPuCWWGPyPyPy (23) PuPuPuCWWGPyPyPy	AAGCAAGTTTTACATAGAGAAGTGAGTTCAGAAAAACTAGCTT	PF3D7_0933100 (conserved Plasmodium protein, unknown function)	1314552 -1317597
PuPuPuCWWGPyPyPy (17) PuPuPuCWWGPyPyPy	AAACATGTTTTCACTTCTTCATCATTCAAACATGTTT	PF3D7_1116100 (serine esterase, putative)	607902 -613394
PuPuPuCWWGPyPyPy (14) PuPuPuCWWGPyPyPy	GGACTTGCTCCCGTACTACCTTGTGGACTTGCTC	PF3D7_0207600 (serine repeat antigen 5 (SERA5))	303593 -307027
PuPuPuCWWGPyPyPy (14) PuPuPuCWWGPyPyPy	AAACATGCTTTTGAATATTCTAAAAAGCTTGTTC	PF3D7_0408600 (sporozoite invasion-associated)	413403 -416357
PuPuPuCWWGPyPyPy (6) PuPuPuCWWGPyPyPy	AAACTAGTTTATAAAAAAGCTAGTTT	PF3D7_0829800 (unspecified product)	1272718-1275456
PuPuPuCWWGPyPyPy (4) PuPuPuCWWGPyPyPy	AAACATGCTTTTAAAAACAAGCTT	PF3D7_1253000 (gametocyte erythrocyte cytosolic protein)	2168181-2169759

*number in brackets = number of random nucleotides separating the two halves of the DNA-binding consensus sequence; † underlined nucleotides = random, intervening nucleotides.

The *Entamoeba histolytica* p53-like DNA-binding consensus sequence failed to have any matches in the 3D7 *P. falciparum* genome (Mendoza *et al.*, 2003). Furthermore, no matches were found for derivatives of this sequence (AGAAATTCATGGGCTAGTGG, AGAAATTCNNGGGCTAGT and AGANATNCNNGGGCTAGT where N represents any nucleotide that did not comply with the canonical vertebrate p53 DNA-binding consensus sequence). Non-canonical binding sites for p53 have been documented although these were not considered as part of this study.

Based on the above findings, only a single canonical p53 DNA binding sequence was used to assess *Pf*p53 DBD binding ability. This was one of the sequences identified within the *falciparum* genome – AACATGCTTTTAAAAACAAGCTT.

3.2.3.5 EMSA for Pfp53

Protein-oligonucleotide interactions can rapidly and sensitively be semi-qualitatively assessed with the aid of an EMSA (Hellman and Fried, 2007). In this study a DIG-labelled system was employed, stated by the manufacturer to have sensitivity at least equal to that of the isotope system (Roche Applied Science, 2004).

GST-*Pf*p53 was used in an array of experiments with the *Pf*p53 DNA-binding consensus sequence using a DIG Gel Shift Kit. Two types of control reactions were employed. The first validated the assay, whereby the Oct2A DNA binding factor, supplied in the kit, was allowed to interact with its known consensus sequence, resulting in a mobility shift, as represented in figure 3.50A lane 2. The functional binding interaction between the protein and the labelled oligonucleotide was almost abolished when 100x excess of unlabelled Oct2A consensus sequence was added to the reaction, thus out-competing the labelled

oligonucleotide and indicating binding specificity (figure 3.50A lane 3). The second control validated that various amounts of GST alone did not unexpectedly facilitate an oligonucleotide signal shift (represented in figure 3.50B).

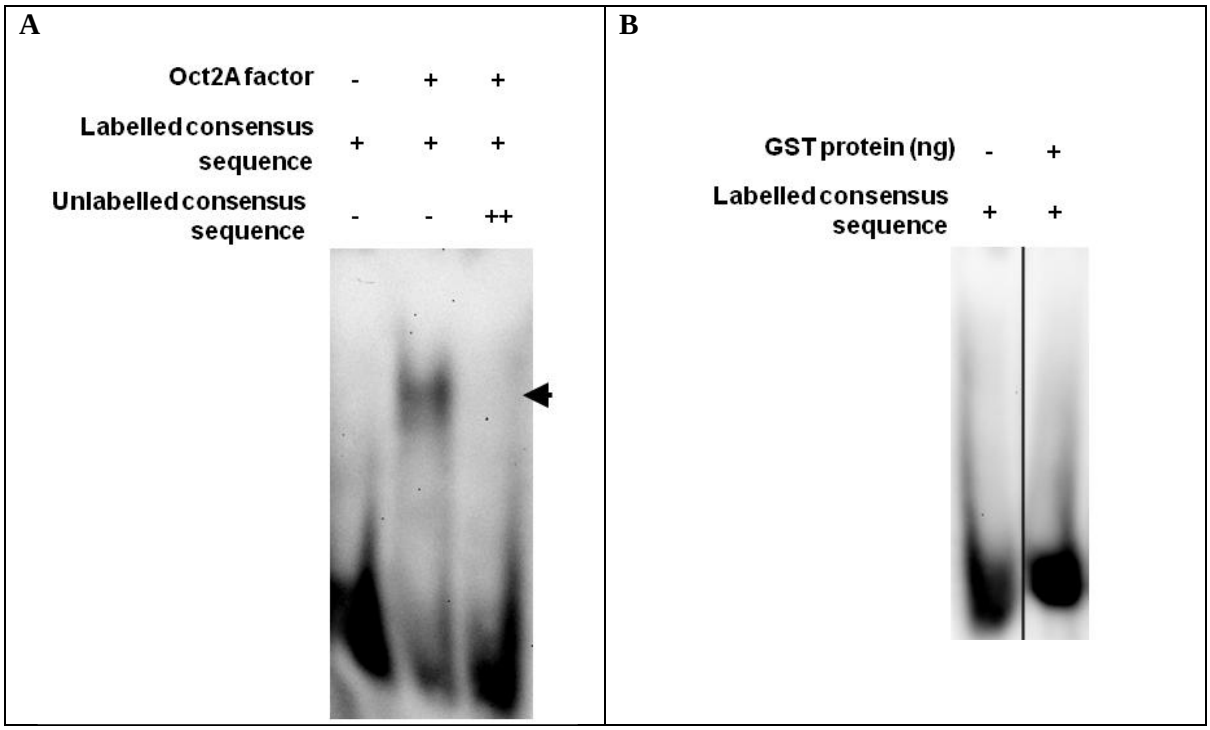

Figure 3.50: Control EMSA reactions.
A) EMSA kit validation. The Oct2A binding factor caused a distinct shift in the signal of its known DNA-binding consensus sequence (marked by the black arrow). This shift was abolished by the addition of excess unlabelled competitor consensus sequence. For the Oct2A factor, + or - represent factor presence or absence respectively; for the unlabelled consensus sequence ++ represents a 100 fold excess relative to the labelled consensus sequence (+).
B) GST control EMSA. GST, at 200ng, failed to induce a signal shift when exposed to the *Pf*p53 DNA-binding consensus sequence. For GST, + or - represent protein presence or absence respectively. The black line represents the joining of two gels.

When the assay was carried out for the GST-*Pf*p53 and labelled p53 consensus sequence, a range of DNA:protein molar ratios were used (2 to 78). In all experiments GST-*Pf*p53 failed to induce an oligonucleotide signal shift, as presented in figure 3.51. Overheating, localized to the central bottom region of some of the gels, was believed to be the cause of the unusual curved migration pattern documented in some cases. These results indicated

that, under the employed conditions, the putative *Pf*p53 DBD was unable to associate with a canonical p53 DNA-binding consensus sequence.

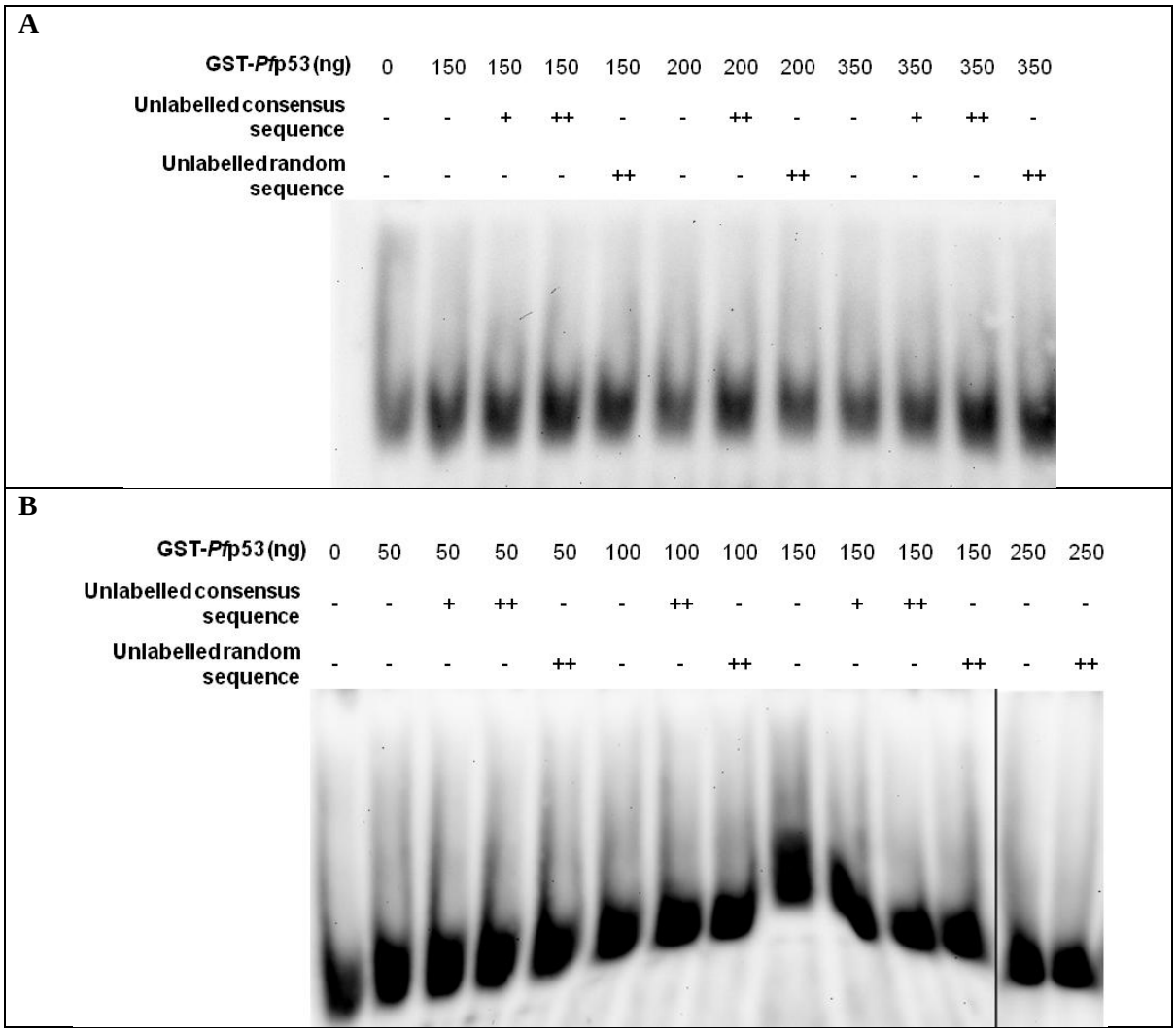

Figure 3.51: EMSA with GST-*Pf*p53 failed to induce any signal shift.
Experiments conducted with increasing amounts of the GST-*Pf*p53 and a constant (A) 2ng or (B) 4ng of DIG-labelled *Pf*p53 DNA-binding consensus sequence. None of the experiments showed a shift in labelled oligonucleotide when separated on a 6% native polyacrylamide gel and detected with an anti-DIG antibody. + represents a 10 fold excess of unlabelled sequence relative to the labelled DNA-binding consensus sequence; ++ represents a 100 fold excess relative to the labelled consensus sequence. Black line represents two gels joined together.

3.2.4 Assessment of *Pf*p53 tetramerization

A C-terminal region, adjacent to the putative DBD, of the *Pf*p53 protein was identified as a putative tetramerization domain (section 3.2.1) and was assessed by means of a

tetramerization assay. The assay was initially validated with BSA, which is able to form oligomers naturally (Payne, 1973). The oligomeric state of BSA can be retained, even after solubilization, in the absence of a cross-linking agent due to the limited accessibility of its disulphide bonds. The addition of a cross-linking agent enhanced the retention of BSA oligomers, but had little effect on dimers, trimers and tetramers, as represented in figure 3.52 (Payne, 1973). Although Tris is known to inhibit glutaraldehyde cross linking, the 500mM Tris GST-elution buffer showed no reduction in BSA oligomer retention relative to other buffering systems without Tris. The final concentration of glutaraldehyde used for GST-*Pf*p53 analysis was within the range used for detecting murine and human p53 oligomers – 0.02% (Payne, 1973, Stenger *et al.*, 1992, Wang *et al.*, 1994).

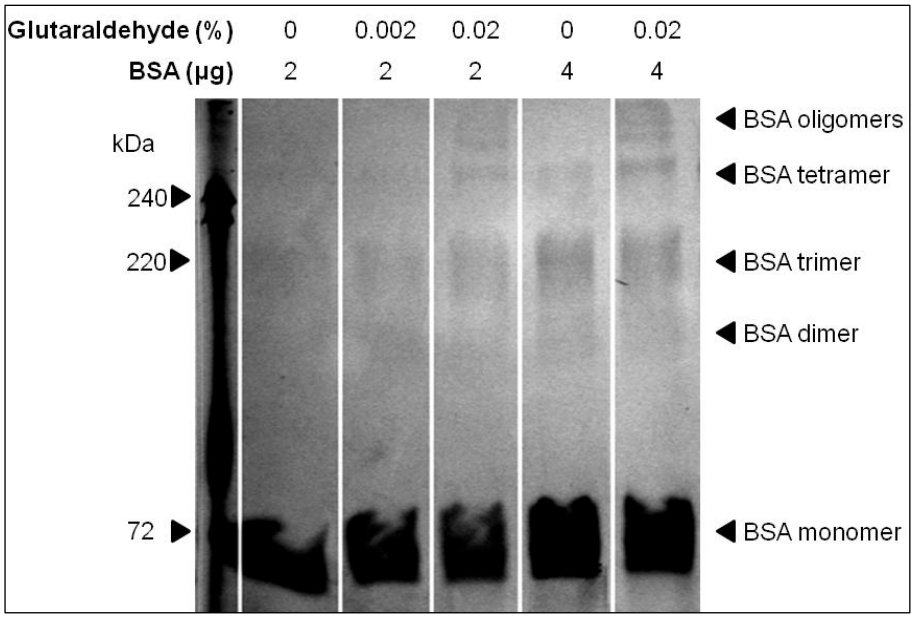

Figure 3.52: Conservation of BSA oligomers in GST elution buffer.
Analysis of BSA oligomerization using SDS-PAGE and Coomassie blue gel staining. As little as 0.002% glutaraldehyde aided in conserving the higher oligomeric states of BSA.

There was difficulty in clearly detecting any oligomeric state for GST-*Pf*p53. Based on figure 3.53 the monomeric GST-*Pf*p53 (~87kDa) was significantly reduced and there was

no dimer (~174kDa) detected. A large amount of protein was retained in the well of the oligomeric GST-*Pf*p53 sample lane, suggesting the protein formed higher oligomers, too large to enter the gel. As presented in figure 3.53, there was a possible tetrameric form (~350kDa) for GST-*Pf*p53 although repeated attempts, with the aid of SDS-PAGE and subsequent Coomassie blue staining or immunoblotting, could not clearly define such a higher oligomeric GST-*P*fp53 population. Attempts to improve protein separation, using a 4-17% gradient gel, and visualization with the aid of the 100x more sensitive silver staining technique relative to Coomassie blue staining (Switzer *et al*., 1979), were unsuccessful.

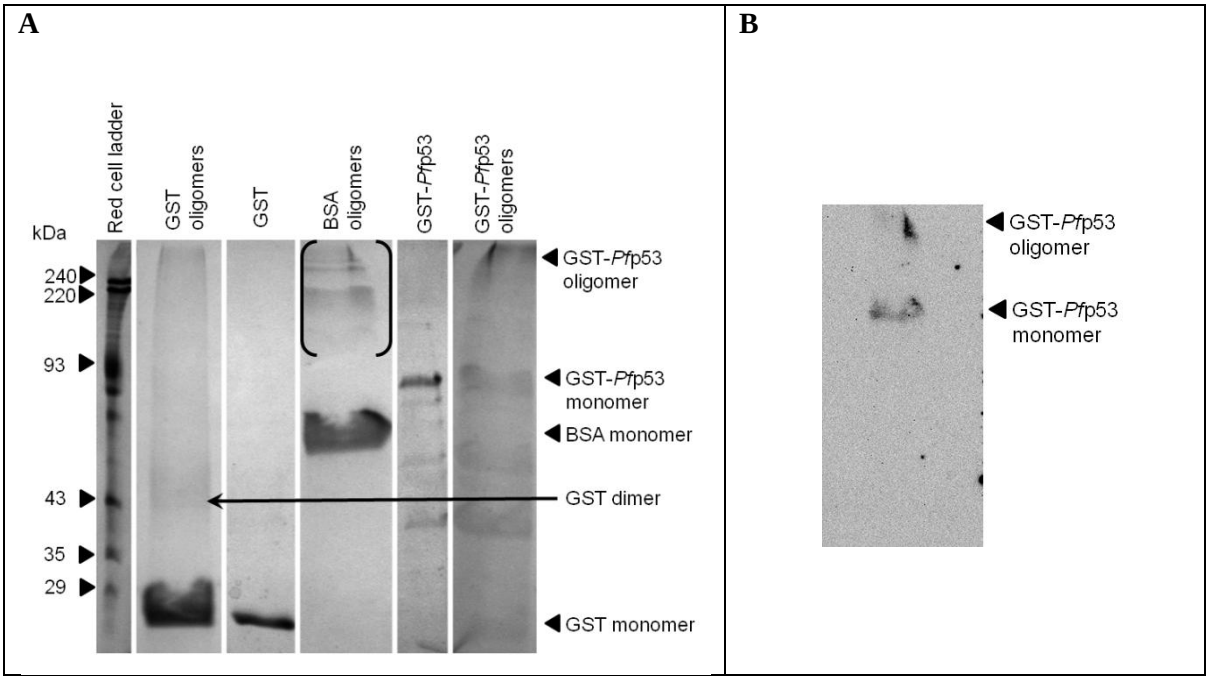

Figure 3.53: SDS-PAGE and western blot analysis of GST-*Pf*p53 oligomers.
Samples were resolved by SDS-PAGE and visualized by A) Coomassie blue staining and B) immunoblotting, using an anti-GST antibody. GST-*Pf*p53 showed a reduced amount of monomer, relative to control GST-*Pf*p53, and a possible tetrameric form (~350kDa). The brackets highlight the various BSA oligomers.

The involvement of the elution impurities in the formation of oligomers was negligible, due to their conserved monomeric state relative to the control elution (figure 3.53).

Although the majority of GST retained a monomeric state when assessed, faint GST dimers were preserved, as theoretically expected (Fabrini *et al.*, 2009), when large quantities of GST was exposed to glutaraldehyde. The reduction in the GST monomeric state and the formation of dimers was negligible when standardized relative to GST-*Pf*p53. This suggested that there was no effect by GST on GST-*Pf*p53 oligomerization and the putative tetramerization domain of *Pf*p53 was a stronger driving force for oligmerization than GST alone. Due to the low yield of GST-*Pf*p53 thrombin-directed removal of the GST-tag was not possible to validate this statement further.

4 DISCUSSION

Although several metazoan PCD machinery homologues have been identified by bioinformatics within the *Plasmodium* genome none have been directly linked to a PCD-like phenotype in the parasite (Nedelcu, 2009, Proto *et al.*, 2013). Currently, the only real evidence supporting PCD in *P. falciparum* has been derived from numerous biochemical and morphological markers which are attributed to metazoan PCD phenotypes (Engelbrecht *et al.*, 2012).

Part of the balance between death prevention and execution, within a metazoan cell, is mediated by specific transcription factors, such as p53, and transcriptional regulators, including MDM2 and the SWI/SNF complex. These regulators have direct involvement in pro-survival responses and both encompass the same functional SWIB/MDM2 domain (Cairns *et al.*, 1996, de la Serna *et al.*, 2000, Lee *et al.*, 2002, Wade *et al.*, 2010). The p53 protein is a well described pro-apoptotic factor within a wide range of eukaryotic organisms (Lu *et al.*, 2009). In *P. falciparum*, two SWIB/MDM2-containing genes have been annotated on PlasmoDB, while a p53 homologue is still outstanding (Aurrecoechea *et al.*, 2009). Novel analysis by Dr. P. Durand identified a putative p53 DBD within the *P. falciparum* genome (Coetzer *et al.*, 2010). This study therefore aimed to elucidate the cellular activities of these three genes within the parasite and to determine their importance in relation to parasite survival and stress response through the implementation of a variety of molecular techniques.

4.1 The solubility of recombinant *P. falciparum* protein domains

Literature readily documents the difficulties associated with recombinant parasite protein expression in a bacterial system. Soluble heterologous expression has been negatively associated with a basic pI, sequence composition, large size, and lack of homology to the proteins of other organisms (Birkholtz *et al.*, 2008). These are not hard and fast rules and deviations are readily observed (Mehlin *et al.*, 2006).

According to Mehlin and colleges (2006) and Vedadi and colleges (2007) recombinant protein expression is favoured for proteins with a pI between 6 and 8 while proteins with a basic pI tend to be insoluble. This was not observed in the current study. Proteins with pI values outside the ideal range were strongly expressed and correlations with solubility were inconsistent. Bioinformatic solubility predictions were unreliable as well. Of the seven *P. falciparum* domains only two (His-*Pf*RS6 and GST-*Pf*MDM2) were expressed at their expected solubility levels. Additionally, neither fusion tag (GST and hexa-histidine) correlated distinctly with enhanced solubility.

The factor which appeared to play a prominent role in dictating soluble expression was protein size. Large protein size, especially when >~60kDa, correlates to poor heterologous expression (Mehlin *et al.*, 2006) and insolubility, although the latter phenomenon is often inconsistent (Mehlin *et al.*, 2006, Vedadi *et al.*, 2007). These inverse relationships were maintained for five out of seven proteins. The only exceptions were the 26kDa His-*Pf*RS6, which expressed poorly, and the 29kDa His-ALV5, which was insoluble. The deviation of the latter domain may have been due to the fact that it was derived from a region of the

protein's inner membrane complex domain and such domains are associated with poor solubility following heterologous expression.

Five out of the seven recombinant proteins assessed during the current study could be isolated and purified with yields sufficient for experimental use. Two of these full length recombinant proteins, GST-*Pf*MDM2 and His-*Pf*ARK3, were isolated with several truncated forms. This is not an uncommon event, although the precise driving force behind the phenomenon is often unknown (Flick *et al.*, 2004, Mehlin *et al.*, 2006). Within both of the mentioned proteins, the sites of truncation appeared to correlate to rare AGA codons. The only other domain to have this codon was GST-*Pf*RS6 and the absence of any detectable truncated forms may have been due to its low expression rate. A modified bacterial line expressing rare tRNAs, to compensate, was used, although this did not prevent truncation. This suggested, as found in other studies, that sequence composition itself was not the only deciding factor (Flick *et al.*, 2004, Vedadi *et al.*, 2007). The faster the rate at which recombinant *P. falciparum* erythrocyte membrane protein 1 was synthesised in a bacterial host cell, the greater the frequency of truncation (Flick *et al.*, 2004). It was proposed that rapid protein synthesis could quickly exhaust the tRNA pool in the cell, in turn inducing early termination in many proteins, including the recombinant one (Flick *et al.*, 2004). The use of lower incubation temperatures (~20°C), to slow the rate of translation, did not prevent the truncation of GST-*Pf*MDM2 or His-*Pf*ARK3.

4.2 Novel binding partner identification with biopanning

The vast majority of proteins operate within the cellular environment as part of a complex (Berggård *et al.*, 2007, Rao *et al.*, 2014). Thus the identification and understanding of

protein-protein interactions is essential. As a result numerous high-throughput techniques have been developed, although none without limitations (Berggård *et al.*, 2007, Rao *et al.*, 2014). Some of the most commonly employed techniques include yeast-two-hybrid systems, phage display biopanning and affinity chromatography (Berggård *et al.*, 2007, Rao *et al.*, 2014).

Affinity chromatography involves the immobilization of a native or recombinant tagged protein of interest onto a surface. Cell lysate is applied, providing the immobilized protein the opportunity to interact and retain specific cell-derived native proteins. These can then be eluted and their identity determined using processes such as mass spectrometry (Berggård *et al.*, 2007, Rao *et al.*, 2014).

A more frequently employed technique is the yeast-two-hybrid approach. Typically a protein of interest is expressed fused to a yeast-specific DBD, while a second protein is expressed fused to a yeast-specific activation domain, required for transcription induction. If the protein of interest and the second protein interact, they will facilitate the formation of a complete transcriptional complex which is transported to the yeast nucleus and induces the expression of a reporter gene (Berggård *et al.*, 2007). Unfortunately this technique can be limited by poor relocation of the interacting complex to the nucleus or transcriptional activation hindrance (Berggård *et al.*, 2007). Previous high throughput yeast two-hybrid studies failed to identify any binding partners for the *Pf*MDM2 and *Pf*SWIB proteins (LaCount *et al.*, 2005).

This study utilized a different technique – phage display technology – in order to determine if novel interactions could be identified for the two parasite SWIB/MDM2 domains. This technique may be similar, at its core, to yeast-two-hybrid analysis but phage display

technology has a far greater throughput. Additionally detection does not depend on effective complex transport and functionality (Willats, 2002, Berggård *et al.*, 2007, Pande *et al.*, 2010). The *P. falciparum* phage display libraries used during this study have previously identified novel *P. falciparum* binding interactions (Lauterbach *et al.*, 2003, Bezuidenhout, 2013, Liebenberg and Coetzer, 2013).

Only a limited number of binding partners were identified for each SWIB/MDM2 domain. One partner was identified for GST-*Pf*MDM2 and three for GST-*Pf*SWIB. Several factors may have contributed to this as outlined below.

Firstly, at the time of mRNA extraction to construct the libraries, only a subset of the parasite's transcriptome would be expressed, limited further by transcript stability (Lanzillotti and Coetzer, 2008). The mRNA for the libraries used in this study was extracted from cultures enriched with late intraerythrocytic asexual life stages, naturally limiting and/or preventing interactions with proteins expressed outside of this time frame (Lanzillotti and Coetzer, 2008). Incomplete conversion of the mRNA into cDNA may have played a further compounding role (Lanzillotti and Coetzer, 2008).

Secondly, the use of the recombinant, as opposed to native, SWIB/MDM2 domains may have limited binding partner detection in various ways. Unfortunately experimentation with the native proteins was not feasible due to a lack in available antibodies for their *in vivo* isolation. Specific binding interactions may require one or more post-translational modifications (Lanzillotti and Coetzer, 2008, Pande *et al.*, 2010). A plethora of post-translational modifications are ascribed to the proteome of *P. falciparum* which cannot be implemented in a bacterial recombinant protein expression system. Knowledge related to these modifications in the two SWIB/MDM2 domains is limited but there are no

documented phosphorylation sites (Solyakov *et al*., 2011). The recombinant domains may also have failed to fold correctly in the bacterial host cell (Baneyx and Mujacic, 2004, Pande et al., 2010) and since the natural conformation of these parasite domains is unknown, this could not be verified. Incorrect conformation would prevent native protein interactions during the assay. The GST-*Pf*MDM2, constituted by almost only the small SWIB/MDM2 domain, may have limited the number of interacting partners which could be identified. Additional domains within the proteins, not expressed as part of the recombinant form, may be responsible for stabilizing or promoting native interactions.

Thirdly, several aspects of the biopanning method may have hindered interactions. The immobilization of the recombinant proteins on magnetic beads may have limited domain accessibility and impeded binding (Lanzillotti and Coetzer, 2008). The use of high stringency wash steps would have eliminated weakly and/or transiently associated binding partners (Lanzillotti and Coetzer, 2008, Pande *et al.*, 2010). The successive rounds of phage amplification could have preferentially selected for certain phage clones that amplified more rapidly and/or out competed other phage (Pande *et al.*, 2010).

Some fourth round identified phage expressed out-of-frame parasite peptides. This was a consequence of the method used for the libraries' creation as there was no control in the translation frame produced when the cDNA was inserted into the phage arms (Lauterbach *et al.*, 2003, Lanzillotti and Coetzer, 2008). While the in-frame sequences had Lys contents of 40% or less, the out-of-frame sequences retained, after the fourth round of biopanning, were constituted by more than 60% Lys residues. The A/T bias of the *P. falciparum* genome was responsible for this enhanced out-of-frame Lys enrichment (Lys codons are

AAA and AAG), resulting in a high charge content and likely promoting non-specific ionic interactions and retention during biopanning (Lanzillotti and Coetzer, 2008).

In addition to the identification of unnatural proteins as binding partners, the biopanning system can present false positives (Willats, 2002, Lanzillotti and Coetzer, 2008, Pande *et al.*, 2010). Here natural parasite proteins or domains are identified but do not represent true binding partners of the immobilized ligand. This is a limitation of all protein-protein interaction systems and verification procedures must be conducted as a result. Surface plasma resonance, confocal microscopy and *in vitro* binding are merely a few examples of such (Berggård *et al.*, 2007, Rao *et al.*, 2014). In this study *in vitro* assays were used as a verification tool for the identified interactions (Lanzillotti and Coetzer, 2006). Several control experiments need to be carried out during this verification process to ensure that association is not a consequence of the system itself.

In this study two control sets were employed – heat denatured ligand and GST protein. Heat denatured ligand showed a substantially reduced interaction with its binding protein (figure 3.19A and 3.20A). The limited interaction could either represent non-specific binding of the ligand onto the beads or the importance of a specific primary sequence in the binding domain of the ligand. Interaction of recombinant GST protein was negligible (less than that of the denatured ligand) and constant, no matter the concentration added to the system. The GST-fused ligand showed a far greater binding capacity with its immobilized binding partner relative to an equal concentration of the GST-tag alone. These findings verified that biopanning identified binding partners were valid. Additional verification techniques could be employed, such as surface plasma resonance, which could also provide information regarding the kinetics of the interaction. Furthermore co-transfections of the SWIB/MDM2 proteins and their identified binding partners would

provide information regarding the physiological location, time and importance of this interaction.

4.3 *Pf*MDM2 and *Pf*SWIB showed structural homology to chromatin remodelling factors

SWIB/MDM2 domains can broadly be divided into two distinct groups based on their functional activities. All group M SWIB/MDM2 domains are key components of MDM2 proteins, facilitating p53 binding and subsequent regulation and inhibition of pro-apoptosis p53-directed transcription (Wade *et al.*, 2010). Group C homologues are involved in activities such as chromatin remodelling and transcriptional regulation (Cairns *et al.*, 1996, Wilson and Roberts, 2011) although for a large part their cellular roles are unknown (Melonek *et al.*, 2012). Both groups are rich in hydrophobic and aromatic amino acid residues; and conform to a classical twisted cleft topology when crystallized (Kussie *et al.*, 1996, Yamada *et al.*, 2004, Yoneyama *et al.*, 2004b, Yoneyama *et al.*, 2004a).

The SWIB/MDM2 domain of *Pf*MDM2 is a likely group C member, based on bioinformatics. The degree of primary sequence identity calculated was within the 'twilight zone' (Rost, 1999) when compared to other group C and M members (16.7 – 23.4% identity) – the greatest identity and similarity were documented relative to group C (eg. 48.1% similarity to the *H. sapiens* chromatin remodelling SWIB/MDM2 domain). Additionally, a conserved group C Trp with unknown function (Bennett-Lovsey *et al.*, 2002) was identified in *Pf*MDM2 (Trp^{80}). This residue is possibly critical for group C domain functioning, explaining its strong retention, and may provide *Pf*MDM2 with similar capabilities.

The predicted secondary and tertiary structures of the *Pf*MDM2 domain, considered as a more reliable means of discerning homology (Geourjon *et al.*, 2001), conformed to that of other SWIB/MDM2 domains. The overall predicted secondary structure was closer to that of group C domains, rich in helices and having a short beta-strand preceding the third helical run (figure 3.3F). Tertiary models were similar to all crystallized SWIB/MDM2 domains but failed to form a complete twisted cleft topology (figure 3.4 F-L). The absence of beta-sheets was unexpected, based on the domain's predicted secondary structure, but deviations between secondary and tertiary states are known phenomena (Geourjon *et al.*, 2001). The yeast SNF12 SWIB/MDM2 domain, implicated in chromosomal remodelling (Cairns *et al.*, 1996), was predicted to share a similar secondary structure (figure 3.3E) and 'incomplete' tertiary topology (figure 3.4T) to *Pf*MDM2. The quality and reliability of the latter prediction was very low (QMEAN of 0.359) but nevertheless demonstrates that only the helical cleft appears necessary for transcriptional regulation in unicellular organisms. Alternatively, the absence of beta-sheets may be compensated for by neighbouring regions, as seen in the crystal structure of the human MDM2 protein. Here, one of the helical stretches was not part of the annotated SWIB/MDM2 domain but instead supplied by a flanking region (Sakurai *et al.*, 2006).

The primary sequence identities calculated for the SWIB/MDM2 domain of *Pf*SWIB were also within 'twilight zone' (Rost, 1999) but greatest when compared to group C members (22.1-24.7% identity). Unlike *Pf*MDM2, the *Pf*SWIB domain did not retain the group C specific Trp residue (Bennett-Lovsey *et al.*, 2002) and instead had a semi-conserved aromatic Tyr^{288} residue, which may play an analogous role to the conserved Trp.

The *Pf*SWIB domain was mainly helical in terms of secondary structure (figure 3.3G) and therefore more like group C domains, which were richer in helical runs relative to group M

members. Five of the seven modelled tertiary structures for this domain were similar to those modelled for *Pf*MDM2 and the yeast domain, forming an incomplete twisted cleft topology. Two of the models formed a complete twisted cleft topology but were amongst some of the lowest QMEAN scoring structures. The generally predicted absence of beta-sheets was expected, based on their absence in the secondary structure predictions. The richer helical content predicted for this domain and frequent topological similarities to a unicellular group C domain (SWIB/MDM2 domain of SNF12), implicated in chromosomal remodelling (Cairns *et al.*, 1996), suggested that *Pf*SWIB was most like a group C family member.

Group M SWIB/MDM2 domains are key components of MDM2 proteins, facilitating p53 binding and subsequent regulation and inhibition of pro-apoptosis p53-directed transcription (Wade *et al.*, 2010). The critical amino acids required for p53 binding were not well conserved in the two parasite domains, with less than half being semi-conserved. There was retention of non-critical hydrophobic and aromatic amino acids, involved in creating a suitable environment for p53 binding (Kussie *et al.*, 1996), but this was not specific for group M domains alone. A similar retention was documented amongst group C domains, suggesting that prominent hydrophobic and aromatic amino acid composition could not be used as a group distinguishing property (Bennett-Lovsey *et al.*, 2002).

The critical amino acids for p53 binding are located in only one of the beta-strands and only two of the alpha helices, highlighting why these topological regions are essential and part of the annotated human SWIB/MDM2 domain (Kussie *et al.*, 1996, Sakurai *et al.*, 2006). The absence of beta-sheets and numerous critical amino acid residues in both *P. falciparum* domains would make an interaction with a potential parasite p53 homologue

unlikely in the conventional manner. However, the known variation in p53 homologue sequence and structure over evolutionary time could account for such fundamental differences in binding interactions (Jin *et al.*, 2000, Derry *et al.*, 2001, Lu *et al.*, 2009), as well as the expected variation in the SWIB/MDM2 domain. More importantly, interaction between p53 and MDM2 has been postulated as a metazoan-stage evolutionary event as no true MDM2 protein homologue has been identified in lower eukaryotes (Lu *et al.*, 2009). Hence the binding of p53 may not be essential or relevant for the *P. falciparum* homologues.

4.4 *Pf*MDM2 is a mitochondrial component

4.4.1 *Pf*MDM2 was located in the mitochondrion

In this study, based on current transcriptomic and proteomic findings (Aurrecoechea *et al.*, 2009), the late intraerythrocytic life stages were considered to be of physiological relevance to *Pf*MDM2. Previous work failed to determine the precise cellular location of this protein (Hu *et al.*, 2010) but it was proven in the current study to have distinct mitochondrial localization in the late life stages. The N-terminal iPSORT predicted signal sequence directed the protein to the mitochondrion, as removal of this region resulted in cytoplasmic retention. The *Plasmodium*-specific bioinformatic algorithm PlasMit failed to detect this sequence suggesting it should not be depended on solely for the identification of mitochondrial localization sequences for parasite proteins.

Mitochondrial localization of group C SWIB/MDM2 homologues has been documented in plants. Plants express four groups of SWIB/MDM2 domain containing proteins, with the so called group I SWIB proteins constituted solely by a SWIB/MDM2 domain. In *Arabidopsis* two group I SWIB proteins have distinct mitochondrial localization –

At1g31760, with exclusive mitochondrial localization, and At2g35605, showing dual mitochondrial and chloroplast localization (Melonek *et al*., 2012). The functional role of these two proteins is unknown, although participation in genomic regulation has been hypothesized (Melonek *et al*., 2012). EMBOSS Needle alignments with the SWIB/MDM2 domain of *Pf*MDM2 revealed strong conservation to that of At1g31760 (39% identity and 51.9% similarity) and At2g35605 (43.3% identity and 55.8% similarity), and hence the parasite protein may play a role similar to these two *Arabidopsis* proteins. Localization of group M domains to the mitochondria has not been previously documented.

4.4.2 *Pf*MDM2 associated with the PF3D7_1303400 protein

Biochemical assessment of *Pf*MDM2 was facilitated with the aid of phage display library technology. To date no other binding partners have been identified for this parasite protein (LaCount *et al.*, 2005). A single, *in vitro*-verified binding partner was documented in this study – a centrally located region of the PF3D7_1303400 protein – *Pf*LisH.

4.4.2.1 Temporal and spatial considerations for the PfMDM2 and PfLisH interaction

Proteomic data have documented *Pf*LisH in the trophozoite and schizont life stages of the asexual intraerythrocytic parasite. Transcriptome analysis indicates expression in the asexual intraerythrocytic life cycle, greatest in the early trophozoite and lowest in the schizont, and in the gametocytes and ookinetes (Aurrecoechea *et al.*, 2009). This has several links temporally with the *Pf*MDM2 expression pattern, providing opportunities for possible interactions.

The cellular compartment of *Pf*LisH needs to be considered as biopanning and the verification binding assays were *in vitro* assays. The cellular location of *Pf*LisH is

unknown but bioinformatics strongly predicted nuclear occupancy (table 3.6 and appendix A). Further work is required to define the location of *Pf*LisH in order to justify or refute the physiological validity of its association with *Pf*MDM2. Under normal conditions it is unlikely that *Pf*LisH and *Pf*MDM2 interact, since *Pf*MDM2 is in the mitochondrion. However, *Pf*MDM2 was predicted by some algorithms to localise to the nucleus and have several nuclear signal sequences. Therefore it could, like *Pf*SWIB, move to the nucleus in response to other stress stimuli and interact with *Pf*LisH.

4.4.2.2 LisH domains are involved in transcriptional regulation

If the interaction between *Pf*MDM2 with *Pf*LisH is physiological relevant then it is a novel finding in the parasite and it has also not been documented in any other eukaryotic organism. The cellular activity of *Pf*LisH is unknown and previous yeast-two hybrid studies failed to identify any interacting proteins (LaCount *et al.*, 2005). The only annotated domain within the protein is the N-terminal LisH motif (Aurrecoechea *et al.*, 2009). Previous bioinformatic analysis identified 114 proteins, from a wide range eukaryotes, having this domain (Emes and Ponting, 2001). It is commonly situated at the N-terminus of a protein and participates in a variety of cellular processes, including protein binding (Thomas Meier and Blobel, 1992, Liu *et al.*, 1996, Conner and Liu, 2000, Miele *et al.*, 2005, Mateja *et al.*, 2006, Mikolajka *et al.*, 2006). Common to these proteins, but not present in the *P. falciparum* protein, are additional domains aiding in molecular interactions (Emes and Ponting, 2001). The LisH motif plays a role in transcriptional regulation, as indicated in table 4.1 (Wei *et al.*, 2003), and it is postulated to function through the recruitment of transcriptional activators.

Table 4.1: Transcriptional regulation involving LisH domains.

Transcriptional regulation proteins having LisH domains	Organism	The gene(s) regulated	Source
Flo8p	*S. cerevisiae*	The flocculation gene FLO1	(Liu *et al.*, 1996)
Leunig	*A. thaliana*	The AGAMOUS gene	(Conner and Liu, 2000)
TBL1	*H. sapiens*	The JNK1 related genes	(Zhang *et al.*, 2002)
Sif2p	*S. cerevisiae*	Telomeric silencing	(Cockell *et al.*, 1998)
P220^{NAT}	*H. sapiens*	The Histone H4 and H2B genes	(Miele *et al.*, 2005) (Wei *et al.*, 2003)

The N-terminal LisH domain of TBL1 interacts with the N-terminal region of the nuclear receptor co-repressor protein which has two SANT (SWI3/ADA2/N-CoR/TFHIIB) domains present in a variety of chromatin-associated complexes, including the SWI/SNF complex (Humphrey *et al.*, 2001, Zhang *et al.*, 2002). SWIB/MDM2 homologues lack SWI3 domains but are core elements of SWI/SNF complexes (Cairns *et al.*, 1996). This latter feature suggests that binding associations with LisH homologues, possibly for complex stabilization, is possible as part of a larger transcriptional complex akin to the SWI/SNF complex (Cairns *et al.*, 1996).

4.4.3 *Pf*MDM2 is an unlikely heat stress participant

Thirty minutes after the termination of heat stress *Pf*MDM2-GFP was still retained in the mitochondrion. Twenty four hours later the episomal fusion protein maintained a punctate green fluorescent signal but no longer aligned completely with the red mitochondrial marker (figure 3.34). This could indicate possible movement of the protein out of the mitochondria or simply be an artefact of the manual microscopy system used. Clearly no nuclear co-localization was detected. Although mitochondrial hyperpolarization has been detected after heat stress for 24 hours with 40°C in late stage intraerythrocytic parasites, no such alterations have been reported under the conditions of this study - 2 hours of 41°C

heat stress (Engelbrecht and Coetzer, 2013). The mitochondrial membrane was thus unlikely to contribute to an observed signal shift.

The At2g35605 protein traffics to both the mitochondria and chloroplast and *Pf*MDM2 may exhibit similar duality. The non-photosynthetic apicoplast of *P. falciparum* shares close contact with the mitochondrion during all stages of the intraerythrocytic life cycle (Van Dooren *et al*., 2005) and is essential for the parasite's survival, although an association with PCD is unknown (Wilson *et al.*, 1996, Waller *et al.*, 1998, Lim and McFadden, 2010). Bioinformatics failed to identify any apicoplast localization sequence for *Pf*MDM2, suggesting that such movement is unlikely. The protein could simply be moving into the cytoplasm, preventing a mitochondrial role or allowing for a cytoplasmic activity to occur. An alternative, and possibly more likely, reason for the shift in location would be parasite mobility. The surviving parasites moved rapidly 24 hours after heat stress termination and this could easily alter the relative location of the green and red fluorescent signals, since images were captured consecutively a few seconds apart and subsequently overlaid. As the MitoSOX^{TM} stain could not be used with fixed parasites, immobilizing the surviving parasites was not an option.

The *P. falciparum* parasite is exposed to a wide range of fluctuating temperatures during its life cycle (Hafalla *et al.*, 2011). On the one hand the periodic fever associated with malaria in the human host has been suggested to reduce the parasite burden on the host by inducing parasite PCD (Deponte and Becker, 2004). On the other hand the parasite must possess a robust, but currently poorly understood, heat shock response system to survive the rapid shifts in environmental temperatures (Kumar *et al.*, 1991, Pallavi *et al.*, 2010, Botha *et al.*, 2011, Muralidharan *et al.*, 2012). The SWI/SNF complex has involvement in

the human and yeast heat stress pathways (Sullivan *et al.*, 2001, Corey *et al.*, 2003, Zhao *et al.*, 2005, Han *et al.*, 2008), in the latter eukaryote, knockout studies have proven the direct involvement of the SWIB/MDM2 homologue SNF12 (Cairns *et al.*, 1996). Based on bioinformatics *Pf*MDM2 is most similar to group C SWIB/MDM2 homologues and therefore should be evaluated as both a PCD and heat stress participant.

The role of *Pf*MDM2 in heat-induced PCD is uncertain. Firstly, vertebrate MDM2 and the human SWI/SNF complex require nuclear localization for PCD regulation, a feature not documented for the parasite protein. Secondly, its binding partner *Pf*LisH has no PCD ties. Thirdly, elevated temperatures, 38.5°C and above, appear to enhance the demise of late asexual intraerythrocytic life stages, relative to early ones (Kwiatkowski, 1989, Long *et al.*, 2001, Porter *et al.*, 2008, Engelbrecht and Coetzer, 2013). As the periodic fever of malaria is linked to egress (Hafalla *et al.*, 2011) the majority of parasites would be rings, having just reinvaded RBC, and only the remaining, lagging late stage parasites would be likely to die and reduce the parasite burden (Deponte and Becker, 2004). For a pro-survival role the SWIB/MDM2 homologue would be required in the rings, where transcriptional profiling indicates *Pf*MDM2 has very low expression levels and current proteomic data indicate it is absent (Aurrecoechea *et al.*, 2009). A great reduction in the parasite population was documented 24 hours after the termination of heat stress. No surviving parasites showed clear *Pf*MDM2-GFP mitochondrial localization, which could indicate that the protein had moved out of the organelle as a pro-survival mechanism. Alternatively the absence of overlap may have been an artefact of the analysis procedure due to the greater mobility of the surviving parasites, relative to control populations, during live imaging. This could have resulted in time delays during red and green fluorescent signal acquisition, since the system employed was not automated. The clear mitochondrial signal shape, seen when

comparing the MitoSox^{TM} and GFP signals in figure 3.34, further supports this conclusion. Future studies are required, with the aid of a mitochondrion specific antibody, to clarify this matter. From the data acquired from this study it was concluded that retention of the protein may therefore be of no consequence to the heat stressed parasites or may represent a pro-survival mechanism. Any change in *Pf*MDM2 localization could not be assessed in those parasites which had died and a role of the protein in PCD of that sub-population could not be evaluated.

The importance of *Pf*MDM2 in a heat stress response pathway is uncertain. The SWI/SNF complex, and therefore a SWIB/MDM2 homologue, is involved in the transcriptional regulation of HSP genes in the nuclei of human and yeast cells (Cairns *et al.*, 1996, Sullivan *et al.*, 2001, Corey *et al.*, 2003, Zhao *et al.*, 2005, Han *et al.*, 2008) but the parasite protein cannot play an analogous role as the mitochondrial genome of the parasite encodes no HSP genes (Feagin, 1992). The LisH domain of the yeast sif2p protein has been shown to be involved in heat-stress survival through transcriptional regulation (Cockell *et al.*, 1998) but as the parasite LisH homologue is likely to be nuclear, its involvement with the mitochondrial *Pf*MDM2 under heat stress seems negligible.

Other stress stimuli, such as high levels of parasitaemia, were not considered as part of this study but have been documented to induce PCD in *P. falciparum* (Deponte and Becker, 2004, Meslin *et al.*, 2007, Totino *et al.*, 2008, Ch'ng *et al.*, 2010). These stimuli may activate different pathways, which may depend on *Pf*MDM2. Different stress stimuli within mammalian cells, such as heat stress, metabolic inhibition and heavy metal poisoning, do not all employ the SWI/SNF complex for transcriptional regulation for example (de la Serna *et al.*, 2000). Therefore even if *Pf*MDM2 does not appear to have a

role in heat-induced PCD it may be involved in other PCD or stress pathways. Commonly the SWI/SNF is involved in pro-survival events during such conditions and therefore a similar activity could be expected for the parasite protein.

4.4.4 Alternative cellular role of *Pf*MDM2 within the parasite

Overall, based on structure, location and the binding partner identified in this study, *Pf*MDM2 does not appear to be a vertebrate MDM2 homologue. Non-PCD roles could be hypothesized for the protein related to DNA synthesis, energy production and the mitochondrial electron transport chain. The late asexual and sexual stages of the parasite, where the transcriptomic and proteomic data suggest greatest physiological relevance of the protein, are associated with preparation for and implementation of rapid DNA synthesis. DNA synthesis is strongly dependent on *de novo* pyrimidine synthesis, as it is the only means by which the parasite can acquire pyrimidines (Gutteridge *et al.*, 1979). It has been suggested that the mitochondrial electron transport chain acts as an electron sink, absorbing the electrons generated by dihydroorotate dehydrogenase during the *de novo* pyrimidine synthesis process (Torrentino-Madamet *et al.*, 2010). DNA synthesis would therefore require the expression of the three protein members of the mitochondrial electron transport chain carried in the mitochondrial genome (Feagin, 1992). *Pf*MDM2 may be involved in this as part of a larger transcriptional complex in the mitochondrion.

During gametocytogenesis, the single mitochondrion branches and elongates and is associated with the formation of cristate structures in the inner mitochondrial membrane; suggesting enhanced metabolic activity, possibly as a preparation for entrance into the midgut of the mosquito and the upcoming energy-expensive sexual development (Torrentino-Madamet *et al.*, 2010). The mitochondrial-encoded cytochrome b gene had a

three-fold increase in expression in the sexual life stages relative to the asexual stages, further supporting the idea of enhanced mitochondrial function in the former and which may involve *Pf*MDM2 (Learngaramkul *et al.*, 1999), although current proteomic data has not documented the protein's presence in this life stage.

4.5 *Pf*SWIB is a likely heat stress response participant

4.5.1 The cytoplasmic distribution of *Pf*SWIB was altered briefly in response to heat stress

Focus was placed on the late intraerythrocytic life stages in this study as proteomic data have only identified the protein in these stages as well as gametocytes and salivary gland sporozoites (Aurrecoechea *et al.*, 2009). Localization algorithms were divided between the nucleus and cytoplasm for this protein (table 3.8 and Appendix A). Experimentally cytoplasmic distribution was documented under control conditions. In *Arabidopsis* one group I SWIB protein resides in the cytoplasm, At3g48600. Its cellular activities are unknown but based on its location genomic association is not possible (Melonek *et al.*, 2012). EMBOSS Needle alignment of this plant protein with the SWIB/MDM2 domain of *Pf*SWIB revealed 22.5% identity and 42.7% similarity, suggesting that these two proteins may share similar cytoplasmic activities.

In response to heat stress, *Pf*SWIB-GFP showed a stage specific distribution pattern. In all schizonts and the majority of trophozoite parasites the fluorescent protein remained in the cytoplasm up to 24 hours after stress termination. In roughly 10% of the trophozoites, *Pf*SWIB-GFP was located in the nucleus 30 minutes after stress termination. The green signal co-localised distinctly in early trophozoites with the nucleus, but a few late

trophozoites showed a partial co-localization pattern, suggesting migration to or from the nucleus (figure 3.37). The perceived nuclear response was brief, since cytoplasmic distribution was documented for all parasites after 2 hours and was maintained up to 24 hours later for *Pf*SWIB-GFP. Bioinformatic analysis did highlight several nuclear localization signals within the protein (figure 3.21), and the elevated temperature may induce the activation of one or more of these signals, possibly through phosphorylation or other posttranslational modifications as documented in proteins such as MDM2 (Meek and Knippschild, 2003). The *Pf*SWIB protein is phosphorylated on seven Ser and Thr residues, two of which are situated in a predicted bipartite nuclear signal sequence and may play a role in regulating cellular location (Aurrecoechea *et al.*, 2009, Solyakov *et al.*, 2011).

Distinct sub-nuclear localization patterns, suggestive of nucleolar and/or chromatin association, have been previously documented for SWIB/MDM2 homologues in response to stress (Mosser *et al.*, 1988, de la Serna *et al.*, 2000, Catalano and O'Day, 2012). The SWI/SNF complex in yeast can rapidly activate heat shock protein 70 (HSP70) gene transcription for cell survival in response to metabolic inhibition and heavy metal poisoning, although the effects of heat stress appeared negligible (de la Serna *et al.*, 2000). The SWIB/MDM2 homologue of *Dictyostelium* showed nuclear localization under normal conditions with enhanced nucleolar localization in response to heat stress (Catalano and O'Day, 2012). The metazoan MDM2 protein also showed nucleolar redistribution in response to stress, inhibiting its pro-survival abilities (Wade *et al.*, 2010). In this study, the precise sub-nuclear localization of the protein, if any, could not be determined.

4.5.2 The SWIB/MDM2 domain of *Pf*SWIB associated with three binding partners

Sequence alignments and tertiary modelling of the SWIB/MDM2 domain of *Pf*SWIB supported the idea of its being a group C SWIB/MDM2 domain relative. In order to further decipher the domain's functional role phage display library technology was employed. No prior binding partners for this protein have been documented (LaCount *et al.*, 2005). This study identified three binding partners for the *Pf*SWIB SWIB/MDM2 domain. One of these, verified with *in vitro* binding assays, was the N-terminal region of the *Pf*ARK3 protein; this binding domain is situated 434 amino acids upstream of a putative kinase domain (Aurrecoechea *et al.*, 2009). The other two partners were a C-terminal region (*Pf*RS6) of a protein annotated to have a ribosomal protein S6e domain, and a portion of the inner membrane complex domain of the *Pf*ALV5 protein (Aurrecoechea *et al.*, 2009). No common binding motif could be identified between these three domains.

4.5.2.1 PfSWIB bound in a concentration dependent manner to PfARK3

Previous bioinformatic work revealed *Pf*ARK3 as an aurora-related kinase, although appearing to have undergone early divergence from this kinase family during evolution (Reininger *et al*., 2011). Aurora kinases, first identified in *Drosophila*, have been identified in a wide range of eukaryotes, ranging from yeast to humans (Chan and Botstein, 1993, Glover *et al.*, 1995). Yeast encodes only a single aurora kinase homologue, IpI1, while higher eukaryotes have been shown to have two or three different types (Aurora A, B and C), participating in various cellular processes and with a strong association to mitosis (Chan and Botstein, 1993, Hsu *et al.*, 2000, Zeitlin *et al.*, 2001, Goto *et al.*, 2002, Kunitoku *et al.*, 2003).

Three Aurora related kinases have been identified within the *Plasmodium* genome which have been shown to be indispensable, by knockout experiments, in the asexual

intraerythrocytic cycle (Solyakov *et al.*, 2011). *Pf*ARK1 (PF3D7_0605300) has been implicated as an essential participant in nuclear mitosis and localization studies revealed its close contact with the nuclear envelope and nuclear membrane (Reininger *et al*., 2011). In the case of the essential phospho-protein *Pf*ARK3 its cellular localization is unpublished, although it has been identified as a nuclear protein (Doerig, 2014, personal communication) and this correlates with the bioinformatics assessment of this study.

Current proteomic data have revealed *Pf*ARK3 translation in the merozoite, trophozoite and schizont life stages while transcriptional data suggest expression throughout the intraerythrocytic life cycle, greatest in the stage V gametocytes and lowest in rings and early trophozoites. There is a massive up-regulation documented for the gene's transcription within the ookinetes as well. In light of these data, the *Pf*SWIB and *Pf*ARK3 would, at a minimum, both be present within the parasite during the trophozoite and schizont life stages. The movement of *Pf*SWIB into the nucleus in response to fever would provide an opportunity for intracellular interaction with *Pf*ARK3.

Previous yeast-two-hybrid studies found that *Pf*ARK3 only associated with a pseudogene (LaCount *et al.*, 2005). This interaction does not exhibit any direct link to PCD or transcriptional regulation but three features of previously characterized aurora kinases are of interest in this study.

Firstly, human Aurora kinase B, and its homologues IpI1 in *S. cerevisiae* and AIR-2 in *C. elegans*, have been shown to play a key role in histone H3 phosphorylation to facilitate correct mitosis (Hsu *et al.*, 2000, Zeitlin *et al.*, 2001, Goto *et al.*, 2002, Kunitoku *et al.*, 2003). Histone phosphorylation has other important cellular consequences as well. H3 phosphorylation by other kinases, specifically at Ser10, alters chromatin structure and is a

requirement in the transcription activation of specific gene subsets in response to specific stimuli, albeit not the only modification (Labrador and Corces, 2003, Yang *et al.*, 2012). Post-translational modifications ascribed to the N-terminal tails of histone proteins have been linked to the histone code hypothesis, where the combination of different post-translation modifications determine a specific function, such as transcription (Jenuwein and Allis, 2001). Heat shocking *Drosophila* cells caused a global decrease in H3 phosphorylation but a local increase in H3 phosphorylation at loci of heat shock transcription factors (Prigent and Dimitrov, 2003). The SWI/SNF complex has been proven to be involved in transcriptional activation of heat stress genes and in yeast cells the removal of the SWIB/MDM2 domain has detrimental effects on heat shock survival (Cairns *et al.*, 1996, Sullivan *et al.*, 2001, Corey *et al.*, 2003, Zhao *et al.*, 2005, Han *et al.*, 2008). Therefore, one could hypothesize that the association of *Pf*SWIB, possibly as part of a SWI/SNF-related complex, with the aurora-related kinase could target specific histones for phosphorylation and transcriptional regulation.

Secondly, human Aurora kinase A has a specific role in apoptosis, specifically regulating both the function and stability of p53 through phosphorylation. The targeting of p53 Ser^{315} enhances the protein's ubiquitination by MDM2 and subsequent degradation, while targeting Ser^{215} inhibits p53 DNA binding and trans-activation activity (Katayama *et al.*, 2004, Liu *et al.*, 2004). Thus, the association of an aurora-related kinase with a SWIB/MDM2 homologue within the parasite may be part of a PCD-like pathway where *Pf*SWIB directs *Pf*ARK3 towards a transcriptional regulator, such as a p53 homologue, to regulate its function and/or stability. *Pf*SWIB lacks a ligase domain required for the classical MDM2-direct ubiquitination and subsequent degradation of a p53 homologue (Honda *et al.*, 1997, Wade *et al.*, 2010). Association with *Pf*ARK3 could compensate,

simply inactivating a p53 homologue through phosphorylation. Bioinformatic evidence indicates the presence of a p53 homologue within the parasite although the function of this protein is uncertain (section 4.6).

Thirdly, the *Pf*SWIB-*Pf*ARK3 association may simply facilitate the phosphorylation of the *Pf*SWIB protein in the nucleus. Seven serines and a single threonine residue have been annotated as phosphorylation sites in *Pf*SWIB (Aurrecoechea *et al.*, 2009, Solyakov *et al.*, 2011); one or more of these may be necessary for its nuclear activities. The role of these phosphorylated residues in the nucleus as well as the cytoplasm, where it resides most of the time, is unknown.

4.5.2.2 PfSWIB interacted with PfALV5 and PfRS6

In this study *Pf*ALV5 and *Pf*RS6 were also identified as binding partners, by biopanning, of *Pf*SWIB. Due to low and insoluble heterologous expression of these two domains respectively, their interactions with *Pf*SWIB could not be verified. However, several control steps, including pre-screening of the library with GST and high stringency washes, were employed to minimize false positive and/or low affinity interactions. Relatively few binding partners were identified, which also implied high specificity. In addition, the verified *Pf*SWIB – *Pf*ARK3 interaction was identified using the same screening protocol.

*Pf*ALV5 was identified as an Alveolin group member of the inner membrane complex, having been localized to this structure by two separate studies (Hu *et al.*, 2010, Kono *et al.*, 2012). It is believed to have been acquired through lateral gene transfer from insects (Kono *et al.*, 2012). The inner membrane complex is a common morphological feature of all alveolate members, constituted by an array of flattened vesicles underneath the plasma

membrane and connected to the organism's cytoskeleton (Gould *et al.*, 2008). To date, no role outside its involvement in this cellular structure has been document for *Pf*ALV5.

Temporally it has been identified, by proteomics, within all the asexual intraerythrocytic life stages of *P. falciparum* (Aurrecoechea *et al.*, 2009). *Pf*SWIB was distributed throughout the cytoplasm and there would therefore be a degree of inner membrane complex association. This association may be functionally relevant, representing a means of membrane sequestration of the *Pf*SWIB protein. Previous studies have documented that HSPs can be retained by cytoskeleton components until stress induces nuclear localization (Schlesinger *et al.*, 1982). It is possible that *Pf*ALV5 and *Pf*SWIB interact in a similar manner, preventing some *Pf*SWIB moving to the nucleus under normal conditions. The other mechanisms involved in *Pf*SWIB cytoplasmic retention are unknown. Yeast-two-hybrid studies have identified four other binding partners for *Pf*ALV5 – a single, known export protein; two functionally unknown proteins; and a putative translational machinery component. Association with the export protein is functionally and spatially expected based on the nature of *Pf*ALV5. Its involvement with direct export of any known signals to activate parasite PCD is unknown. The translation machinery interaction may be of importance as under heat stress the late asexual intraerythrocytic life stages have shown a drastic reduction in protein synthesis (Porter *et al.*, 2008) and this interaction was therefore hypothesised to provide an additional means of regulating translation by recruiting and inhibiting specific machinery. It is unlikely though that *Pf*SWIB has any direct involvement in this interaction.

The last binding partner identified for *Pf*SWIB was *Pf*RS6, a protein putatively annotated to have a ribosomal protein S6e domain (Aurrecoechea *et al.*, 2009). Ribosomes are

complex cellular machinery, composed of proteins and RNA, which facilitate translation of mRNA into protein (Nelson and Cox, 2005). In eukaryotic cytoplasmic ribosomes the S6 protein is located in the A site of the 40S subunit, near the mRNA/tRNA binding site and the interface between the small and large ribosomal subunits (Nygård and Nilsson, 1990). Previous work has proven that S6 phosphorylation, in response to proliferation stimulation, is a prerequisite for increased translation-associated protein synthesis (Thomas *et al.*, 1980, Fumagalli and Thomas, 2000). Stress stimuli, such as heat or oxygen deprivation, have been shown to regulate protein synthesis in eukaryotic cells by the level of S6 phosphorylation – dephosphorylation decreases overall protein synthesis (Glover, 1982, Bailey-Serres and Freeling, 1990, Fumagalli and Thomas, 2000, Williams *et al.*, 2003). Late asexual intraerythrocytic life stages of *P. falciparum* are no strangers to a drastic reduction in metabolic state in response to heat stress (Porter *et al.*, 2008) and *Pf*RS6 may be involved in this process. The protein's role in a PCD pathway or its interaction with *Pf*SWIB is uncertain as associations between SWIB/MDM2 domains and ribosomal proteins are not characterized in literature.

This putative ribosomal protein has been identified by proteomic studies in all the intraerythrocytic asexual life stages as well as various gametocyte stages (Aurrecoechea *et al.*, 2009). The cellular location of *Pf*RS6 is unknown but bioinformatic analysis suggests a strong likelihood of nuclear localization, which is unexpected for a ribosomal protein but would provide it with an opportunity to interact with *Pf*SWIB after heat stress.

Yeast-two-hybrid studies have identified 15 binding partners for this protein (LaCount *et al.*, 2005), as presented in figure 4.1. Four were chromatin-related proteins, supporting the bioinformatic nuclear localization pattern noted for *Pf*RS6 (LaCount *et al.*, 2005) and

suggests that *Pf*SWIB is a group C family member. *Pf*RS6 was also found to associate with a ligase. The vertebrate MDM2 protein encompasses an E3 ligase domain, responsible for the ubiquitination and subsequent degradation of p53 (Honda *et al.*, 1997, Wade *et al.*, 2010). It is possible that the ligase which was bound to *Pf*RS6 was directed by the nuclear *Pf*SWIB to ubiquitinate a p53 homologue. The remaining binding partners for *Pf*RS6 have no link to chromatin remodelling or PCD and it is possible that the *Pf*RS6 protein is pleiotropic in nature, explaining the great variation in its detected binding partners (LaCount *et al.*, 2005).

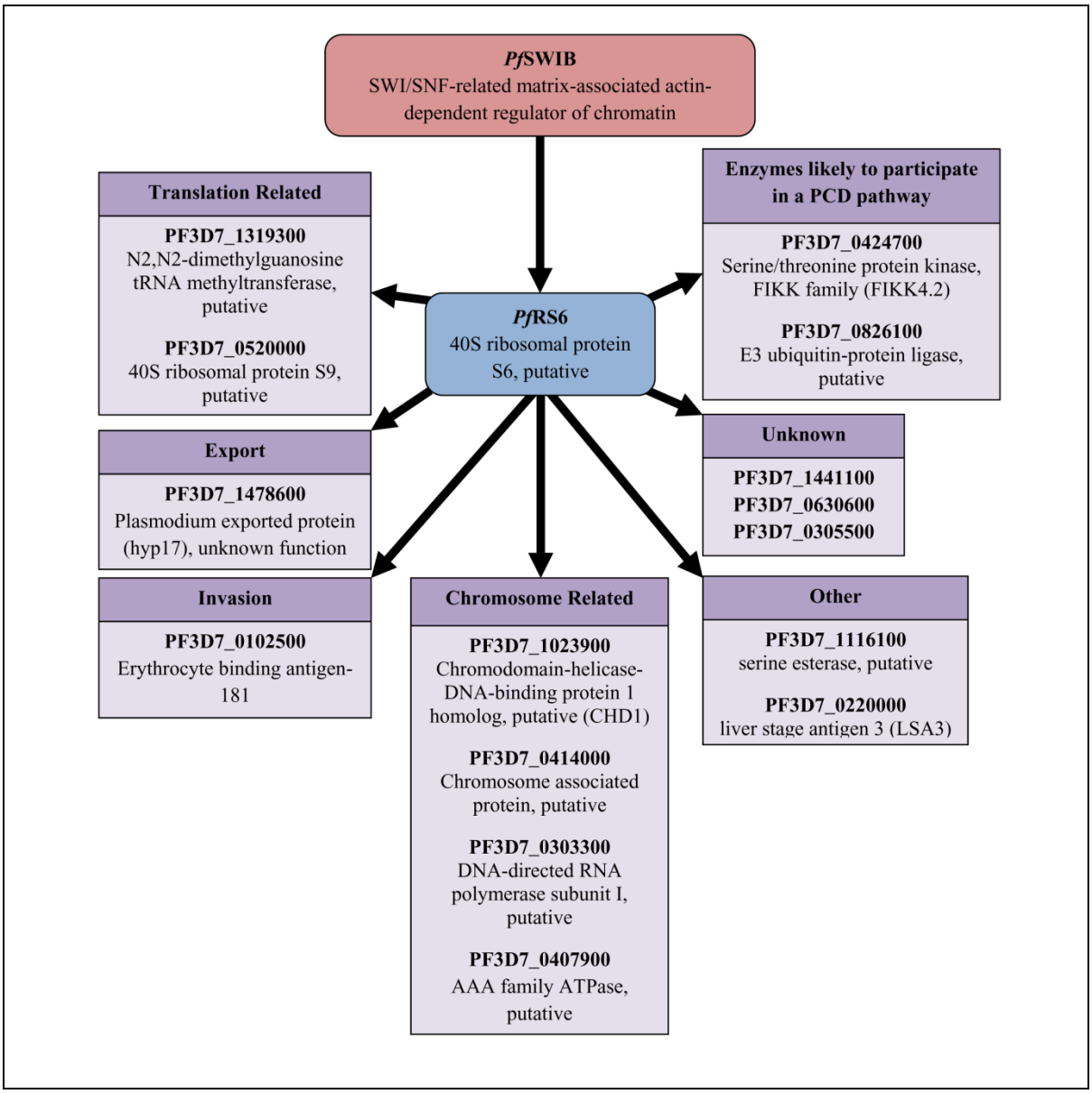

Figure 4.1: Interaction network constructed around the *Pf*SWIB and *Pf*RS6 interaction.
*Pf*SWIB was identified as a putative binding partner of *Pf*RS6, which has been previously proven to interact with a variety of factors, including other chromosome-related proteins and possible PCD participants (LaCount *et al.*, 2005). This interaction network may allow *Pf*SWIB to participate in transcriptional and PCD roles. All proteins presented in purple blocks were identified by high throughput yeast-two-hybrid studies for *Pf*RS6 (LaCount *et al.*, 2005).

4.5.3 The possible role of *Pf*SWIB in response to heat stress

The perceived nuclear response of *Pf*SWIB-GFP was brief. It was only noted 30 minutes after termination of heat stress, after 2 hours all assessed parasites showed a cytoplasmic distribution (figure 3.37). This could imply one of three series of events as outlined below.

4.5.3.1 PfSWIB as a pro-survival PCD factor

The *Pf*SWIB-GFP protein localized to the nucleus briefly (within 30 minutes of heat stress termination) and then may have re-localized to the cytoplasm up to 2 hours later. The majority of late stage parasites died *in vitro* in response to elevated temperatures (Engelbrecht and Coetzer, 2013) and only approximately 10% of trophozoites had a *Pf*SWIB nuclear signal. It could be hypothesized that this nuclear signal represented a pro-survival response, facilitating survival in late stage parasites (de la Serna *et al.*, 2000, Engelbrecht and Coetzer, 2013). Although there was a substantial reduction in parasitaemia 24 hours after heat stress, more than 10% of the population survived suggesting that this cellular phenomenon was an unlikely pro-survival response in the parasite sub-population.

4.5.3.2 PfSWIB as a pro-death factor

The *Pf*SWIB-GFP protein localized to the nucleus briefly and all these parasites may have died and were lost from the population. Commonly SWIB/MDM2 homologues are documented as pro-survival molecules within PCD pathways but the SWIB/MDM2 homologue BAF60a of the mammalian SWI/SNF complex induces p53-directed apoptosis (Oh *et al.*, 2008) and the parasite *Pf*SWIB protein may play a similar pro-PCD role. Several studies have shown that elevated temperatures, 38.5°C and above, significantly inhibited the development and growth of intraerythrocytic asexual parasites, which presented several phenotypic features of necrosis and/or PCD (Engelbrecht *et al.*, 2012). This phenomenon is believed to reduce the host's parasite burden, in turn preventing premature host death before effective parasite transmission (Deponte and Becker, 2004, Porter *et al.*, 2008, Engelbrecht and Coetzer, 2013). Fever is linked to schizont rupture and merozoite re-invasion, with the early life stages surviving *in vitro* heat stress better than late stages (Long *et al.*, 2001, Porter *et al.*, 2008, Engelbrecht *et al.*, 2012, Engelbrecht and

Coetzer, 2013). Thus, removal of lagging late stage parasites, each capable of giving rise to as many as 32 new parasites (Hafalla *et al.*, 2011), could have a significant impact in decreasing the number of parasites. As only trophozoites and not schizonts showed *Pf*SWIB-GFP redistribution, it appeared that life stage is an important contributing factor. Although loss of both late life stages would be advantageous for host survival, schizonts may have crossed a survival point, in terms of *Pf*SWIB-induced death, while trophozoites may still have the potential to be killed off. As the trophozoites aged the redistribution of *Pf*SWIB appeared to weaken, as noted by poor nuclear co-localization of *Pf*SWIB-GFP in a late stage trophozoite parasite.

4.5.3.3 PfSWIB is a possible heat stress response participant

The stress used during this study for PCD induction was elevated temperature, which would activate heat stress survival pathways in the parasite. Therefore, *Pf*SWIB may play a non-PCD, stage specific heat stress regulation role.

The *P. falciparum* parasite is exposed to a wide range of temperatures during its life cycle due to the use of a human host and insect vector (Hafalla *et al.*, 2011). The human host additionally undergoes large temperature fluctuations during the clinical manifestations of the disease, with fever episodes resulting in core body temperature elevations of as much as 5°C for several hours (Ray and Plorde, 2010). As a result, the parasite must possess a robust heat shock response system to survive. This system is poorly understood, although numerous HSP members have been identified and are required for heat shock conditions and normal cellular functioning (Kumar *et al.*, 1991, Pallavi *et al.*, 2010, Botha *et al.*, 2011, Muralidharan *et al.*, 2012). Some of these proteins are elevated in their expression in response to heat shock (Kumar *et al.*, 1991, Botha *et al.*, 2011). No true heat shock factor (HSF) homologues have been identified within the parasite but members of the

Apicomplexa Apetala2 (ApiAP2) transcription family may be responsible instead. PF3D7_1342900, an ApiAP2 family member, has been shown to bind to the cis-element situated upstream of eight *Plasmodium* HSP genes (Campbell *et al.*, 2010). The parasite also encodes a single heat shock factor binding protein (HSBP) homologue, responsible in other eukaryotic systems for the attenuation of the heat shock response. This homologue (PF3D7_1120900) has shown several key features of a HSBP but its precise molecular activity is still elusive (Sayeed *et al.*, 2014).

Nucleosome occupancy, in part, determines the accessibility of regulatory elements and thus is an important contributor to gene activation and repression during the life of a cell (Li and Reinberg, 2011). Under heat stress conditions within human cells the human HSF1 directly recruits the SWI/SNF complex, via interactions with the complex's BRG1 protein, in order to facilitate transcriptional initiation and release of the paused RNA polymerase at the promoter sites of the HSP70 gene (Sullivan *et al.*, 2001, Corey *et al.*, 2003). This activation process is stimulated by ATP-dependent chromatin remodelling at the promoter and along the length of the gene (Sullivan *et al.*, 2001, Corey *et al.*, 2003). Another remodelling complex, an ISWI-related complex, is also present at the HSP70 promoter in the absence of HSP1, under both resting and heat stress conditions, and is believed to keep the structure open for initial RNA polymerase binding but is insufficient for complete transcription (Corey *et al.*, 2003). In yeast, HSP gene expression also involves recruitment of the SWI/SNF complex but this is not essential. It is only required for enhanced initiation and elongation of transcription through chromatin remodelling (Zhao *et al.*, 2005, Han *et al.*, 2008). In *Drosophila* the SWI/SNF complex does not seem to be required for HSP70 transcription but identification of the complex at the promoter was conducted by immunofluorescence which may not have been a suitable means of detection (Armstrong *et*

al., 2002, Corey *et al.*, 2003). The transcriptional regulation of heat shock in *P. falciparum* is not well characterized, but involvement of a SWI/SNF-like complex is plausible. A core member of such a complex in other eukaryotes is a SWIB/MDM2 protein (Wilson and Roberts, 2011), to which *Pf*SWIB shows homology. Furthermore, interactions with *Pf*ARK3 in the nucleus may promote parasite survival through histone phosphorylation and subsequent transcriptional activation of heat shock transcription factors (Hsu *et al.*, 2000, Goto *et al.*, 2002, Prigent and Dimitrov, 2003).

Interestingly, in this study several cellular features documented for *Pf*SWIB were similar to those of eukaryotic heat shock participants, supporting the notion that the protein may participate in thermo-tolerance. Firstly, some heat shock participants are sequestered to the cytoplasm in an inactive state, often associating with elements of the cell cytoskeleton (Akerfelt *et al.*, 2010, Al-Whaibi, 2011). *Pf*SWIB showed cytoplasmic localization under normal growth conditions and was found to associate with a member of the inner membrane complex (*Pf*ALV5), providing the protein an opportunity for sequestration to the inner membrane. If all the *Pf*SWIB-GFP was being sequestered by *Pf*ALV5 then the green fluorescent signal would have been limited to the membrane, but instead a cytoplasmic distribution was documented. Secondly, in response to heat stress some heat shock participants show rapid accumulation in the nucleus that is resolved after stress removal (Akerfelt *et al.*, 2010, Hsu *et al.*, 2010). The *A. thaliana* HSBP homologue revealed cytoplasmic accumulation during unstressed conditions, slight nuclear localization during heat stress and strong nuclear localization for up to 2 hours after the removal of the stress (Hsu *et al.*, 2010). *Pf*SWIB was found within the parasite nucleus 30 minutes after the termination of heat stress and not 2 hours later, suggesting a rapid response which was resolved, provided these parasites had not been lost within the culture

due to death. The different life stages may employ different systems for heat stress survival, explaining the absence of *Pf*SWIB-GFP in the schizont nuclei. The trophozoites revealing a nuclear signal would be hypothesized to survive, analogous to heat stressed *A. thaliana* cells, while the remainder may have been too severely damaged.

*Pf*SWIB contains no HSF or HSP functional domains but yeast and human studies suggest the protein could be involved in a nuclear heat stress response aiding in the activation and/or attenuation of HSP gene translation (Akerfelt *et al.*, 2010). A similar localization pattern has not been described for any other SWIB/MDM2 homologue, and would represent a novel activity within *P. falciparum*.

4.6 The DNA binding and tetramerization domains of *Pf*p53 showed weak homology to other p53 homologues

The identification of a p53-like protein within unicellular eukaryotes, such as *Entamoeba histolytica* and *Monosiga brevicollis*, indicates that this protein family arose before the emergence of multi-cellularity and thus may be present in the *P. falciparum* parasite, if not lost during the evolution of the phylum and/or species (Mendoza *et al.*, 2003, King *et al.*, 2008, Lu *et al.*, 2009, Belyi *et al.*, 2010). Commonly the identification of p53 homologues within organisms outside the vertebrate lineage is complicated by low similarity, thus requiring the use of additional algorithms (Jin *et al.*, 2000, Derry *et al.*, 2001), and *P. falciparum* was no different. A putative p53-DBD was previously detected through the use of a variety of computational methods, such as standard homology methods as well as a novel evolutionary rate-based alignment algorithm FIRE (Functional Inference using the Rates of Evolution) (Coetzer *et al.*, 2010, Durand *et al.*, 2010). The precise borders of the

putative domain within the protein were unclear due to poor sequence similarity, irrespective of the alignments conducted.

Previous studies in other non-vertebrate organisms have revealed a wide but poor level of similarity to the well characterised vertebrate p53 protein; the greatest homology often confined solely to the DBD, with several of the amino acid residues critical for DNA binding being identical (Ollmann *et al.*, 2000, Schumacher *et al.*, 2004, Pankow and Bamberger, 2007, King *et al.*, 2008, Holbrook *et al.*, 2009). The degree of similarity and identity of the parasite protein to the vertebrate p53 was significantly lower, relative to other studied non-vertebrate p53-like homologues (Jin *et al.*, 2000, Kelley *et al.*, 2001, Mendoza *et al.*, 2003, Pankow and Bamberger, 2007), and with very few of the essential amino acid residues conserved for DNA binding. The poor similarity was, in part, the result of the increased size of *Pf*p53, resulting in large gaps separating the regions of conservation, a common feature of parasite proteins when compared to their metazoan counterparts (Pizzi and Frontali, 2000, Pizzi and Frontali, 2001). The alignment quality was significantly improved and was comparable to other studied p53 homologues, when the large gap regions were removed. When the gap regions were present the greatest degree of similarity and identity was documented relative to the Cep-1 protein. Both vertebrate and Cep-1 alignments highlighted the same portion of *Pf*p53 as a putative DBD.

For the putative *Pf*p53 DBD the predicted secondary structure was rich in beta-strands, although these did not align well with those of the other p53 DBD assessed. The structure lacked helices but the human and *Drosophila* domains were also predicted to be poor in helical stretches even though they are required, in part, for DNA binding (Ollmann *et al.*, 2000, Huyen *et al.*, 2004, Ho *et al.*, 2006, Pérez-Cañadillas *et al.*, 2006). Tertiary structure

analysis was weak for this parasite domain, with few template-based modelling algorithms being able to reveal a topology akin to that of other p53 homologue DBDs. All were incomplete structures, lacking many of the topological features required for correct functioning (figure 3.42 C-F). All models were of poor quality when assessed by QMEAN analysis, suggesting low feasibility of the structures in nature. Modelling based on bioinformatics, especially when using standard techniques for p53 homologues, is not always reliable. Therefore, based primarily on amino acid sequence alignments, the putative DBD of *Pf*p53 (residues 8225 to 8508) was expressed and used to assess its DNA binding ability.

Of the other functional domains that are encompassed in the vertebrate p53 protein (Belyi *et al.*, 2010), only a putative tetramerization domain was detected in the *P. falciparum* protein. The vertebrate p53 protein is able to form dimers through interactions between residues of the DBD itself. Tetramerization relies on the linkage of two orthogonally positioned p53 dimers, facilitated by the alpha-helix structure of the tetramerization domain (Miller *et al.*, 1996). A C-terminal region of *Pf*p53 had some similarity to the vertebrate p53 tetramerization domain, although this was significantly lower than that documented for other studied p53-like homologues (Miller *et al.*, 1996, Kelley *et al.*, 2001, Mendoza *et al.*, 2003). As the tetramerization domain of the p53 family has undergone broad diversification during evolution, a low degree of homology was anticipated (Lu *et al.*, 2009). This region in the *P. falciparum* protein was rich in hydrophobic amino acids which are essential for function in the human homologue (Mittl *et al.*, 1998). The predicted secondary structure was constituted by three beta-sheets and a single alpha helix, which did not correspond to the prediction of the human homologue. Although the tertiary model was composed of a short alpha helix, the functional feature of the human

homologue (Miller *et al.*, 1996), the location did not correspond to the secondary structure predictions. Overall, bioinformatic analysis of residues 8551 to 8587 of *Pf*p53 showed only a small degree of correlation to the vertebrate p53 tetramerization domain in its rich hydrophobic content and short helical topology.

The absence of any conserved region for MDM2 binding within the parasite protein correlated with the idea that the vertebrate MDM2-p53 interaction was a late stage evolutionary event (Lu *et al.*, 2009). This may be one of the reasons why *Pf*p53 was not detected during biopanning as a binding partner for either *Pf*MDM2 or *Pf*SWIB. Other possible reasons have been discussed earlier in section 4.2.

4.7 Assessment of the cellular location and DNA binding ability of *Pf*p53

4.7.1 A predicted nuclear localization pattern for *Pf*p53

No localization studies have been conducted for *Pf*p53. The use of the episomal expression system would not be ideal for this protein, for two reasons. Firstly, the large size of *Pf*p53 may cause difficulties in effective construct creation and the use of truncated forms may impede localization, as seen with *Pf*MDM2. Secondly, the system results in continuous episomal protein expression. Over-expression of Dmp53 in *Drosophila* has been associated with prominent cell death and thus a parasite homologue could induce the same response and prevent effective transgenic parasite production (Jin *et al.*, 2000). Another system, such as genome editing where a fluorescent tag is added onto the native protein, maybe a better means to evaluate cellular location in this situation.

In this study, based purely on bioinformatics, *Pf*p53 was suggested to be nuclear, an important location for any functional p53 homologue. Additionally, three regions of the

parasite protein aligned, with high identity, to the three human p53 nuclear localization signals; a feature documented in other non-vertebrate p53 homologues as well (Shaulsky *et al.*, 1990, Kelley *et al.*, 2001, Mendoza *et al.*, 2003). Although this does not imply nuclear localization *in vivo*, it does suggest a possible nuclear role and further supports the notion of the parasite protein as a p53 homologue.

Expression profiles of p53 homologues within lower eukaryotes indicate a key role in embryonic development and germ cell regulation through genomic fidelity (Jin *et al.*, 2000, Derry *et al.*, 2001, Pankow and Bamberger, 2007). Involvement in somatic cells has been hypothesised as a more recent evolutionary event, possibly limited to vertebrate lineages (Jin *et al.*, 2000). Proteomic data, although incomplete, has identified the parasite protein in many of the life stages (Aurrecoechea *et al.*, 2009), with no clear correlation to DNA synthesis or sexual propagation.

4.7.2 The putative DBD of *Pf*p53 did not bind a parasitespecific p53 DNA-binding consensus sequence

All studied eukaryotic p53 homologues are able to bind to the conventional p53 DNA binding consensus sequence (PuPuPuCWWGPyPyPy duplicated but separated by no more than 13 random bp), suggesting that the protein and sequence evolved as a conserved unit (Pankow and Bamberger, 2007). These canonical sequences allow p53 to transcriptionally activate various pro-apoptotic genes, such as Bax and Puma (Toshiyuki and Reed, 1995, Nakano and Vousden, 2001), and factors regulating the cell-cycle, such as 14-3-3σ (Hermeking *et al.*, 1997). Although poorly understood, p53 also facilitates transcriptional repression of anti-apoptotic factors including Bcl-2, Bcl-X, cyclin B1, and survivin, an IAP protein (Amaral *et al.*, 2010, Beckerman and Prives, 2010). In terms of autophagy, p53 is

involved in the transcriptional activation of several genes involved in the inhibition of mammalian target of rapamycin, a negative regulator of autophagy (Maiuri *et al.*, 2010).

The *P. falciparum* genome was found to encode two full length canonical p53 DNA binding consensus sequences, one in the coding region of a gene of unknown function (PF3D7_0829800) and one in a gametocyte erythrocyte cytosolic protein gene (PF3D7_1253000). This supported the possibility of a p53-homologue within the parasite, although its link to PCD or cell cycle regulation was absent. Extending the search, four sequences, composed of the two halves of the canonical p53 DNA consensus sequence separated by a gap exceeding 13bp, were identified. These too failed to correlate to PCD or cell cycle genes. Regulation of the cell cycle appears to be exclusive to vertebrate p53 homologues and thus an unlikely activity of *Pf*p53 (Schumacher *et al.*, 2001, Holbrook *et al.*, 2009).

The *Entamoeba histolytica* p53 homologue was found to associate with a canonical human p53 DNA binding consensus sequence and a sequence derived from the unicellular organism's own genome. The latter sequence deviated by 25% from the canonical sequence (Mendoza *et al.*, 2003) and was not identified in the *P. falciparum* genome. Non-canonical p53 DNA binding sequences (Beckerman and Prives, 2010) were not considered as part of the current study and thus possible p53 homologue targets in the parasite's genome may have been missed.

The DNA binding ability of GST-*Pf*p53 was assessed using one of the p53 DNA binding consensus sequences identified within the *P. falciparum* genome. All experiments were unable to detect any oligonucleotide binding (figure 3.51). It might be assumed, based on

this result and the low sequence homology of the domain, that the putative *Pf*p53 DBD was not capable of binding to DNA but this is not necessarily true. Numerous factors could have contributed towards the observed negative result.

Firstly, the maximum amount of GST-*Pf*p53 used in the EMSA was limited (a maximum of ~300ng). This may have been insufficient for oligonucleotide binding. In conjunction with this, the recombinant domain may not have been biologically active due to incorrect folding and/or the absence of posttranslational modifications (Baneyx and Mujacic, 2004). The *Pf*p53 protein was proven to have 45 Ser and Thr residues that can be phosphorylated, one of which was situated within the putative DBD – Ser^{8238} (Aurrecoechea *et al.*, 2009). This residue was not conserved in relation to known p53 proteins and its importance is uncertain but should not be ignored. Additionally, due to poor homology the precise boundaries of the putative domain were difficult to define and the region used in this study was possibly insufficient for DNA binding.

Secondly, the GST tag would have been able to provide artificial dimerization, in case the domain itself could not do so and thus prevent DNA binding (Klein *et al.*, 2001); although this may have interfered with protein-DNA interaction. Due to the low yield of the fusion protein, thrombin-directed GST-tag cleavage was not a feasible option to verify this suggestion.

Thirdly, the DIG-label added to the 3'-end of the p53 oligonucleotide sequence may have interfered with protein binding (Hellman and Fried, 2007). Lastly, during electrophoresis the protein may dissociate from its bound oligonucleotide sequence, with even slow dissociation reducing shift visibility (Hellman and Fried, 2007).

4.8 *Pf*p53 appeared to form tetramers

Previous work showed that a GST-tag could promote artificial p63 DBD dimerization, required for successful p53 DNA consensus sequence binding (Klein *et al.*, 2001). The vertebrate p53 DBD, unlike human p63, can form dimers on its own and bind naturally to DNA (Miller *et al*., 1996). The use of the GST-tag in this study would facilitate artificial domain dimerization to ensure that oligonucleotide binding was not impeded (Klein et al., 2001).

Evaluation of GST-*Pf*p53 oligomerization was conducted with the aid of a tetramerization assay. This assay showed some dimerization of the GST tag alone under high protein concentrations. The monomeric form of GST-*Pf*p53 was reduced in this assay and no dimers were found. A large quantity of the recombinant protein was retained in the wells, suggesting large aggregate formation – possibly high molecular mass oligomers (figure 3.53). A faint band, detected by anti-GST immunobloting, was evident and suggested the possibility of *Pf*p53 tetramerization. The low yield for GST-*Pf*p53 complicated assessment by creating difficulties in clear oligomeric state visualization and prevented the removal of the GST tag, by thrombin cleavage, to verify intrinsic *Pf*p53 oligmerization. Although suggested with caution, the influence of the GST tag in GST-*Pf*p53 was believed to be negligible as no prominent dimeric form of the recombinant protein was seen. Further research needs to be conducted, at greater concentration, for true validation.

5 CONCLUSION

The 48 hour asexual intraerythrocytic life cycle of *P. falciparum* facilitates exponential population expansion which, if left unregulated, would soon kill the human host before successful parasite transmission to the mosquito. One hypothesized means to regulate this and prevent premature host death is parasite self-induced PCD. A handful of studies have documented the expression of distinct PCD markers in the *P. falciparum* parasite and identified metazoan PCD gene homologues within its genome. Unfortunately no clear link has been established between the two. Therefore there is a gap in our understanding of the parasite's biology. To aid in this arena of research this study evaluated the molecular functions of three putative *P. falciparum* PCD homologues and provides the first description of their localisation within the parasite; their response to elevated temperatures, which mimic fever periods experienced by malaria patients; binding interactions and subsequent links to death/stress pathways.

Bioinformatics suggested that the two parasite SWIB/MDM2 homologues, *Pf*MDM2 and *Pf*SWIB, were chromatin remodelling family members, possibly deviating from the typical twisted cleft topology of this group but structurally similar to the yeast SWIB/MDM2 homologue. Unexpectedly *Pf*MDM2 showed distinct N-terminal-directed mitochondrial localization under both normal and heat-induced PCD conditions, as depicted in figure 5.1. Mitochondrial localization has been documented amongst *Arabidopsis* SWIB proteins, although their functional roles are unknown. The *in vitro* binding partner, *Pf*LisH, was predicted to be nuclear in location and therefore its interaction with *Pf*MDM2, under elevated temperatures, may not be feasible *in vivo*. Their interaction may be physiological relevant under other conditions. It is hypothesized that *Pf*MDM2 plays a role in

mitochondrial maintenance and gene expression, possibly as part of a larger transcriptional complex, and it may also participate in PCD in an unconventional manner.

*Pf*SWIB showed distinct cytoplasmic localization under normal conditions as depicted in figure 5.1, a feature documented in a single *Arabidopsis* SWIB protein of unknown function. After heat stress, the protein revealed a short-lived nuclear localization in a subpopulation of trophozoites (figure 5.1). Three novel *in vitro* binding partners were identified for *Pf*SWIB, one a proven member of the inner membrane complex and the other two likely nuclear components (figure 5.1). These findings suggest that *Pf*SWIB could either play a stage-specific, unconventional PCD role or, more feasibly, a stage-specific, heat-stress regulation role where movement of the protein to the nucleus allows for the survival of trophozoites after exposure to elevated temperatures.

The processes described in figure 5.1 are merely hypothetical, based on the limited work conducted. This study was merely the start on a long road towards fully deciphering the cellular roles of these proteins. More work, including knock downs and co-transfections, is required to verify these postulations, to ascertain if the interactions identified are of physiological relevance and to determine if the SWIB/MDM2 proteins are essential for cellular functioning under normal and PCD conditions. This is essential as it is possible that the roles of these proteins are unique and unrelated to a death pathway.

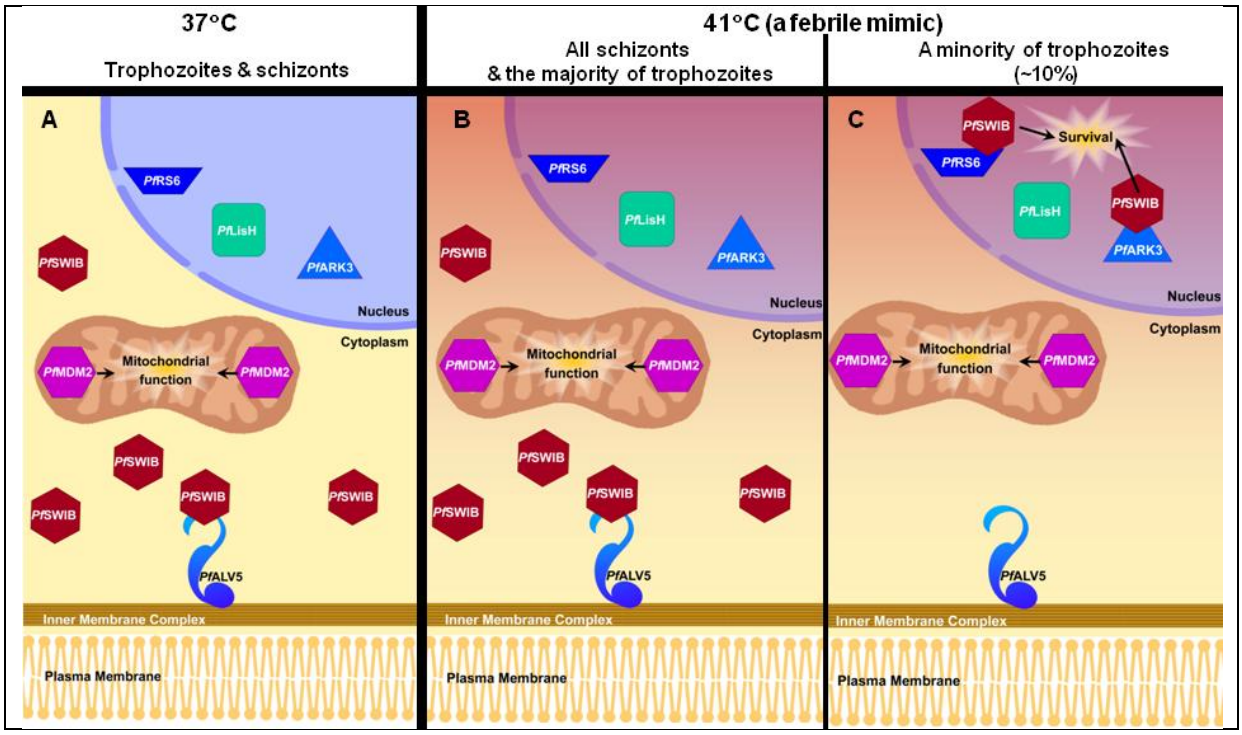

Figure 5.1: **The proposed activities of *Pf*MDM2 and *Pf*SWIB in late asexual intraerythrocytic *P. falciparum* life stages.**
(A) Within the late asexual intraerythrocytic life stages, at 37°C, experimental evidence and bioinformatics suggest that *Pf*MDM2 is involved in mitochondrial functioning and would be unable to interact with its identified binding partner, *Pf*LisH, which is in the nucleus. *Pf*SWIB is cytoplasmic and associates with *Pf*ALV5, a member of the inner membrane complex.
(B) After exposure to elevated temperatures for 2 hours all of the schizonts and the majority of trophozoites retained the normal *Pf*MDM2 and *Pf*SWIB localization pattern, suggesting no stage-specific, heat-related PCD role.
(C) In a minority of trophozoites nuclear *Pf*SWIB was documented briefly. This would provide an opportunity for interaction with nuclear binding partners, *Pf*ARK3 and *Pf*RS6, to bring about stage-specific heat stress regulation and survival to this subpopulation of trophozoite parasites. The location of *Pf*MDM2 was apparently unaffected.

Bioinformatic analysis, based mainly on primary sequence alignments, identified a putative DBD and tetramerization domain within *Pf*p53. Two full length canonical p53 DNA binding consensus sequences within the parasite genome were identified and nuclear localization was predicted for *Pf*p53. The ability of the putative tetramerization domain to facilitate tetramer formation was inconclusive and requires further analysis. The DNA binding function of the parasite protein is currently uncertain, and a metazoan MDM2-p53 interaction seems unlikely in the parasite. Additional studies, such as cellular localization, would help clarify its role in the parasite.

APPENDIX A – BIOINFORMATICS

A Cellular localization predictions

Table A.1: Detailed localization predictions for *P. falciparum* proteins and domains

Protein	Prediction Program	Algorithm Kingdom Specification	Cellular Compartment	Probability of Localization to Specified Compartment (% or yes/no)
***Pf*ALV5**	PlasmoDB - PlasmoAP	n/a	Apicoplast	0
***Pf*ALV5**	PATS Version 1.2.1	n/a	Apicoplast	2.3
***Pf*ALV5**	PSORT Prediction	Plant	Chloroplast stroma	20
***Pf*ALV5**	PSORT Prediction	Plant	Chloroplast thylakoid membrane	20
***Pf*ALV5**	PSORT Prediction	Plant	Chloroplast thylakoid space	20
***Pf*ALV5**	PSORT Prediction	Animal	Cytoplasm	65
***Pf*ALV5**	PSORT Prediction	Plant	Cytoplasm	65
***Pf*ALV5**	WWW PREDOTAR V1.03	Animal	ER	1
***Pf*ALV5**	PSORT Prediction	Animal	Lysosome (lumen)	10
***Pf*ALV5**	MitoProt II - v1.101	n/a	Mitochondria	27
***Pf*ALV5**	iPSORT Prediction	Plant	Mitochondria	no
***Pf*ALV5**	iPSORT Prediction	Non-plant	Mitochondria	no
***Pf*ALV5**	PlasMit	n/a	Mitochondria	1
***Pf*ALV5**	WWW PREDOTAR V1.03	Plant	Mitochondria	1
***Pf*ALV5**	PSORT Prediction	Animal	Mitochondrial matrix space	10
***Pf*ALV5**	NucPred	n/a	Nucleus	20
***Pf*ALV5**	cNLS mapper	n/a	Nucleus (bi-partite)	0
***Pf*ALV5**	cNLS mapper	n/a	Nucleus (monopartite)	0
***Pf*ALV5**	WWW PREDOTAR V1.03	Plant	Plasmid	1
***Pf*ARK3**	PlasmoDB - PlasmoAP	n/a	Apicoplast	0
***Pf*ARK3**	PATS Version 1.2.1	n/a	Apicoplast	2
***Pf*ARK3**	WWW PREDOTAR V1.03	Animal	ER	1
***Pf*ARK3**	PSORT Prediction	Animal	Lysosome	10
***Pf*ARK3**	PSORT Prediction	Plant	Microbody	30
***Pf*ARK3**	PSORT Prediction	Animal	Microbody	10
***Pf*ARK3**	MitoProt II - v1.101	n/a	Mitochondria	50
***Pf*ARK3**	iPSORT Prediction	Plant	Mitochondria	no
***Pf*ARK3**	WWW PREDOTAR V1.03	Plant	Mitochondria	1
***Pf*ARK3**	PSORT Prediction	Plant	Mitochondrial matrix space	10
***Pf*ARK3**	PSORT Prediction	Animal	Mitochondrial matrix space	10
***Pf*ARK3**	iPSORT Prediction	Non-plant	Mitochondrion	no
***Pf*ARK3**	PlasMit	n/a	Mitochondrion	9
***Pf*ARK3**	NucPred	n/a	Nucleus	97

***Pf*ARK3**	PSORT Prediction	Plant	Nucleus	98
***Pf*ARK3**	PSORT Prediction	Animal	Nucleus	98
***Pf*ARK3**	cNLS mapper	n/a	Nucleus (bi-partite)	100
***Pf*ARK3**	cNLS mapper	n/a	Nucleus (monopartite)	97
***Pf*LisH**	PlasmoDB - PlasmoAP	n/a	Apicoplast	0
***Pf*LisH**	PATS Version 1.2.1	n/a	Apicoplast	3
***Pf*LisH**	PSORT Prediction	Plant	Chloroplast thylakoid membrane	10
***Pf*LisH**	WWW PREDOTAR V1.03	Plant	Endoplasmic reticulum	13
***Pf*LisH**	WWW PREDOTAR V1.03	Animal	Endoplasmic reticulum	13
***Pf*LisH**	PSORT Prediction	Animal	Lysosome (lumen)	10
***Pf*LisH**	PSORT Prediction	Animal	Microbody	30
***Pf*LisH**	PSORT Prediction	Plant	Microbody	30
***Pf*LisH**	MitoProt II - v1.101	n/a	Mitochondria	6.7
***Pf*LisH**	iPSORT Prediction	Plant	Mitochondria	No
***Pf*LisH**	iPSORT Prediction	Non-plant	Mitochondria	No
***Pf*LisH**	PlasMit	n/a	Mitochondria	1
***Pf*LisH**	PSORT Prediction	Animal	Mitochondrial matrix space	10
***Pf*LisH**	PSORT Prediction	Plant	Mitochondrial matrix space	10
***Pf*LisH**	NucPred	n/a	Nucleus	94
***Pf*LisH**	PSORT Prediction	Animal	Nucleus	98
***Pf*LisH**	PSORT Prediction	Plant	Nucleus	98
***Pf*LisH**	cNLS mapper	n/a	Nucleus (bipartite)	64
***Pf*LisH**	cNLS mapper	n/a	Nucleus (monopartite)	80
***Pf*LisH**	WWW PREDOTAR V1.03	Plant	Plastid	1
***Pf*MDM2**	PlasmoDB - PlasmoAP	n/a	Apicoplast	No
***Pf*MDM2**	PATS Version 1.2.1	n/a	Apicoplast	10
***Pf*MDM2**	PredSL	n/a	Chloroplast	0
***Pf*MDM2**	iPSORT Prediction	Non-plant	Mitochondria	No
***Pf*MDM2**	iPSORT Prediction	Plant	Mitochondria	Yes
***Pf*MDM2**	MitoProt II - v1.101	n/a	Mitochondria	90
***Pf*MDM2**	PlasMit	n/a	Mitochondria	No
***Pf*MDM2**	PredSL	n/a	Mitochondria	100
***Pf*MDM2**	WWW PREDOTAR V1.03	Animal	Mitochondria	40
***Pf*MDM2**	WWW PREDOTAR V1.03	Plant	Mitochondria	40
***Pf*MDM2**	iPSORT Prediction	Plant	Mitochondria or chloroplast	Yes
***Pf*MDM2**	PSORT Prediction	Animal	Mitochondrial inner membrane	20
***Pf*MDM2**	PSORT Prediction	Plant	Mitochondrial inner membrane	20
***Pf*MDM2**	PSORT Prediction	Animal	Mitochondrial inner membrane space	20
***Pf*MDM2**	PSORT Prediction	Plant	Mitochondrial inner membrane space	20
***Pf*MDM2**	PSORT Prediction	Animal	Mitochondrial matrix space	50
***Pf*MDM2**	PSORT Prediction	Plant	Mitochondrial matrix space	50

***Pf*MDM2**	NucPred	n/a	Nucleus	60
***Pf*MDM2**	PSORT Prediction	Animal	Nucleus	100
***Pf*MDM2**	PSORT Prediction	Plant	Nucleus	100
***Pf*MDM2**	cNLS Mapper	n/a	Nucleus (monopartite signal)	50
***Pf*p53**	PATS Version 1.2.1	n/a	Apicoplast	0
***Pf*p53**	PredSL	Plant	Chloroplast	0
***Pf*p53**	PSORT Prediction	Plant	Chloroplast thylakoid membrane	38
***Pf*p53**	WWW PREDOTAR V1.03	Non-plant	Endoplasmic reticulum	0
***Pf*p53**	WWW PREDOTAR V1.03	Plant	Endoplasmic reticulum	0
***Pf*p53**	PSORT Prediction	Animal	Endoplasmic reticulum (membrane)	85
***Pf*p53**	PSORT Prediction	Animal	Golgi	90
***Pf*p53**	PSORT Prediction	Plant	Golgi	90
***Pf*p53**	PSORT Prediction	Animal	Microbody (peroxisome)	30
***Pf*p53**	iPSORT Prediction	Non-plant	Mitochondria	No
***Pf*p53**	iPSORT Prediction	Plant	Mitochondria	No
***Pf*p53**	PlasMit	n/a	Mitochondria	0
***Pf*p53**	PredSL	Non-plant	Mitochondria	0
***Pf*p53**	PredSL	Plant	Mitochondria	0
***Pf*p53**	MitoProt II - v1.101	n/a	Mitochondria	76
***Pf*p53**	WWW PREDOTAR V1.03	Non-plant	Mitochondria	0
***Pf*p53**	WWW PREDOTAR V1.03	Plant	Mitochondria	0
***Pf*p53**	NucPred	n/a	Nucleus	99
***Pf*p53**	PSORT Prediction	Animal	Nucleus	91
***Pf*p53**	PSORT Prediction	Plant	Nucleus	91
***Pf*p53**	cNLS mapper	n/a	Nucleus (bi-partite)	100
***Pf*p53**	cNLS mapper	n/a	Nucleus (mono-partite)	100
***Pf*p53**	PSORT Prediction	Animal	Plasma membrane	60
***Pf*p53**	WWW PREDOTAR V1.03	Plant	Plastid	0
***Pf*RS6**	PlasmoDB - PlasmoAP	n/a	Apicoplast	0
***Pf*RS6**	PATS Version 1.2.1	n/a	Apicoplast	2.3
***Pf*RS6**	WWW PREDOTAR V1.03	Animal	Endoplasmic reticulum	1
***Pf*RS6**	PSORT Prediction	Animal	Lysosome (lumen)	10
***Pf*RS6**	PSORT Prediction	Plant	Microbody (peroxisome)	30
***Pf*RS6**	PSORT Prediction	Animal	Microbody (peroxisome)	30
***Pf*RS6**	MitoProt II - v1.101	n/a	Mitochondria	7.98
***Pf*RS6**	iPSORT Prediction	Plant	Mitochondria	No
***Pf*RS6**	iPSORT Prediction	Non-plant	Mitochondria	No
***Pf*RS6**	PlasMit	n/a	Mitochondria	1
***Pf*RS6**	WWW PREDOTAR V1.03	Plant	Mitochondria	1
***Pf*RS6**	PSORT Prediction	Plant	Mitochondrial matrix space	10
***Pf*RS6**	PSORT Prediction	Animal	Mitochondrial matrix space	10
***Pf*RS6**	NucPred	n/a	Nucleus	85

***Pf*RS6**	PSORT Prediction	Plant	Nucleus	99
***Pf*RS6**	PSORT Prediction	Animal	Nucleus	99
***Pf*RS6**	cNLS mapper	n/a	Nucleus (bi-partite)	63
***Pf*RS6**	cNLS mapper	n/a	Nucleus (monopartite)	0
***Pf*SWIB**	PlasmoDB - PlasmoAP	n/a	Apicoplast	No
***Pf*SWIB**	PATS Version 1.2.1	n/a	Apicoplast	0
***Pf*SWIB**	PredSL	n/a	Chloroplast	0
***Pf*SWIB**	PSORT Prediction	Animal	Cytoplasm	70
***Pf*SWIB**	PSORT Prediction	Plant	Cytoplasm	70
***Pf*SWIB**	PSORT Prediction	Animal	Lysosome (lumen)	10
***Pf*SWIB**	iPSORT Prediction	Non-plant	Mitochondria	No
***Pf*SWIB**	iPSORT Prediction	Plant	Mitochondria	No
***Pf*SWIB**	MitoProt II - v1.101	n/a	Mitochondria	60
***Pf*SWIB**	PlasMit	n/a	Mitochondria	No
***Pf*SWIB**	PredSL	n/a	Mitochondria	0
***Pf*SWIB**	WWW PREDOTAR V1.03	Animal	Mitochondria	0
***Pf*SWIB**	WWW PREDOTAR V1.03	Plant	Mitochondria	0
***Pf*SWIB**	iPSORT Prediction	Plant	Mitochondria or chloroplast	No
***Pf*SWIB**	PSORT Prediction	Animal	Mitochondrial matrix space	10
***Pf*SWIB**	PSORT Prediction	Plant	Mitochondrial matrix space	10
***Pf*SWIB**	NucPred	n/a	Nucleus	90
***Pf*SWIB**	cNLS Mapper	n/a	Nucleus (bipartite signal)	50
Δm*Pf*MDM2	PlasmoDB - PlasmoAP	n/a	Apicoplast	No
Δm*Pf*MDM2	PATS Version 1.2.1	n/a	Apicoplast	0
Δm*Pf*MDM2	PredSL	n/a	Chloroplast	0
Δm*Pf*MDM2	PSORT Prediction	Animal	Lysosome (lumen)	10
Δm*Pf*MDM2	PSORT Prediction	Plant	Lysosome (lumen)	10
Δm*Pf*MDM2	iPSORT Prediction	Non-plant	Mitochondria	Yes
Δm*Pf*MDM2	iPSORT Prediction	Plant	Mitochondria	No
Δm*Pf*MDM2	MitoProt II - v1.101	n/a	Mitochondria	0
Δm*Pf*MDM2	PlasMit	n/a	Mitochondria	Yes
Δm*Pf*MDM2	PredSL	n/a	Mitochondria	0
Δm*Pf*MDM2	WWW PREDOTAR V1.03	Animal	Mitochondria	0
Δm*Pf*MDM2	WWW PREDOTAR V1.03	Plant	Mitochondria	0
Δm*Pf*MDM2	iPSORT Prediction	Plant	Mitochondria or chloroplast	No
Δm*Pf*MDM2	PSORT Prediction	Animal	Mitochondrial matrix space	10
Δm*Pf*MDM2	PSORT Prediction	Plant	Mitochondrial matrix space	10
Δm*Pf*MDM2	NucPred	n/a	Nucleus	40
Δm*Pf*MDM2	PSORT Prediction	Animal	Nucleus	90
Δm*Pf*MDM2	PSORT Prediction	Plant	Nucleus	90
Δm*Pf*MDM2	cNLS Mapper	n/a	Nucleus (monopartite signal)	50

APPENDIX B – PRIMERS

Table B.1: PCR primers for the amplification of *P. falciparum* genes/domains

Gene	Domain	Vector	Primer Direction	Primer sequence (5' to 3')†	GC content of full length primer (%)	Predicted *P. falciparum* specific T_m (°C)	Predicted Full length primer T_m (°C)	Size of PCR product (bp)
***Pf*p53**	putative DNA binding and tetramerization domain	pGEX-4T-2	Forward	TCA GGA TCC ATG GAA AGG AAA AAA CTG AAC GAA	39.4	49.4	61.3	1602
			Reverse	ACA CTC GAG TCA TTG TCT ATG TAT CCA TGT AAA GGT AA	36.8	51.8	60.8	
***Pf*MDM2**	putative MDM2/SWIB domain	pARL2-GFP	Forward	TCA CTC GAG ATG GGA AAA CAT GAT AAT ACG AA	37.5	45.4	59.1	288
			Reverse	AGG CCT AGG ATG TTT AAA TAA CAA TTT TGG AA	31.3	45.4	57.3	
***Pf*MDM2**	putative MDM2/SWIB domain	pGEX-4T-2	Forward	TCA GGA TCC ATG AAT ACG AAA AAA AAA AGA CCA A	32.4	47.3	58.9	273
			Reverse	TCA CTC GAG TCA TGA CAT ATG TTT AAA TAA CAA	30.3	42.9	56.6	
***Pf*MDM2**	entire gene	pARL2-GFP	Forward	CCT CTC GAG ATG AAA CTT TTG AGA ACA AAC A	38.7	49.0	58.8	411
			Reverse	ACT CCT AGG TTC CTT TCG AAT AGA TGA CAT A	38.7	48.8	58.2	
***Pf*SWIB**	putative MDM2/SWIB domain	pGEX-4T-2	Forward	CCC GGA TCC ATC CCT TTT TTT GAA CTA TCT	43.3	47.2	60.2	480
			Reverse	ATT CTC GAG TCA TTC ATC ATT GGA ACT CAT TTC ATT	33.3	51.2	59.7	
***Pf*SWIB**	entire gene	pARL2-GFP	Forward	GGA CTC GAG ATG GAA CTA TTT GAT AGA GGA AA	40.6	49.3	58.9	2508
			Reverse	GCG CCT AGG AAA ATT ATT ATT ATT ATT ATT ATT ATT ATT GTT	17.8	46.1	55.2	

† Restriction site in forward primers (underlined): For pARL2-GFP: *Xho*I cleavage site (CTC GAG); and for pGEX-4T-2: *BamH*I (GGA TCC).
Restriction site in the reverse primers (underlined): For pARL2-GFP: *Avr*II cleavage site (CCT AGG); and for pGEX-4T-2: *Xho*I cleavage site (CTC GAG).
The restriction sites are preceded by several random nucleotides to enhance the efficiency of digestion by the restriction endonucleases. The reverse primers, for use with the pGEX-4T-2 plasmid, were constructed in such a way to place a stop codon (TGA) at the end of the malaria sequence.

Table B.2: PCR primers for the amplification of biopanning identified binding partners to allow for directional cloning into the pET-15b vector.

Gene	Primer Direction†	Primer sequence (5' to 3') †	GC content of *P. falciparum* specific sequence (%)	GC content of full length primer (%)	Predicted *P. falciparum* specific T_m (°C)	Predicted Full length primer T_m (°C)	Size of PCR product (bp)
***Pf*LisH**	Forward	TCT GTC CAA GAT CAT ATG AGT AAT TGT AGT AGT ACA ACC T	31.8	35.0	48.2	60.3	558
	Reverse	GCC GGA TCC TCA TAT GGG TGC TTT AAT TTG TT	30	43.8	47.5	62.0	
***Pf*ALV5**	Forward	ACA GAA ACA CAT ATG GCA GAT TCA ATC AAA AGT TCA	33.3	33.3	49.3	60.2	735
	Reverse	ATC GGA TCC TTA TGC TCC ACT GTA TTG ATT GTA AA	30.8	37.1	52.3	60.4	
***Pf*RS6**	Forward	TTT GTT TTT CAT ATG GTG AGA GGT TGT ATT GTT GGT	42.9	33.3	52.5	60.1	627
	Reverse	TGC GGA TCC TTA TTT GTC TGG TTT GTT TTG CTT TGT	33.3	38.9	52.3	63.2	
***Pf*ARK3**	Forward	ACA GAA ACT CAT ATG AAA ACT TTA CAA GAA GAG GTA AAT GAA	25.9	28.6	51.6	59.5	1008
	Reverse	AGA GGA TCC TTA TGA CTT AGC TGA TGA TGA TAA TAA GA	30.8	34.2	51.6	59.2	

† Restriction site in forward primers (underlined): *Nde*I cleavage site (CAT ATG). Restriction site in the reverse primers (underlined): *BamH*I cleavage site (GGA TCC). The restriction sites are preceded by several random nucleotides to enhance the efficiency of digestion by the restriction endonucleases. The reverse primers were constructed in such a way to place a stop codon (TAA or TGA) at the end of the malaria sequence.

Table B.3: Vector-specific PCR primers

Vector	Primer Direction	Primer sequence (5' to 3')	GC content (%)	Predicted T_m (°C)	T_a (°C)
pARL2-GFP	Forward	CCG TTA ATA ATA AAT ACA CGC AG	35	59	63
	Reverse	CCA TCT AAT TCA ACA AGA ATT GGG ACA AC	38	63.2	
pET-15b	Forward	TAA TAC GAC TCA CTA TAG GG	40	56.3	55
	Reverse	GCT AGT TAT TGC TCA GCG GT	50	60.4	
T7 phage arms	Forward	GCT AAC TTC CAA GCG GAC CA	55	62.5	50
	Reverse	GCT AGT TAT TGC TCA GCG GT	50	60.4	

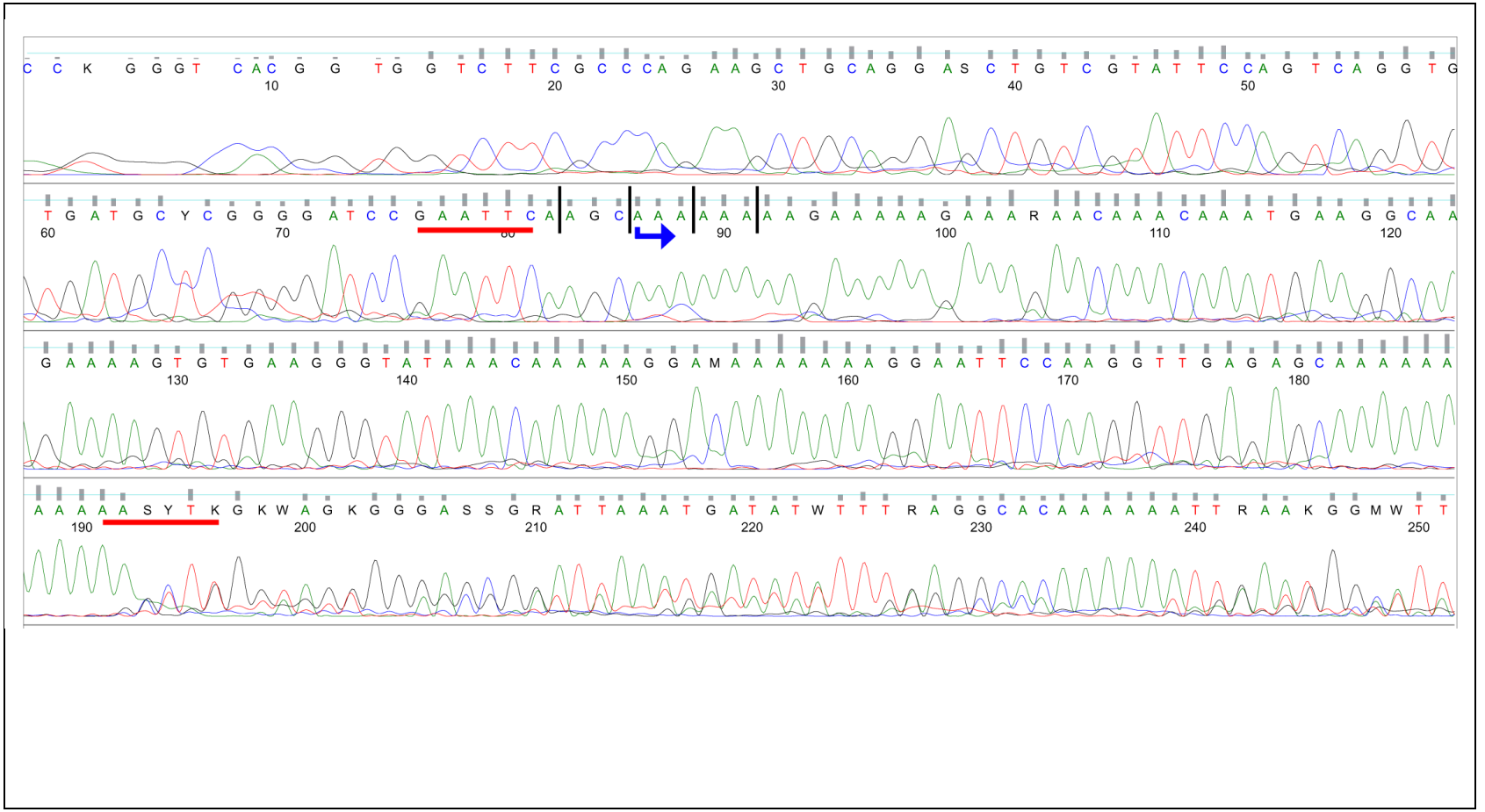

Figure C1: Identification of the *Pf*MDM2 biopanning identified binding partner.

Sequencing results identified the *Pf*LisH domain in the T7 phage expression cassette. The black vertical lines denote cassette's reading frame. The red lines highlight endonuclease restriction sites, flanking the malaria sequence. The blue arrow indicates the start of the malaria transcript.

Output using FinchTV.

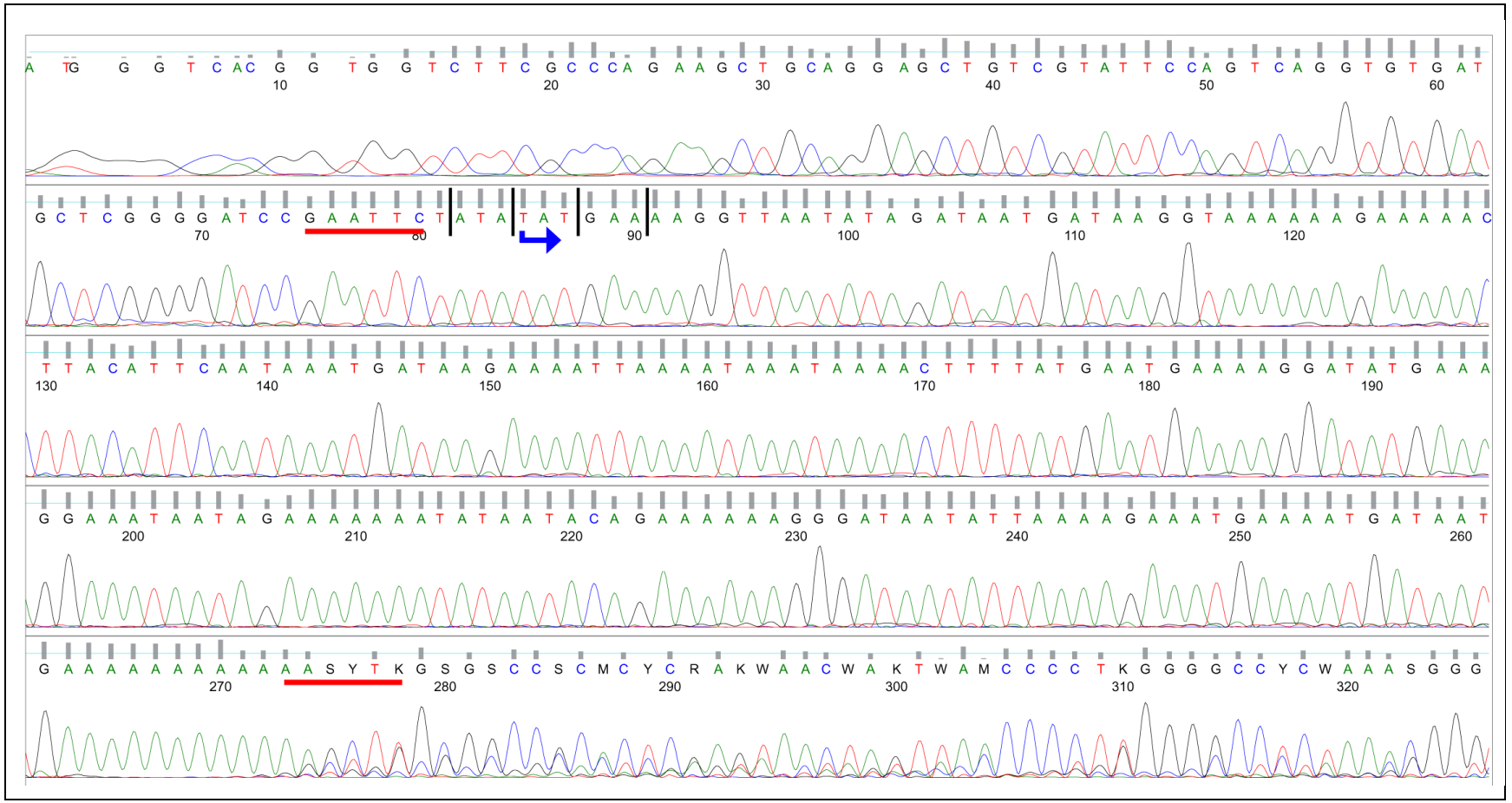

Figure C2: Identification of the *Pf*SWIB biopanning identified binding partner *Pf*ARK3.
Sequencing results identified the *Pf*ARK3 domain in the T7 phage expression cassette. The black vertical lines denote cassette's reading frame. The red lines highlight endonuclease restriction sites, flanking the malaria sequence. The blue arrow indicates the start of the malaria transcript. Output using FinchTV.

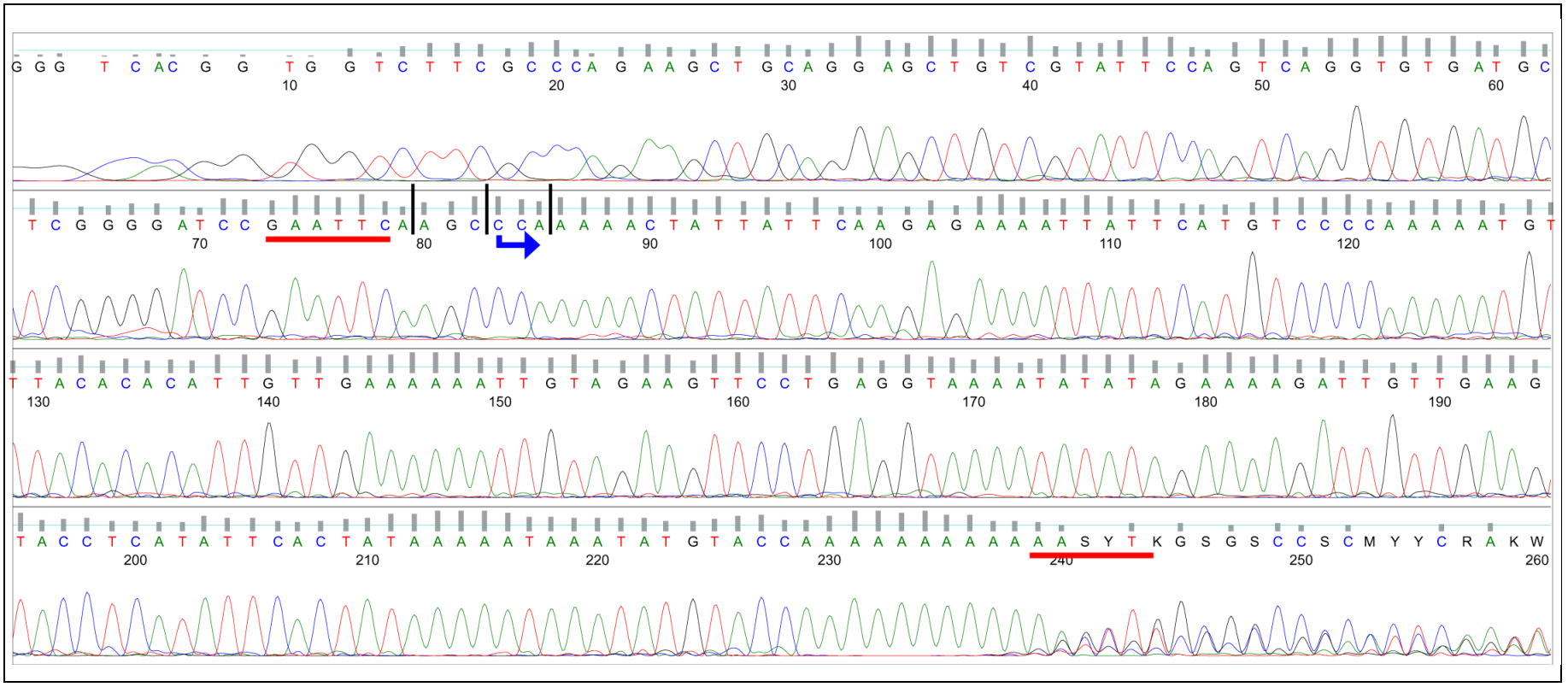

Figure C3: Identification of the *Pf*SWIB biopanning identified binding partner *Pf*ALV5.

Sequencing results identified the *Pf*ALV5 domain in the T7 phage expression cassette. The black vertical lines denote cassette's reading frame. The red lines highlight endonuclease restriction sites, flanking the malaria sequence. The blue arrow indicates the start of the malaria transcript. Output using FinchTV.

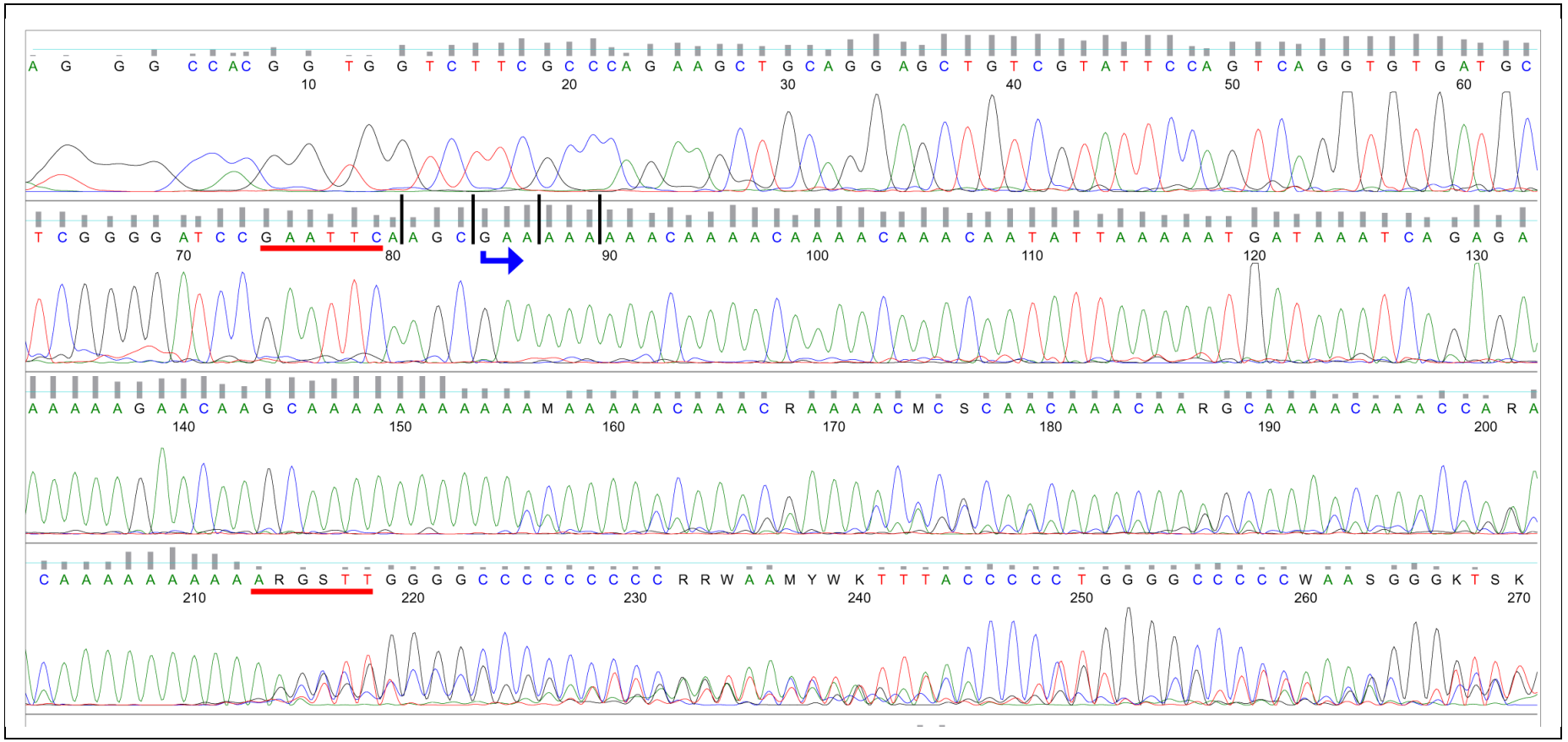

Figure C4: Identification of the *Pf*SWIB biopanning identified binding partner *Pf*RS6.
Sequencing results identified the *Pf*RS6 domain in the T7 phage expression cassette. The black vertical lines denote cassette's reading frame. The red lines highlight endonuclease restriction sites, flanking the malaria sequence. The blue arrow indicates the start of the malaria transcript. Output using FinchTV.

APPENDIX D – VECTOR MAPS AND ISOLATED PLASMID DNA

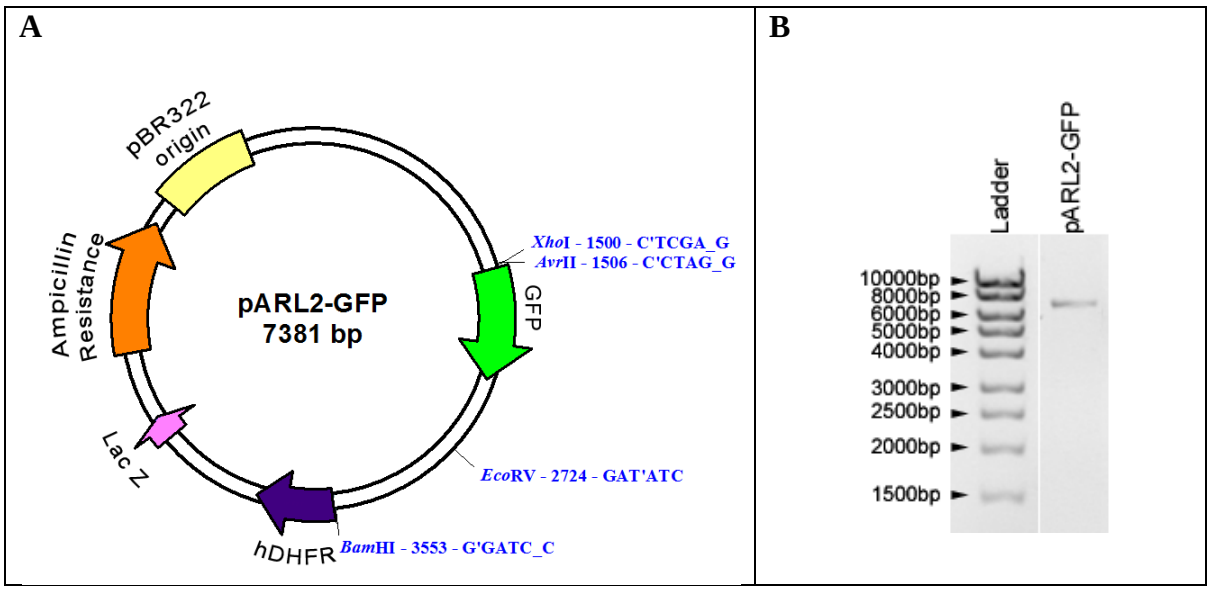

Figure D1: The pARL2-GFP vector

A) A diagram depicting the circular pARL2-GFP vector, modified from the pARL1a^{+} vector (Przyborski *et al.*, 2005), adapted from the LabLife, 2011 diagram.

This low copy number vector encodes the ampicillin resistance gene β-lactamase, facilitating positive-selection after bacterial transformation, and the pBR322 origin of replication, for effective propagation in *E. coli* so to allow for the accumulation of large quantities of the plasmid for subsequent parasite transfection. The plasmid encodes the hDHFR gene, allowing for positive-WR99210 drug selection after parasite transfection (Fidock and Wellems, 1997). The restriction sites employed for directional insertion were *Xho*I and *Avr*II, which precede the open reading and the GFP-tag and thus a 5' initial codon, in frame with the GFP tag, was required in the PCR amplicon. The expression of the GFP-fusion protein is under the control of the chloroquine resistance membrane transporter (*crt*) promoter, allowing for ubiquitous expression during the entire intraerythrocytic, asexual life cycle of the parasite (Aurrecoechea *et al.*, 2009).

B) An agarose gel of digested and dephosphorylated pARL2-GFP vector employed for cloning. The ladder is the MassRuler^{TM} DNA ladder, mixed range.

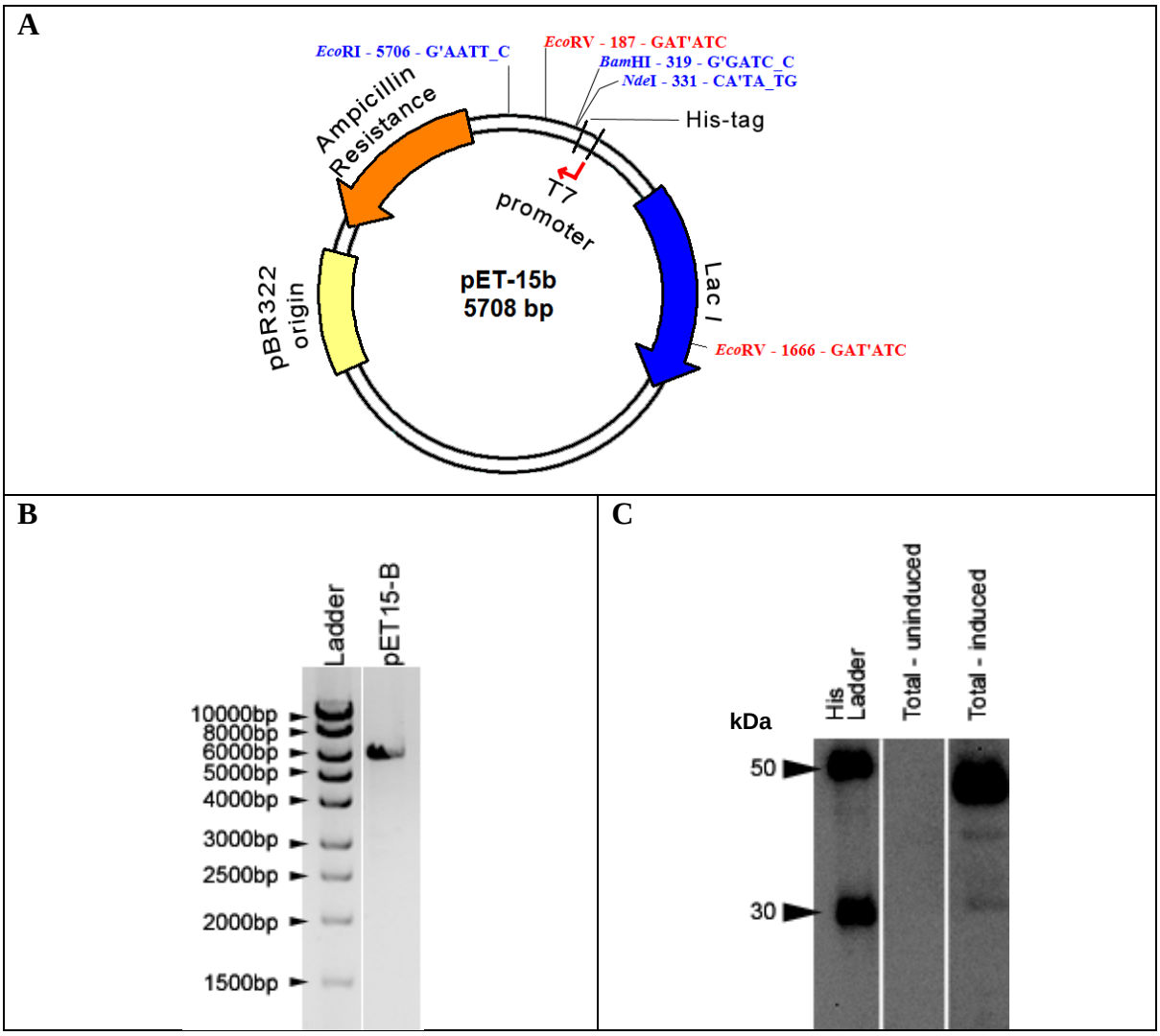

Figure D2: The pET-15b vector

A) A diagram depicting the circular pET-15b vector, adapted from Novagen, 1998 .
This low copy number vector encodes the ampicillin resistance gene β-lactamase, to facilitate positive-selection after bacterial transformation, and the pBR322 origin of replication, for propagation within *E. coli* (Novagen, 2003). In the absence of lactose or an equivalent inducer, such as IPTG, the *lac*I repressor (*Lac*I) inhibits the expression of the T7 RNA polymerase gene, situated in the host cells chromosomes, while in the presence of a suitable induction factor the *lac*UV5 promoter is activated leading to the expression of T7 RNA polymerase, in turn using the T7 promoter on the vector to facilitate recombinant His-tag protein expression (Novagen, 2003). The sites used for directional cloning were *Bam*HI and *Nde*I, situated in the multiple cloning site after the 3' of the penta-His-tag (Novagen, 2003).
B) An agarose of digested and dephosphorylated pET-15b vector employed for cloning. Ladder is the MassRuler^{TM} DNA ladder, mixed range.
C) Comparison of uninduced and induced 20ml cultures for the his-tagged *Pf*LisH protein. No singal was detected at the expected 41kDa mark, based on the migration patter of His-*Pf*LisH indicating, in the uninduced culture at 41kDa, indicating the absence of leaky expression by this vector.

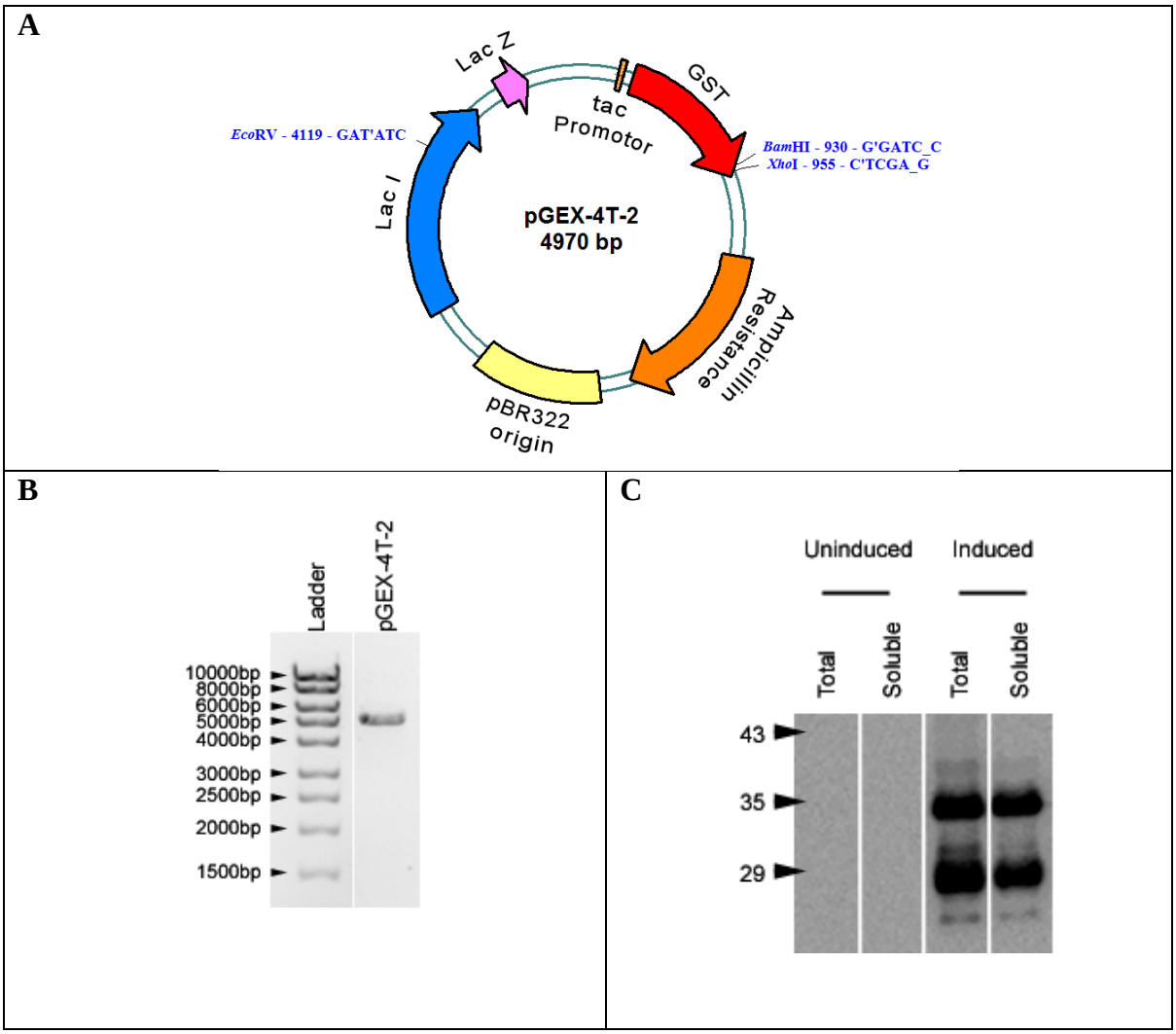

Figure D3: The pGEX-4T-2 vector

A) A diagram depicting the circular pGEX-4T-2 vector, adapted from Healthcare, 2009 .

This low copy number vector encodes for the ampicillin resistance gene β-lactamase, to facilitate positive-selection after bacterial transformation, and the pBR322 origin of replication, for propagation within *E. coli* (Healthcare, 2009). Unlike the pET-15B vector, expression of the recombinant fusion protein is control by a hybrid promoter. The tac promoter is a fusion of the *E. coli trp* and *lac* promoters facilitating enhanced functionality, more so than its parental counterparts, in a lactose repression and induction system (de Boer *et al.*, 1983). In the presence of lactose, or another suitable inducer, the T7 RNA polymerase is expressed in turn leading to recombinant GST-tag protein expression. The sites used for directional cloning were *Bam*HI and *Xho*I, situated downstream of *S. japonicum* GST-tag (Healthcare, 2009).

B) Agarose gel of digested and dephosphorylated pGEX-4T-2 vector employed for cloning. Ladder is the MassRuler^{TM} DNA ladder, mixed range.

C) Comparison of uninduced and induced 20ml cultures for the GST-tagged *Pf*MDM2 protein. Minimal, to no, leaky expression was documented for this vector as indicated by the absence of the GST-*Pf*MDM2 protein within in the uninduced sample at 33.0kDA.

APPENDIX E – LABORATORY CHEMICALS AND EQUIPMENT AND THEIR SUPPLIERS

Chemical, Kit or Equipment	Manufacture or Supplier
0.22µm filters	Millipore, USA
49306 filter	Chroma Technologies, USA
Acid citrate dextrose (ACD) tubes	BD Vacutainer, UK
Acrylamide (C_3H_5NO)	Promega, USA
Agarose	Sigma-Aldrich Corporation, USA
Alexa Fluor® 594 goat anti-mouse antibody	Life Technologies Corporation, USA
Albumax II	Life Technologies Corporation, USA
Ammonium chloride (NH_4Cl)	Saarchem (Pty) Ltd., RSA
Ammonium persulfate ($(NH_4)_2S_2O_8$)	Promega, USA
Ammonium sulphate ($(NH_4)_2SO_4$)	Saarchem (Pty) Ltd., RSA
Ampicillin ($C_{16}H_{19}N_3O_4S$)	Roche, Germany
Anti-GFP rabbit antibody Alexa Fluor® 488 Conjugate	Life Technologies Corporation, USA
Anti-GST HRP conjugated primary antibody	Amersham Biosciences, UK
Anti-His HRP conjugate blocking solution	Qiagen, Germany
anti-His HRP conjugate primary antibody	Qiagen, Germany
Baceriological agar	Merck, Germany
Badelin Sonopuls HD3100 Ultrasonic Homogenizer with microtip MS 73	Bandelin Electronic, Germany
BD Falcon™ round bottom tubes	Becton Dickinson, USA
Beckman Coulter Avanti ® J-E centrifuge	Beckman Coulter, USA
Biorad Gene Pulser® Cuvette	Bio-Rad Laboratories, USA
Bis-acrylamide ($C_7H_{10}N_2O_2$)	Sigma-Aldrich Corporation, USA
Boric acid (H_3BO_3)	Sigma-Aldrich Corporation, USA
Bovine serum albumen (BSA)	Pierce, USA
Bromophenol blue	Merck, Germany
BX41 Olympus Microscope	Olympus, Japan
Calcium chloride ($CaCl_2$)	Merck, Germany
CellSense Dimensions 1.7 Software	Olympus, Japan
Chloramphenicol ($C_{11}H_{12}Cl_2N_2O_5$)	Roche, Germany
Chloroform ($CHCl_3$)	Merck, Germany
Coomassie Brilliant Blue R-250	BDH, UK
CDP-star	Roche, Germany
Cryotubes	Nunc, Denmark
Culture flasks	Thermo Fisher Scientific Inc., USA
DAPI ($C_{16}H_{15}N_5$)	Sigma-Aldrich Corporation, USA
DH5α competent cells	Invitrogen, USA
DIG gel shift kit, 2nd generation	Roche, Germany
Disodium phosphate (Na_2HPO_4)	Saarchem (Pty) Ltd., RSA
Dithiothreitol (DTT) ($C_4H_{10}O_2S_2$)	Boehringer Mannhein, Germany
DMSO (C_2H_6OS)	BDH, UK
DNA MassRuler™	Fermentas International Inc., USA
DNaseI	Fermentas International Inc., USA
D-Sorbitol ($C_6H_{14}O_6$)	Sigma, USA
EDTA ($C_{10}H_{16}N_2O_8$)	Merck, Germany
EGTA ($C_{14}H_{24}N_2O_{10}$)	BDH, UK
Eppendorf centrifuge 5415R	Eppendorf, Germany
Eppendorf centrifuge 5702R	Eppendorf, Germany

Eppendorf Mastercycler Gradient Thermocycler	Eppendorf, Germany
Eppendorf tubes	Eppendorf, Germany
Erlenmeyer 50ml flask	Duran Group, Germany
Ethanol (C_2H_6O)	Merck, Germany
Ethidium bromide	Sigma-Aldrich Corporation, USA
FastAP™ Thermosensitive alkaline phosphatase	Thermo Fisher Scientific Inc., USA
FastDigest® restriction endonucleases	Thermo Fisher Scientific Inc., USA
Filter tips	QSP, USA
Gas mixture	Afrox, RSA
GenElute Plasmid Miniprep kit	Thermo Fisher Scientific Inc., USA
GeneSnap GeneGenius Geldoc scanning system and version 6.05 image acquisition software	Syngene, UK
Gentamycin ($C_{21}H_{43}N_5O_7$)	Sigma, USA
Glacial acetic acid ($C_2H_4O_2$)	Merck, Germany
Glucose ($C_6H_{12}O_6$)	Merck, Germany
Glutathione, reduced ($C_{10}H_{17}N_3O_6S$)	Sigma, USA
Glycerol ($C_3H_8O_3$)	Merck, Germany
HEPES ($C_8H_{18}N_2O_4S$)	Merck, Germany
High Fidelity PCR Enzyme kit®	Thermo Fisher Scientific Inc., USA
Hoechst 33258 pentahydrate ($C_{25}H_{37}Cl_3N_6O_6\bullet5H_2O$)	Invitrogen, USA
Hoefer Mighty Small Mighty Small II SE250 gel cassette	Hoefer Scientific Instruments, USA
Hoefer PR250 orbital bench top shaker	Hoefer Scientific Instruments, USA
Hybond™-C extra supported nitrocellulose membrane	Amersham Biosciences, UK
Hybond™-N nylon membrane	Amersham Biosciences, UK
Hypoxanthine ($C_5H_4N_4O$)	Sigma, USA
Imidazole ($C_3H_4N_2$)	Sigma, USA
Incubator	Heraeus Instruments, Germany
Intelli-Mixer	ELMI Ltd., Latvia
Isopropanol (C_3H_8O)	Merck, Germany
Labcon CPE 50 circulator	Labcon, RSA
Labotec orbital shaker	Thermo Fisher Scientific Inc., USA
Laminar flow hood	Labotec, RSA
Macherey-Nagel NucleoSpin® Gel and PCR Clean-up kit	Separations, RSA
Macherey-Nagel NucleoSpin® plasmid extraction kit	Separations, RSA
MagneGST™ kit	Promega, USA
MagneHis™ kit	Promega, USA
Magnesium chloride ($MgCl_2$)	Merck, Germany
Magnesium sulphate ($MgSO_4$)	Merck, Germany
Maleic acid ($C_4H_4O_4$)	Merck, Germany
Microscope slide	Thermo Fisher Scientific Inc., USA
MitoSOX™ Red mitochondrial superoxide indicator	Invitrogen, USA
Mitotracker™ Green FM	Invitrogen, USA
Monopotassium phosphate (KH_2PO_4)	Merck, Germany
Monosodium phosphate (NaH_2PO_4)	Merck, Germany
MWB2 filter	Olympus, Tokyo, Japan
NanoDrop® 1000	Thermo Fisher Scientific Inc., USA
Nuclease free water	Fermentas International Inc., USA
NucleoBond® Xtra Maxi Plus plasmid DNA preparation kit	Separations, RSA
Nunc tube	Nunc, Germany
Oil immersion Zeiss: Axiostar plus - Transmitted	Zeiss, Germany

Light Microscope	
Olympus DP72 camera	Olympus, Japan
Overnight Express™ Instant TB Medium	Novagen, Inc., USA
Petri Dishes, plastic	Costar, USA
pH meter	Beckman Coulter, USA
Phenol (C_6H_6O)	Merck, Germany
Phusion® Flash High-Fidelity PCR Master Mix	Thermo Fisher Scientific Inc., USA
Ponceau S ($C_{22}H_{12}N_4Na_4O_{13}S_4$)	Sigma-Aldrich Corporation, St. Louis, USA
Potassium acetate (CH_3CO_2K)	Merck, Germany
Potassium chloride (KCl)	Merck, Germany
Protease inhibitor cocktail Set III	Calbiochem®, USA
QIAgen 6xHis Protein Ladder	Qiagen, Germany
QIAgen Anti-His HRP conjugate blocking solution	Qiagen, Germany
QIAgen QIAquick PCR Purification kit®	Qiagen, Germany
Rapi-Diff Staining Kit	Diagnostic Media Products, RSA
RNase A	Thermo Fisher Scientific Inc., USA
Roche Rapid DNA Ligation Kit	Roche Diagnostics, Germany
Rosetta™ 2 (DE3) competent cells	Novagen, Inc., USA
RPMI culture medium	GibcoBRL, USA
Saponin ($C_{27}H_{42}O_3$)	USB, USA
SDS ($NaC_{12}H_{25}SO_4$)	Merck, Germany
Silver nitrate ($AgNO_3$)	Merck, Germany
Slide-A-Lyzer MINI dialysis unit	Pierce, USA
Sodium acetate ($C_2H_3NaO_2$)	Merck, Germany
Sodium bicarbonate ($NaHCO_3$)	PAL Chemicals, UK
Sodium chloride (NaCl)	Merck, Germany
Sodium citrate ($C_6H_7NaO_7$)	Holpro Fine Chemicals, RSA
Sodium hydroxide (NaOH)	Merck, Germany
Sodium thiosulfate ($Na_2S_2O_3$)	Merck, Germany
Sorbitol ($C_6H_{14}O_6$)	Sigma-Aldrich Corporation, USA
Spectra™ Protein Ladder	Pierce, USA
Sterile culture flasks	Nunc, Germany
Sucrose ($C_{12}H_{22}O_{11}$)	Merck, Germany
TEMED ($C_6H_{16}N_2$)	Promega, USA
The SuperSignal® West Pico Chemiluminescent Substrate	Thermo Fisher Scientific Inc., USA
Thermo Biomate 5 Spectrophotometer	Thermo Fisher Scientific Inc., USA
Tris ($C_4H_{11}NO_3$)	Sigma-Aldrich Corporation, USA
Triton-X ($C14H22O(C2H4O)_n$ (n = 9-10))	BDH, UK
Tryptone [Pancreatic Digest of Casein]	Merck, Germany
Tween-20 (C58H114O26)	Calbiochem®, USA
U-25ND25 Olympus neutral density filter	Olympus, Japan
U-MWB2 filter	Olympus, Japan
U-MWU2 filter	Olympus, Japan
VacuCap® 90PF 0.8/0.2µm Filter Unit	Pall Life Sciences, USA
Vacuum pump	Millipore, USA
Water bath	Lauda, Germany
XL10-Gold® Ultracompetent Cells	Stratagene, USA
Yeast Extract	Oxoid, UK
β-mercaptoethanol (C_2H_6OS)	Merck, Germany

6 REFERENCES

Adl, S. M., Simpson, A. G. B., Farmer, M. A., Andersen, R. A., Anderson, O. R., Barta, J. R., Bowser, S. S., Brugerolle, G. U. Y., Fensome, R. A., Fredericq, S., James, T. Y., Karpov, S., Kugrens, P., Krug, J., Lane, C. E., Lewis, L. A., Lodge, J., Lynn, D. H., Mann, D. G., Mccourt, R. M., Mendoza, L., Moestrup, Ø., Mozley-Standridge, S. E., Nerad, T. A., Shearer, C. A., Smirnov, A. V., Spiegel, F. W. & Taylor, M. F. J. R. 2005. The new higher level classification of Eukaryotes with emphasis on the taxonomy of protists. *Journal of Eukaryotic Microbiology,* 52**,** 399-451.

Akerfelt, M., Morimoto, R. I. & Sistonen, L. 2010. Heat shock factors: integrators of cell stress, development and lifespan. *Nature reviews Molecular cell biology,* 11**,** 545-55.

Al-Olayan, E. M., Williams, G. T. & Hurd, H. 2002. Apoptosis in the malaria protozoan, *Plasmodium berghei*: a possible mechanism for limiting intensity of infection in the mosquito. *International Journal for Parasitology,* 32**,** 1133-43.

Al-Whaibi, M. H. 2011. Plant heat-shock proteins: A mini review. *Journal of King Saud University - Science,* 23**,** 139-50.

Ali, M., Al-Olayan, E. M., Lewis, S., Matthews, H. & Hurd, H. 2010. Naturally occurring triggers that induce apoptosis-like programmed cell death in *Plasmodium berghei* ookinetes. *PLoS ONE,* 5**,** e12634.

Amaral, J. D., Xavier, J. M., Steer, C. J. & Rodrigues, C. M. 2010. The role of p53 in apoptosis. *Discovery Medicine,* 9**,** 145-52.

Ameisen, J. C. 1996. The origin of programmed cell death. *Science,* 272**,** 1278-9.

Ameisen, J. C., Idziorek, T., Billaut-Mulot, O., Loyens, M., Tissier, J. P., Potentier, A. & Ouaissi, A. 1995. Apoptosis in a unicellular eukaryote (*Trypanosoma cruzi*): implications for the evolutionary origin and role of programmed cell death in the control of cell proliferation, differentiation and survival. *Cell death and differentiation,* 2**,** 285-300.

Arambage, S. C., Grant, K. M., Pardo, I., Ranford-Cartwright, L. & Hurd, H. 2009. Malaria ookinetes exhibit multiple markers for apoptosis-like programmed cell death *in vitro*. *Parasites and Vectors,* 2**,** doi: 10.1186/756-3305-2-32.

Argentini, M., Barboule, N. & Wasylyk, B. 2001. The contribution of the acidic domain of MDM2 to p53 and MDM2 stability. *Oncogene,* 20**,** 1267.

Armstrong, J. A., Papoulas, O., Daubresse, G., Sperling, A. S., Lis, J. T., Scott, M. P. & Tamkun, J. W. 2002. The *Drosophila* BRM complex facilitates global transcription by RNA polymerase II. *The EMBO Journal,* 21**,** 5245-54.

Arnold, K., Bordoli, L., Kopp, J. & Schwede, T. 2006. The SWISS-MODEL workspace: a web-based environment for protein structure homology modelling. *Bioinformatics,* 22**,** 195-201.

Aurrecoechea, C., Brestelli, J., Brunk, B. P., Dommer, J., Fischer, S., Gajria, B., Gao, X., Gingle, A., Grant, G., Harb, O. S., Heiges, M., Innamorato, F., Iodice, J., Kissinger, J. C., Kraemer, E., Li, W., Miller, J. A., Nayak, V., Pennington, C., Pinney, D. F., Roos, D. S., Ross, C., Stoeckert, C. J., Treatman, C. & Wang, H. 2009. PlasmoDB: a functional genomic database for malaria parasites. *Nucleic Acids Research,* 37**,** D539-43.

Bailey-Serres, J. & Freeling, M. 1990. Hypoxic stress-induced changes in ribosomes of maize seedling roots. *Plant Physiology,* 94**,** 1237-43.

Bakkenist, C. J. & Kastan, M. B. 2003. DNA damage activates ATM through intermolecular autophosphorylation and dimer dissociation. *Nature,* 421**,** 499-506.

Baneyx, F. & Mujacic, M. 2004. Recombinant protein folding and misfolding in *Escherichia coli*. *Nature Biotechnology,* 22**,** 1399-408.

Baton, L., Warr, E., Hoffman, S. & Dimopoulos, G. 2008. Programmed Cell Death during Malaria Parasite Infection of the Vertebrate Host and Mosquito Vector. *In:* Pérez Martín, J. M. (ed.) *Programmed Cell Death in Protozoa.* New York: Springer Publishing.

Baton, L. A. & Ranford-Cartwright, L. C. 2005. Spreading the seeds of million-murdering death*: metamorphoses of malaria in the mosquito. *Trends in parasitology,* 21**,** 573–80.

Bayles, K. W. 2014. Bacterial programmed cell death: making sense of a paradox. *Nature Reviews Microbiology,* 12**,** 63-9.

Beckerman, R. & Prives, C. 2010. Transcriptional regulation by p53. *Cold Spring Harbor Perspectives in Biology,* 2**,** a000935.

Belyi, V. A., Ak, P., Markert, E., Wang, H., Hu, W., Puzio-Kuter, A. & Levine, A. J. 2010. The origins and evolution of the p53 family of genes. *Cold Spring Harbor Perspectives in Biology,* 2**,** a001198.

Bendall, L. J. & Green, D. R. 2014. Autopsy of a cell. *Leukemia,* 28**,** 1341-3.

Bender, A., Van Dooren, G. G., Ralph, S. A., Mcfadden, G. I. & Schneider, G. 2003. Properties and prediction of mitochondrial transit peptides from *Plasmodium falciparum*. *Molecular and Biochemical Parasitology,* 132**,** 59-66.

Benkert, P., Künzli, M. & Schwede, T. 2009. QMEAN server for protein model quality estimation. *Nucleic Acids Research,* 37**,** W510-4.

Benkert, P., Tosatto, S. C. E. & Schomburg, D. 2008. QMEAN: A comprehensive scoring function for model quality assessment. *Proteins: Structure, Function, and Bioinformatics,* 71**,** 261-77.

Bennett-Lovsey, R., Hart, S. E., Shirai, H. & Mizuguchi, K. 2002. The SWIB and the MDM2 domains are homologous and share a common fold. *Bioinformatics,* 18**,** 626-30.

Berggård, T., Linse, S. & James, P. 2007. Methods for the detection and analysis of protein–protein interactions. *Proteomics,* 7**,** 2833-42.

Bezuidenhout, B. C. 2013. *The apaptor protein 1 medium subunit of Plasmodium falciparum.* PhD, University of the Witwatersrand.

Bialik, S., Zalckvar, E., Ber, Y., Rubinstein, A. D. & Kimchi, A. 2010. Systems biology analysis of programmed cell death. *Trends in Biochemical Sciences,* 35**,** 556-64.

Birkholtz, L. M., Blatch, G., Coetzer, T. L., Hoppe, H. C., Human, E., Morris, E. J., Ngcete, Z., Oldfield, L., Roth, R., Shonhai, A., Stephens, L. & Louw, A. I. 2008. Heterologous expression of *plasmodial* proteins for structural studies and functional annotation. *Malaria Journal,* 7**,** 197.

Birnboim, H. C. & Doly, J. 1979. A rapid alkaline extraction method for the isolation of plasmid DNA. *Nucleic Acids Research,* 7**,** 1513-23.

Bjellqvist, B., Basse, B., Olsen, E. & Celis, J. E. 1994. Reference points for comparisons of two-dimensional maps of proteins from different human cell types defined in a pH scale where isoelectric points correlate with polypeptide compositions. *Electrophoresis,* 15**,** 529-39.

Bjellqvist, B., Hughes, G. J., Pasquali, C., Paquet, N., Ravier, F., Sanchez, J. C., Frutiger, S. & Hochstrasser, D. 1993. The focusing positions of polypeptides in immobilized pH gradients can be predicted from their amino acid sequences. *Electrophoresis,* 14**,** 1023-31.

Blackburn, G. M., Gait, M. J., Loakes, D. & Williams, D. M. 2006. *Nucleic Acids in Chemistry and Biology,* Cambridge, The Royal Society of Chemistry.

Blomqvist, K. 2008. Thawing of glycerolyte-frozen parasites with NaCl. *In:* Moll, K., Ljungström, I., Perlmann, H., Scherf, A. & Wahlgren, M. (eds.) *Methods in Malaria Research.* Fifth ed. Paris: Malaria Research and Reference Reagent Resource Center.

Botha, M., Chiang, A., Needham, P., Stephens, L., Hoppe, H., Külzer, S., Przyborski, J., Lingelbach, K., Wipf, P., Brodsky, J., Shonhai, A. & Blatch, G. 2011. *Plasmodium falciparum* encodes a single cytosolic type I Hsp40 that functionally interacts with Hsp70 and is upregulated by heat shock. *Cell Stress and Chaperones,* 16**,** 389-401.

Brameier, M., Krings, A. & Maccallum, R. 2007. NucPred--predicting nuclear localization of proteins. *Bioinformatics,* 23**,** 1159-60.

Bruce-Chwarr, L. J. 1988. *History of Malaria from Prehistory to Eradication,* Edinburg, Churchill Livingstone.

Buchan, D. W., Ward, S. M., Lobley, A. E., Nugent, T. C., Bryson, K. & Jones, D. T. 2010. Protein annotation and modelling servers at University College London. *Nucleic Acids Research,* 38**,** W563-8.

Cairns, B. R., Kim, Y. J., Sayre, M. H., Laurent, B. C. & Kornberg, R. D. 1994. A multisubunit complex containing the SWI1/ADR6, SWI2/SNF2, SWI3, SNF5, and SNF6 gene products isolated from yeast. *Proceedings of the National Academy of Sciences of the United States of America,* 91**,** 1950-4.

Cairns, B. R., Levinson, R. S., Yamamoto, K. R. & Kornberg, R. D. 1996. Essential role of Swp73p in the function of yeast Swi/Snf complex. *Genes & Development,* 10**,** 2131-44.

Campbell, T. L., De Silva, E. K., Olszewski, K. L., Elemento, O. & Llinás, M. 2010. Identification and Genome-Wide Prediction of DNA Binding Specificities for the ApiAP2 Family of Regulators from the Malaria Parasite. *PLoS Pathogens,* 6**,** e1001165.

Canman, C. E., Lim, D.-S., Cimprich, K. A., Taya, Y., Tamai, K., Sakaguchi, K., Appella, E., Kastan, M. B. & Siliciano, J. D. 1998. Activation of the ATM Kinase by ionizing radiation and phosphorylation of p53. *Science,* 281**,** 1677-9.

Catalano, A. & O'day, D. 2012. Nucleoplasmic/nucleolar translocation and identification of a nuclear localization signal (NLS) in *Dictyostelium* BAF60a/SMARCD1 homologue Snf12. *Histochemistry and Cell Biology,* 138**,** 515-30.

Ch'ng, J. H., Kotturi, S. R., Chong, A. G. L., Lear, M. J. & Tan, K. S. W. 2010. A programmed cell death pathway in the malaria parasite *Plasmodium falciparum* has general features of mammalian apoptosis but is mediated by clan CA cysteine proteases. *Cell Death and Disease,* 1**,** e26.

Chan, C. S. & Botstein, D. 1993. Isolation and characterization of chromosome-gain and increase-in-ploidy mutants in yeast. *Genetics,* 135**,** 677-91.

Chan, W. M., Mak, M. C., Fung, T. K., Lau, A., Siu, W. Y. & Poon, R. Y. C. 2006. Ubiquitination of p53 at Multiple Sites in the DNA-Binding Domain. *Molecular Cancer Research,* 4**,** 15-25.

Chen, J., Lin, J. & Levine, A. J. 1995. Regulation of transcription functions of the p53 tumor suppressor by the mdm-2 oncogene. *Molecular Medicine,* 1**,** 142-52.

Cheng, J., Randall, A., Sweredoski, M. & Baldi, P. 2005. SCRATCH: a protein structure and structural feature prediction server. *Nucleic Acids Research,* 33**,** w72-6.

Cheng, Q., Chen, L., Li, Z., Lane, W. S. & Chen, J. 2009. ATM activates p53 by regulating MDM2 oligomerization and E3 processivity. *The EMBO Journal,* 28**,** 3857-67.

Cho, Y., Gorina, S., Jeffrey, P. & Pavletich, N. 1994. Crystal structure of a p53 tumor suppressor-DNA complex: understanding tumorigenic mutations. *Science,* 265**,** 346-55.

Christofferson, D. E. & Yuan, J. 2010. Necroptosis as an alternative form of programmed cell death. *Current Opinion in Cell Biology,* 22**,** 263-8.

Claros, M. G. & Vincens, P. 1996. Computational Method to Predict Mitochondrially Imported Proteins and their Targeting Sequences. *European Journal of Biochemistry,* 241**,** 779-86.

Clontech. 2012. *In-Fusion® Molar Ratio Calculator* [Online]. TAKARA BIO Inc.,. Available: http://bioinfo.clontech.com/infusion/molarRatio.do [Accessed 30 July 2011].

Cockell, M., Renauld, H., Watt, P. & Gasser, S. M. 1998. Sif2p interacts with the Sir4p amino-terminal domain and antagonizes telomeric silencing in yeast. *Current Biology,* 8**,** 787-S2.

Coetzer, T. L., Durand, P. M. & Nedelcu, A. M. 2010. Genomic evidence for elements of a programmed cell death pathway in Plasmodium: exploiting programmed parasite death for malaria control? . *Blood,* 116.

Computational Biology Research Centre. 2012. *MAFFT version 6: Multiple alignment program for amino acid or nucleotide sequences* [Online]. Computational Biology Research Centre,. Available: http://mafft.cbrc.jp/alignment/server/ [Accessed].

Conner, J. & Liu, Z. 2000. LEUNIG, a putative transcriptional corepressor that regulates AGAMOUS expression during flower development. *Proceedings of the National Academy of Sciences of the United States of America,* 97**,** 12902-7.

Corey, L. L., Weirich, C. S., Benjamin, I. J. & Kingston, R. E. 2003. Localized recruitment of a chromatin-remodeling activity by an activator *in vivo* drives transcriptional elongation. *Genes & Development,* 17**,** 1392-401.

Cornillon, S., Foa, C., Davoust, J., Buonavista, N., Gross, J. D. & Golstein, P. 1994. Programmed cell death in Dictyostelium. *Journal of Cell Science,* 107**,** 2691-704.

Cote, J., Quinn, J., Workman, J. L. & Peterson, C. L. 1994. Stimulation of GAL4 derivative binding to nucleosomal DNA by the yeast SWI/SNF complex. *Science,* 265**,** 53-60.

Cowman, A. F., Berry, D. & Baum, J. 2012. The cellular and molecular basis for malaria parasite invasion of the human red blood cell. *The Journal of Cell Biology,* 198**,** 961-71.

Cowman, A. F., Crabb, B. S., Maier, A. G., Tonkin, C. J., Healer, J., Gibson, P. & De Koning-Ward, T. 2008. Preparation of *P. falciparum* genomic DNA. *In:* Moll, K., Ljungström, I., Perlmann, H., Scherf, A. & Wahlgren, M. (eds.) *Methods in Malaria Research.* Fifth ed. Paris: Malaria Research and Reference Reagent Resource Center.

Cox, F. 2010. History of the discovery of the malaria parasites and their vectors. *Parasites & Vectors,* 3**,** 5.

De Boer, H. A., Comstock, L. J. & Vasser, M. 1983. The tac promoter: a functional hybrid derived from the trp and lac promoters. *Proceedings of the National Academy of Sciences of the United States of America,* 80**,** 21-5.

De La Serna, I. L., Carlson, K. A., Hill, D. A., Guidi, C. J., Stephenson, R. O., Sif, S., Kingston, R. E. & Imbalzano, A. N. 2000. Mammalian SWI-SNF Complexes Contribute to Activation of the hsp70 Gene. *Molecular and Cellular Biology,* 20**,** 2839-51.

Dearnley, M. K., Yeoman, J. A., Hanssen, E., Kenny, S., Turnbull, L., Whitchurch, C. B., Tilley, L. & Dixon, M. W. A. 2012. Origin, composition, organization and function of the inner membrane complex of *Plasmodium falciparum* gametocytes. *Journal of Cell Science,* 125**,** 2053-63.

Deleo, A. B., Jay, G., Appella, E., Dubois, G. C., Law, L. W. & Old, L. J. 1979. Detection of a transformation-related antigen in chemically induced sarcomas and other transformed cells

of the mouse. *Proceedings of the National Academy of Sciences of the United States of America,* 76**,** 2420-4.

Deponte, M. & Becker, K. 2004. *Plasmodium falciparum* – do killers commit suicide? *Trends in parasitology,* 20**,** 165-9.

Derry, W. B., Putzke, A. P. & Rothman, J. H. 2001. *Caenorhabditis elegans* p53: role in apoptosis, meiosis, and stress resistance. *Science,* 294**,** 591-5.

Desai, M., Ter Kuile, F. O., Nosten, F., Mcgready, R., Asamoa, K., Brabin, B. & Newman, R. D. 2007. Epidemiology and burden of malaria in pregnancy. *The Lancet Infectious Diseases,* 7**,** 93-104.

Dias, S. S., Milne, D. M. & Meek, D. W. 2006. c-Abl phosphorylates Hdm2 at tyrosine 276 in response to DNA damage and regulates interaction with ARF. *Oncogene,* 25**,** 6666-71.

Dick, S. A. & Megeney, L. A. 2013. Cell death proteins: an evolutionary role in cellular adaptation before the advent of apoptosis. *Bioessays,* 35**,** 974-83.

Dingwall, A. K., Beek, S. J., Mccallum, C. M., Tamkun, J. W., Kalpana, G. V., Goff, S. P. & Scott, M. P. 1995. The Drosophila snr1 and brm proteins are related to yeast SWI/SNF proteins and are components of a large protein complex. *Molecular Biology of the Cell,* 6**,** 777-91.

Durand, P., Hazelhurst, S. & Coetzer, T. 2010. Evolutionary rates at codon sites may be used to align sequences and infer protein domain function. *BMC Bioinformatics,* 11**,** 151.

El-Deiry, W. S., Kern, S. E., Pietenpol, J. A., Kinzler, K. W. & Vogelstein, B. 1992. Definition of a consensus binding site for p53. *Nature Genetics,* 1**,** 45-9.

Elfring, L. K., Deuring, R., Mccallum, C. M., Peterson, C. L. & Tamkun, J. W. 1994. Identification and characterization of Drosophila relatives of the yeast transcriptional activator SNF2/SWI2. *Molecular and Cellular Biology,* 14**,** 2225-34.

Emes, R. D. & Ponting, C. P. 2001. A new sequence motif linking lissencephaly, Treacher Collins and oral–facial–digital type 1 syndromes, microtubule dynamics and cell migration. *Human Molecular Genetics,* 10**,** 2813-20.

Engebrecht, J., Brent, R. & Kaderbhai, M. A. 1987. Unit 1.6: Minipreps of Plasmid DNA. *In:* Ausubel, F. M., Brent, R., Kingston, R. E., Moore, D. D., Seidman, J. G., Smith, J. A. & Struhl, K. (eds.) *Current Protocols in Molecular Biology.* John Wiley & Son, Inc.

Engelbrecht, D. & Coetzer, T. L. 2013. Turning up the heat: heat stress induces markers of programmed cell death in *Plasmodium falciparum* in vitro. *Cell Death and Disease,* 4**,** e971.

Engelbrecht, D., Durand, P. M. & Coetzer, T. L. 2012. On programmed cell death in *Plasmodium falciparum*: status quo. *Journal of Tropical Medicine,* 2012**,** 646534.

Escalante, A. A. & Ayala, F. J. 1994. Phylogeny of the malarial genus *Plasmodium*, derived from rRNA gene sequences. *Proceedings of the National Academy of Sciences of the United States of America,* 91**,** 11373-7.

Escalante, A. A. & Ayala, F. J. 1995. Evolutionary origin of *Plasmodium* and other Apicomplexa based on rRNA genes. *Proceedings of the National Academy of Sciences of the United States of America,* 92**,** 5793-7.

European Bioinformatics Institute. 2012. *Tools for Sequence Analysis* [Online]. Cambridge: European Bioinformatics Institute,. Available: http://www.ebi.ac.uk/Tools/sequence.html [Accessed 29 June 2012].

Fabrini, R., De Luca, A., Stella, L., Mei, G., Orioni, B., Ciccone, S., Federici, G., Lo Bello, M. & Ricci, G. 2009. Monomer−Dimer Equilibrium in Glutathione Transferases: A Critical Re-Examination. *Biochemistry,* 48**,** 10473-82.

Fairbanks, G., Steck, T. L. & Wallach, D. F. 1971. Electrophoretic analysis of the major polypeptides of the human erythrocyte membrane. *Biochemistry,* 10**,** 2606-17.

Feagin, J. E. 1992. The 6-kb element of *Plasmodium falciparum* encodes mitochondrial cytochrome genes. *Molecular and Biochemical Parasitology,* 52**,** 145-8.

Fidock, D. & Wellems, T. 1997. Transformation with human dihydrofolate reductase renders malaria parasites insensitive to WR99210 but does not affect the intrinsic activity of proguanil. *Proceedings of the National Academy of Sciences of the United States of America,* 94**,** 10931-6.

Flick, K., Ahuja, S., Chene, A., Bejarano, M. & Chen, Q. 2004. Optimized expression of *Plasmodium falciparum* erythrocyte membrane protein 1 domains in *Escherichia coli*. *Malaria Journal,* 3**,** 1-8.

Foth, B. J., Ralph, S. A., Tonkin, C. J., Struck, N. S., Fraunholz, M., Roos, D. S., Cowman, A. F. & Mcfadden, G. I. 2003. Dissecting Apicoplast Targeting in the Malaria Parasite Plasmodium falciparum. *Science,* 299**,** 705-8.

Freedman, D. A., Epstein, C. B., Roth, J. C. & Levine, A. J. 1997. A genetic approach to mapping the p53 binding site in the MDM2 protein. *Molecular Medicine,* 3**,** 248-59.

Fuchs, Y. & Steller, H. 2011. Programmed Cell Death in Animal Development and Disease. *Cell,* 147**,** 742-58.

Fujioka, H. & Aikawa, M. 1999. The Malaria Parasite and its Life-Cycle. *In:* Wahlgren, K. M. & Perlmann, P. (eds.) *Malaria: Molecular & Clinical Aspects.* Amsterdam: Harwood Academic Publishers.

Fulda, S. 2012. Autophagy and cell death. *Autophagy,* 8**,** 1250-1.

Fumagalli, S. & Thomas, G. 2000. S6 Phosphorylation and Signal Transduction. *In:* Sonenberg, N., Hershey, J. W. B. & Mathews, M. B. (eds.) *Translational Control of Gene Expression.* CSHL Press.

Gasteiger, E., Hoogland, C., Gattiker, A., Duvaud, S., Wilkins, M. R., Appel, R. D. & Bairoch, A. 2005. Protein Identification and Analysis Tools on the ExPASy Server. *In:* Walker, J. M. (ed.) *The Proteomics Protocols Handbook.* Totowa: Humana Press.

Geourjon, C., Combet, C., Blanchet, C. & Deléage, G. 2001. Identification of related proteins with weak sequence identity using secondary structure information. *Protein Science,* 10**,** 788-97.

Glover, C. V. 1982. Heat shock induces rapid dephosphorylation of a ribosomal protein in Drosophila. *Proceedings of the National Academy of Sciences of the United States of America,* 79**,** 1781-5.

Glover, D. M., Leibowitz, M. H., Mclean, D. A. & Parry, H. 1995. Mutations in aurora prevent centrosome separation leading to the formation of monopolar spindles. *Cell,* 81**,** 95-105.

Goto, H., Yasui, Y., Nigg, E. A. & Inagaki, M. 2002. Aurora-B phosphorylates Histone H3 at serine28 with regard to the mitotic chromosome condensation. *Genes to Cells,* 7**,** 11-7.

Gould, S. B., Tham, W.-H., Cowman, A. F., Mcfadden, G. I. & Waller, R. F. 2008. Alveolins, a New Family of Cortical Proteins that Define the Protist Infrakingdom Alveolata. *Molecular Biology and Evolution,* 25**,** 1219-30.

Grabski, A., Mehler, M. & Drott, D. 2005. The Overnight Express Autoinduction System: High-density cell growth and protein expression while you sleep. *Nature Methods,* 2**,** 233-5.

Guex, N. & Peitsch, M. C. 1997. SWISS-MODEL and the Swiss-PdbViewer: an environment for comparative protein modeling. *Electrophoresis,* 18**,** 2714-23.

Gutteridge, W. E., Dave, D. & Richards, W. H. G. 1979. Conversion of dihydroorotate to orotate in parasitic protozoa. *Biochimica et Biophysica Acta (BBA) - General Subjects,* 582**,** 390-401.

Guttery, D. S., Holder, A. A. & Tewari, R. 2012. Sexual Development in *Plasmodium*: Lessons from Functional Analyses. *PLoS Pathog,* 8**,** e1002404.

Hafalla, J. C., Silvie, O. & Matuschewski, K. 2011. Cell biology and immunology of malaria. *Immunological Reviews,* 240**,** 297-316.

Hall, T. A. 1999. BioEdit: a user-friendly biological sequence alignment editor and analysis program for Windows 95/98/NT. *Nucleic Acids Symposium Series,* 41**,** 95 - 8.

Han, Q., Lu, J., Duan, J., Su, D., Hou, X., Li, F., Wang, X. & Huang, B. 2008. Gcn5- and Elp3-induced histone H3 acetylation regulates hsp70 gene transcription in yeast. *Biochemical Journal,* 409**,** 779-88.

Healthcare, G. 2009. Glutathione S-transferase (GST) Gene Fusion System. *In:* Healthcare, G. (ed.). Buckinghamshire: GE Healthcare.

Hellman, L. M. & Fried, M. G. 2007. Electrophoretic mobility shift assay (EMSA) for detecting protein-nucleic acid interactions. *Nat. Protocols,* 2**,** 1849-61.

Hermeking, H., Lengauer, C., Polyak, K., He, T.-C., Zhang, L., Thiagalingam, S., Kinzler, K. W. & Vogelstein, B. 1997. *14-3-3σ* Is a p53-Regulated Inhibitor of G2/M Progression. *Molecular Cell,* 1**,** 3-11.

Ho, W. C., Fitzgerald, M. X. & Marmorstein, R. 2006. Structure of the p53 core domain dimer dound to DNA. *Journal of Biological Chemistry,* 281**,** 20494-502.

Hoffmann-Rohrer, U. W. & Kruchen, B. 2011. *Roche Applied Science Lab FAQs: Find a Quick Solution,* Germany, Roche Diagnostics.

Holbrook, L. A., Butler, R. A., Cashon, R. E. & Van Beneden, R. J. 2009. Soft-shell clam (*Mya arenaria*) p53: a structural and functional comparison to human p53. *Gene,* 433**,** 81-7.

Holstege, F. C., Jennings, E. G., Wyrick, J. J., Lee, T. I., Hengartner, C. J., Green, M. R., Golub, T. R., Lander, E. S. & Young, R. A. 1998. Dissecting the regulatory circuitry of a eukaryotic genome. *Cell,* 95**,** 717-28.

Honda, R., Tanaka, H. & Yasuda, H. 1997. Oncoprotein MDM2 is a ubiquitin ligase E3 for tumor suppressor p53. *FEBS letters,* 420**,** 25–7.

Hsu, J.-Y., Sun, Z.-W., Li, X., Reuben, M., Tatchell, K., Bishop, D. K., Grushcow, J. M., Brame, C. J., Caldwell, J. A., Hunt, D. F., Lin, R., Smith, M. M. & Allis, C. D. 2000. Mitotic phosphorylation of histone H3 Is governed by Ipl1/aurora kinase and Glc7/PP1 phosphatase in budding yeast and nematodes. *Cell,* 102**,** 279-91.

Hsu, S. F., Lai, H. C. & Jinn, T. L. 2010. Cytosol-localized heat shock factor-binding protein, AtHSBP, functions as a negative regulator of heat shock response by translocation to the nucleus and is required for seed development in *Arabidopsis*. *Plant Physiology,* 153**,** 773-84.

Hu, G., Cabrera, A., Kono, M., Mok, S., Chaal, B. K., Haase, S., Engelberg, K., Cheemadan, S., Spielmann, T., Preiser, P. R., Gilberger, T.-W. & Bozdech, Z. 2010. Transcriptional profiling of growth perturbations of the human malaria parasite Plasmodium falciparum. *Nat Biotech,* 28**,** 91-8.

Humphrey, G. W., Wang, Y., Russanova, V. R., Hirai, T., Qin, J., Nakatani, Y. & Howard, B. H. 2001. Stable histone deacetylase complexes distinguished by the presence of SANT domain proteins CoREST/kiaa0071 and Mta-L1. *Journal of Biological Chemistry,* 276**,** 6817-24.

Hurd, H. & Carter, V. 2004. The role of programmed cell death in Plasmodium-mosquito interactions. *International Journal for Parasitology,* 34**,** 1459-72.

Hurd, H., Grant, K. M. & Arambage, S. C. 2006. Apoptosis-like death as a feature of malaria infection in mosquitoes. *Parasitology,* 132**,** S33-S47.

Huyen, Y., Jeffrey, P. D., Derry, W. B., Rothman, J. H., Pavletich, N. P., Stavridi, E. S. & Halazonetis, T. D. 2004. Structural Differences in the DNA Binding Domains of Human p53 and Its *C. elegans* Ortholog Cep-1. *Structure,* 12**,** 1237-43.

Integrated DNA Technologies. 2012. *OligoAnalyzer 3.1* [Online]. Integrated DNA Technologies, Inc. Available: http://eu.idtdna.com/analyzer/Applications/OligoAnalyzer/ [Accessed 30 June 2011 2011].

Jensen, J. B., Boland, M. T. & Akood, M. 1982. Induction of crisis forms in cultured *Plasmodium falciparum* with human immune serum from Sudan. *Science,* 216**,** 1230-3.

Jenuwein, T. & Allis, C. D. 2001. Translating the histone code. *Science,* 293**,** 1074-80.

Jin, S., Martinek, S., Joo, W. S., Wortman, J. R., Mirkovic, N., Sali, A., Yandell, M. D., Pavletich, N. P., Young, M. W. & Levine, A. J. 2000. Identification and characterization of a p53 homologue in *Drosophila melanogaster*. *Proceedings of the National Academy of Sciences of the United States of America,* 97**,** 7301-6.

Jones, D. T. 1999. Protein secondary structure prediction based on position-specific scoring matrices. *Journal of Molecular Biology,* 292**,** 195-202.

Kaczanowski, S., Sajid, M. & Reece, S. 2011. Evolution of apoptosis-like programmed cell death in unicellular protozoan parasites. *Parasites and Vectors,* 4**,** 44.

Katayama, H., Sasai, K., Kawai, H., Yuan, Z.-M., Bondaruk, J., Suzuki, F., Fujii, S., Arlinghaus, R. B., Czerniak, B. A. & Sen, S. 2004. Phosphorylation by aurora kinase A induces Mdm2-mediated destabilization and inhibition of p53. *Nature Genetics,* 36**,** 55-62.

Kawai, H., Wiederschain, D. & Yuan, Z.-M. 2003. Critical Contribution of the MDM2 Acidic Domain to p53 Ubiquitination. *Molecular and Cellular Biology,* 23**,** 4939-47.

Kelley, L. A. & Sternberg, M. J. E. 2009. Protein structure prediction on the Web: a case study using the Phyre server. *Nat. Protocols,* 4**,** 363-71.

Kelley, M. L., Winge, P., Heaney, J. D., Stephens, R. E., Farell, J. H., Van Beneden, R. J., Reinisch, C. L., Lesser, M. P. & Walker, C. W. 2001. Expression of homologues for p53 and p73 in the softshell clam (*Mya arenaria*), a naturally-occurring model for human cancer. *Oncogene,* 20**,** 748-58.

Kern, S. E., Kinzler, K. W., Bruskin, A., Jarosz, D., Friedman, P., Prives, C. & Vogelstein, B. 1991. Identification of p53 as a sequence-specific DNA-binding protein. *Science,* 252**,** 1708-11.

Kerr, J. F., Wyllie, A. H. & Currie, A. R. 1972. Apoptosis: a basic biological phenomenon with wide-ranging implications in tissue kinetics. *British Journal of Cancer,* 26**,** 239-57.

King, N., Westbrook, M. J., Young, S. L., Kuo, A., Abedin, M., Chapman, J., Fairclough, S., Hellsten, U., Isogai, Y., Letunic, I., Marr, M., Pincus, D., Putnam, N., Rokas, A., Wright, K. J., Zuzow, R., Dirks, W., Good, M., Goodstein, D., Lemons, D., Li, W., Lyons, J. B.,

Morris, A., Nichols, S., Richter, D. J., Salamov, A., Sequencing, J. G. I., Bork, P., Lim, W. A., Manning, G., Miller, W. T., Mcginnis, W., Shapiro, H., Tjian, R., Grigoriev, I. V. & Rokhsar, D. 2008. The genome of the choanoflagellate *Monosiga brevicollis* and the origin of metazoans. *Nature,* 451**,** 783-8.

Klein, C., Georges, G., Künkele, K.-P., Huber, R., Engh, R. A. & Hansen, S. 2001. High Thermostability and Lack of Cooperative DNA Binding Distinguish the p63 Core Domain from the Homologous Tumor Suppressor p53. *Journal of Biological Chemistry,* 276**,** 37390-401.

Kono, M., Herrmann, S., Loughran, N. B., Cabrera, A., Engelberg, K., Lehmann, C., Sinha, D., Prinz, B., Ruch, U., Heussler, V., Spielmann, T., Parkinson, J. & Gilberger, T. W. 2012. Evolution and Architecture of the Inner Membrane Complex in Asexual and Sexual Stages of the Malaria Parasite. *Molecular Biology and Evolution,* 29**,** 2113-32.

Kosugi, S., Hasebe, M., Matsumura, N., Takashima, H., Miyamoto-Sato, E., Tomita, M. & Yanagawa, H. 2009a. Six Classes of Nuclear Localization Signals Specific to Different Binding Grooves of Importin α. *The Journal of Biological Chemistry,* 284**,** 478-85.

Kosugi, S., Hasebe, M., Tomita, M. & Yanagawa, H. 2009b. Systematic identification of cell cycle-dependent yeast nucleocytoplasmic shuttling proteins by prediction of composite motifs. *Proceedings of the National Academy of Sciences of the United States of America,* 106**,** 10171-6.

Krief, S., Escalante, A. A., Pacheco, M. A., Mugisha, L., André, C., Halbwax, M., Fischer, A., Krief, J.-M., Kasenene, J. M., Crandfield, M., Cornejo, O. E., Chavatte, J.-M., Lin, C., Letourneur, F., Grüner, A. C., Mccutchan, T. F., Rénia, L. & Snounou, G. 2010. On the Diversity of Malaria Parasites in African Apes and the Origin of *Plasmodium falciparum* from Bonobos. *PLoS Pathog,* 6**,** e1000765.

Kroemer, G., Galluzzi, L., Vandenabeele, P., Abrams, J., Alnemri, E. S., Baehrecke, E. H., Blagosklonny, M. V., El-Deiry, W. S., Golstein, P., Green, D. R., Hengartner, M., Knight, R. A., Kumar, S., Lipton, S. A., Malorni, W., Nuñez, G., Peter, M. E., Tschopp, J., Yuan, J., Piacentini, M., Zhivotovsky, B. & Melino, G. 2009. Classification of cell death: recommendations of the Nomenclature Committee on Cell Death 2009. *Cell death and differentiation,* 16**,** 3-11.

Kumar, N., Koski, G., Harada, M., Aikawa, M. & Zheng, H. 1991. Induction and localization of Plasmodium falciparum stress proteins related to the heat shock protein 70 family. *Molecular and Biochemical Parasitology,* 48**,** 47-58.

Kunitoku, N., Sasayama, T., Marumoto, T., Zhang, D., Honda, S., Kobayashi, O., Hatakeyama, K., Ushio, Y., Saya, H. & Hirota, T. 2003. CENP-A Phosphorylation by Aurora-A in Prophase

Is Required for Enrichment of Aurora-B at Inner Centromeres and for Kinetochore Function. *Developmental Cell,* 5**,** 853-64.

Kussie, P. H., Gorina, S., Marechal, V., Elenbaas, B., Moreau, J., Levine, A. J. & Pavletich, N. P. 1996. Structure of the MDM2 Oncoprotein Bound to the p53 Tumor Suppressor Transactivation Domain. *Science,* 274**,** 948-53.

Kwiatkowski, D. 1989. Febrile temperatures can synchronize the growth of *Plasmodium falciparum in vitro*. *The Journal of Experimental Medicine,* 169**,** 357-61.

Lablife. 2011. *pARL2-GFP* [Online]. LabLife. Available: https://www.lablife.org/lab?a=shared_view&oid=g1764.e8a00d4fa783a183e0149cbde5b271ab9c87fee5 [Accessed 15 March 2012].

Labrador, M. & Corces, V. G. 2003. Phosphorylation of histone H3 during transcriptional activation depends on promoter structure. *Genes & Development,* 17**,** 43-8.

Lacount, D. J., Vignali, M., Chettier, R., Phansalkar, A., Bell, R., Hesselberth, J. R., Schoenfeld, L. W., Ota, I., Sahasrabudhe, S., Kurschner, C., Fields, S. & Hughes, R. E. 2005. A protein interaction network of the malaria parasite Plasmodium falciparum. *Nature,* 438**,** 103-7.

Laemmli, U. K. 1970. Cleavage of Structural Proteins during the Assembly of the Head of Bacteriophage T4. *Nature,* 227**,** 680 - 5.

Lambert, C., Léonard, N., De Bolle, X. & Depiereux, E. 2002. ESyPred3D: Prediction of proteins 3D structures. *Bioinformatics,* 18**,** 1250-6.

Lambros, C. & Vanderberg, J. P. 1979. Synchronization of *Plasmodium falciparum* Erythrocytic Stages in Culture. *The Journal of Parasitology,* 65**,** 418-20.

Lanzillotti, R. & Coetzer, T. L. 2006. The 10 kDa domain of human erythrocyte protein 4.1 binds the *Plasmodium falciparum* EBA-181 protein. *Malaria Journal,* 5**,** doi:10.1186/475-2875-5-100.

Lanzillotti, R. & Coetzer, T. L. 2008. Phage display: a useful tool for malaria research? *Trends in parasitology,* 24**,** 18-23.

Laurent, B. C., Treitel, M. A. & Carlson, M. 1991. Functional interdependence of the yeast SNF2, SNF5, and SNF6 proteins in transcriptional activation. *Proceedings of the National Academy of Sciences of the United States of America,* 88**,** 2687-91.

Lauterbach, S., Lanzillotti, R. & Coetzer, T. 2003. Construction and use of Plasmodium falciparum phage display libraries to identify host parasite interactions. *Malaria Journal,* 2**,** 47.

Le Chat, L., Sinden, R. E. & Dessens, J. T. 2007. The role of metacaspase 1 in *Plasmodium berghei* development and apoptosis. *Molecular and Biochemical Parasitology,* 153**,** 41-7.

Learngaramkul, P., Petmitr, S., Krungkrai, S. R., Prapunwattana, P. & Krungkrai, J. 1999. Molecular Characterization of Mitochondria in Asexual and Sexual Blood Stages of *Plasmodium falciparum*. *Molecular Cell Biology Research Communications,* 2**,** 15-20.

Lee, D., Kim, J. W., Seo, T., Hwang, S. G., Choi, E.-J. & Choe, J. 2002. SWI/SNF Complex Interacts with Tumor Suppressor p53 and Is Necessary for the Activation of p53-mediated Transcription. *Journal of Biological Chemistry,* 277**,** 22330-7.

Li, G. & Reinberg, D. 2011. Chromatin higher-order structures and gene regulation. *Current Opinion in Genetics & Development,* 21**,** 175-86.

Lichtman, J. W. & Conchello, J.-A. 2005. Fluorescence microscopy. *Nature Methods,* 2**,** 910-9.

Liebenberg, D. & Coetzer, T. L. Year. Identification of binding partners for a putative *P. falciparum* inhibitor of apoptosis (IAP) protein. *In:* 6th MIM Pan-African Malaria Conference, 2013 Durban, South Africa. 170.

Lim, L. & Mcfadden, G. I. 2010. The evolution, metabolism and functions of the apicoplast. *Philosophical Transactions of the Royal Society B: Biological Sciences,* 365**,** 749-63.

Liu, H., Styles, C. A. & Fink, G. R. 1996. Saccharomyces cerevisiae S288C Has a Mutation in FL08, a Gene Required for Filamentous Growth. *Genetics,* 144**,** 967-78.

Liu, Q., Kaneko, S., Yang, L., Feldman, R. I., Nicosia, S. V., Chen, J. & Cheng, J. Q. 2004. Aurora-A Abrogation of p53 DNA Binding and Transactivation Activity by Phosphorylation of Serine 215. *Journal of Biological Chemistry,* 279**,** 52175-82.

Liu, W., Li, Y., Learn, G. H., Rudicell, R. S., Robertson, J. D., Keele, B. F., Ndjango, J.-B. N., Sanz, C. M., Morgan, D. B., Locatelli, S., Gonder, M. K., Kranzusch, P. J., Walsh, P. D., Delaporte, E., Mpoudi-Ngole, E., Georgiev, A. V., Muller, M. N., Shaw, G. M., Peeters, M., Sharp, P. M., Rayner, J. C. & Hahn, B. H. 2010. Origin of the human malaria parasite *Plasmodium falciparum* in gorillas. *Nature,* 467**,** 420-5.

Liu, Z., Miao, J. & Cui, L. 2011. Gametocytogenesis in malaria parasite: commitment, development and regulation. *Future Microbiology,* 6**,** 1351-69.

Lockshin, R. A. & Williams, C. M. 1964. Programmed cell death—II. Endocrine potentiation of the breakdown of the intersegmental muscles of silkmoths. *Journal of Insect Physiology,* 10**,** 643-9.

Lohrum, M. A. E., Ashcroft, M., Kubbutat, M. H. G. & Vousden, K. H. 2000. Identification of a cryptic nucleolar-localization signal in MDM2. *Nature Cell Biology,* 2**,** 179-81.

Long, H. Y., Lell, B., Dietz, K. & Kremsner, P. G. 2001. *Plasmodium falciparum*: *in vitro* growth inhibition by febrile temperatures. *Parasitology Research,* 87**,** 553-5.

Lu, W.-J., Amatruda, J. F. & Abrams, J. M. 2009. p53 ancestry: gazing through an evolutionary lens. *Nat Rev Cancer,* 9**,** 758-62.

Macrae, J., Dixon, M., Dearnley, M., Chua, H., Chambers, J., Kenny, S., Bottova, I., Tilley, L. & Mcconville, M. 2013. Mitochondrial metabolism of sexual and asexual blood stages of the malaria parasite Plasmodium falciparum. *BMC Biology,* 11**,** 1-10.

Maiuri, M. C., Galluzzi, L., Morselli, E., Kepp, O., Malik, S. A. & Kroemer, G. 2010. Autophagy regulation by p53. *Current Opinion in Cell Biology,* 22**,** 181-5.

Marois, E. 2011. The multifaceted mosquito anti-*Plasmodium* response. *Current Opinion in Microbiology,* 14**,** 429-35.

Mateja, A., Cierpicki, T., Paduch, M., Derewenda, Z. S. & Otlewski, J. 2006. The Dimerization Mechanism of LIS1 and its Implication for Proteins Containing the LisH Motif. *Journal of Molecular Biology,* 357**,** 621-31.

Mckinney, K., Mattia, M., Gottifredi, V. & Prives, C. 2004. p53 Linear Diffusion along DNA Requires Its C Terminus. *Molecular Cell,* 16**,** 413-24.

Meek, D. W. & Knippschild, U. 2003. Posttranslational Modification of MDM2. *Molecular Cancer Research,* 1**,** 1017-26.

Mehlin, C., Boni, E., Buckner, F. S., Engel, L., Feist, T., Gelb, M. H., Haji, L., Kim, D., Liu, C., Mueller, N., Myler, P. J., Reddy, J. T., Sampson, J. N., Subramanian, E., Van Voorhis, W. C., Worthey, E., Zucker, F. & Hol, W. G. J. 2006. Heterologous expression of proteins from Plasmodium falciparum: Results from 1000 genes. *Molecular and Biochemical Parasitology,* 148**,** 144-60.

Melonek, J., Matros, A., Trosch, M., Mock, H. P. & Krupinska, K. 2012. The core of chloroplast nucleoids contains architectural SWIB domain proteins. *Plant Cell,* 24**,** 3060-73.

Mendoza, L., Orozco, E., Rodríguez, M. A., García-Rivera, G., Sánchez, T., García, E. & Gariglio, P. 2003. Ehp53, an *Entamoeba histolytica* protein, ancestor of the mammalian tumour suppressor p53. *Microbiology,* 149**,** 885-93.

Meslin, B., Barnadas, C., Boni, V., Latour, C., De Monbrison, F., Kaiser, K. & Picot, S. 2007. Features of Apoptosis in *Plasmodium falciparum* Erythrocytic Stage through a Putative Role of PfMCA1 Metacaspase-Like Protein. *Journal of Infectious Diseases,* 195**,** 1852-9.

Meslin, B., Beavogui, A. H., Fasel, N. & Picot, S. 2011. *Plasmodium falciparum* Metacaspase PfMCA-1 Triggers a z-VAD-fmk Inhibitable Protease to Promote Cell Death. *PLoS ONE,* 6**,** e23867.

Miele, A., Braastad, C. D., Holmes, W. F., Mitra, P., Medina, R., Xie, R., Zaidi, S. K., Ye, X., Wei, Y., Harper, J. W., Van Wijnen, A. J., Stein, J. L. & Stein, G. S. 2005. HiNF-P Directly Links the Cyclin E/CDK2/p220NPAT Pathway to Histone H4 Gene Regulation at the G1/S Phase Cell Cycle Transition. *Molecular and Cellular Biology,* 25**,** 6140-53.

Mikolajka, A., Yan, X., Popowicz, G. M., Smialowski, P., Nigg, E. A. & Holak, T. A. 2006. Structure of the N-terminal Domain of the FOP (FGFR1OP) Protein and Implications for its Dimerization and Centrosomal Localization. *Journal of Molecular Biology,* 359**,** 863-75.

Miller, L. H., Baruch, D. I., Marsh, K. & Doumbo, O. K. 2002. The pathogenic basis of malaria. *Nature,* 415**,** 673-9.

Miller, M., Lubkowski, J., Rao, J. K. M., Danishefsky, A. T., Omichinski, J. G., Sakaguchi, K., Sakamoto, H., Appella, E., Gronenborn, A. M. & Clore, G. M. 1996. The oligomerization domain of p53: Crystal structure of the trigonal form. *FEBS letters,* 399**,** 166–70.

Mittl, P. R., Chene, P. & Grutter, M. G. 1998. Crystallization and structure solution of p53 (residues 326-356) by molecular replacement using an NMR model as template. *Acta Crystallogr D Biol Crystallogr,* 54**,** 86-9.

Molecular Probes, I. 2005. MitoSOX™ Red mitochondrial superoxide indicator for live-cell imaging. *In:* Technologies, I. D. (ed.). Invitrogen.

Molecular Probes, I. 2008. MitoTracker® Mitochondrion-Selective Probes. *In:* Technologies, I. D. (ed.). Invitrogen.

Momand, J., Zambetti, G. P., Olson, D. C., George, D. & Levine, A. J. 1992. The mdm-2 oncogene product forms a complex with the p53 protein and inhibits p53-mediated transactivation. *Cell,* 69**,** 1237-45.

Mondal, P. K. & Dutta, S. 2014. Review on apoptosis and its role in cancer. *World Journal of Pharmacy and Pharmaceutical Sciences,* 3**,** 713-28.

Moore, D. D. & Dowhan, D. 1987. Unit 2.1: Purification and Concentration of DNA from aqueous solutions. *In:* Ausubel, F. M., Brent, R., Kingston, R. E., Moore, D. D., Seidman, J. G., Smith, J. A. & Struhl, K. (eds.) *Current Protocols in Molecular Biology.* John Wiley & Son, Inc.

Morrison, D. A. 2009. Evolution of the Apicomplexa: where are we now? *Trends in parasitology,* 25**,** 375-82.

Mosser, D. D., Theodorakis, N. G. & Morimoto, R. I. 1988. Coordinate changes in heat shock element-binding activity and HSP70 gene transcription rates in human cells. *Molecular and Cellular Biology,* 8**,** 4736-44.

Muralidharan, V., Oksman, A., Pal, P., Lindquist, S. & Goldberg, D. E. 2012. *Plasmodium falciparum* heat shock protein 110 stabilizes the asparagine repeat-rich parasite proteome during malarial fevers. *Nature Communication,* 3**,** 1310.

Mutai, B. K. & Waitumbi, J. N. 2010. Apoptosis stalks *Plasmodium falciparum* maintained in continuous culture condition. *Malaria Journal,* 9 Suppl 3**,** S6.

Nakano, K. & Vousden, K. H. 2001. *PUMA,* a Novel Proapoptotic Gene, Is Induced by p53. *Molecular Cell,* 7**,** 683-94.

Nanodrop Technologies, I. 2007. *Technical support bulletin T009: 260/280 and 260/230 Ratios NanoDrop® ND-1000 and ND-8000 8-Sample Spectrophotometers* [Online]. Wilmington. Available: www.nanodrop.com [Accessed 10 August 2011].

Nedelcu, A. 2009. Comparative Genomics of Phylogenetically Diverse Unicellular Eukaryotes Provide New Insights into the Genetic Basis for the Evolution of the Programmed Cell Death Machinery. *Journal of Molecular Evolution,* 68**,** 256-68.

Nelson, D. L. & Cox, M. M. 2005. *Lehninger, Principles of Biochemistry, 4th edition.,* New York, W. H. Freeman and Company.

Nkuo, T. K. & Deas, J. E. 1988. Sera from Cameroon induce crisis forms during *Plasmodium falciparum* growth inhibition studies *in vitro*. *Transactions of the Royal Society of Tropical Medicine and Hygiene,* 82**,** 380–3.

Normark, J. 2008. Freezing of patient isolates and strains with glycerolyte. *In:* Moll, K., Ljungström, I., Perlmann, H., Scherf, A. & Wahlgren, M. (eds.) *Methods in Malaria Research.* Fifth ed. Paris: Malaria Research and Reference Reagent Resource Center.

Novagen 1998. pET-15b Vector. United States.

Novagen 2003. pET System Manual. *In:* Novagen (ed.) 10 ed. United States: Novagen.

Novagen 2004. *Competent Cells,* Germany, EMD Biosciences, Inc.

Novagen 2011. T7Select® System Manual. Darmstadt.

Novy, R. & Morris, B. 2001. Use of glucose to control basal expression in the pET system innovations. *InNovations,* 13**,** 8-10.

Nyakeriga, A. M., Perlmann, H., Hagstedt, M., Berzins, K., Troye-Blomberg, M., Zhivotovsky, B., Perlmann, P. & Grandien, A. 2006. Drug-induced death of the asexual blood stages of *Plasmodium falciparum* occurs without typical signs of apoptosis. *Microbes and Infection,* 8**,** 1560-8.

Nygård, O. & Nilsson, L. 1990. Translational dynamics. *European Journal of Biochemistry,* 191**,** 1-17.

Oakley, M. S. M., Kumar, S., Anantharaman, V., Zheng, H., Mahajan, B., Haynes, J. D., Moch, J. K., Fairhurst, R., Mccutchan, T. F. & Aravind, L. 2007. Molecular factors and biochemical pathways induced by febrile temperature in intraerythrocytic *Plasmodium falciparum* parasites. *Infection and Immunity,* 75**,** 2012-25.

Oh, J., Sohn, D. H., Ko, M., Chung, H., Jeon, S. H. & Seong, R. H. 2008. BAF60a interacts with p53 to recruit the SWI/SNF complex. *Journal of Biological Chemistry,* 283**,** 11924-34.

Okamoto, N., Spurck, T. P., Goodman, C. D. & Mcfadden, G. I. 2009. Apicoplast and Mitochondrion in Gametocytogenesis of Plasmodium falciparum. *Eukaryotic Cell,* 8**,** 128-32.

Ollmann, M., Young, L. M., Di Como, C. J., Karim, F., Belvin, M., Robertson, S., Whittaker, K., Demsky, M., Fisher, W. W., Buchman, A., Duyk, G., Friedman, L., Prives, C. & Kopczynski, C. 2000. Drosophila p53 Is a Structural and Functional Homolog of the Tumor Suppressor p53. *Cell,* 101**,** 91-101.

Ollomo, B., Durand, P., Prugnolle, F., Douzery, E., Arnathau, C., Nkoghe, D., Leroy, E. & Renaud, F. 2009. A New Malaria Agent in African Hominids. *PLoS Pathog,* 5**,** e1000446.

Pallavi, R., Acharya, P., Chandran, S., Daily, J. & Tatu, U. 2010. Chaperone expression profiles correlate with distinct physiological states of Plasmodium falciparum in malaria patients. *Malaria Journal,* 9**,** 236.

Pande, J., Szewczyk, M. M. & Grover, A. K. 2010. Phage display: Concept, innovations, applications and future. *Biotechnology Advances,* 28**,** 849-58.

Pankow, S. & Bamberger, C. 2007. The p53 Tumor Suppressor-Like Protein nvp63 Mediates Selective Germ Cell Death in the Sea Anemone *Nematostella vectensis*. *PLoS ONE,* 2**,** e782.

Papoulas, O., Beek, S. J., Moseley, S. L., Mccallum, C. M., Sarte, M., Shearn, A. & Tamkun, J. W. 1998. The Drosophila trithorax group proteins BRM, ASH1 and ASH2 are subunits of distinct protein complexes. *Development,* 125**,** 3955-66.

Park, J. H., Park, E. J., Hur, S. K., Kim, S. & Kwon, J. 2009. Mammalian SWI/SNF chromatin remodeling complexes are required to prevent apoptosis after DNA damage. *DNA Repair (Amst),* 8**,** 29-39.

Pavletich, N. P., Chambers, K. A. & Pabo, C. O. 1993. The DNA-binding domain of p53 contains the four conserved regions and the major mutation hot spots. *Genes & Development,* 7**,** 2556-64.

Payne, J. W. 1973. Polymerization of proteins with glutaraldehyde. Soluble molecular-weight markers. *The Biochemical Journal,* 135**,** 867-73.

Pérez-Cañadillas, J. M., Tidow, H., Freund, S. M. V., Rutherford, T. J., Ang, H. C. & Fersht, A. R. 2006. Solution structure of p53 core domain: Structural basis for its instability. *Proceedings of the National Academy of Sciences of the United States of America,* 103**,** 2109-14.

Phelan, M. L., Sif, S., Narlikar, G. J. & Kingston, R. E. 1999. Reconstitution of a core chromatin remodeling complex from SWI/SNF subunits. *Mol Cell,* 3**,** 247-53.

Picot, S., Burnod, J., Bracchi, V., Chumpitazi, B. F. & Ambroise-Thomas, P. 1997. Apoptosis related to chloroquine sensitivity of the human malaria parasite *Plasmodium falciparum*. *Transactions of the Royal Society of Tropical Medicine and Hygiene,* 91**,** 590-1.

Pishchany, G. & Skaar, E. P. 2012. Taste for Blood: Hemoglobin as a Nutrient Source for Pathogens. *PLoS Pathog,* 8**,** e1002535.

Pizzi, E. & Frontali, C. 2000. Divergence of Noncoding Sequences and of Insertions Encoding Nonglobular Domains at a Genomic Region Well Conserved in Plasmodia. *Journal of Molecular Evolution,* 50**,** 474-80.

Pizzi, E. & Frontali, C. 2001. Low-Complexity Regions in Plasmodium falciparum Proteins. *Genome Research,* 11**,** 218-29.

Porro, M., Viti, S., Antoni, G. & Saletti, M. 1982. Ultrasensitive silver-stain method for the detection of proteins in polyacrylamide gels and immunoprecipitates on agarose gels. *Analytical Biochemistry,* 127**,** 316–21.

Porter, H., Gamette, M. J., Cortes-Hernandez, D. G. & Jensen, J. B. 2008. Asexual Blood Stages of *Plasmodium falciparum* Exhibit Signs of Secondary Necrosis, but not Classical Apoptosis after Exposure to Febrile Temperature (40 C). *Journal of Parasitology,* 94**,** 473-80.

Prigent, C. & Dimitrov, S. 2003. Phosphorylation of serine 10 in histone H3, what for? *Journal of Cell Science,* 116**,** 3677-85.

Promega 2009a. Technical Manual: MagneGST™ Protein Purification System. Madison: Promega Corporation.

Promega 2009b. Technical Manual: MagneHis™ Protein Purification System. Madison: Promega Corporation.

Proto, W. R., Coombs, G. H. & Mottram, J. C. 2013. Cell death in parasitic protozoa: regulated or incidental? *Nature Reviews Microbiology,* 11**,** 58-66.

Prugnolle, F., Durand, P., Neel, C., Ollomo, B., Ayala, F. J., Arnathau, C., Etienne, L., Mpoudi-Ngole, E., Nkoghe, D., Leroy, E., Delaporte, E., Peeters, M. & Renaud, F. 2010. African great apes are natural hosts of multiple related malaria species, including *Plasmodium falciparum*. *Proceedings of the National Academy of Sciences of the United States of America*.

Prugnolle, F., Durand, P., Ollomo, B., Duval, L., Ariey, F., Arnathau, C., Gonzalez, J.-P., Leroy, E. & Renaud, F. 2011. A Fresh Look at the Origin of *Plasmodium falciparum*, the Most Malignant Malaria Agent. *PLoS Pathog,* 7**,** e1001283.

Przyborski, J. M., Miller, S. K., Pfahler, J. M., Henrich, P. P., Rohrbach, P., Crabb, B. S. & Lanzer, M. 2005. Trafficking of STEVOR to the Maurer's clefts in Plasmodium falciparum-infected erythrocytes. *The EMBO Journal,* 24**,** 2306-17.

Ramsdale, M. 2012. Programmed cell death in the cellular differentiation of microbial eukaryotes. *Curr Opin Microbiol,* 15**,** 646-52.

Rao, V. S., Srinivas, K., Sujini, G. N. & Kumar, G. N. S. 2014. Protein-protein interaction detection: methods and analysis. *Int J Proteomics,* 2014**,** 147648.

Rapley, R. 2005. Chapter 5: Molecular biology, bioinformatics and basic techniques. *In:* Wilson, K. & Walker, J. (eds.) *Principles & Techniques of Biochemistry of Molecular Biology* Cambridge: Cambridge University Press.

Ray, C. G. & Plorde, J. J. 2010. Sporozoa. *In:* Ryan, K. J. & Ray, C. G. (eds.) *Sherris Medical Microbiology.* 5th ed. New York: McGraw Hill.

Reininger, L., Wilkes, J. M., Bourgade, H., Miranda-Saavedra, D. & Doerig, C. 2011. An essential Aurora-related kinase transiently associates with spindle pole bodies during *Plasmodium falciparum* erythrocytic schizogony. *Molecular Microbiology,* 79**,** 205-21.

Rich, S. M., Leendertz, F. H., Xu, G., Lebreton, M., Djoko, C. F., Aminake, M. N., Takang, E. E., Diffo, J. L. D., Pike, B. L., Rosenthal, B. M., Formenty, P., Boesch, C., Ayala, F. J. & Wolfe, N. D. 2009. The origin of malignant malaria. *Proceedings of the National Academy of Sciences of the United States of America*.

Rich, S. M., Licht, M. C., Hudson, R. R. & Ayala, F. J. 1998. Malaria's Eve: Evidence of a recent population bottleneck throughout the world populations of *Plasmodium falciparum*. *Proceedings of the National Academy of Sciences of the United States of America,* 95**,** 4425-30.

Roche Applied Science 2004. *DIG Gel Shift Kit, 2nd Generation,* Germany, Roche Applied Science.

Roche Applied Science 2011. *Rapid DNA Ligation Kit,* Germany, Roche Applied Science.

Rosenberg, R., Wirtz, R. A., Schneider, I. & Burge, R. 1990. An estimation of the number of malaria sporozoites ejected by a feeding mosquito. *Transactions of the Royal Society of Tropical Medicine and Hygiene,* 84**,** 209-12.

Rost, B. 1999. Twilight zone of protein sequence alignments. *Protein Engineering,* 12**,** 85-94.

Roth, J., Dobbelstein, M., Freedman, D. A., Shenk, T. & Levine, A. J. 1998. Nucleo-cytoplasmic shuttling of the hdm2 oncoprotein regulates the levels of the p53 protein via a pathway used by the human immunodeficiency virus rev protein. *The EMBO Journal,* 17**,** 554-64.

Rotter, V., Abutbul, H. & Ben-Ze'ev, A. 1983. P53 transformation-related protein accumulates in the nucleus of transformed fibroblasts in association with the chromatin and is found in the cytoplasm of non-transformed fibroblasts. *The EMBO Journal,* 2**,** 1041-7.

Russo, I., Oksman, A. & Goldberg, D. E. 2009a. Fatty acid acylation regulates trafficking of the unusual Plasmodium falciparum calpain to the nucleolus. *Mol Microbiol,* 72**,** 229-45.

Russo, I., Oksman, A., Vaupel, B. & Goldberg, D. E. 2009b. A calpain unique to alveolates is essential in Plasmodium falciparum and its knockdown reveals an involvement in pre-S-phase development. *Proc Natl Acad Sci U S A,* 106**,** 1554-9.

Sakamuro, D., Sabbatini, P., White, E. & Prendergast, G. C. 1997. The polyproline region of p53 is required to activate apoptosis but not growth arrest. *Oncogene,* 15**,** 887-98.

Sakurai, K., Schubert, C. & Kahne, D. 2006. Crystallographic analysis of an 8-mer p53 peptide analogue complexed with MDM2. *Journal of the American Chemical Society,* 128**,** 11000-1.

Sambrooke, J. & Russell, D. W. 2001. *Molecular Cloning: A Laboratory Manual,* New York, Cold Spring Harbour Laboratory Press.

Sat, B., Hazan, R., Fisher, T., Khaner, H., Glaser, G. & Engelberg-Kulka, H. 2001. Programmed Cell Death in Escherichia coli: Some Antibiotics Can Trigger mazEF Lethality. *JOURNAL OF BACTERIOLOGY,* 183**,** 2041–5.

Sayeed, S., Shah, V., Chaubey, S., Singh, M., Alampalli, S. & Tatu, U. 2014. Identification of heat shock factor binding protein in *Plasmodium falciparum*. *Malaria Journal,* 13**,** 118.

Schlesinger, M. J., Aliperti, G. & Kelley, P. M. 1982. The response of cells to heat shock. *Trends in Biochemical Sciences,* 7**,** 222-5.

Schnitzler, G., Sif, S. & Kingston, R. E. 1998. Human SWI/SNF interconverts a nucleosome between its base state and a stable remodeled state. *Cell,* 94**,** 17-27.

Schrodinger, Llc 2010. The PyMOL Molecular Graphics System, Version 1.3r1.

Schumacher, B., Hofmann, K., Boulton, S. & Gartner, A. 2001. The *C. elegans* homolog of the p53 tumor suppressor is required for DNA damage-induced apoptosis. *Current Biology,* 11**,** 1722-7.

Schumacher, B., Hofmann, K., Boulton, S. & Gartner, A. 2004. The C. elegans homolog of the p53 tumor suppressor is required for DNA damage-induced apoptosis. *Current Biology,* 11**,** 1722-7.

Schwede, T., Kopp, J., Guex, N. & Peitsch, M. C. 2003. SWISS-MODEL: an automated protein homology-modeling server. *Nucleic Acids Research,* 31**,** 3381-5.

Shaner, N. C., Steinbach, P. A. & Tsien, R. Y. 2005. A guide to choosing fluorescent proteins. *Nature Methods,* 2**,** 905-9.

Shaulsky, G., Goldfinger, N., Ben-Ze'ev, A. & Rotter, V. 1990. Nuclear accumulation of p53 protein is mediated by several nuclear localization signals and plays a role in tumorigenesis. *Molecular and Cellular Biology,* 10**,** 6565-77.

Shivaswamy, S. & Iyer, V. R. 2008. Stress-dependent dynamics of global chromatin remodeling in yeast: Dual role for SWI/SNF in the heat shock stress response. *Molecular and Cellular Biology,* 28**,** 2221-34.

Sim, B. K., Toyoshima, T., Haynes, J. D. & Aikawa, M. 1992. Localization of the 175-kilodalton erythrocyte binding antigen in micronemes of *Plasmodium falciparum* merozoites. *Molecular and Biochemical Parasitology,* 51**,** 157-9.

Singh, B., Sung, L. K., Matusop, A., Radhakrishnan, A., Shamsul, S. S. G., Cox-Singh, J., Thomas, A. & Conway, D. J. 2004. A large focus of naturally acquired Plasmodium knowlesi infections in human beings. *The Lancet,* 363**,** 1017-24.

Smith, M. A. & Schnellmann, R. G. 2012. Calpains, mitochondria, and apoptosis. *Cardiovascular Research,* 96**,** 32-7.

Solyakov, L., Halbert, J., Alam, M. M., Semblat, J.-P., Dorin-Semblat, D., Reininger, L., Bottrill, A. R., Mistry, S., Abdi, A., Fennell, C., Holland, Z., Demarta, C., Bouza, Y., Sicard, A.,

Nivez, M.-P., Eschenlauer, S., Lama, T., Thomas, D. C., Sharma, P., Agarwal, S., Kern, S., Pradel, G., Graciotti, M., Tobin, A. B. & Doerig, C. 2011. Global kinomic and phospho-proteomic analyses of the human malaria parasite *Plasmodium falciparum*. *Nature Communication,* 2**,** 565.

Speidel, D. 2010. Transcription-independent p53 apoptosis: an alternative route to death. *Trends in Cell Biology,* 20**,** 14-24.

Srivastava, I. K., Rottenberg, H. & Vaidya, A. B. 1997. Atovaquone, a broad spectrum antiparasitic drug, collapses mitochondrial membrane potential in a malarial parasite. *J Biol Chem,* 272**,** 3961-6.

Stenger, J. E., Mayr, G. A., Mann, K. & Tegtmeyer, P. 1992. Formation of stable p53 homotetramers and multiples of tetramers. *Molecular Carcinogenesis,* 5**,** 102-6.

Stommel, J. M., Marchenko, N. D., Jimenez, G. S., Moll, U. M., Hope, T. J. & Wahl, G. M. 1999. A leucine-rich nuclear export signal in the p53 tetramerization domain: regulation of subcellular localization and p53 activity by NES masking. *The EMBO Journal,* 18**,** 1660-72.

Stratagene 2004. *XL10-Gold® ultracompetent cells*, Stratagene,.

Sullivan, E. K., Weirich, C. S., Guyon, J. R., Sif, S. D. & Kingston, R. E. 2001. Transcriptional activation domains of human heat shock factor 1 recruit human SWI/SNF. *Molecular and Cellular Biology,* 21**,** 5826-37.

Switzer, R. C., Merril, C. R. & Shifrin, S. 1979. A highly sensitive silver stain for detecting proteins and peptides in polyacrylamide gels. *Analytical Biochemistry,* 98**,** 231–7.

Takahashi, N., Jetten, A. M. & Breitman, T. R. 1991. Retinoylation of cytokeratins in normal human epidermal keratinocytes. *Biochem Biophys Res Comm,* 180**,** 393-400.

Taliaferro, W. H. & Taliaferro, L. G. 1944. The effect of immunity on the asexual reproduction of *Plasmodium brasilianum*. *The Journal of Infectious Diseases,* 75**,** 1-32.

Tanimura, S., Ohtsuka, S., Mitsui, K., Shirouzu, K., Yoshimura, A. & Ohtsubo, M. 1999. MDM2 interacts with MDMX through their RING finger domains. *FEBS letters,* 447**,** 5–9.

The Eupathdb Project Team. 2012. *PlasmoDB 8.2* [Online]. Strategies WDK Available: http://plasmodb.org/plasmo/ [Accessed 15 March 2012 2012].

Thermo Fisher Scientific 2011. Product Information: High Fidelity PCR Enzyme Mix. *Thermo Fisher Scientific, Inc.*

Thermo Fisher Scientific Inc 2011. Fermentas FastDigest Restriction Enzymes. *In:* Thermo Fisher Scientific Inc (ed.). Thermo Fisher Scientific Inc,.

Thomas, G., Siegmann, M., Kubler, A.-M., Gordon, J. & Jimenez De Asua, L. 1980. Regulation of 40S ribosomal protein S6 phosphorylation in Swiss mouse 3T3 cells. *Cell,* 19**,** 1015-23.

Thomas Meier, U. & Blobel, G. 1992. Nopp 140 shuttles on tracks between nucleolus and cytoplasm. *Cell,* 70**,** 127-38.

Tilley, L., Dixon, M. W. A. & Kirk, K. 2011. The *Plasmodium falciparum*-infected red blood cell. *The International Journal of Biochemistry & Cell Biology,* 43**,** 839-42.

Tirasophon, W., Ponglikitmongkol, M., Wilairat, P., Boonsaeng, V. & Panyim, S. 1991. A novel detection of a single *Plasmodium falciparum* in infected blood. *Biochemical and Biophysical Research Communications,* 175**,** 179-84.

Tompa, P. 2002. Intrinsically unstructured proteins. *Trends in Biochemical Sciences,* 27**,** 527-33.

Tonkin, C. J., Van Dooren, G. G., Spurck, T. P., Struck, N. S., Good, R. T., Handman, E., Cowman, A. F. & Mcfadden, G. I. 2004. Localization of organellar proteins in Plasmodium falciparum using a novel set of transfection vectors and a new immunofluorescence fixation method. *Molecular and Biochemical Parasitology,* 137**,** 13-21.

Torrentino-Madamet, M., Desplans, J., Travaille, C., James, Y. & Parzy, D. 2010. Microaerophilic respiratory metabolism of *Plasmodium falciparum* mitochondrion as a drug target. *Curr Mol Med,* 10**,** 29-46.

Toshiyuki, M. & Reed, J. C. 1995. Tumor suppressor p53 is a direct transcriptional activator of the human *bax* gene. *Cell,* 80**,** 293-9.

Totino, P. R. R., Daniel-Ribeiro, C. T., Corte-Real, S. & Ferreira-Da-Cruz, M. D. F. 2008. *Plasmodium falciparum*: Erythrocytic stages die by autophagic-like cell death under drug pressure. *Experimental Parasitology,* 118**,** 478-86.

Towbin, H., Staehelin, T. & Gordon, J. 1979. Electrophoretic transfer of proteins from polyacrylamide gels to nitrocellulose sheets: procedure and some applications. *Proceedings of the National Academy of Sciences of the United States of America,* 76**,** 4350-4.

Trager, W. & Jensen, J. B. 1976. Human malaria parasites in continuous culture. *Science,* 193**,** 673-5.

Treich, I., Ho, L. & Carlson, M. 1998. Direct interaction between Rsc6 and Rsc8/Swh3,two proteins that are conserved in SWI/SNF-related complexes. *Nucleic Acids Research,* 26**,** 3739-45.

Unger, T., Nau, M. M., Segal, S. & Minna, J. D. 1992. p53: a transdominant regulator of transcription whose function is ablated by mutations occurring in human cancer. *The EMBO Journal,* 11**,** 1383-90.

Uren, A. G., O'rourke, K., Aravind, L., Pisabarro, M. T., Seshagiri, S., Koonin, E. V. & Dixit, V. M. 2000. Identification of Paracaspases and Metacaspases: Two Ancient Families of Caspase-like Proteins, One of which Plays a Key Role in MALT Lymphoma. *Molecular Cell,* 6**,** 961-7.

Vaidya, A. B. & Mather, M. W. 2009. Mitochondrial evolution and functions in malaria parasites. *Annual Review of Microbiology,* 63**,** 249-67.

Van Dooren, G. G., Marti, M., Tonkin, C. J., Stimmler, L. M., Cowman, A. F. & Mcfadden, G. I. 2005. Development of the endoplasmic reticulum, mitochondrion and apicoplast during the asexual life cycle of *Plasmodium falciparum*. *Molecular Microbiology,* 57**,** 405-19.

Van Wye, J. D. & Haldar, K. 1997. Expression of green fluorescent protein in *Plasmodium falciparum*. *Molecular and Biochemical Parasitology,* 87**,** 225-9.

Vardi, A., Berman-Frank, I., Rozenberg, T., Hadas, O., Kaplan, A. & Levine, A. 1999. Programmed cell death of the dinoflagellate *Peridinium gatunense* is mediated by CO2 limitation and oxidative stress. *Current Biology,* 9**,** 1061–4.

Vedadi, M., Lew, J., Artz, J., Amani, M., Zhao, Y., Dong, A., Wasney, G., Gao, M., Hills, T., Brokx, S., Qiu, W., Sharma, S., Diassiti, A., Alam, Z., Melone, M., Mulichak, A., Wernimont, A., Bray, J., Loppnau, P., Plotnikova, O., Newberry, K., Sundararajan, E., Houston, S., Walker, J., Tempel, W., Bockharev, A., Kozieradzki, I., Edwards, A., Arrowsmith, C., Roos, D., Kain, K. & Hui, R. 2007. Genome-scale protein expression and structural biology of *Plasmodium falciparum* and related Apicomplexan organisms. *Molecular and Biochemical Parasitology,* 151**,** 100 - 10.

Vu, T. T., Tran, V. B., Phan, N. T., Le, T. T., Luong, V. H., O'brien, E. & Morris, G. E. 1995. Screening donor blood for malaria by polymerase chain reaction. *Transactions of the Royal Society of Tropical Medicine and Hygiene,* 89**,** 44-7.

Wade, M., Wang, Y. V. & Wahl, G. M. 2010. The p53 orchestra: Mdm2 and Mdmx set the tone. *Trends in Cell Biology,* 20**,** 299-309.

Waller, R. F., Keeling, P. J., Donald, R. G. K., Striepen, B., Handman, E., Lang-Unnasch, N., Cowman, A. F., Besra, G. S., Roos, D. S. & Mcfadden, G. I. 1998. Nuclear-encoded proteins target to the plastid in *Toxoplasma gondii* and *Plasmodium falciparum*. *Proceedings of the National Academy of Sciences of the United States of America,* 95**,** 12352-7.

Waller, R. F., Reed, M. B., Cowman, A. F. & Mcfadden, G. I. 2000. Protein trafficking to the plastid of *Plasmodium falciparum* is via the secretory pathway. *The EMBO Journal,* 19**,** 1794-802.

Wang, P., Reed, M., Wang, Y., Mayr, G., Stenger, J. E., Anderson, M. E., Schwedes, J. F. & Tegtmeyer, P. 1994. p53 domains: structure, oligomerization, and transformation. *Mol Cell Biol,* 14**,** 5182-91.

Wang, W., Cote, J., Xue, Y., Zhou, S., Khavari, P. A., Biggar, S. R., Muchardt, C., Kalpana, G. V., Goff, S. P., Yaniv, M., Workman, J. L. & Crabtree, G. R. 1996. Purification and

biochemical heterogeneity of the mammalian SWI-SNF complex. *The EMBO Journal,* 15**,** 5370-82.

Wang, Y., Schwedes, J. F., Parks, D., Mann, K. & Tegtmeyer, P. 1995. Interaction of p53 with its consensus DNA-binding site. *Molecular and Cellular Biology,* 15**,** 2157–65.

Waning, D. L., Lehman, J. A., Batuello, C. N. & Mayo, L. D. 2010. Controlling the Mdm2-Mdmx-p53 Circuit. *Pharmaceuticals (Basel),* 3**,** 1576-93.

Waters, A. P., Thomas, A. W., Van Dijk, M. R. & Janse, C. J. 1997. Transfection of malaria parasites. *Methods,* 13**,** 134-47.

Wei, Y., Jin, J. & Harper, J. W. 2003. The Cyclin E/Cdk2 Substrate and Cajal Body Component p220NPAT Activates Histone Transcription through a Novel LisH-Like Domain. *Molecular and Cellular Biology,* 23**,** 3669-80.

Welburn, S. C., Barcinski, M. A. & Williams, G. T. 1997. Programmed cell death in Trypanosomatids. *Parasitology Today,* 13**,** 22-5.

White, N. J., Turner, G. D. H., Day, N. P. J. & Dondorp, A. M. 2013. Lethal malaria: Marchiafava and Bignami were right. *Journal of Infectious Diseases,* 208**,** 192-8.

Wickham, M. E., Culvenor, J. G. & Cowman, A. F. 2003. Selective Inhibition of a Two-step Egress of Malaria Parasites from the Host Erythrocyte. *Journal of Biological Chemistry,* 278**,** 37658-63.

Wickman, G., Julian, L. & Olson, M. F. 2012. How apoptotic cells aid in the removal of their own cold dead bodies. *Cell death and differentiation,* 19**,** 735-42.

Wilkinson, D. L. & Harrison, R. G. 1991. Predicting the solubility of recombinant proteins in *Escherichia coli*. *Biotechnology (N Y),* 9**,** 443-8.

Willats, W. G. 2002. Phage display: practicalities and prospects. *Plant Molecular Biology,* 50**,** 837-54.

Williams, A. J., Werner-Fraczek, J., Chang, I.-F. & Bailey-Serres, J. 2003. Regulated phosphorylation of 40S ribosomal protein S6 in root tips of maize. *Plant Physiology,* 132**,** 2086-97.

Wilson, B. G. & Roberts, C. W. M. 2011. SWI/SNF nucleosome remodellers and cancer. *Nature Reviews Cancer,* 11**,** 481-92.

Wilson, R. J. M., Denny, P. W., Preiser, P. R., Rangachari, K., Roberts, K., Roy, A., Whyte, A., Strath, M., Moore, D. J., Moore, P. W. & Williamson, D. H. 1996. Complete gene map of the plastid-like DNA of the malaria parasite *Plasmodium falciparum*. *Journal of Molecular Biology,* 261**,** 155-72.

World Health Organization 2013. WHO global malaria programme: World malaria report 2013. Geneva, Switzerland: World Health Organization.

Wu, J. I., Lessard, J. & Crabtree, G. R. 2009. Understanding the words of chromatin regulation. *Cell,* 136**,** 200-6.

Yamada, K., Saito, K., Nameki, N., Inoue, M., Koshiba, S., Shirouzu, M., Terada, T., Yabuki, T., Aoki, M., Matsuda, T., Seki, E., Hirota, H., Yoshida, M., Tanaka, A., Osanai, T., Arakawa, T., Carninci, P., Kawai, J., Hayashizaki, Y., Kigawa, T. & Yokoyama, S. 2004. Solution structure of the SWIB domain of mouse BRG1-associated factor 60a (PDB ID: 1UHR).

Yang, W., Xia, Y., Hawke, D., Li, X., Liang, J., Xing, D., Aldape, K., Hunter, T., Alfred yung, W. K. & Lu, Z. 2012. PKM2 Phosphorylates Histone H3 and Promotes Gene Transcription and Tumorigenesis. *Cell,* 150**,** 685-96.

Yonekawa, T. & Thorburn, A. 2013. Autophagy and cell death. *Essays in Biochemistry,* 55**,** 105-17.

Yoneyama, M., Tochio, N., Koshiba, S., Inoue, M., Kigawa, T. & Yokoyama, S. 2004a. Solution structure of the SWIB/MDM2 domain of the hypothetical protein At5g08430 from *Arabidopsis thaliana* (PDB ID 1V32).

Yoneyama, M., Tochio, N., Koshiba, S., Inoue, M., Kigawa, T. & Yokoyama, S. 2004b. Solution structure of the SWIB/MDM2 domain of the hypothetical protein At5g14170 from *Arabidopsis thaliana* (PDB ID: 1V31).

Zangger, H., Mottram, J. C. & Fasel, N. 2002. Cell death in *Leishmania* induced by stress and differentiation: programmed cell death or necrosis? *Cell death and differentiation,* 9**,** 1126-39.

Zeitlin, S. G., Shelby, R. D. & Sullivan, K. F. 2001. CENP-A is phosphorylated by Aurora B kinase and plays an unexpected role in completion of cytokinesis. *The Journal of Cell Biology,* 155**,** 1147-58.

Zhang, J., Kalkum, M., Chait, B. T. & Roeder, R. G. 2002. The N-CoR-HDAC3 nuclear receptor corepressor complex inhibits the JNK pathway through the Integral Subunit GPS2. *Molecular Cell,* 9**,** 611-23.

Zhang, Y. & Xiong, Y. 2001. A p53 amino-terminal nuclear export signal inhibited by DNA damage-induced phosphorylation. *Science,* 292**,** 1910-5.

Zhao, J., Herrera-Diaz, J. & Gross, D. S. 2005. Domain-wide displacement of histones by activated heat shock factor occurs independently of Swi/Snf and is not correlated with RNA polymerase II density. *Molecular and Cellular Biology,* 25**,** 8985-99.

Zielonka, J. & Kalyanaraman, B. 2010. Hydroethidine- and MitoSOX-derived red fluorescence is not a reliable indicator of intracellular superoxide formation: another inconvenient truth. *Free Radical Biology & Medicine,* 48**,** 983-1001.

Zuegge, J., Ralph, S., Schmuker, M., Mcfadden, G. I. & Schneider, G. 2001. Deciphering apicoplast targeting signals – feature extraction from nuclear-encoded precursors of Plasmodium falciparum apicoplast proteins. *Gene,* 280**,** 19-26.